Max-Planck-Institut für Biochemie

Abteilung Strukturforschung

Biologische NMR-Arbeitsgruppe

Structural studies of kinases involved in the cell cycle control

and

the structural basis of regulation of insulin-like growth factor binding proteins (IGFBPs)

Sudipta Majumdar

Vollständiger Abdruck der von der Fakultät für Chemie der Technischen Universität München zur Erlangung des akademischen Grades eines

Doktors der Naturwissenschaften

genehmigten Dissertation.

Vorsitzender: Univ.-Prof. Dr. Johannes Buchner

Prüfer der Dissertation: 1. apl. Prof. Dr. Luis Moroder

2. Univ.-Prof. Dr. Dr. Adelbert Bacher

Die Dissertation wurde am 19.12.2005 bei der Technischen Universität München eingereicht und durch die Fakultät für Chemie am 14.03.2006 angenommen.

I would like to dedicate my thesis to my mother and father ....

Acknowledgements

I would like to thank everyone who contributed to this work.

I am grateful to Professor Robert Huber for giving me the opportunity to work in his department and I am also greatful to Professor Dr. Luis Moroder for being my Doktorvater.

To my supervisor Doctor Tad A. Holak, for his support, guidance, discussions and encouragement for my work.

I am thankful to my laboratory mates: Michael Brüggert, Till Rehm, Grzegorz Popowicz, Loy D'Silva, Magda Wisniewska, Marcin Krajewski, Narashima Rao Nolabothula, Mariusz Kamionka, Ola Mikolajka, Pawel Smialowski, Przemyslaw Ozdowy, Dorota Ksiazek, Tomasz Sitar, Dr. Ashwani Thakur, Anna Woscowicz and Anna Benzinger for creating the motivating atmosphere.

My special thanks goes to Sreejesh, Madhumita, Mahavir, Joma, and Igor for their technical advises and discussion. Ulli Rothweiler and Dr. Brigitte Kracht- for their help in the matters of bureaucracy and German language.

Last but not the least I would like to thank my mother and father for their kind support and sacrifices, which is helping me to achieve my goal. I would also like to acknowledge my wife Geetanjali for her patience, care and love, also in the hardest moment of time.

Publications

Parts of this thesis have been or will be published in due course:

- P. Smialowski, M. Singh, A. Mikolajka, **S. Majumdar**, J. K. Joy, N. Nalabothula, M. Krajewski, R.Degenkolbe, H. U. Bernard and T. A. Holak. (2005) NMR and mass spectrometry studies of putative interactions of cell cycle proteins pRb and CDK6 with cell differentiation proteins MyoD and ID-2. *Biochem. Biophys. Acta Proteomics*. **1750**, 48-60.

- A. Benzinger, G. Popowicz, J. K. Joy, **S. Majumdar**, T. A. Holak, and Heiko Hermeking. (2005) The crystal structure of the non-liganded 14-3-3sigma protein: insights into determinants of isoform specific ligand binding and dimerization. *Cell Res*. **15**, 219-227.

- Siwanowicz, G. Popowicz, L. D'Silva, **S. Majumdar**, J. K. Joy, M. Wisniewska, S. M. Firth, R. Huber, R. C. Baxter, and T. A. Holak. (Submitted in *J. Mol. Biol*.) Molecular architecture of the insulin-like growth factor binding proteins.

- M. Krajewski, **S. Majumdar**, U. Rothweiler, L. D'Silva and T. A. Holak. (In preperation) Targeting ligand-protein and protein-protein interactions in the NMR competition binding experiments.

- J. K. Joy, **S. Majumdar** and T. A. Holak. (In preparation) Structural insights into the interaction between insulin growth factor and its binding proteins.

- **S. Majumdar**, L. D'Silva and T. A. Holak. (In preparation) Interaction studies of the flavonoid derivatives on the ATP binding cleft of CDK2 by NMR spectroscopy.

Contents

1. INTRODUCTION

1.1 Cell cycle

E. Krebs and E. Fisher in the 1950's discovered protein phosphorylation and protein kinases that opened the way to an amazing flow of data on how protein kinases are regulated and control cell fate. Among the estimated 1000 human protein kinases the family of cyclin dependent kinases (CDKs) has been extensively studied because of their essential cellular functions (Cohen, 2002; Knockaert et al., 2002).

CDKs play pivotal role in controlling the cell cycle (CDK1, 2, 3, 4, 6, 7), in apoptosis (CDK2), in neuronal function (CDK5) and in transcription (CDK7, 8, 9). CDC2 was the first member of this family, which was discovered for its cell cycle function in yeast. At present thirteen CDKs and 25 cyclin box-containing proteins have been identified in humans (Knockaert et al., 2002). Those known to interact in a complex are listed in Table 1. In addition there are several CDK related kinases with no identified cyclin partner. These are recognized by the sequence homology and by the presence of the variation of the conserved '*PSTAIRE*' motif located in the cyclin binding domain. They are *PCTAIRE*, *PFTAIRE*, *PITAIRE*, *KKIALRE*, *PISSLRE*, *NKIAMRE* and *PITSLRE*s instead of *PSTAIRE* motif. Cyclins F, G, M, O, and P do not have any CDK partners and are known as 'orphan' cyclins (Meijer et al., 2000; Meyerson et al., 1992).

1.1.1 Cell cycle: different phases and control

The transient activation of various CDKs and by the association with different cyclins, control the progression of the cell division cycle through the G1→S→G2→M phases. In early to mid G1 the first set of cyclins (D1, D2, D3) are activated by the mitogenic signals (Matsushime et al., 1991; Xiong et al., 1991; Motokura et al., 1991). Mitogen induced Ras signaling promotes transcription of the cyclin D1 gene via a kinase cascade that depends on the sequential activities of Raf-1, mitogen induced protein kinase (MEK1 and MEK2) and extracellular signal regulated protein kinases (ERKs). ERKs act posttranslationally to regulate cyclin D-CDK assembly because ectopically expressed cyclin subunits do not efficiently associate with CDKs in the absence of mitogenic signals. The turnover of D-type cyclins depends on a separate Ras signaling pathway-involving phosphatidylinositol 3-kinase (PI3K) and Akt (protein kinase B), which negatively regulate the phosphorylation of cyclin D1 on a single threonine residue (Thr286) by glycogen synthase kinase-3β

(GSK3β). Inhibition of this signaling pathway leads to cyclin D1 phosphorylation, enhances its nuclear export, and accelerates its ubiquitin-dependent proteasomal degradation in the cytoplasm (Hunter et al., 1994).

Table 1. CDKs known to make pairs with the cyclins and have been identified for their distinctive role in the cell cycle (Meijer et al. 2000)

CDKs	Partners	Functions
CDK1	cyclin B	Prophase to metaphase transition, regulation of topoisomerase-2
	Ringo	β-Amyloid-induced cytotoxicity
CDK2	cyclin A	G1→S transition, S phase and G2 phase, centrosome duplication, regulation of Sp1-mediated transcription
	cyclin E	Apoptosis in thymocytes, mesangial cells DNA damage-induced apoptosis
CDK3	cyclin E	G1→S transition
CDK4	cyclin D	G1 phase excitotoxin-induced neuronal cell death, dopamine and glutamate signaling, neurite outgrowth, neurone migration, induction of acetylcholine receptors
CDK5	p35, p25	Apoptosis
	p39, p29	Golgi membrane traffic, insulin exocytosis by β-cells phototransduction, neurotransmitter release(VDCC*) Lens cell differentiation, myogenesis
CDK6	cyclin D	G1phase neuronal cell death
CDK7	cyclin H	CDK1, 2 activation, basal transcription (TFIIH)
CDK8	cyclin C	Basal transcription, regulation of CDK7–cyclin H
CDK9	cyclin K	Signal transduction RNA transcription (P-TEFb), HIV-Tat-dependent transcription
	cyclin T	MyoD-mediated myocyte differentiation
CDK11	cyclin L	RNA processing or transcriptional apoptosis, dopamine and glutamate signaling
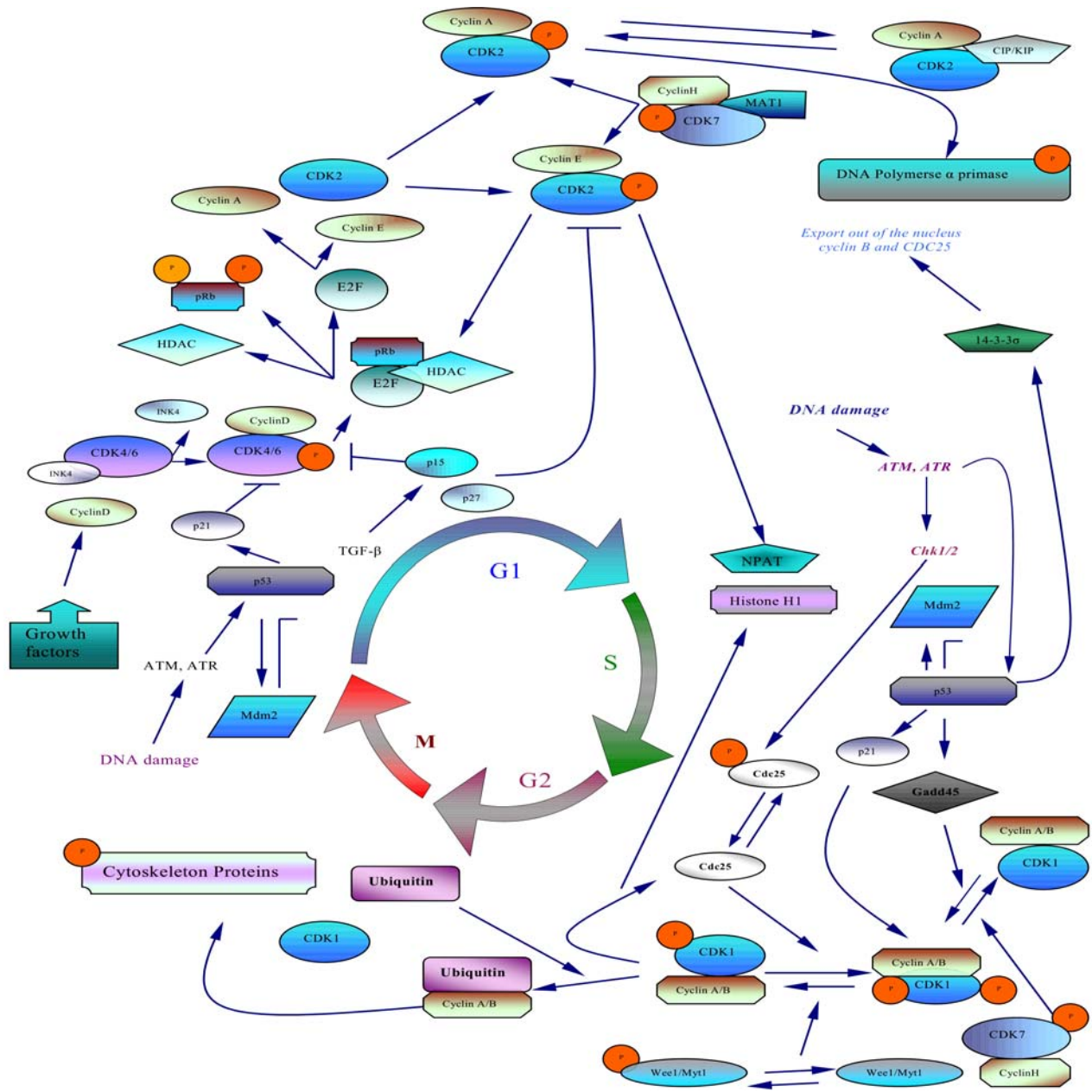
Fig. 1. Schematic representation of the cell cycle. Details regarding the different phases are described in the text.

G1 cyclins assemble with CDK4 and CDK6, which in turn gets activated by phosphorylation, with a CDK activating kinase (CAK) (Matsushime et al., 1992; Meyerson et al., 1994). These activated CDKs (CDK4-cyclin D1 and CDK6-cyclin D3) phosphorylate the retinoblastoma protein pRb. Phosphorylation of pRb causes dissociation of the E2F/DP1/pRb complex and turns off its transcriptional suppressor activity (de-Gregori et al., 1995; Arata et al.,

2000; Sherr, 1996). Release of E2F/DP1 results in transcriptional activation of a set of genes required for entry into S-phase including thymidylate synthetase, dihydro-folate reductase, cyclin A and cyclin E. Cyclin E activates CDK2, which acts to further phosphorylate pRB that in turn makes the pRB hyperphosphorylated and results in an irreversible commitment to cell division and transition into S-phase (Lukas et al., 1997; Lundberg et al., 1998).
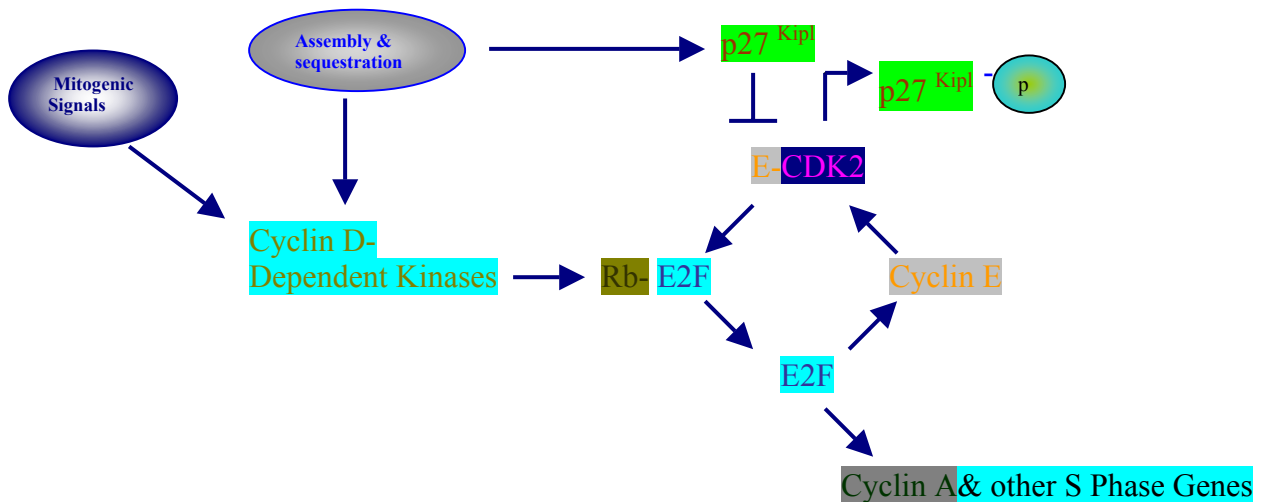
Fig. 2. Schematic representation of the activation of S-phase genes.

During S-phase, CDK2-cyclin A phosphorylates different substrates allowing DNA replication and inactivation of the G1 transcription factors. Around the time of S→G2 transition CDK1 associates with cyclin A. After that CDK1-cyclin B appears and triggers the G2→M transition by phosphorylating substrates like the nuclear lamins. Cyclin B proteolysis, transition to anaphase and completion of mitosis requires phosphorylation of 'Anaphase Promoting Complex' (APC) by CDK1-cyclin B.

Some CDKs directly influence transcription. The CDK7-cyclin H/MAT1 complex, a component of the TFIIH transcription factor, is responsible for the phosphorylation of the C-terminal domain of the large subunit of RNA polymerase II, which is required for the elongation process (Adamczewski et al., 1996; Feaver et al., 1994; Roy et al., 1994; Serizawa et al., 1995). CDK8-cyclin C phosphorylates CTD RNA pol II, but on different sites. P-TEFb, a component of the positive transcription elongation factor has CDK9-cyclin T (Grana et al., 1994; Garriga et al., 2003; Zhu et al., 1997; Peng et al., 1998). It is responsible for the TAT associated kinase activity involved

in the HIV 1 Tat transactivation (Shore et al., 2003; Peng et al., 1998; Michels et al., 2003; Wimmer et al., 1999).

Activation and inactivation of these successive waves of cyclin-CDK assemblies are tightly regulated by posttranslational modifications and intracellular translocations. They are coordinated and dependent on the completion of previous steps through so called checkpoint controls. For example, they are controlled by association with pRb and pRb related p107 and p130 proteins, which comprise the 'pocket protein' family of cell cycle regulators. pRb and the p107/p130 pair are required for the repression of distinct sets of genes potentially due to their selective interactions with E2Fs that are engaged at specific promoter elements (Aslanian et al., 2004; Cam et al., 2003; Classon et al., 2001; Ginsberg 2004; Stevaux et al., 2002). In the G1 to S phase transition pRb binds to the E2F family of transcription factors and the resulting pRb-E2F complex not only blocks transcriptional activation by E2F but also forms an active transcriptional repressor complex at the promoter of cell cycle genes that can block transcription by recruiting histone deacetylase (HDAC) and the remodeling chromatin complex (SWI/SNF complex) (Rayman et al., 2002; Nicolas et al., 2003; Zhang et al., 2000; Harding et al., 2004). SWI/SNF proteins form an 11-subunit complex of approximately 2 mega Daltons. When bound to nucleosomes, the SWI/SNF complex alters the path of DNA bending around the nucleosome core in an ATP-dependent reaction that does not by itself displace the underlying histones. This complex is able to disrupt the nucleosome structure in a sequence–independent manner (Strober et al., 1996; Dunaief et al., 1994).

The pRb-E2F-HDAC repression can be removed by the sequential phosphorylation of pRb. pRb contains at least 16 consensus sequences for CDK phosphorylation (Knudsen et al., 1996; Knudsen et al., 1997). Phosphorylation of the C-terminal domain of pRb (Ser807, Ser811, Thr821 and Thr826) by cyclin D-CDK4/6 triggers an initial intramolecular interaction with the central pRb pocket domain that inhibits HDAC binding, thereby blocking active transcriptional repression by the pRb-pocket (Hinds et al., 1992; Dowdy et al., 1993; Ewen et al., 1994; Kato et al., 1993; Hatakeyama et al., 1994). Phosphorylation of Ser608, Ser612, Ser780 or Ser788 by cyclin E-CDK2 does not affect the pocket activity or structure but the phosphorylation of Ser567 disrupts the A-B interface preventing pRb from binding and inactivating E2F (Mittnacht et al., 1994; Roberts et al., 1994; Weinberg et al., 1995; Harbour et al., 1999). Cyclin D-CDK4/6 is the kinase that normally

disrupts HDAC and blocks active repression in vivo because it is activated in G1, before cyclin E-CDK2. Inactivation of E2F would not be prevented until near the end of G1, when cyclin E-CDK2 is activated (Harbour et al., 1999). Studies show that cyclin E-CDK-2 and its cooperation with E2F is required for the efficient initiation of DNA replication. Such a progressive loss of activities allows differential regulation of genes involved in cell cycle progression (Harbour et al., 1999).

1.1.2 The ARF tumor suppressor – regulator in G1 phase

The ARF proteins are encoded by INK4a gene by alternative splicing of its exon (Quelle et al., 1995; Kamijo et al., 1997). Introduction of ARF into cells results in the p53-dependent cell cycle arrest, indicating that ARF acts upstream of p53 (Quelle et al., 1995; Mao et al., 1995; Stone et al., 1995; Duro et al., 1995).

p53 is a homotetrameric transcription factor that induces either cell cycle arrest or apoptosis, depending on the biological setting (Ko et al., 1996; Levine, 1997). Cells lacking p53 alone are refractory to ARF-induced arrest, and ARF protein expression is greatly increased (Kamijo et al., 1998; Stott et al., 1998). ARF stabilizes p53 by antagonizing the p53-negative regulator MDM2. MDM2 binds to the transactivation domain of the p53 to inhibit p53-dependent gene expression and it also manifests an ubiquitin ligase activity that appears to target p53 for proteasomal degradation (Kamijo et al., 1998; Pomerantz et al., 1998; Zhang et al., 1998). MDM2 is itself a p53-responsive gene that normally acts in feedback control to terminate the p53 response. ARF can interfere with all of the known functions of MDM2, including its ability to block p53 transcription, to ubiquitinate p53, and to enforce p53 transport into the cytoplasm where it is degraded in proteasomes (Oliner et al., 1993; Momand et al., 1992; Honda et al., 1997; Barak et al., 1993). ARF was found to bind to a central region of MDM2 to a segment distinct from MDM2's nuclear import and export signals, its NH2-terminal p53 binding domain, and the COOH–terminal RING domain, the integrity of which is required for the E3 ubiquitin ligase activity (Tao et al., 1999; Zhang et al., 1999; Weber et al., 1999; Haupt et al., 1997; Kubbutat et al., 1997; Midgley et al., 1997).

ARF expression is activated by overexpression of oncoproteins such as MYC, EIA, E2F1, RAS and V-ABL. It connects the pRb pathway with MDM2 and p53. ARF acts as a fuse to inappropriate mitogenic signals flowing through the cyclin D-CDK-pRb-E2F circuit, inducing p53

under conditions in which abnormal proliferative signals are generated. In short, ARF normally acts to protect cells from MYC overexpression by facilitating MYC–induced, p53–dependent apoptosis. Cells corrupted in the ARF-MDM2-p53 pathway are resistant to MYC-induced killing, enabling MYC to act as a pure growth promoter in this setting. In these way cells, which have received the oncogenic insult undergo a p53-dependent growth arrest or apoptosis (Zindy et al., 1998; de-Stanchina et al., 1998; Bates et al., 1998; Palmero et al., 1998; Radfar et al., 1998).

1.1.3 bHLH proteins and CDKs

The basic helix loop helix (bHLH) proteins are crucial for the coordination of differentiation processes in the cell cycle (Norton 2000). These proteins form both homo- and heterodimers. Dimerization and interaction with the basic region are essential for DNA binding and transcriptional activity (Lassar 1991; Massari et al., 2000). The bHLH contains MyoD, myogenin, E12, E47, E2-5/ITF1, NeuroD/BETA2, and TAL (Massari et al., 2000). Id-1 to Id-4 are mammalian HLH proteins (Norton et al., 1998). These proteins promote cell proliferation by binding to transcription factors from the bHLH proteins and inhibit their ability to bind DNA.

MyoD plays a key role in the differentiation of all skeletal muscle lineages (Weintraub et al., 1991). A forced expression of MyoD in a variety of different cell backgrounds, including normal, transformed, and tumor cell lines, was shown to induce growth arrest. This feature was correlated with the presence of the MyoD bHLH domain (Crescenzi et al., 1990). Researchers found that MyoD interacted with human CDK4 and CDK6 through a conserved 15-amino-acid region situated at the C-terminus of MyoD. This C-terminus fragment was shown to be sufficient to inhibit CDK4-dependent phosphorylation of pRb (Zhang et al., 1999; Zhang et al., 1999).

1.2 Cyclin dependent kinases and their regulation

CDKs are composed of a protein kinase catalytic subunit and a regulatory cyclin subunit. The typical CDK catalytic subunit contains a 300 amino acids catalytic core that is completely inactive when monomeric and unphosphorylated (Bondt et al., 1993; Morgan et al., 1994). The inactive monomeric CDK subunit becomes activated through protein conformational changes accompanied by its association with the specific cyclin molecule and phosphorylation of a conserved and essential

threonine residue within the activation segment of the kinase (Thr160 of CDK2) (Kobayashi et al., 1992; Morgan et al., 1994). Mutation of the equivalent residue from a number of species abolishes cell cycle kinase activity and the kinase activity of CDK2-cyclin A is increased 300- fold on phosphorylation of Thr160 (Poon et al., 1994; Fisher et al., 1994). When Ser was replaced in place of Thr160 the phosphorylation was more efficient but the dephosphorylation of CDK2 got delayed. Therefore one reason for the conservation of threonine as the site of activating phosphorylation may be to favor unphosphorylated CDK2 following the degradation of cyclins (Fesquet et al., 1993; Solomon et al., 1993; Matsuoka et al., 1994; Krek et al., 1991). The control of activity of these kinases is necessary for progression through G1 and is affected at multiple levels:

1. Activation and accumulation of the cyclins with response to the cell signals.
2. Proper assembly of cyclin-CDK complexes.
3. Specific phosphorylation and dephosphorylation events.
4. Inhibitory proteins.

The primary regulator of CDK activity is the cyclin subunit. Each CDK interacts with a specific subset of cyclins. Cyclin function is primarily controlled by changes in cyclin levels, which increase characteristically at specific cell cycle stages. Homology among cyclins is often limited to a relatively conserved domain of about 100 amino acids, the cyclin box which is responsible for CDK binding and activation (Kobayashi et al., 1992; Lees et al., 1993). Constant synthesis during the cell cycle results in a roughly linear increase in cyclin concentration until at mitosis cycle degradation abruptly increases, producing a rapid decline in cyclin levels. Cyclin degradation probably involves the ubiquitin-dependent proteolytic machinery, and requires a small sequence motif (the destruction box) near the amino terminus of mitotic cyclins (Glotzer et al., 1991).

In CDK2, Thr160 lays in the T-loop that block the protein substrate-binding site; its side chain is inaccessible to solvent suggesting that the loop must move to allow phosphorylation (Fesquet et al., 1993; Matsuoka et al., 1994). Cyclin binding enhances phosphorylation and the later enhances the binding of some CDK-cyclin partners. CAK (CDK activating kinase) is a hetero trimeric complex composed of a catalytic subunit, p40^{MO15}/CDK7, a regulatory subunit, cyclin H and an assembly factor, MAT1. CAK can activate all the major CDK-cyclin substrates involved in vertebrate cycle (Fisher et al., 1994, Matsuoka et al., 1994; Krek et al., 1991; Gu et al., 1992).

Final activation of the CDKs requires dephosphorylation of the inhibitory pThr14 and pTyr15 sites by the dual specificity phosphatase CDC25. CDC25 activity decreases during mitosis, largely because of increased phosphorylation. During mitosis, the kinase responsible for this phosphorylation is activated and the corresponding phosphatase is inhibited (Zeng et al., 1998; Gyuris et al., 1993; Harper et al., 1993; Hanon et al., 1994).

Genetic and biochemical studies have implicated KAP (kinase-associated phosphatase also termed Cdi1, Cip2) as one of the protein phosphatases responsible for dephosphorylating the activating pThr160 residue of human CDK1, CDK2 and CDK3. The enzyme, is a member of the dual specificity phosphatase (DSP) family and is capable of dephosphorylating artificial protein substrates containing both pThr and pTyr residues.

The CDK-cyclin complexes can also be inhibited by phosphorylation at two sites near the amino terminus (Thr14 and Tyr15) in human CDK1 and CDK2 (Furnari et al., 1997; Lorka 1992). The kinases responsible for these two phosphorylation events include the Myt1 and Wee1 kinases, which phosphorylate CDK1 on Thr14 and Tyr15, respectively (Morgan et al., 1994).

Phosphorylation of Thr14 and Tyr 15 is particularly important in the control of CDK1 activation at mitosis. Like the Thr161 phosphorylation, phosphorylation Thr14 and Tyr15 roughly parallels the rise in cyclin B levels that occurs as cells approach mitosis. CDK1-cyclin B complexes are thus maintained in an inactivate state, until Thr14 and Tyr15 dephosphorylation at the end of G2 activates CDK1 (Strausfeld et al., 1991, Zeng et al., 1998). So the CDKs are controlled through several different processes involving the binding of activating cyclin subunits, phosphorylation and by the inhibitory Cip or INK4 subunits, the later is described in the next section.

1.3 Inhibitors of CDKs

The CDK inhibitors also known as CKIs can either physically block activation or block substrate/ATP access. Most antiproliferative signals lead to the induction of CDK inhibitors. For example senescence, contact inhibition, extracellular anti-mitogenic factors like TGF-β and cell cycle check points like the p53 DNA damage, induce $p16^{INK4a}$, $p27^{Cip2}$, $p15^{INK4b}$, and $p21^{Cip1}$, respectively. The inhibitors of CDKs are categorized in two families according to their structural similarities and modes of action. They are the INK4 family and the Cip/Kip family.

1.3.1 The INK4 family

The INK4 proteins (named for their ability to <u>in</u>hibit CD<u>K</u>4) specifically target the cyclin D dependent kinases. Four proteins are currently known in this family. They are p16^{INK4a}, p15^{INK4b}, p18^{INK4c}, and p19^{INK4d} (Sherr et al., 1995; Ruas et al., 1998). The presence of the ankyrin repeats is the common structural feature of these proteins. In humans, INK4a and INK4b are closely linked on the short arm of chromosome 9, whereas INK4c maps to chromosome 1 and INK4d maps to chromosome 19. INK4 proteins are expressed in a cell-type specific manner. p15^{INK4b} is induced by TGFβ (Serrano et al., 1993; Hannon et al., 1994; Hirai et al., 1995; Chan et al., 1995; Kamb et al., 1994). Among all the CKIs both INK4 and Cip/Kip, only p16^{INK4a} is classified as a tumor suppressor. p18^{INK4c} and p19^{INK4d} preferentially bind CDK6.

INK4 proteins sequester CDK4/6 into binary CDK-INK4 complexes, liberating bound Cip/Kip proteins, and thereby indirectly inhibiting cyclin E/CDK2 to ensure cell cycle arrest. The INK4 proteins by inhibiting cyclin D-dependent kinases make pRb to remain hypophosphorylated and able to repress transcription of S-phase genes (Guan et al., 1994, Lukas et al., 1995; Medema et al., 1995). In the absence of pRb, cyclin E expression is increased, and inhibition of cyclin D-CDK4 complexes does not inhibit S-phase entry. So the simple conceptual pathway is as follows:

INK4 proteins $\Rightarrow$ *cyclin D-dependent kinases* $\Rightarrow$ *pRb* $\Rightarrow$ *E2Fs* $\Rightarrow$ *S-phase entry.*

1.3.2 Cip/Kip Family

The Cip (<u>C</u>DK <u>i</u>nteracting <u>p</u>rotein)/Kip (<u>k</u>inase <u>i</u>nhibitory <u>p</u>rotein) family has three proteins. They are p21^{Cip1}, p27^{Kip1} and p57^{Kip2} (el-Deiry et al., 1993; Harper 1993; Polyak et al., 1994; Toyoshima et al., 1994; Lee et al., 1995; Matsuoka et al., 1995). These proteins act as stoichiometric inhibitors and share a homologous inhibitory domain, which is both necessary and sufficient for binding and inhibition of CDK2 and CDK4 containing complexes. They preferentially act on CDK2 complexes in vivo. Cip/Kip proteins are required for the assembly of the active cyclin D-dependent holoenzymes (Soos et al., 1996; Blain et al., 1997; La-Baer et al., 1997; Cheng et al., 1999).

p21^{Cip1} was the first CKI identified. This protein was also named Sdi1 (senescent cell derived inhibitor) and Waf1 (wild type p53activated fragment). p21^{Cip1} is involved in the p53-dependent DNA damage-induced G1 arrest. The amount of p21^{Cip1} protein increases following

exposure to DNA damaging agents. In addition to the ability to associate with cyclin-CDK complexes, p21[Cip1] also associates with proliferating cell nuclear antigen (PCNA) a subunit of DNA polymerase delta (Kopundrioukoff et al., 2000). The PCNA–CDK2 complex is present in the nucleus throughout the cell cycle and is preferentially formed during the S-phase in the cytoplasm. CDK2-cyclin A phosphorylates two DNA replication proteins, RF-Cp145 (the PCNA binding region of replication factor C) and ligase1. PCNA acts as a connector for DNA ligase1 with CDKs-cyclins, by contributing the recognition step preceding phosphorylation and stimulate phosphorylation (Koundrioukoff et al., 2000; Bravo, 1986). This is an additional way in which p21[Cip1] can inhibit DNA synthesis. Both its involvement in the DNA damage check point and its possible role in PCNA inactivation, suggest that p21[Cip1] has a major role in regulating replication in committed cells.

In cycling cells p27[Kip1] remains bound to the CDK-cyclin D complex. So under certain conditions this protein will interfere with the cyclin D dependent activities. The understanding of how these proteins work together is important. In one model, cells were treated with TGFβ, which accumulated p15[INK4b] and lead to the reduction of cyclin D-CDK4 complexes that in turn increased the level of p27[Kip1] in the cell by releasing it from the bound state. This allows p27[Kip1] to interact with CDK2. Once cyclin E-CDK2 is activated, it phosphorylates p27[Kip1]. p27 inhibits CDK2 activity until the G1 transition at which point p27 levels decrease (Yam et al., 1999). A family of small proteins that include Cks1, bind to CDK2 and mediates the interaction between CDK2 and p27. In late G1, cyclin E-CDK2 phosphorylate p21 and p27. Skp2 degrades the ubiquitinated Cip/Kip proteins. Cks1 controls the ability of Skp2 to bind p27, by allowing a change in conformation that increases its affinity for p27 (Mongay et al., 2001; Bourne et al., 1996; Spruck et al., 2001). This converts p27[Kip1] to a form that is recognized by ubiquitin ligases and is targeted for destruction in proteasomes. Therefore cyclin E-CDK2 antagonizes the action of its own inhibitor. It follows that once cyclin E-CDK2 is activated, unbound p27[Kip1] is rapidly degraded, contributing to the irreversibility of passage through the restriction point. If cells are persistently stimulated with mitogens, the cyclin D dependent kinase activity remains high in subsequent cycles, p27[Kip1] can be found in complexes with the cyclin D-CDKs. However, when mitogens are withdrawn, cyclin D is rapidly degraded, and previously sequestered Cip/Kip proteins are mobilized to inhibit cyclin E-

CDK2, thereby arresting progression usually within a single cycle (Reynisdottir et al., 1997; Muller et al., 1997; Perez-Roger et al., 1997). The p57^{Kip2} locus is imprinted in both mouse and humans, and only the maternal allele is expressed. Targeted disruption of p57 in mice showed a role for this CKI in the control of the commitment/withdrawal decision as well as differentiation and apoptosis (Lee et al., 1995; Matsuoka et al., 1995).

1.4 The gene knockout studies

Table 2. The knockout studies conducted in mice

Cyclin D1	Cyclin D2	Cyclin D3	Cyclins D1, D2 and D3	CDK4	CDK6	CDK4 and CDK6
Viable	Viable	Viable	Dead	Viable	Viable	Embryonic lethality
Small body size	Defective ovarian granulosa cell development female sterility	Hypoplastic thymus with loss of T-cell maturation	Severe hematopoietic deficits affecting number and proliferative capacity of stem cells and multipotential progenitors	Small body size	Thymic and splenic hypoplasia	Small embryos
Hypoplastic retinopathy				Most males and females are sterile	Mild defects in hematopoiesis	Failure of hematopoiesis
Defective beast Lobuloal-veolar developm-ent during pregnancy	Males have hypoplastic testes but are fertile Abnormal postnatal cerebellar development due to reduce number of neurons.		Liver damage	Abnormal development of pancreatic-islet cells leads to insulin-dependent diabetes	T-lymphocytes exhibit delayed S phase entry	Severe megaloblastic anemia
			Death due to anemia and defects in heart development			Reduced S phase fraction
	Impaired proliferation of peripheral B-lymphocytes					Some D-type cyclins associate with and activate CDK2

Table 2. The knockout studies conducted in mice (continued)

Cyclins E1 and E2	CDK2
Dead	Viable
Cardiac anomalies of varying severity in rescued embryos	Meiotic failure
Reduced endoreduplication in megakaryocytes	Gonadal hypertrophy, and male and female sterility
Increased G1 phase and undergo senescence	Delayed entry into S-phase and/or decreased ability to re-enter the cell cycle
Quiescent cells cannot re-enter the cell cycle due to a failure in loading MCM proteins onto prereplication origins	

All the recent studies on knockout mice of CDKs and cyclins suggest that one CDK can compensate the other to some extent. For example in G1 phase the knockout studies revealed that the role of CDK4 and CDK6 could be compensated by CDK2 and in the S phase the role of CDK2 can be compensated by CDK1. However, the appearance of tissue-specific defects in the mutants clearly establishes that they are not totally interchangeable. It will be more interesting to determine why certain tissues are more sensitive to the loss of certain CDKs and cyclins than others. Table 2 describes the knockout studies conducted in different mice models and their effect.

1.5 Cyclin dependent kinase 2

1.5.1 History

A human homolog of CDC2/CDC28 of *Schizosaccharomyces pombe* and *Saccharomyces cerevisiae,* respectively, was identified as p34CDC2, a serine-threonine protein kinase (Ninomiya-Tsuji, 1991; Lee et al., 1987). Using a human cDNA expression library to search for suppressors of CDC28 mutations in *Saccharomyces cerevisiae*, a second functional p34 homolog, CDK2, and cell division kinase was identified. This gene is expressed as a 2.1 kb transcript encoding a polypeptide of 298 amino acids. This protein retained nearly all of the amino acids highly conserved among previously identified p34 homolog from other species, but was considerably divergent from all

previous p34CDC2 homologs, exhibiting approximately 65% identity. Furthermore, this gene encoded the human homolog of the *Xenopus* Eg1 gene, sharing 89% amino acid identity, and defined a second subfamily of CDC2 homologs. A 2.4 kb DNA fragment from the upstream region of CDK2 contained five transcription initiation sites within 72-bp stretch. A 200bp sub fragment that confers 70% of maximal basal promoter activity contained 2 synergistically acting Sp1 sites. Like CDK4, CDK2 mapped to 12q13 (Ninomiya-Tsuji et al., 1991; Shiffman, 1996; Demetrick, 1994).

1.5.2 Role of CDK2 in different phases of the cell cycle

The role of CDK2 in different phases of the cell cycle has already been described in the earlier sections of the thesis. The other inhibitors, which influence the CDK2 activity apart from Cip/ Kip proteins, are described in the table below (Meijer et al., 2000).

Table 3. Endogenous inhibitors of CDK2 and their roles in the cell cycle

Cip/Kip proteins	p27, p21, p57	Main regulator of CDK2 activity. Described in the earlier sections
MYC		Oncoprootein that induces CDK2 activity. Down-regulation of MYC induces cell cycle arrest by down-regulation of CDK2
Interferon/TNF (Tumor Necrosis Factor)		Reduces CDK2 activity by the combination of cytokines
Insulin receptor kinase		CDK2 activity is inhibited as this protein recruits p27
PKC-protein kinase C		Association with cyclinA-CDK2 ultimately leads to the inhibition of kinase activity
Cell-cell contact		Inhibits CDK2 by p27 recruitment and cyclin A down-regulation

1.5.3 CDK2 and oncoproteins

B-MYB is a target of cyclin A-CDK2 and its activity is regulated by the later through phosphorylation (Ziebold et al., 1997; Saville et al., 1998). There are six sites in the B-MYB that are recognized by CDK2 (Bartsch et al., 1999). V-JUN shares the capacity of the MYC, E2F, and E1A oncoproteins and accelerates G1 transition in the absence of the mitogenic signals. V-JUN accelerates the production of cyclin A, which increases kinase activity of the cyclin A-CDK2 complex. As a result the pRb gets phosphorylated, the E2F/p107 complex persists after mitogen withdrawal and triggers DNA synthesis. V-JUN also deregulates the cyclin E-CDK2 complex without affecting cyclin D-CDK4 (Clark et al., 2000).

1.5.4 Association of viral oncoproteins with CDK2

Table 4. Association of viral oncoproteins with CDK2 and their control

Source	*Protein*	*Associations*	*Functions*
Polyomavirus (Lane et al., 1979)	SV40T-antigen	CDK2-cyclin A	CDK2-cyclin A binds with T antigen of SV40, forms replication initiation complex in S-phase Complexes with p53 and p300
Papillomavirus (Scheffner et al., 1993)	E6, E7	pRb, p107, and p130, cyclin A and E	CDK2-cyclin A/E7and CDK2-cyclin E/E7 show high kinetic activity Overrides the p21 inhibition E1 helicase binds cyclin E-CDK2, regualte papilomavirus replication Accelerates ubiquitin-mediated degradation by p53
Human Cytomegalovirus (HCMV) (Bresnahan et al., 1997)	IEI, 2	CDK2	Activates CDK2 Induces cyclins, pRb MYC and FOS oncogenes are upregualted
Adenovirus (Bagchi et al., 1990)	E1A	CDK2-cyclin A, pRb, p27	Act downstream of p27 and cyclin E-CDK2 Binds pRb and dissociates it from E2F Prevent growth arrest either by p27 or p16

1.6 Binding partners of CDK2

1.6.1 CDK2 and the regulatory C-terminal domain of p53

The tumor suppressor protein p53 is involved in a DNA-damage cell-cycle checkpoint pathway that modulates apoptotic and growth arrest pathways (Jayaraman et al., 1999). The biochemical activity of p53 most tightly linked to its biological function as a damage-responsive protein involves its ability to bind to DNA sequence-specifically (el-Deiry et al., 1992) and function as a transcription factor (Pietenpol et al., 1994). p53 is composed of at least four functional domains that regulate its activity as a transcription factor: (i) an N-terminal trans-activation domain, which is required for interaction with components of the transcriptional machinery, including p300/CBP (Avantaggiati et al., 1997; Lee et al., 1998); (ii) a central conserved core DNA binding domain containing most of the inactivating mutations found in human tumors (Cho et al., 1994); (iii) a tetramerization domain that facilitates sequence-specific DNA binding (Clore et al., 1995); and (iv) a C-terminal negative regulatory domain whose phosphorylation primes the latent sequence-specific DNA binding function of p53 for activation (Hupp et al., 1995).

- NTD   >   1-93 aa   (N-terminal domain)
- DBD   >   102-292 aa   (DNA binding domain)
- CTD   >   293-393 aa   (C-terminal domain)
- CTRD >   363 –393 aa   (C-terminal regulatory domain)

Each of these domains of p53 contains multiple sites for modification. The combined actions of many enzymes coordinately modulate the p53-dependent gene expression in response to cellular stress (Webley et al., 2000). Protein kinases that target the N-terminus of p53 and regulate its biochemical function include the DNA-activated protein kinase (DNA-PK) (Lees-Miller et al., 1992), ATM (Banin et al., 1998, Canman et al., 1998), and ATR (Tibbetts et al., 1999). Radiation-dependent changes in steady-state phosphorylation can occur at Ser15 (Shieh et al., 1997), Thr18 (Craig et al., 1999; Webley et al., 2000), or Ser20 (Craig et al., 1999; Shieh et al., 1999), and as these modifications lie within the MDM2 and/or p300 interaction site, they presumably affect these two biochemical pathways in cells.

The C-terminal negative regulatory domain of p53 is also a target of enzymes that post-translationally modify p53 and affect its *in vitro* DNA binding function. The un-phosphorylated p53

protein assembles into a latent tetrameric state and phosphorylation of its negative regulatory domain at Ser392 can activate the specific DNA binding function of p53 by reducing the energy barrier to activation (Hupp et al., 1995), presumably by stabilizing the p53 tetramer. Protein kinase phosphorylation at Ser392 and Ser315 can stimulate p53's specific DNA binding function *in vitro* (Hupp et al., 1995; Wang et al., 1995). So it is important to know whether cellular factors actually target the C-terminal domain of p53 in response to DNA damage. Steady-state phosphorylation at one of these sites (Ser392) increases in response to DNA damage, *in vivo* under conditions in which p53 protein levels do not change and where p53 becomes active as a transcription factor (Blaydes et al., 1998), suggesting that signal transduction pathways respond to DNA damage by post-translationally activating the p53 function. One major site of phosphorylation in the C-terminal negative regulatory domain for which a role in the stress-induced activation of p53 has not been defined *in vivo* is the cyclin dependent kinase site at Ser315. Phosphorylation of p53 at this site has been shown to enhance the sequence-specific DNA-binding activity of p53 protein *in vitro* (Fuchs et al., 1995; Wang et al., 1995), possibly by co-operating with other modifications within the C-terminal negative regulatory domain (Hansen et al., 1996). There is a cyclin A-CDK2 binding motif within the C-terminal negative regulatory domain of p53. This docking site is defined as a cyclin A box motif based on the primary amino acid sequence homology of small inhibitory peptides derived from this region of p53 to the cyclin A box in the tumor suppressor pRb. In addition, single amino acid mutations of the cyclin A box in the full-length p53 protein reduces the rate of cyclin A-CDK2 phosphorylation of p53 thus highlighting the importance of the cyclin A interaction site for catalyzing cyclin A-dependent kinase phosphorylation of p53.

1.6.2. CDK2 and 14-3-3σ protein
The 14-3-3 proteins comprise a family of highly conserved acidic proteins, and there are at least seven different mammalian isoforms. Several activities have been ascribed to these proteins, including signal transduction of Raf-1 and cell cycle regulation. 14-3-3ε and 14-3-3β were the first known proteins of the family. Later on 14-3-3ζ and σ came into play. 14-3-3σ can bind to CDK2, cyclin A-CDK2, cyclin E-CDK2, cyclin B-CDC2, cyclin D-CDK4, and emerged as a class of potent

inhibitors of cyclin A-CDK2 (Fantl et al., 2002; Li et al., 1995; Ford et al., 1994; Aitken et al., 1992).

The σ protein has a distinctive sequence *AAWRVLSS*. The cyclin-CDK binding partners share this RXL motif. Sequence analysis of human CDK reveals that there are two possible 14-3-3 binding sites (*GVTS*229*MP* and *YKPS*236*FP*) located in the C-terminal region of CDK2 which share a homologous sequence to what has been predicted as the 14-3-3σ binding sites. Therefore it is possible that 14-3-3σ may bind to this region to regulate CDK activities and cell cycle progression (Laronga et al., 2000). It has also been revealed that there is a leucine rich NES-like sequence *(*202*STLIMQLLR-DNLTLW*212*)* in the 14-3-3σ. The binding of 14-3-3σ to CDK2 can cause the sequestration of CDK2 and CDC2 into the cytoplasm, and the NES of 14-3-3σ is required for this biological function (Laronga et al., 2000).

1.6.3 INCA1, the novel binding partner of CDK2

This novel cyclin A1-CDK2 interaction partner was identified last year in a yeast triple-hybrid system. Several novel proteins (INCA1, KARCA1, and PROCA1), as well as the known proteins GPS2 (<u>G</u>-protein <u>p</u>athway <u>s</u>uppressor <u>2</u>), Ku70, receptor for activated protein kinase C1/guanine nucleotide-binding protein β-2-like-1, and mRNA-binding motif protein 4 were identified as interaction partners. These proteins link the cyclin A1-CDK2 complex to diverse cellular processes such as DNA repair, signaling, and splicing. The most frequently isolated unknown gene, which was named INCA1 (<u>in</u>hibitor of <u>C</u>DK interacting with <u>c</u>yclin <u>A1</u>) was characterized and cloned. The INCA1 sequence was analyzed for intracellular localization signals. INCA1 did not show any transmembrane domains or docking sites for a GPI anchor, suggesting that it was not membrane-bound. A signal sequence for nuclear localization (*RRKKRR,* aa 75–80) was found within the INCA1 sequence (Diederichs et al., 2004).

The nuclear INCA1 protein is evolutionarily conserved and lacks homology to any known gene. Cyclin A1 and all interaction partners were highly expressed in testis with varying degrees of tissue specificity. The highest expression levels were observed at different time points during testis maturation, whereas expression levels in germ cell cancers and infertile testes decreased. These findings and consensus sequences for potential phosphorylation by cyclin-dependent kinases in the

INCA1 sequence led to the hypothesis that the cyclin A1-CDK2 complex phosphorylated INCA1. Cloning and analysis of different INCA1 fragments indicated strong phosphorylation of the C-terminus (aa 149–221). The N-terminus (aa 1–74) was weakly phosphorylated by cyclin A1-CDK2, whereas the intermediate fragment was also phosphorylated by CDK2 alone. Human and murine INCA1 contain four potential phosphorylation sites that were conserved between species; 167*TPGR* matched exactly the consensus site for CDK phosphorylation, whereas 23*SP*, 176*SP*, and 179*SP* only showed a conserved SP motif necessary for CDK phosphorylation in both species.

In the genomic sequences upstream of the INCA1 gene, a functional promoter corroborating the identification of the full-length transcript and an intact genomic locus of INCA1 was identified. This promoter was dependent on the transcription factor Sp1, which also regulates the cyclin A1 promoter. In vitro, INCA1 was phosphorylated by cyclin A1 or cyclin A2 in complex with CDK2, but at least in testis, the tissue-specific expression pattern of cyclin A1 and INCA1 might indicate that cyclin A1 is physiologically the more relevant interacting partner. In healthy tissue, INCA1 expression was highest in testis, followed by intermediate expression levels in ovary, pancreas, lung, liver, and spleen. Therefore, expression patterns of cyclin A1 and INCA1 correlated well with regard to the testis, whereas expression in other organs was not closely correlated. The induction of INCA1 in testis maturation hints at a potential role in spermatogenesis (Diederichs et al., 2004).

1.7 Structural study of CDKs

1.7.1 The structure of monomeric CDK

The high degree of primary sequence homology among members of the CDK family (55-65%) suggests that any one structure of the CDK provide a useful framework for understanding all members of the family. Out of all the CDKs known till today, the crystal structure of CDK2 best describes the overall protein structure of the whole CDK family.

The structure of monomeric CDK2 has the same overall fold as other eukaryotic protein kinases. The structure consists of an N- terminal lobe rich in β-sheets (five antiparallel β-sheets, β1-5) and a single large α-helix, a larger C- terminal lobe, rich in α-helices contains a pseudo-4-helical bundle (α2, 3, 4, 6), a small ribbon (β6-8), two additional helices (α5, 7) and a deep cleft at the junction of the two lobes that is the site of ATP binding and catalysis. In the monomeric CDK2

structure, two regions differed from the canonical kinase structure and were predicted to function as regulatory elements. One is a α-helix present in other protein kinases but having the unique PSTAIRE amino acid sequence only in cyclin dependent kinases; the other is a regulatory loop that, like most other kinases, has the activating phosphorylation site. This regulatory loop (the T- loop, residues 145-172, containing the Thr160 phosphorylation site) completely blocks the core of the protein substrate-binding cleft.
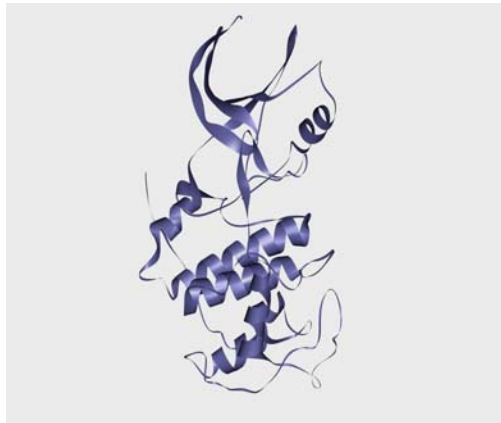
Fig. 3. Crystal structure of unphosphorylated CDK2.

Conserved regions include the glycine rich loop of the ATP binding site (between β1-β2), the highly conserved PSTAIRE motif in the α1 helix, the GDSEID motif at the N- terminal end of α5 and the T- loop. The inhibitory phosphorylation sites Thr14 and Tyr15 are both in the middle of the glycine rich loop that serves as a phosphate anchor in ATP binding. The hydroxyl group of Tyr15 is distant from ATP whereas the hydroxyl group of Thr14 is very close to the γ-phosphate of ATP. Thr160, is found at the apex of the T- loop blocking the protein substrate-binding site. The hydroxyl group of the Thr160 is oriented towards the glycine-rich loop of the ATP-binding site (Bondt et al., 1993).

1.7.2 The structure of cyclin A

The cyclin A fragment 173-432 has a globular structure consisting of 12 α-helices. The molecule contains a structural repetition, having two sequential 90 amino acid domains with identical folds (residues 208-303 and 309-399). The repeats are connected by a linker of five amino acids, and pack loosely against each other across an interface that contains three buried water molecules. The first

repeat coincides with the cyclin box (residues 209-310). As expected it is the binding site for the PSTAIRE helix and making contacts with the T- loop and the N- terminal β-sheet of CDK2. The structural motifs of five helices observed twice in the cyclin A fragment is common to other members of the cyclin family and is termed the cyclin fold.
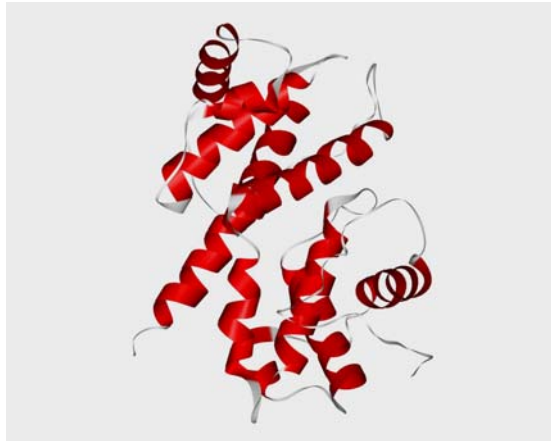
Fig. 3. Crystal structure of cyclin A.

The hydrophobic core of the motif is formed by the α3 helix whose central portion is surrounded by the remaining four helixes. Helices 4 and 5, which pack against helix 3, are partially exposed to solvent and contact CDK2. The most significant of the packing interactions involves Ala235 and 264 from the α2 and α3 helices, respectively (equivalent to Ala333 and 363 from the second repeat), where the tight packing allows no substitution. This pair of residues is highly conserved among cyclin family members (Brown et al., 1995; Jeffrey et al., 1995).

1.7.3 Crystal structure of the complex between cyclin and CDK
Binding of cyclin to CDK2 activates the kinase by causing conformational changes but there are no distinct conformational changes in the cyclin itself. Cyclin A contacts the PSTAIRE helix and moves this helix into the catalytic cleft and rotates it by 90°. It also changes the T- loop structure and position, moving parts of it by over 20 Å. PSTAIRE helix has a catalytic site residue, Glu51, conserved among eukaryotic protein kinases. Without the cyclin the glutamic acid side chain is outside the catalytic cleft.

When the cyclin binds, the change in the helix brings the glutamic acid side chain inside the catalytic cleft, where, together with a lysine residue, an aspartic acid residue, and a magnesium ion it coordinates the ATP phosphate atoms and correctly orients them for catalysis. The T- loop is positioned in front of the catalytic cleft entrance.
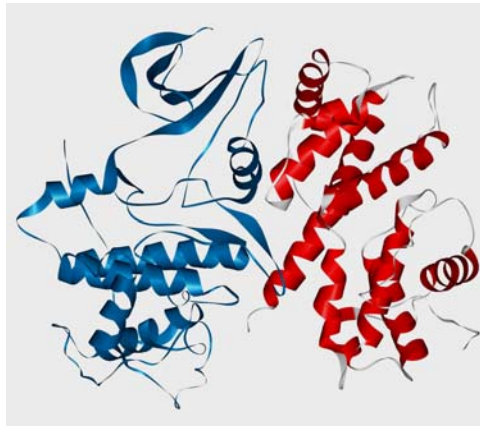
Fig. 4. Crystal structure of the binary complex of cyclin A-CDK2.

Upon cyclin binding, T- loop is moved away and largely relieves the blocking of the catalytic cleft. These changes also expose the phosphorylation site on the T-loop, setting the stage for the full activation of the kinase (Jeffrey et al., 1995).
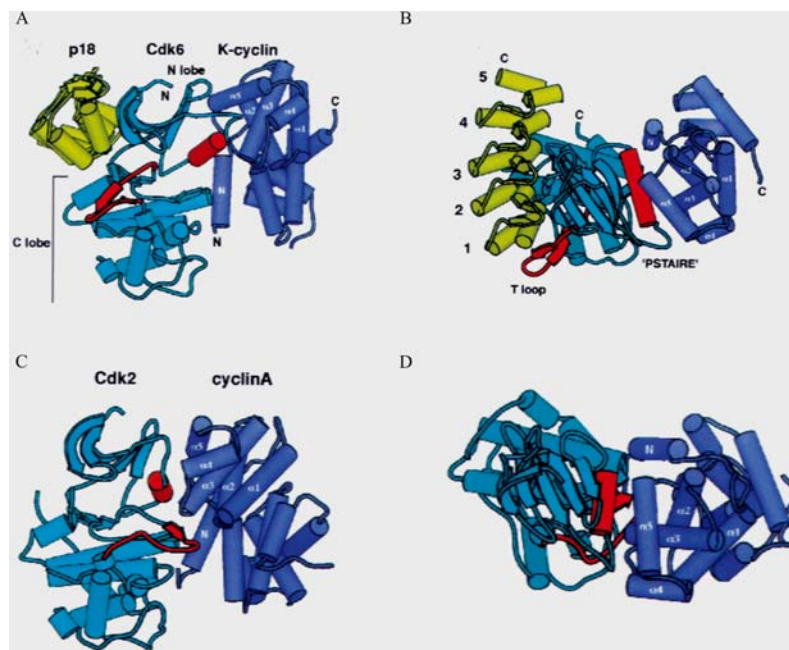
Fig. 5. A. Schematic view of p18–CDK6–cyclin K. p18 is shown in yellow, CDK6 in cyan, cyclin K in purple. The T-loop and PSTAIRE elements of CDK6 are highlighted in red, and the helices of the first cyclin repeat are labeled. N and C termini are labeled where visible. The p18–CDK6 and cyclin K–CDK6 interfaces do not overlap and lie on opposite sides of the kinase, burying a total of 4350 Å2 of surface area. *B*. Top view of the p18–CDK6–cyclin K complex, approximately orthogonal to view in *A*. The ankyrin repeats of p18 are numbered. The PSTAIRE helix is central to the CDK6–cyclin K interface, but the T- loop packs on the other side of the kinase. *C*. View of CDK2–cyclin A complex superimposed on the C lobe of CDK6 in the same orientation as in A. Both the PSTAIRE helix and T- loop, in red, pack against cyclin A. *D*. View of superimposed CDK2–cyclin A complex from same viewpoint as *B*.

The CDK6 structure in the p18–CDK6–cyclin K complex has a large number of conformational changes compared with the active conformation of CDK2 (Jeffrey et al., 1995) or of other protein kinases. In this inactive CDK6 structure, the N- and C- lobes are rotated 13° away from each other, resulting in the misalignment of ATP-binding residues. The N- lobe PSTAIRE helix, which contains an invariant active site residue (Glu61), is displaced by 4.5 Å away from the active site and is rotated by 16°. A C- lobe loop (T- loop, residues 162–182), which contains the threonine that is phosphorylated (Thr177) on the full activation of the kinase (Russo et al., 1996) and that forms part of the polypeptide substrate-binding site (Brown et al., 1999), is displaced by >30 Å. Finally, an additional loop at the back of the catalytic cleft (residues 99–102), which would hydrogen bond to ATP, is displaced by several angstroms. In the p18–CDK6–cyclin K complex, not only does the cyclin K fail to carry out most of these conformational changes but p18 causes the misalignment of additional residues involved in ATP binding and catalysis. In the CDK2–cyclin A complex, the T- loop makes multiple contacts with the PSTAIRE helix, the cyclin, and other parts of the C- lobe. As these contacts would not be possible in p18–CDK6–cyclin K (because of the misalignment of the lobes and PSTAIRE helix), the T- loop instead adopts a hairpin structure and packs on the C lobe in a position near the first ankyrin repeat of p18 (Fig. 5 A, B), which is opposite from its position in the active CDK. The T- loop phosphorylation site (Thr177) is displaced by 23 Å from the equivalent residue in the unphosphorylated CDK2–cyclin A complex. The inactive conformation of the T- loop is essentially identical to that in the p16–CDK6 and p19–CDK6 complexes (Brotherton et al., 1998; Russo et al., 1998).

1.7.4 Changes upon phosphorylation of CDKs; the final activation

When the T- loop becomes phosphorylated on Thr160 (CDK2), it undergoes an additional conformational change. This change is induced by the phosphate group acting as an organizing

center in this region being bound by 3 arginine side chains, each coming from a differenet part of the structure (one from the N- lobe, one from the C- lobe, and one from the T- loop). The arginine residues in turn hydrogen bond to other CDK and cyclin groups and extend the organizing influence of the phosphate group. The significance of this CDK region is that it is part of the catalytic cleft, and in particular the putative polypeptide substrate interaction site. Phosphorylation thus completes the re-organization of the substrate-binding site that was started by the cyclin (Jeffrey et al., 1995; Russo et al., 1996).

1.7.5 Structure of the CDK-cyclin complex bound with INK4 inhibitors

In the structure of the p16^{INK4} bound to CDK6, the inhibitor binds next to the catalytic cleft, opposite from where the cyclin would bind, and interacts with both the N- and C- lobes to form a continuous interface (Russo et al., 1998; Brotherton et al., 1998). The INK4 and the cyclin binding sites on the CDK do not overlap. So the INK4 binds to the cyclin-CDK complex without dissociating the cyclin. It blocks cyclin binding indirectly, in part by causing allosteric changes in the CDK that propagate to and alter the cyclin binding site.
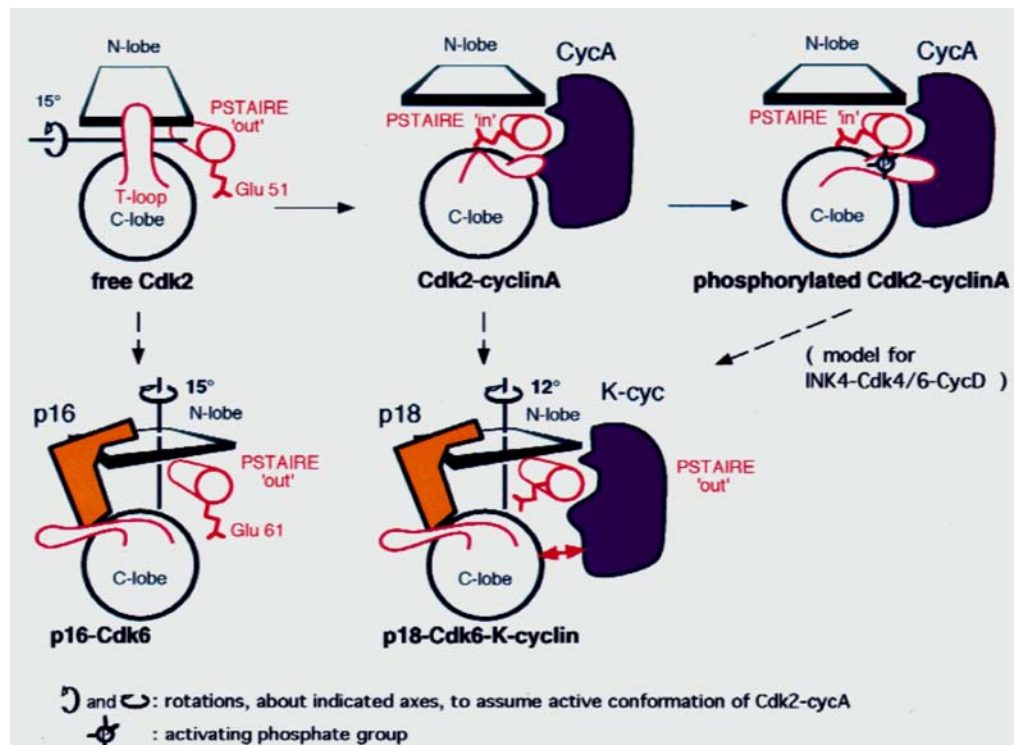
Fig. 6. Schematic representation of the different conformations of the CDK. CDKs undergo extensive conformational changes on binding of activating or inhibiting subunits. The major determinants of activity are the positions and conformation of the *PSTAIRE* helix and T- loop, as well as the relative disposition of the kinase N- and C- lobes. The *PSTAIRE* helix adopts a position further away from the catalytic cleft in inactive CDKs (labeled as 'out') than in active CDKs ('in'). The *PSTAIRE* helix conformation correlates with the location of a conserved active site residue (CDK2, Glu 51; CDK6, Glu 61) either inside or outside the catalytic cleft.

The interactions p16 makes with the two lobes are associated with a rotation of the lobes (roughly 15°) through a vertical axis, compared to the other CDK structures. The functional significance of this twist is that at the other end of the catalytic cleft, the N- and C- lobes, and the *PSTAIRE* helix, are misaligned with respect to cyclin binding in the consensus manner. This is best seen in a superposition of the p16-CDK6 and cyclin A-CDK2 complexes where the position of the N- lobe in the p16 complex would be incompatible with the cyclin binding both the N- and C- lobes. Both p16 and cyclin need to interact with both CDK lobes for their function, but it appears that they need them in different relative orientations. A close look at the catalytic cleft shows that the ATP binding site, which is adjacent to the p16 binding site, is distorted. These distortions would not eliminate ATP binding, but they would significantly reduce ATP affinity and may well disorient any bound ATP (Russo et al., 1998).

1.7.6 Structure of the CDK-cyclin complex bound with Cip inhibitors

The members of the Cip/Kip family have a Leu-Phe-Gly (*LFG*) motif, which is conserved (Jeffrey et al., 1995; Zhu et al., 1996). In the ternary complex of cyclin A2-CDK2/p27, the p27 inhibitory domain has a non-globular, extended structure that consists sequentially of a rigid coil and amphipathic α-helix, and an amphipathic β-hairpin, a β-strand and a 3_{10}-helix (Russo et al., 1996). The fully active form of the enzyme can be completely shut down by the binding of the Cip family of inhibitors (Polyak et al., 1994). The *LFG* motif and the cyclin interactions (cyclin box) are likely to serve the first anchor in complex formation. The mechanism by which p27^{Kip1} inhibits the kinase is through the insertion of a small 3_{10}-helix inside the catalytic cleft of CDK2.

Comparison of the CDK2-cyclin A2/p27 and the ATP-CDK2-cyclin A complexes shows that the p27 helix mimics the ATP substrate, both in its position and in the contacts it makes to the active site groups. A tyrosine side chain of p27, conserved among all Cip proteins, mimics the van der Waals contacts made by the ATP purine group and also the hydrogen bonds made by the N1 and N6

groups of ATP. At the C-terminus of the p27 helix, the backbone carbonyl groups hydrogen bond to the active site lysine residue that would hydrogen bond to the nucleotide phosphates in the ATP complex.
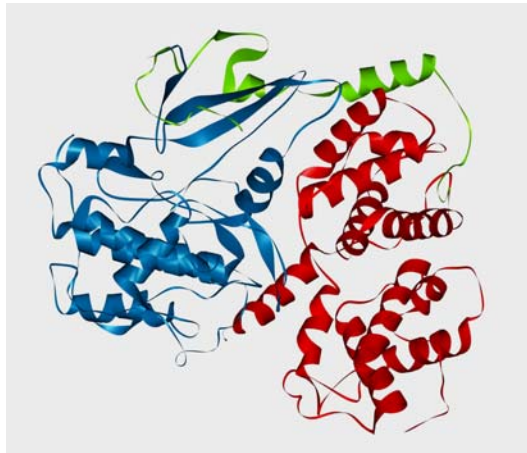
Fig. 7. Crystal structure of the ternary complex of cyclin A-CDK2 with N- terminal residues (1-96) of p27. Green represents the residues of p27, red denotes cyclin A and blue represents CDK2.
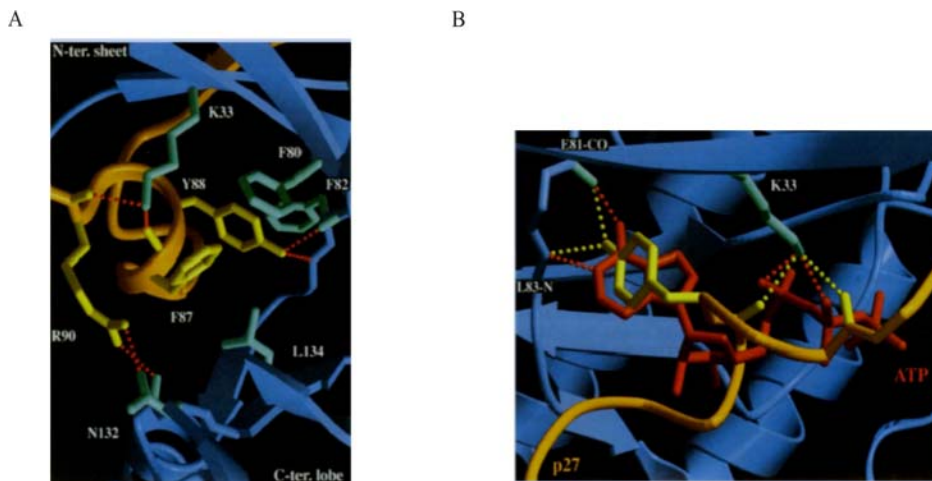
Fig. 8. A. p27 3_{10}-helix bind in the widened catalytic cleft of CDK2 making multiple van der Walls and hydrogen-bond cotacts (red dotted lines). To make the contacts easier to see, parts of the N- and C- terminal lobes that would be above the plane of the figure are not shown, Hydrogen-bonds contacts not mentined in the text include ones by the Arg90 side chain of p27 to the Asn132 side chain and Gln131 backbone carbonyl group of CDK2. *B*. The p27 3_{10}-heix mimics the ATP in the binary complex in its position and its CDK2 contacts. Composite figure shows the ATP (red) from the phosphorylated binary complex positioned by superimposing the CDK2 molecules in the binary and tertiary complexes. The hydrogen bonds that ATP makes in binary complexes are indicated as red dotted lines and thosee made by p27 as yellow dotted lines. The second strand of the β-sheet is not shown because it would obstruct the view of the catalytic cleft.

26

The insertion of the p27 helix into the catalytic cleft thus directly blocks ATP binding. In the absence of the 3_{10}-helix p27 can still inhibit the kinase. This occurs because on binding the kinase p27 also changes the shape of the catalytic cleft, and specifically the roof of the catalytic cleft formed by the N- lobe β- sheet in its p27 and ATP bound forms. On p27 binding, the kinase β- sheet loses many of its ATP interacting elements, such as the glycine rich loop that will bind the ATP phosphate groups. In the absence of p27 the N- lobe β- sheet is highly curved being partially folded upon itself and has a small hydrophobic core. When p27 binds, it removes the first β- strand of CDK2, gains access to the hydrophobic core, inserts one of its one strand in place of the CDK strand, flattens the CDK2 β- sheet, and forms an intermolecular β- sandwich, with a new, mixed hydrophobic core. In essence, the CDK2 N- lobe and p27 co-refold into a new structure (Russo et al., 1996).

1.7.7 Structural basis for specificity of substrates for CDKs

The generic substrate sequence recognized by CDK2-cyclin A is *S/TPXK/R*, where *S* or *T* are the phosphoacceptor residues, *X* is any amino acid, and *K/R* denote a preference for a basic residue (Higashi et al., 1995; Holmes et al., 1996; Kitawaga et al., 1996; Zarkowski et al., 1997). For basic understanding, numbers represents the positions of amino acids, P0 is the *S/T*, P+1 is *P*, *X* is P+2 and *K/R* is P+3.
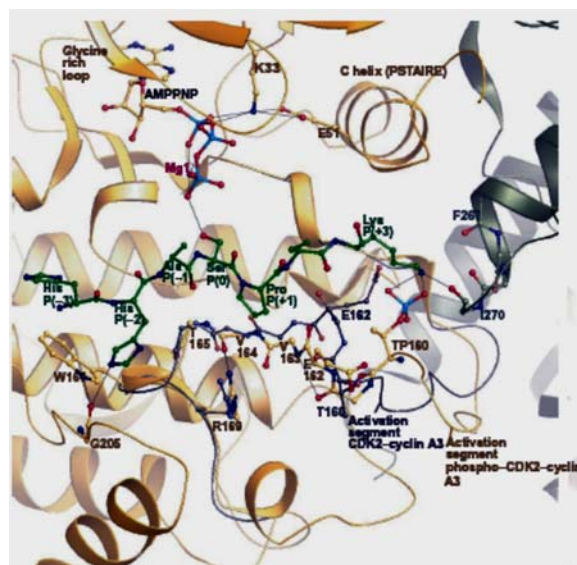
Fig. 9. Contacts between CDK2 and the substrate peptide. Interactions of the substrate peptide with phospho-CDK2–cyclin A3 in the region of the activation segment and other selected residues. CDK2 is shown in yellow with the C (*PSTAIRE*) helix in red and the activation segment in magenta. Cyclin A3 is shown in khaki. Conventional view of the CDK2–cyclin A3 complex, also showing the peptide substrate (green ball-and-stick diagram) and the recruitment peptide (cyan ball-and-stick diagram). The activation segment of the partially active CDK2–cyclin A3 complex is shown in grey. For further details, see text.

The specificity of CDK2 for a proline at the P+1 position of the substrate, following the phosphorylatable serine, is explained by the substrate's contacts with the activation segment, which forms a suitably shaped pocket to accept the proline. The activation segment residue V164 has an unusual left-handed conformation that results in carbonyl oxygen atom being directed away from the substrate. Binding of any residue except proline at the P+1 site would be unfavorable because of an uncompensated hydrogen bond from the substrate's main-chain nitrogen. In P+2 position the substrate does not make any contacts with the protein, but still the presence of a long aliphatic amino acid or a positively charged residue e.g. arginine, methionine or lysine, in the P+2 position favors phosphorylation (Brown et al., 1999). A major interaction occurs in the P+3 position that explains the specificity of a basic residue. The interaction occurs with the lysine side chain in the P+3 position. The lysine is hydrogen bonded to the Thr160 phosphate and to the main chain oxygen of residue I270 on cyclin A3. (Brown et al., 1999; Jeffrey et al., 1995). Catalysis takes place with the help of the Mg^{2+}. Mg^{2+} is bound in octahedral coordination and chelates the α- and γ-phosphates. The substrate (serine) is hydrogen bonded with the conserved catalytic aspartate, D127, and the conserved lysine K129. D127 is poised to assist catalysis by both orientational effects and general acid/general base catalysis, while K129 may assist in stabilizing the negative charge in the transition state (Bondt et al., 1993).

1.7.8 Structural basis for specificity of substrate recruitment for CDKs

The presence of the *RXL* motif either in the substrate or in an inhibitor is the recognition sequence for cyclin A that is quite remote from the phosphoacceptor site in CDK2 (Adams et al., 1996; Chen et al., 1996; Dynlacht et al., 1997; Schulman et al., 1998; Adams et al., 1999). It has been shown that the *RXL* recognition site is located at an exposed hydrophobic site on the cyclin A molecule, which is conserved in cyclins A, B, D, and E. The recruitment site is 40 Å from the catalytic site of CDK2. Examination of substrates of CDKs show no fixed relationship between sites of

phosphorylation and those of recruitment, and it may be that there is no fixed route for communication.
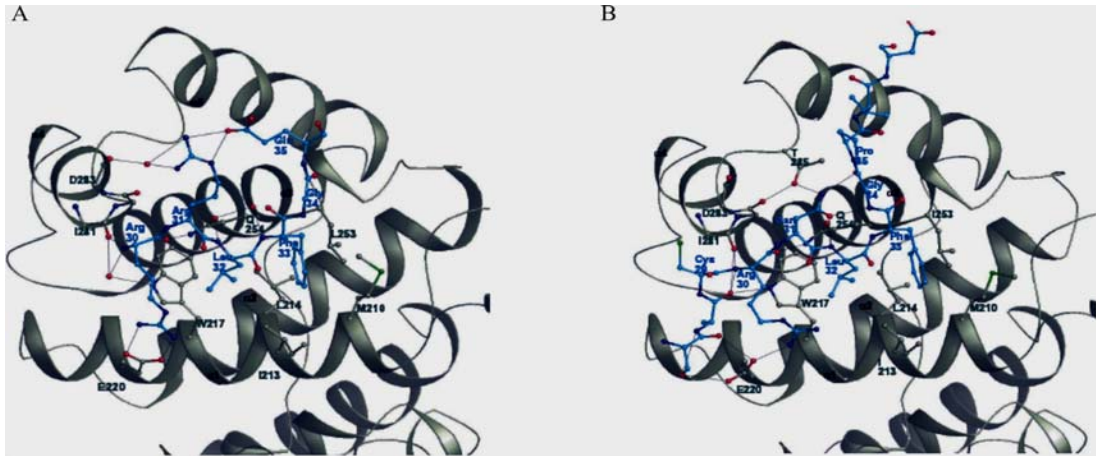
Fig. 10. The recruitment-peptide-binding site of the phospho CDK2–cyclin A3 complex. *A*. Diagram showing residues RRLFGE from the recruitment peptide of p107 bound at the hydrophobic site on cyclin A3, making contacts with residues from successive turns of the α1 and α3 helices. The view, which is rotated~90° from that shown in Fig. 9, shows the complete fold of the cyclin box. *B*. Similar view of the equivalent residues from the phospho-CDK2–cyclin A3/p27^{KIP1} complex.

The central feature in target recognition appears to be the leucine of the RXL motif reinforced by a non-polar residue that is either immediately adjacent or next adjacent to it in the substrate. The primary role of the RXL- recognition motif may be to increase the local concentration of substrates relative to the catalytic site and to increase phosphorylation of otherwise poorly phosphorylated substrate.

The important common features of the substrate recognition are:

1. the non polar pocket in cyclin that recognizes the leucine at P0
2. the contacts from the substrate main chain atoms at sites P0, P-2 and P-4 to polar groups of the cyclin
3. van der Waals contacts at both the P2, P-3 and P-4 sites
4. charge–charge contact from Arg (if present) at P-2 to Glu220 on the cyclin.

Cyclin A residues that are involved in contacts (Met210, Ile213, Trp217, Leu253, Gln254, Asp283) is conserved in cyclins A, B, D, and E, but Glu220, although conserved in cyclins A, D, and E is gluatmine in cyclin B (Brown et al., 1999).

1.8 CDK2 and apoptosis

CDK2 plays a role in cellular apoptosis. In this process signals deregulate the CDK2 kinase activity by inhibiting p27. Inhibition of CDK2 kinase activity efficiently blocks cell cycle**.** In human endothelial cells the caspase 3 mediated cleavage of p27 and p21 results in activation of CDK2-cyclin kinetic activity (Kim et al., 2001).

1.8.1 CDK2 in cancer

Cell cycle deregulation associated with cancer occurs through mutation of proteins important at different levels of the cell cycle. In cancer, mutations have been observed in genes encoding CDK, cyclins, CDK-activating enzymes, CKI, CDK substrates, and checkpoint proteins (Sherr 1996). Alterations of CDK molecules in cancer have been reported, although with low frequency. CDK4 overexpression that occurs as a result of amplification has been identified in cell lines of melanoma, sarcoma, and glioma (Wolfel et al., 1995). Mutations in CDK4 and CDK6 genes, resulting in loss of CKI binding, have also been identified (Easton et al., 1998). CDK1 and CDK2 have been reported to be overexpressed in a subset of colon adenomas, a greater overexpresion was seen in focal carcinomas in adenomatous tissues (Kim et al., 1999).

Cables is a novel cell cycle regulatory protein that interacts with CDK2, CDK3, and CDK5. Cables inhibits CDK2 activity by enhancing CDK2 Tyr15 phosphorylation by Wee1, which consequently leads to inhibition of cell growth. Loss of Cables expression was found in many human cancers, especially colon and endometrial cancer (Zhang et al., 2005). A major mechanism governing MYC's effects on the cell cycle progression in breast cancer cells appears to be *via* the activation of cyclin E-CDK2 through loss of p21[WAF1/Cip1] (Prall et al., 2001; Lai et al., 2001; Mukherjee et al., 2005).

1.9 Non-physiological inhibitors of CDK2

1.9.1 Specificity and properties of the non-physiological inhibitors

Frequent deregulation of CDKs in cancers has lead to the search of different compounds that can specifically inhibit the kinases. 6-dimethylaminopurine and isopentyladenine were the first inhibitors of CDKs. The selectivity of these compounds decreased in clinical trials. This is because

the amino acids constituting the ATP binding region in the CDK family is more or less conserved. The CDK group of inhibitors falls into three classes:

1. non-selective: deschloroflavopiridol, flavopiridol, oxindole16, etc
2. selective: CDK1-5 and CDK9 – olomucine, roscovitine, purvalanol B, etc.
3. CDK4 and 6, fascaplysin, CINK4, etc.

The CDK inhibitors help to trigger apoptosis. All CDK inhibitors are small, hydrophobic and can bind competitively to the ATP binding site of CDKs. CDKs, which have been studied, are CDK1, CDK2, CDK4 & 6. Recent studies are focusing on the other kinases like CDK7, 8, 9. But till now no inhibitor has been developed that will inhibit the cell cycle by specifically inhibiting a particular CDK. CDK inhibitors also protect normal cells from apoptosis from the toxic effects of chemotherapy. Some inhibitors were found to prevent chemotherapy-induced alopecia by arresting the cell cycle and reducing the sensitivity of the epithelium to many active oncogenic agents (Davis et al., 2001).

1.9.2 Designing inhibitors for CDK2

The CDK2-ATP binding site is divided into four main parts for the development of a potent inhibitor (Davies et al., 2002). The regions are listed in Table 5 and in Fig. 8.
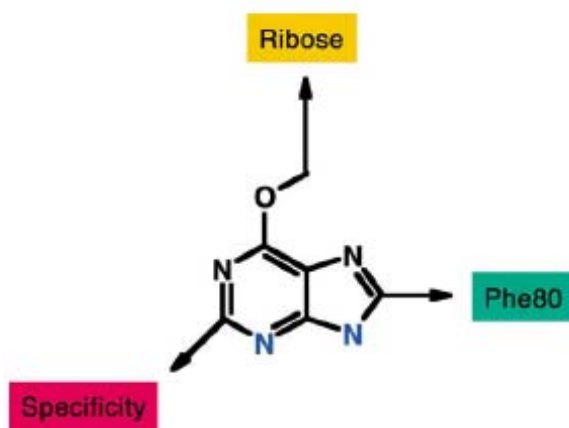
Fig. 8. A generic O6-substituted purine indicating inhibitor positions that probe the various subsites. Hinge region (blue), Phe80 (green), ribose/phosphate (yellow), and specificity surface (red)

Table 5. Binding regions of CDK2 inhibitors

Hinge region	Phe80 pocket	Ribose-phosphate site	Surface interactions
Residues 81-84 N1 of ATP accepts hydrogen bond from Leu83, N6 donates a hydrogen bond to carbonyl of Glu81	Shallow cavity at the back of ATP binding cleft formed by the side chain of Phe80	Residues 11-18, an extensive solvent pocket formed by the glycine loop, undergoes conformational changes during cyclin binding and phosphorylation	Regions outside the ATP cleft His84, Gln85, Lys89, in CDK2 and Asp84, Gln85 and Thr89 in CDK4
Adenine portion of ATP form hydrophobic contacts with residues Ile10, Val18, Ala131, Phe82, and Leu134	Not used by ATP but a lot of inhibitors use this place	Lys33 and Asp145 form a salt bridge with the phosphate-binding site of CDK2 Glu51 stabilizes Lys33 via salt bridge to coordinate the α & β phosphates of ATP	Inhibitors contact with the hydrophobic tunnel formed by Ile10, Phe80, and His84. Some inhibitors form hydrogen bonds with the Asp86 eg. [(3-benzylidene) indolin2-ones]
Three hydrogen bonds should form with the inhibitor and the protein. a) oxygen of Glu81 b) nitrogen of Leu83 c) oygen of Leu83	Hydrophobic interaction site	Hydrogen bond formation between ribose 2'- and 3' - hydroxyl groups Flavopiridol form hydrogen bond between piperidine ring and Lys33 and Asp145 while the other inhibitors show hydrophobic interactions in this region	Targeting this region may afford selectivity because CDKs differ considerably in this region
Presence of methyl group in N9 position abolishes the binding due to steric hindrances	Isopropyl and hydroxyethyl substituents were useful in binding but sugar moieties abolished binding	Highly hydrated and flexible nature of the pocket makes it difficult to design inhibitors which will make hydrogen bonds with the Lys33 and Asp145	

1.10 Chalcones

Chalcones are derivatives of flavonoids and isoflavonoids and are abundant in edible plants. Chemically chalcones consist of open chain flavonoids in which the two aromatic rings are joined by a three-carbon α-, β- unsaturated carbonyl system. Chalcones are synthesized in the laboratory using Claisen-Schimdt aldol condensation (Frederic et al., 1999). Chalcones have been reported to

show promising therauptic efficacy against human cancers. Some of them include inhibition of angiogenes, interfering with p53-MDM2 interaction, induction of mitochondrial uncoupling and membrane collapse and disruption of the cell cycle (Stoll et. al., 2001; Kumar et al., 2003; Won et al., 2005).

Butein (3,4,2', 4'-tetrahydroxychalcone, a plant phenol, is one of the major biologically active components of the bark and stems of *Rhus verniciflua Stokes*. Butein was first used as an inhibitor of cAMP-dependent phosphodiesterase. The compound was isolated from the plant *Dalbergia odorifera T Chen*. Later on studies revealed that it specifically inhibited the tyrosine kinase activities of the EGF receptors. Butein was also reported to inhibit PKC (protein kinase C), which is a serine–threonine kinase and protein kinase A. The inhibition was competitive to ATP and non-competitive to the phosphate acceptor for the EGF receptor (Yang et al., 1998). The methoxylated chalcone is probably the most potent inhibitor of microtubule assembly in human leukaemia cells (Lawrence et al., 2003). In the recent studies (with the piepridinyl chalcones) it has been shown that the levels of pRb, CDK4 and E2F go down in the cells treated with this compound. These antitumor properties of chalcones prompted us to characterize the interaction of some chalcones with CDK2.

1.11 Pharmacological inhibitors

When CDK inhibitors are used as pharmacological tools in cell biology to demonstrate the involvement of a particular CDK in a cellular process, selectivity is a key issue. By contarst, absolute selectivity might not be the best approach to cure complex disorders where multiple pathways are deregulated. Indeed, combinations of effects rather than a single effect might yield better therauptic agents. Indentification of the 'good' and 'bad' targets might help to circumvent toxic side effects. Table 6 lists all compounds that have been co-crystallized with CDK2, with the exception of SU9516 that was modeled with CDK2, alsterpaullone and indolylmethylene-indolinone 8a modelled with CDK1, and fascaplysin and compound 15b modeled with CDK4. Deschloroflavopiridol was co-crystallized with CDK2. Fig. 9 describes the chemical structures of most studied inhibitors of CDK2 (Meijer et al., 2000).

Table 6. Characteristics of pharmacological inhibitors of CDKs. The IC_{50} values of each compound tested on the indicated kinases are provided in micromolar concentrations.

Inhibitor	Class	CDK1-cyclin B	CDK2-cyclin A, E	CDK5-p25	CDK4-cyclin D
N6-Isopentenyladenine	Purine (adenine)	45	50 (A)	80	>100
Olomoucine	Purine (adenine)	7	7	3	>1000
(R)-Roscovitine	Purine (adenine)	0.45	0.7	0.16	>100
Purvalanol B	Purine (adenine)	0.006	0.006 (A), 0.009 (E)	0.006	>10
Aminopurvalanol (NG97)	Purine (adenine)	0.033	0.033 (A), 0.028 (E)	0.02	-
OL567	Purine (adenine)	0.23	-	-	-
H717	Purine (adenine)	0.23	0.050 (E)	-	2
NU2058	Purine (guanine)	5*	12*	-	-
NU6027	Pyrimidine	2.5*	1.3*	-	-
Hymenialdisine	Pyrroloazepine	0.022	0.07 (A), 0.04 (E)	0.028	0.6
Deschloroflavopiridol	Flavone	-	-	-	-
Flavopiridol	Flavone	0.4	0.1 (A)	-	0.4
Staurosporine	Indololocarbazole	0.006	0.007	-	<10
Fascaplysin	-	>100	>50 (A), >50 (E)	20	0.35 (D1)
Compound 66	Pyridopyrimidine	0.675	0.129 (A), 0.410 (E)	-	0.032
PD0183812	Pyridopyrimidine	>40	0.21 (A), 0.17 (E)	-	0.008
Oxindole 16 (compound 3)	Oxindole (indolinone)	0.78	0.06	-	-
Oxindole 91	Oxindole (indolinone)	0.11	0.010 (A)	-	0.13
Indolylmethylene-indolinone 8a	Indolinone	5.8	-	25	-
Indolylmethylene-indolinone 8e	Indolinone	2.2	-	1.8	-
Indirubin-3'-monoxime	Oxindole (indolinone)	0.18	0.44 (A), 0.25 (E)	0.1	3.33
Indirubin-5-sulfonate	Oxindole (indolinone)	0.055	0.04 (A), 0.15 (E)	0.065	0.3
SU9516	Oxindole (indolinone)	0.04	0.022 (A)	-	0.2
Compound 26a	Diarylurea	0.12	0.078	-	0.042
Compound 15b	Diarylurea	1.8	0.44 (A)	-	0.0023
PKF049365	Arylpyrazole	1.3	1.6	-	-
PNU112455A	Aminopyrimidine	-	2* (E)	2*	-
Alsterpaullone	Benzazepinone	0.035	0.015 (A) 0.2 (E)	0.04	>10
CINK4	Triaminopyrimidine	>100	>50 (A), >50 (E)	25	1.5 (D1)
Anilinoquinazoline 2	Quinazoline	1	-	-	-
Quinazoline 51	Quinazoline	-	0.65 (E)	-	>2.1

1.12 Clinical studies of CDK inhibitors

Till today around 70 different inhibitors of CDKs are known. Some of these inhibitors are being tested in the clinical trials. These include flavopiridol, roscovitine, UCN-01 and BMS387032. (Achenbach et al., 2000; Senderowicz et al., 1999; Senderowicz, 2003). In pre-clinical and clinical

studies, flavopiridols induced programmed cell death, promoted cell differentiation, inhibited angiogenesis, and modulated transcriptional events. Flavopiridols not only use the classical pathway of drug-induced apoptosis, they also trigger other pathways, which are still under investigation.
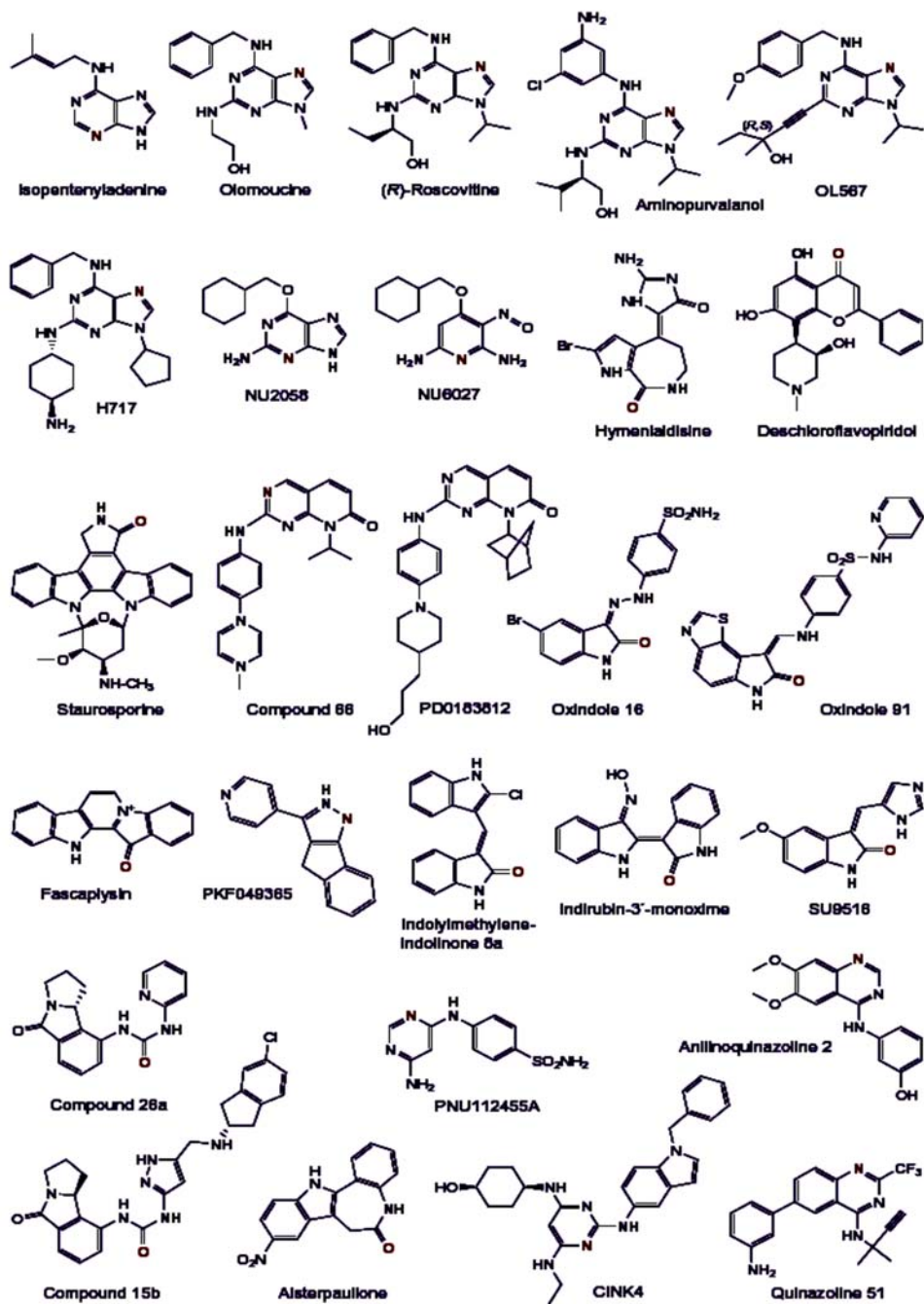
Fig. 9. Structures of some of the most studied pharmacological inhibitors of cyclin dependent kinases (CDKs). Only those that have been co-crystallized with CDK2 or modeled with CDK2 (CINK4), CDK1 (PNU112455A and alsterpaullone) or CDK4 (anilinoquinazoline 2 and quinazoline 51) are shown (see Table 6 for references). The molecules are grouped by chemical families. The two or three atoms that interact with the backbone nitrogen and oxygen atoms of Leu83 and Glu81 (or Glu94 and Val96 in CDK4) are shown in red (H-bond acceptors) and blue (H-bond donors). Note that H-bond acceptor and donor atoms are not identical in all purines because isopentenyladenine, olomoucine, roscovitine, purvalanol (H717) and NU2058 are bound in totally different orientations within the CDK2 ATP-binding pocket.

A flavopiridol-induced apoptosis is not blocked by Bcl-2 overexpression. Flavopiridol can trigger apoptosis in the absence of caspase 3 or caspase 8, since it can utilize alternate pathways for the induction of cell death. (Motwani et al., 2000; Robey et al., 2001; Schwartz, 2001; Casagrande et al., 2001). Extensive clinical trials were carried out with the purine inhibitor, roscovitine. The conclusion was that rosocovitine in combination with chemotherapy and radiotherapy will be helpful in causing the cell cycle arrest. UCN-01 (7- hydroxystaurosporine) inhibits CDK2 in a concentration dependent fashion. UCN-01 acts via p21 (Wang et al., 1996); it induces the expression of p21, which finally stops the kinetic activity of CDK2. UCN-01 has been successful in clinical trials (Sausville et al., 2001; Bunch et al., 1996; Akiyama et al., 1997). The CDK2 inhibitory activity of the compound BMS387032 (oxazole containing CDK2 inhibitor) was superior to that of the flavopiridol, which was less selective to all CDK complexes studied. The results from phase I trials demonstrated good tolerability. Main adverse events include: fatigue and gastrointestinal disorders (Senderowicz, 2003).

Other specific inhibitors include SU9516 (Lane et al., 2001), DPC 2313 (Du Pont compound), PNU-252808 (Pharmacia Upjohn Pharmaceuticals), BMS-239091 (Bristol-Meyers Squibb Pharmaceuticals), NU2058 and NU6027 (Astra Zeneca Pharamceuticals). These compounds are highly specific to a particular kinase. For example the inhibitor SU9516, a novel three-substituted indoline, inhibits CDK2 with a greater selectivity than other CDKs (Lane et al. 2001). All these inhibitors are on their way to clinical trial.

2. The IGF system

2.1 Introduction

The IGF system involves two ligands, insulin-like growth factor-I and -II (IGF-I and IGF-II) that interact with specific type 1 or type 2 IGF receptors (IGF-IR and IGF-IIR). There are six high affinity IGF binding proteins (IGFBPs), which modulate IGF availability and bioactivity. This ensemble of mutually interacting proteins is referred to as "the IGF system." It plays the key role in regulation of cell development, metabolism and survival through life.

Human IGF-I and IGF-II are single-chain polypeptides. IGF-I (70 amino acids) is a basic protein and IGF-II (67 amino acids) being slightly acidic. The amino acids of both IGF-I and -II are grouped into domains A, B (similar to insulin), domain C (analogous to the connecting peptide of proinsulin) and the C-terminus octapeptide (the D region, 63–70) that has no counterpart in insulin and proinsulin (Baxter et al., 1992). Both IGF factors contain three disulphide bonds, and display approximately 62 percent sequence homology with each other and 47 percent with insulin (Fig. 10).

```
Chain B:     G₁PETLCGAEL₁₀VDALQF₁₆VCGD₂₀RGFY₂₄FNKPT₂₉ IGF-I
          AYRP₄SETLCGGEL₁₃VDTLQF₁₉VCGD₂₃RGFY₂₇FSRPA₃₂ IGF-II
          FV₂NQHLCGSHL₁₁VEALYL₁₇VCGE₂₁RGFF₂₅YT-PK₂₉ SCI

Chain C:     G₃₀YGSSSRRAPQ₄₀T                         IGF-I
          S₃₃--RVSRRSR₄₀                              IGF-II

Chain A:     G₄₂IVDECCFR₅₀SCDLR₅₅RLEMY₆₀CA₆₂          IGF-I
          G₄₁IVEECCFR₄₉SCDLA₅₄LLETY₅₉CA₆₁             IGF-II
          GₐIVEQCCTS₉ICSLY₁₄QLENY₁₉CN₂₁               SCI

Chain D:     P₆₃LKPAKSA₇₀                             IGF-I
          T₆₂--PAKSE₆₇                                IGF-II
```

Fig. 10. Sequence and structure alignment of IGFs and single-chain insulin (SCI). Residues that make contacts with miniNBP-5 within 4 Å are highlighted in lime; residues responsible for binding to IGF-IR in grey, residues in blue showed no electron density in the structure of the miniNBP-5/IGF-I binary complex.

In addition to the classical IGF-I, molecules a truncated form of IGF-I known as DES(1-3)IGF-I has been found in fetal and adult human brain (Humbel, 1990). DES(1-3)IGF-I is the product of differential processing of pro-IGF-I lacking the first three residues at the amino terminus: Gly-Pro-Glu (GPE). The biological potency of this truncated form is 10 times higher than that of the full-length form and is explained by reduced binding to IGF-binding proteins (Francis et al., 1988;

Beck et al., 1993; Ballard et al., 1996). IGF-I is composed primarily of three helical segments corresponding to the B-helix (IGF-I residues 7-18) and two A-helices (IGF-I residues 43-47 and 54-58) of insulin. The hydrophobic core includes three disulfide linkages between Cys6 and Cys48, Cys18 and Cys61, and Cys47 and Cys52. Residues of the C-chain (Ser34-Thr41) form a flexible loop. Similarly, two N-terminal and six C-terminal residues showed no electron density, indicating motional flexibility in these regions.

2.2 IGF receptors

The IGFs interact with specific cell surface receptors, designated type I and type II IGF receptors (IGF-IR and IGF-IIR). The IGF-IR is a membrane glycoprotein of 300-350 kDa, consisting of two α-subunits (135 kDa each) and two β- subunits (90 kDa each) (Yamasaki et al., 1993). Disulphide bonds connect both alpha and beta-subunits to form a functional heterotetrameric receptor complex. In analogy with the insulin receptor, IGF-I receptor subunits are encoded within a single 180 kDa polypeptide precursor that is glycosylated, dimerised and proteolytically processed to yield the mature α-2-β-2-form of the receptor. The α- subunit is entirely extracellular and contains the ligand-binding site, and a cysteine-rich domain. The β- subunit contains the hydrophobic transmembrane domain with a short extracellular region, and a tyrosine kinase domain in its cytoplasmic portion.

The structure of the first three domains of the extracellular portion of IGF-IR (L1-Cys-rich-L2, residues 1-462) has been determined to a 2.6 Å resolution (Garrett et al., 1998). The L domains (L stands for "large") each adopt a compact shape consisting of a single-stranded right-handed β-helix. The Cys-rich region is composed of eight disulphide-bonded modules, seven of which form a rod-shaped domain. The receptor fragment is not active in terms of IGF binding. The physiological functions of insulin and IGFs are very different, while their receptor structures are similar. The IGF-IR binds IGF-I with a high affinity (ca. 0.1 nM), IGF-II with a 10-fold lower affinity, and insulin with a 100-1000 fold lower affinity (Bohannon et al., 1988; Lesniak et al., 1988). On the other hand, IR demonstrates high-affinity binding to insulin (ca. 0.1 nM), 10-fold lower affinity binding to IGF-II, and a 100-fold lower affinity binding to IGF-I. The structural differences between both receptors are also involved in different intracellular signaling. For example, the IR contains two distal tyrosine residues, whereas the IGF-IR contains three tyrosine residues, and the tyrosine kinase domains of

both receptors show distinct preferences for the tyrosine phosphorylation domains of insulin receptor substrate 1 (IRS 1) (De Meyts et al., 1994). The IGF-II receptor (IGF-IIR) consists of a single glycosylated polypeptide of approximately 260 kDa. It is primarily extracellular, having a short cytoplasmic tail and consists of 15 repeat mannose-6-phosphate (M6P)-binding units (August et al., 1983; Kornfeld, 1992).

IGF-I binding to a cysteine-rich domain in the extracellular α subunit of IGF-IR causes autophosphorylation of three tyrosines in the activation loop of the tyrosine kinase domain in the cytoplasmic portion of the β- subunit, which results in amplification of tyrosine kinase activity and further autophosphorylation of additional tyrosine residues. The IRSs (insulin receptor substrates) are known as "docking" proteins and constitute a family of four structurally related adaptor proteins that can link the IGF-I receptor to downstream signal transduction mediators regulating cellular growth. IRS 1 has multiple tyrosines, which associates with SH2 domain-containing proteins including growth factor receptor bound-2 protein (Grb2) and p85 regulatory subunit of phosphoinositol-3 (PI-3) kinase, p110. Phosphorylation of IRS 1 and 2 leads to activation of two downstream signaling cascades: 1) the mitogen-activated protein kinase (MAPK) and the 2) phosphatidylinositol 3-kinase (P3K) cascades (Fig. 11).

Stimulation of growth factor receptor-bound protein 2 (Grb2) by activated IRS 1/2 or Shc leads to the coupling of Grb2 with the guanyl nucleotide exchange factor, which in turn activates Ras. In the Ras pathway, phosphorylation of c-Raf 1 activates the downstream protein kinase, MAP kinase kinase 1 (also known as MEK or MKK1) or MAP kinase kinase 2 (MKK2). MKK1 and MKK2 activate two members of the MAP kinase family; extracellular signal related protein kinase (ERK)-1 and -2. Phosphorylated ERK-1 and (or) ERK-2 are translocated to the nucleus where in turn they phosphorylate a variety of transcription factors including c-FOS, c-JUN and c-MYC. This signaling cascade is important for cellular growth and mitogenesis (Hernandez-Sanchez et al., 1995). The c-MYC protooncogene encodes a nuclear transcription factor that is both necessary and sufficient to trigger entry of certain cell types into the S-phase of the cell cycle (Cole, 1986). IGF-IR-activated IRS 1 binds the regulatory p85 alpha-subunit of PI-3 kinase, and this complex activates the 110-kDa catalytic subunit, which phosphorylates phosphoinositides, generating PI-3 phosphate,

PI-3, 4-bisphosphate, and PI-3, 4, 5- triphosphate (Myers et al., 1996). These phosphatidylinositides in turn activate protein kinases including p70 ribosomal protein S6 kinase ($p70^{s6k}$), and protein kina-
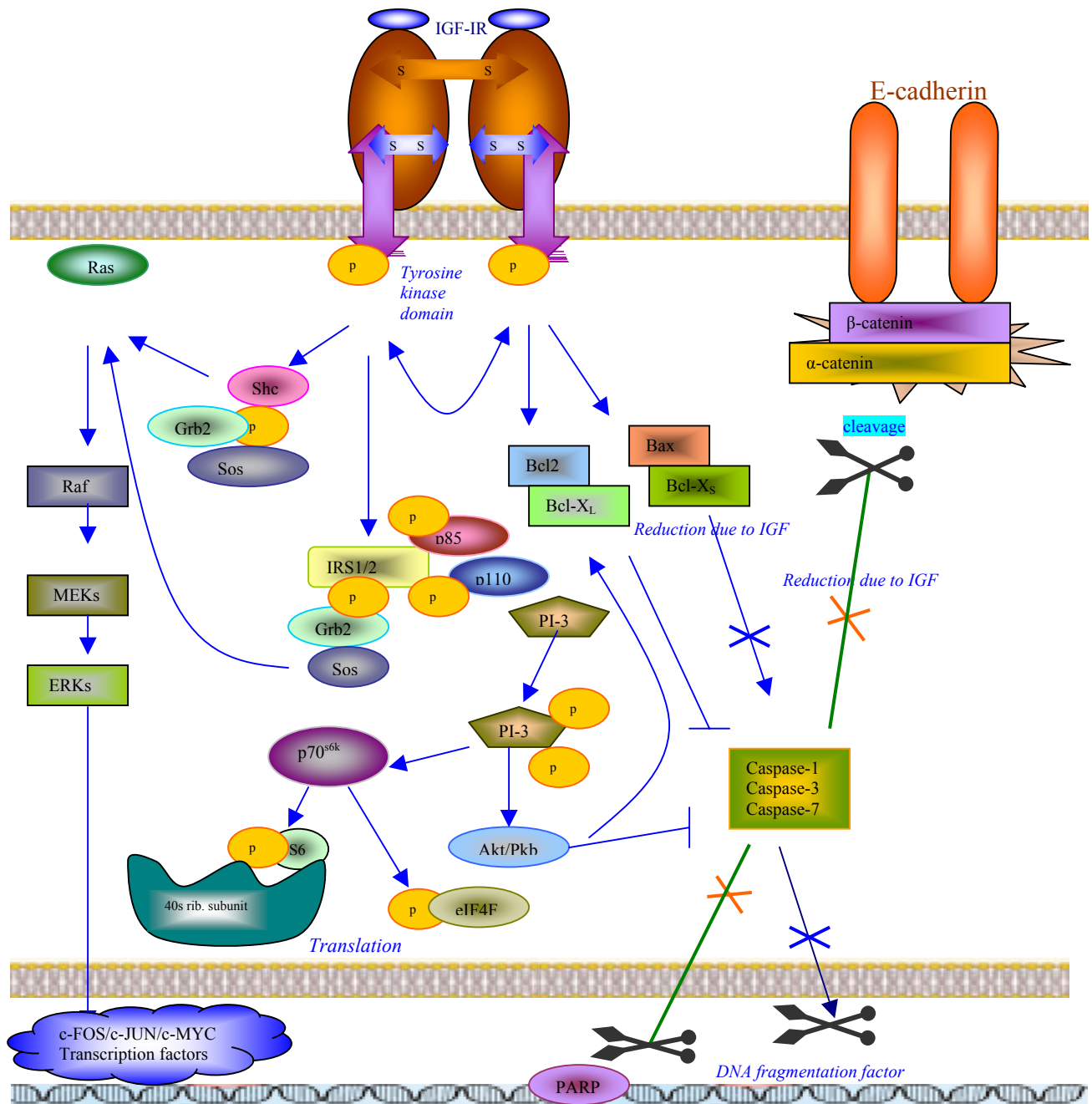
Fig. 11. Schematic presentation of the intracellular signaling pathways of the IGF-I receptor. The initial response of the IGF-IR to IGF-I binding is to undergo autophosphorylation on specific tyrosine residues. The intrinsic tyrosine kinase activity of the IGF-I receptor is enhanced and phosphorylates multiple substrates, including IRS 1 and IRS 2, on tyrosine residues. Proteins containing SH2-domains such as PI-3 kinase (p85/p110) and Grb2 associate with specific phosphotyrosine-containing motifs within IRS 1 and IRS 2. A similar response occurs with Shc. The ras/raf/MAP kinase pathway is activated by the association of IRS 1 and Shc with Grb2, which in turn is associated with the mammalian guanine nucleotide exchange factor protein son of sevenless (Sos). The PI-3 kinase/Akt cascade plays primary role in regulation of apoptosis. Activated Akt kinase phosphorylates proapoptotic factor Bad on a serine residue, resulting in its dissociation from anti-apoptotic protein, B- cell lymphoma –X (Bcl-x_L). The anti-apoptotic protein Bcl-2 and apoptotic proteins Bax and Bcl-x_s are also phosphorylated either by Akt or IGF-IR. This and Akt pathway converge on the inhibition of caspases, especially caspase-3, which is then blocked from performing an apoptosis-initiating cleavage of poly(adenosine diphosphate ribose) polymerase (PARP) and blocked from degrading β-catenin, part of the cadherin cell-adhesion system. Akt activates p70^{s6k}, which in turn phosphorylates S6 protein of 40S ribosomal subunit and translation initiation factor-4 (eIF4F), resulting in a stimulation of protein synthesis

se B (PKB/Akt) as well as other less characterised downstream molecules (Datta et al., 1997; Du et al., 1998; Myers et al., 1994). This pathway is important for IGF-mediated survival, enhancement of cellular motility and protein synthesis, retaining of cell-to-cell junctions and protection from programmed cell death.

2.3 Insulin-like growth factor binding proteins

IGFs are unlike other endocrine hormones, such as growth hormone and insulin, which are secreted from storage vesicles in an endocrine gland in response to releasing factors such as GH releasing factor or glucose. In contrast, the IGFs are not stored in an endocrine gland and are therefore not released acutely into the blood by releasing factors. However, the IGFs are stored in the blood and in tissues in a different, and somewhat unique manner for a protein hormone; they are stored bound to specific IGFBPs.

The precursor forms of all six IGFBPs have secretory signal peptides of between 20 and 39 amino acids, and the mature proteins are all found extracellularly. All IGFBPs bind IGFs with high affinity but in addition possess several specific, distinct functional binding sites that are not shared. The latter confer unique biological properties to each IGFBP. The common major binding reaction is the association with IGFs that regulates their free level and hence all the important cellular activities of the IGFs discussed above. Most of the IGF-I and IGF-II molecules in serum are found in a 150-kDa ternary complex formed by an IGF, IGFBP-3 – the predominant IGFBP in plasma, and a 85 kDa leucine-rich glycoprotein known as the acid labile subunit (ALS) (Hashimoto et al., 1997;

Boisclair et al., 2001; Baxter, 1994). To a smaller degree, IGFBP-5 also forms such a complex (Twigg et al., 2000). The ALS-protein plays an important role in regulating the affinity of IGFBP-3 to IGF-I, thus regulating the levels of free IGFs. In addition, ALS-proteins increase the molecular mass of the IGF-IGFBP-3 complex so that the access of the circulating IGFs to the extracellular fluid and thus to the various tissues is limited. IGFs are released from the 150-kDa complexes by limited proteolysis of IGFBP-3 and cross the vascular endothelial barrier alone or associated with smaller IGFBPs.

The other 20-25% of the IGFs is associated with lower mass IGFBPs, and less then 1% of IGFs circulate in the free forms (Baxter, 1994; Hashimoto et al., 1997). However, not only can IGFBPs inhibit IGF actions, all, except IGFBP-4, can potentiate specific activities of the IGFs under certain experimental conditions (Firth et al., 2002). In addition, the IGFBPs have IGF-independent receptor-mediated actions on cells, which can also be inhibitory or stimulatory. It is broadly agreed that the functions of IGFBPs which regulate the endocrine actions of IGFs are: 1) regulation of the rate of transport of IGFs from the vascular compartment to enhance the growth-potentiating effects of IGFs, 2) prolongation of the plasma half-lives of IGFs and 3) inhibition of the insulin-like activity of IGFs. In the tissues the release of IGFs from the IGFBPs can be modulated by three mechanisms, which function to decrease the affinity of the IGFBPs to the IGFs and act as a sustaining local source of IGFs to the IGF receptor. They transport the IGFs to and from the extracellular fluid and control the level of the biologically active, free IGFs since binding partially inactivates the IGFs. IGFBPs also prolong the half-life of IGFs, increasing it from 7-9 min to 30-40 min.

2.3.1 IGF independent actions of IGFBPs

IGF-I-independent, direct cellular actions have been demonstrated for IGFBP-1, -2, -3 and –5. Jones and coworkers showed that IGFBP-1 stimulated the migration of Chinese hamster ovary (CHO) and fibroblast cells by binding via its C-terminal integrin receptor recognition RGD sequence to the cellular α5β1 integrin (fibronectin receptor) (Jones et al., 1993). It is possible, that IGFBP-1 competes with fibronectin and blocks integrin-mediated effect required for cell migration. The Arg-Gly-Asp motif in IGFBP-1 also appears to be involved in the induction of focal adhesion kinase dephosphorylation, cell detachment, and subsequent apoptosis, because IGFBP-1 and a synthetic

Arg-Gly-Asp- containing peptide had similar effects in initiating these events in breast cancer cells (Perks et al., 1999). Thus, it appears that the effect of IGFBP-1 on integrin function could be cell specific. IGFBP-2, the only other IGFBP with RGD sequence, binds to αvβ3 integrin and found to mediate reduced migration and was associated with reduced *in vivo* tumor growth.

Table 7. General characteristics of the human IGFBPs

	IGFBP-1	IGFBP-2	IGFBP-3	IGFBP-4	IGFBP-5	IGFBP-6
IGF preference	IGF-I≥IGF-II	IGF-II>IGF-I	IGF-I≥IGF-II	IGF-I>IGF-II	IGF-II>IGF-I	IGF-II>>IGF-I
Molecular weight	25 kDa	31 kDa	43-45 kDa	24 kDa	29 kDa	28-30 kDa
Serum concentration	2-15 nM	2-15 nM	100 nM	2-15 nM	2-15 nM	2-15 nM
Binds ALS			+		+	
Nuclear target sequence			+		+	
Heparin binding residues			+		+	+
RGD sequence	+	+				
ECM binding	+	+	+		+	+
N-glycosylation			+	+		
O-glycosylation					+	+
Serine-phosphorylation sites	+		+		+	

Most studies on the IGF-independent actions of IGFBPs have focused on IGFBP-3 and IGFBP-5. IGFBP-3 is an important cell growth inhibitor and a potential anti-cancer agent. It directly inhibits the proliferation of chicken embryo fibroblasts (Delbe et al., 1991), the estrogen receptor-negative human breast cancer cell line Hs578T (Oh et al., 1993) and prostate cancer cells (Cohen et al., 1993). Transfection of the IGFBP-3 gene into mouse fibroblasts decreases proliferation (Cohen et al., 1993). One of the initial key experiments demonstrated a growth inhibitory effect of overexpressed IGFBP-3 in fibroblasts isolated from IGF-IR-deficient mice (Valentinis et al., 1995). The protein directly induces apoptosis in a prostate cancer cell line, mediates at list in part the growth inhibitory actions of retinoic acid, TGFβ and the tumor suppressor gene p53 (Oh et al., 1993; Leal et al., 1997; Rajah et al., 1997). Transforming growth factor β and retinoic acid, which are known to inhibit cell growth and induce apoptosis in a variety of normal and malignant cell types, also induce the expression and secretion of IGFBP-3 (Martin et al., 1992; 1995, Babajko et al., 1996). In 1995, Buckbinder and coworkers first identified IGFBP-3 as one of the p53-inducible

genes. Although the precise mechanism of growth regulation by IGFBP-3 is unknown, one plausible explanation is that IGFBP-3 is transported to the nucleus where it directly or indirectly modulates gene transcription. The basic carboxyl-terminal domain of IGFBP-3 contains a region with strong sequence homology to nuclear localization signals (NLS). In addition, this basic region shares homology with the DNA-binding domains of several transcription factors (Turner et al., 1989). Based on sequence homology between the basic carboxyl-terminal regions of IGFBP-3 and IGFBP-5 (IGFBP-3, amino acids 215–232; IGFBP-5, amino acids 201–218), be targeted to the nuclei of cells and to interact directly with DNA. Both IGFBP-3 and -5 have been indeed identified in the nuclei of opossum kidney cells, mink lung epithelial cells and T47D breast cancer cells (Schedlich et al., 1998).

Taylor and coworkers have isolated a 75 kDa receptor which transports IGFBP-3 intracellularly into the α-granules of megakaryocytes, and thus potentially makes it possible for the protein to reach cell nucleus (Taylor et al., 2001). Inhibition of receptor-mediated endocytosis does not however affect nuclear uptake of IGFBP-3, suggesting that it uses also an alternative non-classical import pathway for transport across the plasma membrane (Schedlich et al., 1998). Lee and coworkers observed cellular internalization of IGFBP-3 occurring via interaction with caveolin, one of two (next to clathrin) major proteins mediating endocytic uptake (Lee et al., 2004). Both IGFBP-3 and −5 possess caveolin docking domains in their C-domains.

The transforming growth factor-β receptor (TβR-V), a membrane glycoprotein with Ser-specific protein kinase activity, was found to be identical to IGFBP-3 receptor, which mediates IGF-independent growth inhibition (Leal et al., 1997; Leal et al., 1999; Wu et al., 2000). Findings of Huang and coworkers suggest that the growth inhibition results from dephosphorylation of insulin receptor substrates, IRS-1 and -2, by the IGFBP-3-bound TβR-V (Huang et al., 2004).

IGFBP-5 stimulates mitogenesis of endothelial, osteoblast and other cell types independent of IGF (Andress et al., 1992, 1993, 1995). Cell association is required, but receptor has not been isolated. Fragments of the IGFBPs have been reported to have both inhibitory and stimulatory actions (Binoux et al., 1999). IGFBP-5 (1-169) directly stimulates osteoblast proliferation suggesting a regulatory role in bone formation (Andress et al., 1992). The C-terminal metal binding domain (MBD) of IGFBP-3 has been shown to mediate cellular uptake and nuclear localization of

C-terminally conjugated not related partner proteins: green fluorescent protein (GFP) and horseradish peroxidase (HRP). A 12-amino acid long MBD peptide triggered apoptosis as effectively as an intact IGFBP-3 in chemically or nutritionally stressed human embryonic kidney (HEK) cells (Singh et al., 2004). It has been also shown that the E7 protein encoded by human papillomavirus type 16 binds to intracellular IGFBP-3 and triggers its proteolytic cleavage, preventing its proapoptotic functions, hence overriding senescence (Mannhardt et al., 2000).

2.4 Structure of IGFBPs

The molecular size of the six IGFBPs ranges from 22 to 32 kDa. The N- and C-terminal thirds of all the IGFBPs are homologous and heavily cross-liked by disulfide bonds whose positions are conserved (Fig. 12). The middle regions have a minimal homology and only IGFBP-4 has a disulfide bond in this region. Secondary structure predictions and accessibility to proteolysis suggests that the linker region is exposed and lacks significant structure. Several studies aimed at establishing the disulfide bond linkages of IGFBPs using conventional biochemical methods. Only mapping of disulfides in IGFBP-6, containing six amino-terminal cysteine bridges, one less than other IGFBPs, produced complete and accurate map of all the linkages in both N- and C-domains (Neumann et al., 1999). In a study on IGFBP-4, Chelius and coworkers established 8 out of 10 disulfide bonds and narrowed the remaining assignment to 2 possibilities (Chelius et al., 2001). All IGFBPs examined so far (IGFBP-1, -2, -4, -6) have an identical intradomain disulphide-bonding pattern of the C-domain (Forbes et al., 1998; Neumann et al., 1998; Standker et al., 2000). Regions of amino acid sequence homology and the conserved N- and C-terminus disulfide cross- linking pattern in IGFBPs suggest maintenance of a conserved structure across all IGFBPs in these regions. IGFBPs with reduced disulfides exhibit no IGF binding activity, suggesting the importance of the bridging for maintaining structural elements required for ligand binding (Landale et al., 1995; Hashimoto et al., 1997; Qin et al., 1998; Neumann et al., 1999). Several properties of IGFBPs and IGFs, such as the intrinsic disorder of the central one-third of the IGFBPs, the highly disulfide bridged folded domains, and rapid aggregation of IGFs have hindered structural studies with these proteins (reviewed in Clemmons, 2001, in Hwa et al., 1999; in Carrick et al., 2002; Cooke et al., 1991; Torres et al., 1995). Only in the last few years have reports on structural characterization of

small domains of IGFBPs appeared. The first direct information on IGFBP folding came from the NMR study of miniNBP-5, a short amino-terminal fragment spanning residues 40-92 (Kalus et al., 1998), which was later confirmed by X-ray crystallography (Zeslawski et al., 2001).

```
IGFBP-1               A P W Q C A P C S A E K L A L C P P V S A S - - - - - 22
IGFBP-2             E V L F R C P P C T P E R L A A C G P P P V A P P A A V 28
IGFBP-3 G A S S G G L G P V V R C E P C D A R A L A Q C A P P P A V - - - - - 30
IGFBP-4             D E A I H C P P C S E E K L A R C R P P V G - - - - - - 22
IGFBP-5           L G S F V H C E P C D E K A L S M C - P P S P L G - - - - 24
IGFBP-6             A L A R C P G C G Q G V Q A G C - P G G - - - - - - - 19

IGFBP-1 - - - - - - - - - - C S E - - - - V T R S A G C G C C P M C A L P L G 43
IGFBP-2 A A V A G G A R M P C A E - - - - L V R E P G C G C C S V C A R L E G 59
IGFBP-3 - - - - - - - - - - C A E - - - - L V R E P G C G C C L T C A L S E G 51
IGFBP-4 - - - - - - - - - - C E E - - - - L V R E P G C G C C A T C A L G L G 43
IGFBP-5 - - - - - - - - - - C - E - - - - L V K E P G C G C C M T C A L A E G 44
IGFBP-6 - - - - - - - - - - C V E E E D G G S P A E G C A E A E G C L R R E G 44

IGFBP-1 A A C G V A T A R C A R G L S C R A L P G E Q Q P L H A L T R G Q G A 78
IGFBP-2 E A C G V Y T P R C G Q G L R C Y P H P G S E L P L Q A L V M G E G T 94
IGFBP-3 Q P C G I Y T E R C G S G L R C Q P S P D E A R P L Q A L L D G R G L 86
IGFBP-4 M P C G V Y T P R C G S G L R C Y P P R G E V K P L H T L M H G Q G V 78
IGFBP-5 Q S C G V Y T E R C A Q G L L C L P R Q D E E K P L H A L L H G R G V 79
IGFBP-6 Q E C G V Y T P N C A P G L Q C H P P K D D E A P L R A L L L G R G R 79

IGFBP-1 C V Q E S D A S A P H A A E A G S P E S P E S T E I T E E E L L D M F 113
IGFBP-2 C E K R R D A E Y G A S P E Q V A D N G D D H S E G G L V E N H V D S 129
IGFBP-3 C V N A S A V S R L R A Y L L P A P P A P G N A S E S E E D R S A G S 121
IGFBP-4 C M E L A E I E A I Q E S L Q P S D K D E G D H P N N S F S P C S A H 113
IGFBP-5 C L N E K S Y R E Q V K I E R D S R E H E E P T T S E M A E E T Y S P 114
IGFBP-6 C L P A R A P A V A E E N P K E S K P Q A G T A R P Q D V N R R D Q Q 114

IGFBP-1 H L M A P S E E D H S I L W D A I S T Y D G S K A L H V T N I K K W K 148
IGFBP-2 T M N M L G G G G S A G R K P L K S G M K E L A V F R E K V T E Q H R 164
IGFBP-3 V E S P S V S S T H R V S D P K F H P L H S K I I I I K K G H A K D S 156
IGFBP-4 D R R C L Q K H F A K I R D R S T S G G K M K V N G A P R E D A R P V 148
IGFBP-5 K I F R P K H T R I S E L K A E A V K K D R R K K L T Q S K F V G G A 149
IGFBP-6 N R P G T S T T P S Q P N S A G V Q D T E M                         136

IGFBP-1                                         E P C R E I L Y 156
IGFBP-2 Q M G K G G K H H L G L E E P K K L R P P P A R     T P C Q Q E L D 196
IGFBP-3 Q R Y K V D Y E S Q S T D T Q N F S S E S K R E T E Y G P C R R E M E 191
IGFBP-4 P Q                                       G S C Q S E L H 158
IGFBP-5 E N T A H P R I I S A P E M R Q E S E Q     G P C R R H M E 177
IGFBP-6                                         G P C R R H L D 144

IGFBP-1 R V V E S L A K A Q E T S - - G E - E - I S K F Y L P N C N K N G F Y 187
IGFBP-2 Q V L E R I S T M R L P D E R G P L E H L Y S L H I P N C D K H G L Y 231
IGFBP-3 D T L N H L K F L N V L S V R G - - - - V - - - H I P N C D K K G F Y 219
IGFBP-4 R A L E R L A A S Q - - S - R T H - E D L Y I I P I P N C D R N G N F 189
IGFBP-5 A S L Q E L K A S E M R V P R A - - - - V Y - - - L P N C D R K G F Y 205
IGFBP-6 S V L Q Q L Q T E V Y - - - R G - A Q T L Y - - - V P N C D H R G F Y 172

IGFBP-1 H S R Q C E T S M D G E A G L C W C V Y P W N G K R I P G S P E I - R 221
IGFBP-2 N L K Q C K M S L N G Q R G E C W C V N P N T G K L I Q G A P T I - R 266
IGFBP-3 K K K Q C R P S K G R K R G F C W C V D K Y - G Q P L P G Y T T K G K 253
IGFBP-4 H P K Q C H P A L D G Q R G K C W C V D R K T G V K L P G - G L E P K 223
IGFBP-5 K R K Q C K P S R G R K R G I C W C V D K Y - G M K L P G M - E Y V D 238
IGFBP-6 R K R Q C R S S Q G Q R R G P C W C V D R M - G K S L P G S P D - G N 205

IGFBP-1 G D P N C Q M Y F N V Q N                         234
IGFBP-2 G D P E C H L F Y N E Q C E A R G V H T Q R M Q     289
IGFBP-3 E D V S C Y S M Q S K                             264
```

```
IGFBP-4 G E L D C H Q L A D S F R E                                237
IGFBP-5 G D F Q C H T F D S S N E V                                252
IGFBP-6 G S S S C P T G S S G                                      216
```

Fig. 12. Sequence alignment of human IGFBP-1 to -6. Conserved residues are indicated by cyan shading. Blue box – caveolin scaffolding docking domain (Lee et al., 2004); yellow – nuclear localization sequences (NLS) (Schedlich et al., 1998); purple – potential integrin-binding sequences; green – potential N-glycosylation sites; magenta – identified O-glycosylation sites; red – phosphorylated serines (Jones et al., 1993; Hoeck et al., 1994), lettering in magenta - heparin-binding domains (Booth et al., 1995); underlined – metal binding domain (MBD) (Singh et al., 2004). In **bold** – amino acids, after which cleavage occurs (Binoux et al., 1999).

The structure of this minimum-binding region of the N-terminal domain can be described as a compactly arranged, short three-stranded antiparallel β-sheet (residues 46–47, 59–61, 78–82). As expected, the fold of miniNBP-5 determined by NMR was conserved in the crystal structure with IGF-I, although complex formation did rigidify the miniNBP-5 loop at residues 62–69.

Headey and coworkers have recently determined a solution structure of the carboxyl-terminal domain of IGFBP-6 (residues 161-240 of the full-length precursor) using NMR (Headey et al., 2004). The domain consists of a thyroglobulin type-1 fold comprising a α-helix followed by a loop, a three-stranded anti-parallel β- sheet incorporating a second loop, and finally a disulfide bonded flexible third loop. The structure is in an agreement with a model proposed for C-terminal domain of IGFBP-4 (residues 136-237) based on the crystal structure of homologous protein, p41 (a proteolytic fragment of MHC class II) (Mazebourg et al., 2004).

2.5 IGF in cancer

The link between cancer and IGF signaling is also consistent with recent epidemiological studies showing an increased relative risk for the development of colon, prostate, breast, lung, and bladder cancers in individuals with circulating IGF-I levels in the upper quartile of the normal range (Chan et al., 1998). These findings were confirmed in animal models, where reduced circulating IGF-I levels result in significant reductions in cancer development, growth, and metastases, whereas increased circulating IGF-I levels are associated with enhanced tumor growth (Wu et al., 2003). Characteristic alterations detected in primary hepatocellular (HCC) and cutaneous carcinomas, breast carcinomas and hepatoma cell lines, comprise the overexpression of the IGF-IR (sometimes accompanied by its hyperphosphorylation), emerging as critical event in malignant transformation and growth of tumors (Sharf et al., 2003).

Preventing the IGF-IR interaction with its ligand can be achieved either by neutralization of circulating IGFs or blocking the IGF binding site on IGF-IR. The strategies aiming at elimination of active IGFs utilize either specific antibodies or inhibitory IGFBPs (Arteaga et al., 1989; Firth et al., 2002). Antibody-mediated blockade of ligand binding to the IGF-IR inhibited downstream signaling of IGFs pathways and, as a result, the mitogenic and proliferative potential of IGF-I and IGF-II were significantly reduced. Direct reduction of IGF-IR expression has been approached by using antisense strategy through either oligonucleotides (Grzmil et al., 2004), stable transfections, or siRNAs (Neuenschwander et al., 1995). Certain compounds of the group cyclolignans have recently been reported to be potent and selective inhibitors of tyrosine phosphorylation of the IGF-IR (Girnita et al., 2004).

The IGF system plays a central role in many aspects of tumorigenesis. The approaches to its control listed above have numerous drawbacks and problems, including lack of specificity, difficulty of drug delivery, etc. A better understanding of this complex system will facilitate the development of novel approaches to diagnose and treat various human cancers.

3. Goals of the Study

The work on structural analysis of CDKs, their binding partners, and inhibitors (both endogenous and chemical) would greatly improve our understanding of the structure-function relationship of this multi-dimensional protein family. A precise model of the interaction between CDKs and their binding partners can be created based on high-resolution 3-D structures of the interacting proteins, kinetic data from binding studies on truncated variants, and information on their dynamic behaviour from NMR experiments. Knowledge of structural determinants of pRb, p53, INCA1 on CDK2-cyclin A binding site would place at our disposal a means to regulate the actions of the CDKs, arguably one of the most important cell cycle regulators.

In the cell cycle, endogenous inhibitors INK4 and Cip/Kip help to regulate the CDKs. Numerous cases of CDK deregulation because of mutation in these endogenous inhibitors in human cancers prompted us to study several small molecule inhibitors with NMR spectroscopy focusing on the ATP/inhibitor binding site of CDK2.

While IGFBPs have different actions, all IGF-dependent actions, positive or negative, depend on binding to a high-affinity binding site on IGFBPs. Therefore, elucidation of structural determinants of various IGFBPs in IGF binding is important for a general understanding of the biology of the IGF system and may shed light on how different IGFBPs exhibit specific actions. Design and *in silico* modeling of novel, low molecular weight ligands with therapeutic potential should be possible based on new interaction sites revealed in this study.

4. Materials and laboratory methods

4.1 Materials

4.1.1 *E. coli* strains and plasmids

Cloning strains: XL1-Blue (Stratagene, USA), One Shot TOP10 (Invitrogen, Holland), DH5α (Novagen, Canada).

Plasmids: pET28a (+) (Novagen, Canada), pET-46 Ek/LIC (Novagen, Canada), pET-41 Ek/LIC (Novagen, Canada), pGEX-4T-2 (Amersham Biosciences, Sweden).

Protein expresion strains: One shot$^®$ BL21 (DE3) (Invitrogen, Holland), One shot$^®$ BL21 Star™ (DE3) (Invitrogen, Holland), One shot$^®$ BL21 Star™ (DE3) pLysS (Invitrogen, Holland).

4.1.2 Cell growth media and stocks

4.1.2.1 One litre LB medium: 10 g bacto tryptone, 5 g bacto yeast extract, and 10 g sodium chloride. pH adjusted to 7.0. For the preparation of agar plates the medium was supplemented with 15 g agar.

4.1.2.2 One litre TB medium: 12 g bacto tryptone, 24 g bacto yeast extract, 10 g sodium chloride, 4 ml glycerol, 800 ml deionized water. The medium was autoclaved, cooled; 100 ml sterile K-phosphate and glucose were added. The final concentration of glucose was 0.5%. 1 l of K-phosphate buffer pH 7.1 contained 23.1 g KH_2PO_4, 125.4 g K_2HPO_4,

4.1.2.3 Minimal medium (MM) for uniform enrichment with ^{15}N: For 1 l MM: 0.5 g NaCl, 1.3 ml trace elements solution, 1 g citric acid monohydrate, 36 mg ferrous citrate, 4.02 g KH_2PO_4, 7.82 g K_2HPO_4, 1 ml Zn-EDTA solution, 1 g NH_4Cl or $^{15}NH_4Cl$, pH was adjusted to 7.0 with NaOH. The mixture was autoclaved and upon cooling separately sterilized 25 ml glucose, 560 µl thiamin, antibiotics, 2 ml of 1 M $MgSO_4$ were added.

4.1.2.4 Defined medium for selective ^{15}N labeling of proteins: For 1 l of medium:

400 mg Ala, Gln, Glu, Arg, Gly, Ile, Val

255 mg Asp, Met

> 125 mg cytosine, guanosine, uracil
>
> 100 mg Asn, Leu, His, Lys, Pro, Thr, Tyr
>
> 50 mg Phe, thymine, thymidine
>
> 1.6 g Ser

10 mg $CaCl_2$, 2 g NaAc, 10 g K_2HPO_4, 1 g citric acid, 1.3 ml trace element solution, 36 mg ferrous citrate, 1 ml Zn-EDTA solution, 1 g NH_4Cl, pH was adjusted to 7.0 with NaOH. The mixture was autoclaved and to the cooled medium, separately sterilized solutions of 25 ml glucose, 560 μl thiamin, antibiotics and 2 ml of 1 M $MgSO_4$ were added. 50 mg Cys, Trp, nicotinic acid, 0.1 mg Biotin, *X* mg ^{15}N-amino acid was also added. The other half portion of the ^{15}N-amino acid was sterile filtered and added at the time of induction.

4.1.3 Stock solutions

Glucose: 20% (w/v) in deionised H_2O, autoclaved

Ampicillin: 100 mg/ml of ampicillin in deionised H_2O, sterilized by filtration, stored in aliquots at -20°C. Working concentration: 100 μg/ml

Kanamycin: 50 mg/ml of kanamycin in deionised H_2O, sterile filtrated and stored in aliquots at -20 °C

Chloramphenicol: 33 mg/ml of chloramphenicol in deionised H_2O, sterile filtrated and stored in aliquots at -20 °C

Thiamin: 1%, in deionised H_2O, sterilized by filtration

$MgSO_4$:   1 M, in deionised H_2O, sterilized by filtration

Zn-EDTA solution: 5 mg/ml EDTA, 8.4 mg/ml $Zn(Ac)_2$

Trace elements solutions: 2.5 g/l H_3BO_3, 2.0 g/l $CoCl_2$, 1.13 g/l $CuCl_2$, 9.8 g/l $MnCl_2$, 2.0 g/l Na_2MoO_4, pH lowered with citric acid or HCl

4.1.4 Protein purification buffers for Ni-NTA chromatography

Buffers for protein purification:

(A) IGF BPs (denaturing conditions)

Buffer A:	6 M guanidinium chloride, 100 mM NaH_2PO_4, 10 mM Tris, 10 mM β-mercaptoethanol, pH 8.0
Buffer B:	6 M guanidinium chloride, 100 mM NaH_2PO_4, 10 mM Tris, 10 mM β-mercaptoethanol, pH 6.5
Buffer C:	6 M guanidinium chloride, 100 mM NaAc, 10 mM β-mercaptoethanol, pH 4.0
Buffer D:	6 M guanidinium chloride, pH 3.0
Buffer E: (Refolding buffer)	200 mM Arginine HCl, 1 mM EDTA, 100 mM Tris, 2 mM red GSH, 10% (v/v) glycerol, 0.05% NaN_3, pH 8.4

Ion exchange and gel filtration buffers:

Buffer P (0):	8 mM KH_2PO_4, 16 mM Na_2HPO_4, pH 7.2
Buffer P (1000):	8 mM KH_2PO_4, 16 mM Na_2HPO_4, 1 M NaCl, pH 7.2
PBS:	140 mM NaCl, 2.7 mM KCl, 10 mM Na_2HPO_4, 1.8 mM KH_2PO_4, pH 7.3

Protease buffers:

(Thrombin cleavage buffer):	60 mM NaCl, 60 mM KCl, 2.5 mM $CaCl_2$, 50 mM Tris, pH 8.0
(Factor Xa cleavage buffer):	100 mM NaCl, 4 mM $CaCl_2$, 50 mM Tris, pH 8.0

(B) CDK2 and p27 (native conditions)

Lysis buffer or binding buffer:	500 mM NaCl, 50 mM NaH_2PO_4, 10 mM β-mercaptoethanol, pH 7.5
Wash buffer:	500 mM NaCl, 50 mM NaH_2PO_4, 20 mM imidazole, 10 mM β-mercaptoethanol, pH 7.5
Elution buffer:	500 mM NaCl, 50 mM NaH_2PO_4, 250 mM imidazole, 10 mM β-mercaptoethanol, pH 7.5
Gel filtration buffer:	140 mM NaCl, 2.7 mM KCl, 10 mM Na_2HPO_4, 1.8 mM KH_2PO_4, 5 mM DTT, pH 7.5

<div align="center">Or</div>

<div align="center">200 mM NaCl, 40 mM HEPES, 5 mM DTT, pH 7.5</div>

<div align="center">Or</div>

<div align="center">20 mM HEPES, 1 mM EDTA, pH 7.4</div>

(C) Cyclin A2 constructs and INCA1 constructs (native conditions)

Lysis buffer or binding buffer:	500 mM NaCl, 50 mM Tris HCl, 20 ml glycerol, 0.05% Triton X-100, 100 mM $MgCl_2$, 0.01% NaN_3, 10 mM β-mercaptoethanol, pH 7.5
Wash buffer:	500 mM NaCl, 50 mM Tris HCl, 100 mM $MgCl_2$, 5 mM PMSF, 20 mM imidazole, 10 mM β-mercaptoethanol, pH 7.5
Elution buffer:	500 mM NaCl, 50 mM Tris HCl, 100 mM $MgCl_2$, 5 mM PMSF, 250 mM imidazole, 10 mM β-mercaptoethanol, pH 7.5
Gel filtration buffer:	100 mM $MgCl_2$, 50 mM Tris HCl, 5 mM DTT, pH 7.5

(D) p53 C-terminal constructs (native conditions)

Lysis buffer or binding buffer:	500 mM NaCl, 50 mM Tris HCl, 0.05% Triton X-100, 0.01% NaN_3, 10 mM β-mercaptoethanol, pH 7.5
Wash buffer:	500 mM NaCl, 50 mM Tris HCl, 5 mM PMSF, 20 mM imidazole, 10 mM β-mercaptoethanol, pH 7.5
Elution buffer:	500 mM NaCl, 50 mM Tris HCl, 5 mM PMSF, 250 mM imidazole, 10 mM β-mercaptoethanol, pH 7.5
Gel filtration buffer:	200 mM NaCl, 40 mM HEPES, 5 mM DTT, pH 7.5

(E) pRb C-terminal constructs

Lysis buffer or binding buffer:	300 mM NaCl, 50 mM NaH_2PO_4, 10 mM β-mercaptoethanol, pH 7.5
Wash buffer:	300 mM NaCl, 50 mM NaH_2PO_4, 20 mM imidazole, 10 mM β-mercaptoethanol, pH 7.5

Elution buffer: 300 mM NaCl, 50 mM NaH$_2$PO$_4$, 250 mM imidazole, 10 mM β-mercaptoethanol, pH 7.5

Gel filtration buffer: 200 mM NaCl, 40 mM HEPES, 5 mM DTT, pH 7.5

(F) 14-3-3σ protein

Lysis buffer or binding buffer: 300 mM NaCl, 50 mM NaH$_2$PO$_4$, 10 mM imidazole, 10 mM β-mercaptoethanol, pH 8.0

Wash buffer: 300 mM NaCl, 50 mM NaH$_2$PO$_4$, 20 mM imidazole, 10 mM β-mercaptoethanol, pH 7.5

Elution buffer: 500 mM NaCl, 50 mM NaH$_2$PO$_4$, 250 mM imidazole, 10 mM β-mercaptoethanol, pH 7.5

Gel filtration buffer: 100 mM NaCl, 100 mM KCl, 5 mM DTT, pH 8.0

4.1.5 Buffers for GST purification of INCA1 and cyclin A2

Lysis buffer or binding buffer: 140 mM NaCl, 2.7 mM KCl, 10 mM Na$_2$HPO$_4$, 1.8 mM KH$_2$PO$_4$, 0.05% Triton X-100, 5 mM DTT, pH 7.5

Wash buffer: 140 mM NaCl, 2.7 mM KCl, 10 mM Na$_2$HPO$_4$, 1.8 mM KH$_2$PO$_4$, 0.05% Triton X-100, 5 mM DTT, pH 7.5

Lysis buffer: 50 mM Tris, 10 mM glutathione (reduced), 5 mM DTT, pH 8.0

4.1.6 Reagents and buffers for the SDS-PAGE

Anode buffer (+): 200 mM Tris, pH 8.9

Cathode buffer (-): 100 mM Tris, pH 8.25, 100 mM tricine, 0.1% SDS

Separation buffer: 1 M Tris, pH 8.8, 0.3% SDS

Stacking buffer: 1 M Tris, pH 6.8, 0.3% SDS

Separation acrylamide: 48% acrylamide, 1.5% bis-acrylamide

Stacking acrylamide: 30% acrylamide, 0.8% bis-acrylamide

4.1.6.1 Preperation of polyacrylamide gels

Separation gel:	1.675 ml H_2O, 2.5 ml separation buffer, 2.5 ml separation acrylamide, 0.8 ml glycerol, 25 µl APS, 2.5 µl TEMED
Intermediate gel:	1.725 ml H_2O, 1.25 ml separation buffer, 0.75 ml separation acrylamide, 12.5 µl APS, 1.25 µl TEMED
Stacking gel:	2.575 ml H_2O, 0.475 ml stacking buffer, 0.625 ml stacking acrylamide, 12.5 µl 0.5 M EDTA, pH 8.0, 37.5 µl APS, 1.9 µl TEMED

4.1.7 Protein visualization

Coomassie-blue solution:	45% ethanol, 10% acetic acid
Destaining solution:	5% ethanol, 10% acetic acid

4.1.8 Enzymes and other proteins

BSA, BamHI, EcoRI, HindIII, XhoI (New England BioLabs, USA), Pfu turbo DNA Polymerase (Stratagene, USA), T4 DNA Ligase (Roche, Germany), DpnI (Stratagene, USA), Factor Xa (Sigma, USA, Novagen, Canada), Thrombin (Sigma, USA), Enterokinase (Novagen, Canada).

4.1.9 Kits and reagents

QIAquick PCR Purification Kit	Qiagen (Germany)
QIAprep Spin Miniprep Kit	Qiagen (Germany)
Quick change site-directed mutagenesis Kit	Stratagene (USA)
Pre-Crystallization Test (PCT)	Hampton Research (USA)

4.1.10 Protein and nucleic acid markers

Prestained Protein Marker:	New England Bio Labs (USA)
Broad Range (6-175 kDa) 1 kb DNA-Leiter:	Peq Lab (Germany)

4.1.11 Chromatography equipment, columns and media

AKTA explorer 10 (Amersham Pharmacia, Sweden), Bio Logic LP System (Bio-Rad, USA), HiLoad 26/60 Superdex 75 pg (Amersham Pharmacia, Sweden), HiLoad 10/30 Superdex 75 pg (Amersham Pharmacia, Sweden), Mono Q HR 5/5, 10/10 (Amersham Pharmacia, Sweden), Mono S 8 ml (Amersham Pharmacia, Sweden), Ni-NTA-agarose (Qiagen, Germany), Glutathione Sepharose Transferase Fast Flow (Amersham Pharmacia, Sweden), Superdex 200 HR 10/30 pg (Amersham Pharmacia, Sweden).

4.2 Laboratory methods and principles

4.2.1 Choice of the expression vector

The plasmid-encoded transcription signals: transcription initiation and termination sites and "strong" promoters, either hybrid or of phage origin, make high levels of mRNA synthesis. A long half-life of the mRNA is assured when specifically designed *E. coli* strains are used, for instance BL21 Star, characterized by deletions of genes encoding specific RNAses. The level of translation, which determines an overall yield of an over expressed proteins, depends on properties of the transcript RNA: its sequence and the quality of its codons, rather than on the strength of the promoter. The hairpin type secondary structure assumed by mRNA leads to attenuation of ribosome progression, greatly reducing protein production.

The phenomenon of a 'codon bias' arises from a different codon usage by eukaryotic and prokaryotic organisms: from the existing possible triplets encoding one amino acid, the former group of organisms sometimes choose different ones than the latter. As a result, a pool of amino acyl-tRNAs and aa-tRNA synthetases present in *E. coli* differs from the one found in human cells. In particular, Arg codons AGA, AGG, CGG, CGA, Ile codon AUA, Leu codon CUA, Gly codon GGA and Pro codon CCC are rarely used. This impact appears to be highest when these codons are present near the N-terminus and when they appear consecutively. Several laboratories have shown that the yield of a protein whose genes contain rare codons can be dramatically improved when the cognate tRNA is increased within the host (Rosenberg et al., 1993). *E. coli* strains are commercially available that have artificially introduced copies of genes encoding the tRNAs, either at the genomic level or in a plasmid (Rossetta from Invitrogen; BL21 RP or RIL from Novagen). The choice of the

expression vector and fusion partner/tag is dictated by such parameters of the recombinant protein as its toxicity to *E. coli* and solubility.

Tightly controlled expression system are preferred, such as a pET system based on the phage T7 RNA polymerase, enabling a high level of control over a basal expression of genes encoding toxic proteins. The system provides several levels of control due to additional plasmid, which express T7 lysozyme, a natural T7 RNA polymerase inhibitor. Large, vector encoded fusion tags, such as glutathione S-transferase (GSH), thioredoxin or maltose binding protein (MBP) often increase solubility and promote proper folding of recombinant fusion partners. For proteins directed into inclusion bodies, use of a 6-histidine fusion peptide (His-tag) makes use of immobilized metal chromatography (IMAC) possible under strong denaturing/reducing conditions, enabling rapid purification.

It is often required for functional studies of a recombinant protein and for crystallization purposes that the fusion tag is removed. This is usually achieved with an aid of a specific restriction protease. The enzymes most commonly used are serine proteases of the blood coagulation cascade: Factor Xa (cleaves after *R* in a *IEGRX* sequence *X ≠ P*) and thrombin (cleaves after *R* in *LVPRGS*). The sequences encoding the desired cleavage site are introduced by means of PCR, in 5'-overhangs of forward and treatment of the fusion protein with these enzymes results in unwanted cleavage at sites possessing a certain degree of homology to the recognition sequences with degradation susceptible proteins. The enzymes are used for removal of only short N-terminal His-tag.

In choosing the restriction protease, enzymes–target protein compatibility has to be considered for example the optimal cleavage conditions for the enzymes may not be appropriate for the stability of the protein in question. For instance, Factor Xa requires the presence of 1-2 mM Ca^{2+} in the buffer and oxidizing conditions, and will not work in the presence of chelating agents, phosphate buffer, reducing agents or high salt. Presence of even small amounts of detergents may hamper its selectivity. Pre-scission protease on the other hand requires strong reducing conditions.

Plasmids pET28a, pET-46 Ek/LIC, pET-41 Ek/LIC, pGEX-4T-2, were selected as vectors of choice for expression of the proteins discussed in this work. All amino-terminal constructs and mutants of IGFBP-4, 14-3-3σ, CDK2 and cyclin A2 were cloned into pET28a in frame to a His/T7-tag of the following sequence: *MGSSHHHHHHCCGLVPRGSHMASMTGGQQMGRGSIEGR*.

Treatment with Factor Xa (the cleavage site in bold) yielded IGFBP-4 and 14-3-3σ proteins with native N-termini. Both Factor Xa and thrombin sites were introduced. Ligation independent cloning was performed with CDK2, cyclin A2, p53, pRb, and INCA1 in pET-46 Ek/LIC. The vector has a 15 amino acid histidine tag, which can be cleaved by Enterokinase protease.

4.2.2 DNA techniques

Preparation of plasmid DNA: The isolation of plasmid DNA from *E. coli* was carried out using plasmid purification kits from Qiagen. The kits employ a standard alkalic lysis of the precipitated bacteria in the presence of RNAse and strong ionic detergent, SDS, followed by neutralization/DNA renaturation with acetate. For purification, a crude cell elute was loaded onto a silica gel column, washed with an ethanol-containing buffer, and eluted in a small volume, yielding up to 20 µg of the plasmid DNA.

PRIMERS USED IN THE STUDY	Tm	Bases	GC %
14-3-3σ (Fwd): 5'-GGT AAT TGA GGG TCG CAT GGA GAG AGA GCC AGT CTG ATC- 3'	60	39	53.8
14-3-3σ (Rev): 5' -AGA GGA GAG TTA GAG CCT CAG CTC TGG GGC TCC TGG GG- 3'	61	38	60.5
CDK2, BamHI (Fwd): 5' -CGC GGA TCC ATG GAG AAC TTC CAA AAG- 3'	66.5	27	51.9
CDK2, EcoRI (Rev): 5' -CCG GAA TTC TCA GAG TCG AAG ATG GGG- 3'	68	27	55.6
CDK2, Thr/Enk/LIC (Fwd): 5' - GAC GAC GAC AAG ATG CTG GTG CCG CGC GGC AGC ATG GAG AAC TTC CAA AAG- 3'	81.6	54	59.3
CDK2, Enk/LIC (Fwd): 5' -GAC GAC GAC AAG ATG GAG AAC TTC CAA AAG GTG GAA AAG- 3'	71.6	39	46.2
CDK2, (LIC) (Rev): 5' -GAG GAG AAG CCC GGT TTA TCA GAG TCG AAG ATG GGG TAC TGG CTT GGT- 3'	78	48	54.2
cyclin A2, (full length), BamHI (Fwd): 5' -CGC GGA TCC ATG TTG GGC AAC TCT GCG CCG- 3'	75	30	66.7
cyclin A2, (full length), EcoRI (Rev): 5' -CCG GAA TTC TTA CAG ATT TAG TGT CTC TGG TGG- 3'	68.3	33	45.5
cyclin A2, (short), BamHI (Fwd): 5' -CGC GGA TCC AGT GTT AAT GAA GTA CCA GAC TAC- 3'	69.5	33	48.5
cyclin A2, (short), Enk/LIC (Fwd): 5' -GAC GAC GAC AAG ATG AAT GAA GTA CCA GAC TAC CAT GAG- 3'	76.8	39	46.2
cyclin A2, (short), Enk/LIC (Rev): 5' -GAG GAG AAG CCC GGT TTA CAG ATT TAG TGT CTC TGG TGG- 3'	78.9	39	51.3
p27, (short), BamHI (Fwd): 5' -CGC GGA TCC ATG TCA AAC GTG CGA GTG TCT AAC GGG- 3'	57	36	58.3
p27, (short), EcoRI (Rev): 5' -CCG GAA TTC TCA TTT GGG GGG CCG CGG GGG	61	37	64.8

TCT GTA G- 3'			
p53 (CTD), Enk/LIC (Fwd): 5' -GAC GAC GAC AAG ATG GGG GAG CCT CAC CAC GAG CTG CCC- 3'	80	39	66.7
p53 (CTD), Thr/LIC (Fwd): 5' -GAC GAC GAC AAG ATG CTG GTG CCG CGC GGC AGC GGG GAG CCT CAC CAC GAG-3'	87.4	57	71.9
p53 (TD), Enk/LIC (Rev): 5' -GAG GAG AAG CCC GGT TCA TCA CCC AGC CTG GGC ATC CTT GAG- 3'	84.8	42	61.9
p53 (CTRD), Enk/LIC (Fwd): 5' -GAC GAC GAC AAG ATG AGG GCT CAC TCC AGC CAC CTG AAG- 3'	76.8	39	59
p53 (CTRD), Thr/LIC (Fwd): 5' -GAC GAC AAG ATG CTG GTG CCG CGC GGC AGC AGG GCT CAC TCC AGC CAC CTG AAG- 3'	85.2	57	66.7
p53 (CTRD), Trp,Enk/LIC (Fwd): 5'-GAC GAC GAC AAG ATG TGG AGG GCT CAC TCC AGC CAC- 3'	81.2	36	61.1
p53, Enk/LIC (Rev): 5' -GAG GAG AAG CCC GGT TCA CTA GTC TGA GTC AGG CCC TTC TGT CTT GAA CAT- 3'	78.2	51	52.9
INCA1, Enk/LIC (Fwd): 5' -GAC GAC GAC AAG ATG CAG GTG CAG GAT GAT GGA GTC- 3'	78.9	36	55.6
INCA1 (2ndconstruct), Enk/LIC (Fwd): 5'-GAC GAC GAC AAG ATG CTT TGG AGA AGA AAG AAG AGG AGG- 3'	77.8	39	48.7
INCA1 (3rd construct), Enk/LIC (Fwd): 5' -GAG GAG AAG ATG CAG CTG CTT TGG TCT CCC TGG AGC- 3'	82.1	39	59
INCA1, Enk/LIC (Rev): 5' -GAG GAG AAG CCC GGT TTA CTC TTC AGA CGC TGC CAA CTG- 3'	81	39	56.4

A polymerase chain reaction was employed to amplify desired DNA fragments and genes, introduce restriction sites, STOP codons and sequences encoding restriction protease cleavage sites. The primers were prepared according to standardized principles regarding the length, GC-content, melting temperature and occurrence of secondary structures of the hairpin type. All primers used for cloning and mutageneses are listed in table.

4.2.3 PCR conditions

A polymerase chain reaction was employed to amplify desired DNA fragments and genes, introduce restriction sites, STOP codons and sequences encoding restriction protease cleavage sites. The primers were prepared according to standardized principles regarding the length, GC-content, melting temperature and occurrence of secondary structures of the hairpin type. Two different kinds of recombinant thermostable DNA polymerases were used.

	Melting temp.	Annealing temp.	Synthesis temp.
P$_{wo}$	94 °C	55 °C	72 °C
Pfu Turbo	95 °C	55 °C	68 °C

4.2.4 Digestion with restriction enzymes

Usually, 1-2 units of each restriction enzyme were used per 1 µg of plasmid DNA to be digested. The digestion was performed in a buffer specified by the manufacturer at the optimal temperature (37 °C) for 2-16 h. The fragments ends that occurred after digestion were cohesive.

4.2.5 Purification of PCR and restriction digestion products

DNA obtained after restriction digestion was purified from primers, nucleotides, enzymes, buffering substances, mineral oil, salts, agarose, ethidium bromide, and other impurities, using a silica-gel column (QIAquick PCR purification Kit, Qiagen) or Gel Extraction Kit, Qiagen. The QIAquick system uses a simple bind-wash-elute procedure. A binding buffer was added directly to the PCR sample or other enzymatic reaction, and the mixture was applied to the spin column. Nucleic acids absorbed to the silica-gel membrane in the high-salt conditions provided by the buffer. Impurities and short fragments of single or double-stranded DNAs were removed by the wash step and pure DNA was eluted with a small volume of 10 mM Tris pH 8.0 or ddwater.

4.2.6 Agarose gel electrophoresis of DNA

For verification of the presence and length of PCR or restriction digestion products, agarose gel electrophoresis was performed. For this purpose 1% agarose in TBE buffer plus ethidium bromide was prepared. The solution was poured into a horizontal gel chamber to polymerise. The DNA samples were mixed with 6× sample buffer prior loading. Electrophoresis was carried out at 100-120 V DC. Results were evaluated using UV illumination.
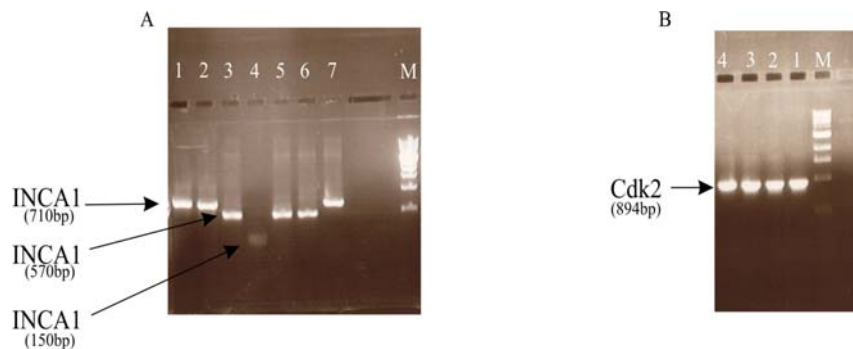

Fig. 1. 1%agraose gel photographs. *A*. Shows the purified DNA constructs of INCA1 and *B* shows the purified DNA fragment of CDK2 according to their corresponding base pairs. Gel A and B has 1kb marker. The last marker band on the gels corresponds to the size of 500bp.

4.2.7 Transformation of *E. coli*

A number of factors have been elucidated that produced an increase in transformation efficiency. Such factors include: prolonged incubation of bacteria with $CaCl_2$, addition of multiple cations, such as Mg^{2+}, Cs^{2+} or Rb^{2+}, into the transformation mixture and treatment of bacteria with dimethyl sulfoxide (DMSO), polyethylene glycol, hexamine-cobalt and dithiothreitol in the presence of both monovalent and divalent cations (Shung et al., 1989). After incubation with DNA, in order to make the cells keep the plasmid and to be certain they survive, the cells were heat shocked for several seconds to induce heat shock genes, which aid in survival and recovery. The cells were then incubated at 37°C without selective pressure. Sufficient time was given for expression of antibiotic resistance genes. Plating on selective media enabled recovery of those cells that actually received the DNA.

Transformation by electroporation employs high voltage, which temporarily puncture bacterial cell walls. High mortality of cells treated in this way implicates the need for high concentrations of bacteria.

4.2.8 Transformation of chemically competent cells

1µl of a ligation mix or ca. 50 µg of plasmid DNA was added to 50 µl of chemically competent cells. The mixture was incubated on ice for 30 min followed by a heat shock of 30 s at 42 °C, 200 µl of 2× LB medium was added and kept for half an hour in 37 °C in a table top shaker. 20-50 µl of the mixture was spread out on LB agar plates that included selective antibiotic and incubated in 37 °C.

4.2.9 Transformation by electroporation

1µl of an aqueous solution of plasmid DNA (ca. 100 ng/µl) was added to 50 µl of electrocompetent cells, the mixture was pipetted into a 2 mm electroporation cuvette. The electroporation was performed in an electroporation vessel (Gene pulser) at 1650 V. The suspension was then transferred into an eppendorf tube and mixed with 1 ml LB medium. After 1 h of incubation at 37°C, cells were plated as described above.

4.3 Protein chemistry; methods and techniques

4.3.1 Sonication

Sonication is a simple method used for disruption of cells by ultrasounds. The bubbles grow during the rarefying phase of the sound wave, and then are collapsed during the compression phase. On collapse, shock wave passes through the medium. The whole process of gas bubble nucleation, growth and collapse due to the action of intense sound waves is called cavitation. The collapse of the bubbles converts sonic energy into mechanical energy in the form of shock waves equivalent to several thousand atmospheres (300 MPa) pressure. The collapse of which produces sheer forces that are able to break cells. The advantage of this method for cell disruption over French press, freezing and thawing or lysozyme digestion is comparatively low viscosity of the lysate due to the nucleic acid fragmentation.

Pulsed mode of operation was applied (output control 8, 60% duty cycle) and sonication was carried out on ice, in 4 steps of 4 min each, with 4 min intervals between steps, to avoid overheating of the sample.

4.3.2 SDS polyacrylamide gel electrophoresis (SDS-PAGE)

SDS polyacrylamide gel electrophoresis was performed at various stages of purification to verify samples' purity, identify the eluted proteins in chromatography purification, progression of enzymatic digestion etc. Tricine, used as the trailing ion instead of glycine, allows a resolution of proteins at lower acrylamide concentrations than in glycine-SDS-PAGE systems. A resolution of proteins, especially in the range between 5 and 20 kDa, is thus achieved without the necessity to use urea. The guanidinium HCl-free protein samples were prepared by mixing 20 µl of protein solution with 5 µl of sample buffer (SB) followed by 3 min incubation at 100 °C. Due to rapid precipitation of SDS in contact with guanidine, the samples to be examined by PAGE after Ni-NTA chromatography under denaturing conditions had to be prepared in a following fashion: 20 µl of the protein solution in a denaturing buffer was diluted with 400 µl 20% trichloroacetic acid (TCA). The sample was incubated for 5 min at room temperature followed by centrifugation for 5 min at $20000 \times$ g. Supernatant was discarded by suction; the precipitated protein pellet was washed once by vortexing with 400 µl ethanol. After centrifugation and ethanol removal, the protein pellet was resuspended in 20 µl of $2\times$ SB and the sample was boiled for 3 min.

4.3.3 Visualization of separated proteins

For visualization of the protein bands, the gels were stained in a Coomassie-blue solution. Background was cleared by incubation of the gel in a destaining solution. Both processes were greatly accelerated by brief heating with microwaves of the gel submerged in an appropriate solution.

4.4 Protein expression, refolding and purification

4.4.1 IGFBPs

The One Shot® BL21 Star™ (DE3) chemically competent cells were transformed with the plasmid DNA according to the protocol described above. Growth media contained kanamycin (for pET28a and pET41 Ek/LIC transformed cells) or ampicillin (for pGEX-4T-2 and pET46 Ek/LIC transformed cells) as selective antibiotics. Use of ampicillin as a selective antibiotic requires special care because β-lactamase is made in substantial amounts and is secreted into the medium, where it can destroy all of the ampicillin. In addition, ampicillin is susceptible to hydrolysis under acidic media conditions created by bacterial metabolism. It would not be feasible to add enough ampicillin to the medium to keep the cells under selection all the way to saturation. The pre-cultures were grown at 28 °C, to slow bacterial growth, for 12 h.

The overnight cultures of 10 ml were used as an inoculum for the 1litre culture. The cells were induced at OD_{600}=0.8-0.9 by addition of IPTG (1 mM final concentration) and cells were grown for the next 3 h with vigorous shaking at 37 °C. The cells were harvested by centrifugation (5500× g, 20 min, 4 °C). Bacterial pellets were resuspended in buffer A and left for solubilisation at room temperature overnight. The cell suspension was sonicated 4 minutes using a macro tip (output control 8, 60%) and centrifuged at 60000× g for 1 h at 18 °C. The resulting supernatant was incubated with a Ni-NTA slurry (Qiagen), equilibrated previously with buffer A for 1 h at room temperature with gentle agitation. Next, the mixture was loaded onto an empty column and washed with buffer A and B. The protein was eluted with buffer C. The fractions containing the desirable protein were pooled, concentrated and dialyzed against buffer D for removal of reducing agents. Subsequently, refolding of the protein was performed. For this purpose, the protein sample was stepwise diluted in buffer E in a 1:50 volume proportion. The refolding mixture was left with

stirring at 4 °C. After 3 days, the mixture was concentrated and dialyzed against a low salt phosphate buffer, and then was loaded onto a cation exchange column (Mono S). Bound proteins were fractionated with linear NaCl gradient. Fractions containing the protein of interest were pooled and dialysed against thrombin or Factor Xa cleavage buffers. Factor Xa digestion was performed for 72 h at room temperature in the 50 mM Tris buffer pH 8.0, 150 mM NaCl, 4 mM $CaCl_2$ using 1 U of the activated protease (Novagen) per 1 mg of the fusion protein. Thrombin cleavage was carried out in the same conditions; 2 U of thrombin (Sigma) was used per 1 mg of protein.

The proteins of interest were separated from the His-tag and protease by gel filtration on the Superdex 75 prep grade 26/60 HR column. The buffer used contained 140 mM NaCl, 2.7 mM KCl, 10 mM Na_2HPO_4, 1.8 mM KH_2PO_4, 0.05% NaN_3, pH 7.3.

4.4.2 CDK2, cyclin A2, p53, pRb and p27

The overnight culture of 10 ml was used as an inoculum for the 1 l culture. The cells were induced at OD_{600}=0.8-0.9 by addition of IPTG (0.5 mM final concentration) and cells were grown for the 18 h with vigorous shaking at 20 °C for CDK2. Cyclin A2, p53 (C-terminal domain), pRb (C-terminal domain) and p27 (N-terminal domain) were induced at OD_{600}=0.8 by addition of IPTG (0.5 mM final concentration) and cells were grown for 12-15 h with vigorous shaking at 18 °C. The cells were harvested by centrifugation (5500× g, 20 min, 4°C). The resulting supernatant, after lysis of the cells was incubated with a Ni-NTA slurry (Qiagen), (equilibrated previously with the lysis buffer of that particular protein) for 2 h at 4 °C with gentle agitation. Purification of the proteins under native conditions was done according to their respective buffers listed in the section 4.1.3. For CDK2 an additional cation exchange column (Mono S) was used for more purity.

4.4.3 GST purification of INCA1 and cyclin A2 (full length)

The purification protocol was similar to that of the shorter construct of cyclin A2. Only the resulting supernatant after lysis of the cells was incubated with GST-bed, which was pre-equilibrated with lysis buffer and kept for 5-6 h at 4 °C with gentle agitation. Proteins were further purified with the GST buffers listed in section 4.1.5.

4.5 Baculovirus expression system

Baculoviruses are the most prominent viruses known to affect the insect population. They are double-stranded, circular, supercoiled DNA molecules in a rod-shaped capsid. More than 500 baculovirus isolates (based on hosts of origin) have been identified, most of which originated in arthropods, particularly insects of the order Lepidoptera. Two of the most common isolates used in foreign gene expression are *Autographa californica* multiple nuclear polyhedrosis virus (AcMNPV) and *Bombyx mori* (silkworm) nuclear polyhedrosis virus (BmNPV). Wild-type baculoviruses exhibit both lytic and occluded life cycles that develop independently throughout the three phases of virus replication.

4.5.1 Baculoviruses as expression vectors

The major difference between the naturally occurring *in vivo* infection and the recombinant *in vitro* infection is that the naturally occurring polyhedrin gene within the wild-type baculovirus genome is replaced with a recombinant gene or cDNA. These genes are commonly under the control of polyhedrin and p10 promoters. During the very late phase of infection, the inserted heterologous genes are placed under the transcriptional control of the strong AcMNPV polyhedrin promoter. Thus, recombinant product is expressed in place of the naturally occurring polyhedrin protein. The following morphological changes are typical of monolayer *Sf* 9 cells infected with recombinant AcMNPV.

Early Phase: Infection begins with the adsorptive endocytosis of one or more competent virions by a cell in a high metabolic state (peak replication rate). The nucleocapsids pass through the cytoplasm to the nucleus. When the virions enter the nucleus, they release the contents of the capsid. Within 30 min of infection, viral RNA is detectable. Within the first 6 h of infection, the cellular structure changes, normal cellular functions decline precipitously, and early-phase proteins become evident.

Late Phase: Within 6 to 24 h after infection, an infected cell ceases many normal functions, stops dividing, and logarithmically increases the production of viral genome and budded virus. The virogenic stroma (an electrondense nuclear structure) becomes well developed. Infected cells increase in diameter and have enlarged nuclei. The cells may demonstrate reduced refractivity under phase contrast microscopy. Infected cultures stop growing.

Very Late Phase: Within 20 to 36 h after infection, cells cease production of budded virus and begin the assembly, production, and expression of recombinant gene product. In monolayer cultures, areas of infection display decreased density as cells die and lyse. Likewise, in suspension cultures, cell densities begin to decrease. Infected cells continue to be increased in diameter and have enlarged nuclei. The cytoplasm may contain vacuoles, and the nuclei may demonstrate granularity. As the infected cells die, plaques develop in immobilized cultures. The plaques can be identified under a microscope as regions of decreased cell density, or by eye as regions of differential refractivity.

4.6 Advantages of BEVS technology

More than 600 recombinant genes have been expressed in baculoviruses to date. Since 1985, when the first protein (IL-2) was produced in large scale from a recombinant baculovirus, use of BEVS has increased dramatically. Baculoviruses offer the following advantages over other expression vector systems.

• Ease of scale up: Baculoviruses have been reproducibly scaled up for the large-scale production of biologically active recombinant products.

• High levels of recombinant gene expression: In many cases, the recombinant proteins are soluble and easily recovered from infected cells late in infection when host protein synthesis is diminished.

• Accuracy: Baculoviruses can be propagated in insect hosts, which post-translationally modify peptides in a manner similar to that of mammalian cells.

4.7 *Sf* 9 cell line

The *Sf* 9 cell line is the traditional cell line used with baculovirus and originated at the USDA Insect Pathology Laboratory. The cell line originated from the IPLBSF-21 cell line, derived from the pupal ovarian tissue of the fall army worm *Spodoptera frugiperda*. It grows well in monolayer and suspension culture. The *Sf* 9 cell line is aclonal isolate of IPLBSF-21-AE. The cell line is suitable for transfection, plaque formation, plaque purification, generating high titre stocks and expression of recombinant proteins. The *Sf* 9 cell line is suitable for use in expressing recombinant proteins with

baculovirus and other insect expression systems. In our study this cell line was used for the expression of CDK6.

4.8 Generating a recombinant virus by homologous recombination

The most common baculovirus used for gene expression is AcMNPV. AcMNPV has a large (130-kb), circular, double-stranded DNA genome. The gene of interest is cloned into a transfer vector containing a baculovirus promoter flanked by baculovirus DNA derived from a nonessential locus-in this case, the polyhedrin gene. Transfer vector pAcG2T was used for the study. The vector is a derivative of the pAcCL29 vector. It has a GST tag. The cdk6 gene was amplified using 5'-*CGT AAC AGT TTT GTA ATA AAA AAC C*- 3'as forward primer and 5'-*CAA CAA CGC ACA GAA TCT AGA C*- 3' as reverse primer. The gene was then cloned in frame with the GST open reading frame using the restriction sites BamHI and EcoRI. The fusion protein was under the control of the strong AcMNPV polyhedrin promoter. The gene was transformed and amplified in *E. coli* strains using DH5α, under ampicillin selection and purified using the standard protocols mentioned above. For construction of recombinant virus a co-transfection of the purified recombinanat pAcG2T vector and linearized Baculovirus DNA [BacuGold^{TM} viral DNA (BD-Pharmingen)] was performed in the *Sf* 9 cell line using BaculoGold^{TM} transfection kit. BaculoGold^{TM} DNA is an engineered baculoviral DNA incorporating a lethal deletion. Co-transfection of the BaculoGold^{TM} DNA and a complementing baculovirus transfer vector restores viability by homologous recombination and rescues the virus along with the desired recombinant gene.

2×10^6 *Sf* 9 cells were seeded onto 60 mm tissue culture plates and allowed to adhere to the plate to form an adhesion culture. Initial cell density was 50% confluent. The medium of the culture was removed and 1 ml of transfection buffer A was added to the cells. Separately 0.5 μg of BaculoGold DNA (Pharmingen) and 8 μg of recombinant baculovirus transfer vector containing the insert were mixed well by vortexing and then the mixture was incubated for 5 min. 1 ml of transfection buffer B was added to the mixture. Medium was aspirated off from cells that were previously allowed to attach to the plate and replaced with 1 ml of the transfection buffer A. The previously prepared transfection buffer B/DNA mix was then added drop wise to the experimental cotransfection plate. After every 2 to 3 drops, the plate was gently rocked to mix the drops with the

medium and then the plates were incubated at 27 °C for 4 h. After 4 h the medium was aspirated and 3 ml fresh pre warmed SF 900 medium was added. The plates were then further incubated at 27 °C for 4-5 days, following which the plates were checked for signs of infection under a phase contrast microscope. Infected cells appeared larger with enlarged nuclei. The supernatant was then collected and assayed for cotransfection efficiencies by the end-point dilution assay.

4.9 Endpoint dilution assay (EPDA)

1×10^{6} *Sf* 9 cells per well were seeded and allowed to attach firmly on an 8-well EPDA plate. 1 μl, 10 μl, 100 μl, and 200 μl of the recombinant virus supernatant were then added to separate wells. All plates were incubated at 27 °C for three days. After incubation, infected cells were identified from uninfected once based on the enlargement of nucleus of infected cell. After the lysis was complete the cells and the supernatant was taken and centrifuged, which removed all the cell debris and only the viral DNA was left in the supernatant. This process was continued two to three times which usually gave a virus titer of 2×10^8 /ml virus particles.

4.10 Plaque assay for insect cells

1×10^{6} *Sf* 9 cells per well were seeded and allowed to attach firmly on a 10 cm plate. The old medium was changed and fresh medium was added. Dilutions typically, 0.1% to 1% of the resulting progeny were used to infect the cells. The recombinants were identified by altered plaque morphology.

4.11 Insect cell culture media commonly used in BEVS applications
Commonly used insect cell culture media are listed below.
- Grace's Supplemented (TNM-FH), Sf-900 II SFM
- IPL-41 EXPRESS-FIVE™ SFM
- Schneider's Drosophila

Liquid media contained photo labile components in the dark at 4 °C to 8 °C. Fetal bovine serum (FBS) has been the primary growth supplement used in insect cell culture medium. For BEVS applications, the early formulations were generally poorly defined and too rich in protein. Most

commercially available serum-free insect media are essentially simple variations of IPL-41 basal medium supplemented with undefined protein hydrolysates and a lipid/surfactant emulsion. Second-generation serum free formulations are Sf-900 II SFM and EXPRESS-FIVE™. SFM are specifically designed for large-scale production of recombinant proteins. They contain optimized concentrations of amino acids, carbohydrates, vitamins, and lipids that reduce or eliminate the effect of rate-limiting nutritional restrictions or deficiencies. Both Sf-900 II SFM and EXPRESS-FIVE SFM media support faster population doubling times and higher saturation cell densities than do traditional media. The optimized formulations offer the following advantages over sera:

- Eliminate the need for costly fetal bovine and other animal sera supplements.
- Increase cell and product yields.

4.12 SF 900 II SFM medium

It is a protein free medium without L-methionine and L-cystine. It is capable of supporting long-term cell growth (>20 passages). It is a protein free medium, which supports increased cell growth of a variety of insect cell lines as well as significantly increasing the production of recombinant proteins using the Baculovirus Expression Vector System. It is a serum free medium designed for growth of *Sf* 9 and other lepidopteran cell lines and production of insect virus and rDNA proteins. This medium contains a biologically active raw material, which is a critical growth-promoting component. We used this media for the growth of the *Sf* 9 cells.

4.13 Cell handling techniques

Passaging /subculturing refers to diluting cells back to a density that maintains log phase growth and maximum viability.

Adherent culture: Adherent cultures should be passaged at confluency and are typically diluted at a 1:5 dilution (volume of cells: final volume of medium) in order to maintain log phase growth.

Suspension culture: Suspension cultures should be passaged before they reach a density of 2.0 to 2.5×10^6 cells/ml. Floaters are a normal occurrence and are often seen in older cultures and

cultures, which have overgrown. Floaters are cells that are either loosely attached or suspended in the medium.

Viability: Cell viability refers to the percent of cells in a culture that are living. Trypan blue dye molecules are excluded from viable cell membranes, but readily enter non-living (viable) cells. Cells that are blue are dead.

Confluency: Confluency is a marker for when to subculture your cells. A confluent monolayer is an adherent cell culture in which the cells have formed a single layer over the entire surface area available for growth. Cells that are repeatedly passaged at densities past confluency display decreased doubling times, decreased viabilities, and a decreased aluility to attach. The culture is considered to be unhealthy. Cell cultures that have not reached confluency are more difficult to dislodge, and require more mechanical force to dislodge them form the monolayer. When repeatedly subcultured before confluency cells display-doubling times and decreased viabilities.

Log phase culture: Cells in log phase are optimal for transfections, plaque assays, generating high–titer stocks, expression studies, and seeding suspension cultures. Cells that are dividing every 18-72 hours and are 95% or greater in viability are considered to be in log phase.

Growth temperature: Cells should be maintained at 27 °C in a non-humidified environment. Fresh cell culture medium should be equilibrated to room temperature before use. Insect cells will begin to show increased doubling times at temperatures between 27 °C and 30 °C. Above 30 °C cells may display decreased viabilities.

Procedure: While removing medium from a plate containing a cell monolayer the plate was tilted at a 45° angle so that medium flows to one edge. Aspirated the medium completely using a pipette. Carefully and slowly added the medium against the side edge of the plate. To disperse cells, the flask was plated slowly by hand forward and backward, then side-to-side. This was repeated four times, so that the liquid reached all areas of the growth surface. For addition and removal of medium (flasks and plates) from a flask of cells, the flask was tilted so that the entire medium flows to one corner, away from the cell monolayer. Medium was carefully removed with a pipette. During addition of the medium, same process was repeated.

4.14 Initiation of cell culture from the frozen stock

Removed vial of cells from dry ice and placed in a 37 °C water bath. Thawed rapidly with gentle agitation. Removed the cells from the water bath. Decontaminated the outside of the vial by treating with 70% ethanol. Dried the vial and placed on ice. Pre wet a 75 cm^2 flask by coating the adherent surface with 8 ml of SF 900 II medium with a 5% of FBS (fetal bovine serum). Transferred the 1 ml cell suspension directly into the medium. Transferred flask to a 27 °C incubator and allowed the cells to attach for 30-45 min. After the attachment of the cells the medium was removed. This was done to remove the DMSO from the freezing medium. 10 ml of fresh medium was added. After 24 h, the medium was changed. Viability of the cells was counted. Continued to incubate until the cells have formed a confluent monolayer. Adherent culture: Checked cells daily until a confluent monolayer had formed. The cells were passaged at confluency. Repeated subculturing of cells at densities past confluency would result in decreased doubling times and decreased viability. Log phase growth could be maintained by splitting cells at a 1:5 dilution. After 30 passages cells lose their viability and infectivity. Dislodged monolayers in adherent cell culture by tapping the flask until monolayer loosens.

Suspension culture: Log phase adherent cells were grown to start the spinner of desired size with 1×10^6 cells/ml. The cells were removed from flasks, counted and checked for viability, which was 95%. Incubated the spinner flask at 27 °C with constant stirring at 100 rpm. When the cells reached a density of about $2\text{-}2.5 \times 10^6$ cells/ml that was usually after 24 h, fresh medium was added to dilute their density back to 1×10^6 cells/ml. Cells were checked daily for density and viability. A spinner flask with a vertical impeller was used. The vertical impeller provides better aeration. The impeller was submerged 1 cm into the medium to ensure adequate aeration. The total culture volume in a spinner should be ½ the indicated volume of the spinner for proper aeration. The addition of medium was sufficient to replenish cell nutrients. Cell viability of 95% or more was required for high yield of protein.

4.15 Purification of CDK6

The *Sf* 9 cells were grown to a count of 2×10^6 cells/ml. The culture was infected with 10 ml of the viral titer (0.05×10^{-3}/ml) for 1 litre culture. Cells were harvested after 58 h of infection and lysed with Modified Buffer, pH 8.0,

71

$$50 \text{ mM } Na_2HPO_4$$

$$250 \text{ mM NaCl}$$

One cocktail protease inhibitor tablet (Roche), for 50ml of buffer was used.

For 1 l culture, 30 ml of the modified buffer was used to lyse the cells. Cells were sonified in the macro tip of the sonicator machine with a duty cycle of 65, output: 8, time: 30 s and a cooling time of 1 min. The procedure was repeated for 4 times. Centrifuged the sample in 75,000× g for 2 hours. The pH of the lysate was adjusted to 8.0. GST bed was equilibrated with Modified PBS buffer, pH 8.0,   140 mM NaCl

$$10 \text{ mM } Na_2HPO_4$$

$$2.7 \text{ mM KCl}$$

$$0.05\% \text{ } NaN_3$$

Lysate was kept in the GST bed for binding for 2 hours. The bed was washed with Modified PBS buffer. After 4 washes, thrombin was added in the bed. Stock concentration of thrombin was 2.5 U/ml, and 20 units were added. After 4 h of cleavage the protein was eluted with the PBS buffer. The protein was concentrated down to 5 ml and loaded on Superdex 75 column for gel filtration and eluted with the gel filtration buffer, pH 8.0,

$$280 \text{ mM NaCl}$$

$$10 \text{ mM } Na_2HPO_4$$

$$2.7 \text{ mM KCl}$$

4.16 Determination of protein concentration

The concentration of proteins in solution was estimated by means of the Bradford colorimetric assay. 5 μl of the protein sample was added to 1 ml (10 × diluted stock) Bradford reagent (Bio-Rad). After gentle mixing, it was measured at A_{595} and converted to the protein concentration on the basis of a calibration curve prepared for known concentrations of BSA. A precise protein concentration determination was performed spectrophotometrically. Absorption at 280 nm was measured and converted to the protein concentration on the basis of theoretical extinction coefficients.

4.17 Protein crystallization

4.17.1 (NBP-4/IGF-I) complex

 The binary (NBP-4/IGF-I) complex was prepared by mixing equimolar amounts of the respective components. The complexes were separated from any excess of either protein by gel filtration on the Superdex 75 prep grade 26/60XR column. The buffer used contained 5 mM Tris, pH 8.0, 50 mM NaCl and 0.01% NaN_3. Initials screening of crystallization conditions for NBP-4(3-82)/IGF-I, binary complex yielded 3 hits. The X-ray quality crystals were obtained from 23% PEG 1500, 25 mM Tris pH 7.8. They appeared in several days and grew to a final size of ca. 0.4×0.2×0.2 mm. Crystals of NBP-4 (1-92)/IGF-I was grown from the Index solution 74 (0.2 M lithium sulfate monohydrate, 0.1 M Bis-Tris pH 5.5 and 25% w/v PEG 3350). The optimization of the conditions was achieved by dilution of the original solution by the factor of 1/16, 1/8 and 1/4, varying the size of drops and the ratios of protein and precipitant. Large, up to 0.8 mm, long plates or plate cluster crystals grew throughout the range of these conditions.

4.17.2 14-3-3σ crystals

Initial screening for crystals was performed with Crystal Screen I and II (Hampton Research). Crystallization of the protein was carried out with the sitting drop vapor diffusion method. The protein crystallized under many different conditions, however it was difficult to obtain well-diffracting crystals. The best crystals were obtained from 40 % PEG 4000, 0.6 M ammonium sulfate and 0.1 M Tris pH 9.0 after micro seeding. They appeared after several weeks and grew to a final size of ca. $0.3 \times 0.2 \times 0.1$ mm. Crystals were flash frozen after soaking for ca. 30 sec in a drop of a reservoir solution containing 30% (v/v) glycerol as a cryoprotectant. The crystals belong to the space group $P2_12_12_1$ with unit cell dimensions a =71.65 Å, b = 80.85 Å, c = 99.13 Å and contained one dimer molecule per asymmetric unit.

4.18 Data collection and molecular replacement

4.18.1 NBP-4 (3-82)/IGF-I: Prior to plunge freezing, the crystals of the NBP-4 (3-82)/IGF-I binary complex were soaked for ca. 30 s in a drop of a reservoir solution containing 15% v/v ethylene glycol as cryoprotectant. The crystals belonged to the space group $P2_12_12_1$ and contained

one complex per an asymmetric unit. A lower-resolution dataset (up to 2.1 Å) was collected from a plunge frozen crystal at a rotating anode laboratory source. The high-resolution dataset up to 1.6 Å was collected on the MPG/GBF beamline BW6 at DESY, Hamburg, Germany. Collected data were integrated, scaled and merged by XDS and XSCALE programs (Kabsch, 1993). The structure was determined by molecular replacement using the Molrep program from the CCP4 suite (CCP4, 1994). The structure of the complex of IGF-I and a fragment of the N-terminal domain of IGFBP-5 (miniNBP-5, PDB entry 1H59) was used as a probe structure (Zeslawski et al., 2001). Rotation search in the Patterson space yielded one peak of height 7.56 σ over the highest noise peak of 3.75 σ. Translation search gave a 16.28 σ peak over the noise height of 9.49 σ. The initial R-factor of the model was 0.49. At this stage the free atom model improvement was performed using Arp/wArp (Perrakis et al., 2001). As the next step an iterative model building was performed using Arp/wArp (Perrakis et al., 1999). The initial model consisted of 137 residues and was completed and revised manually using Xfit software (McRee, 1999). Arp/wArp was used to add solvent atoms (Lamzin et al., 1993).

Table 1. Data collection statistics

Space group	$P2_12_12_1$
Cell constants (Å)	a=34.47, b=54.28, c=74.55
Resolution range (Å)	37-1.6
Wavelength (Å)	1.542, 1.05
Observed reflections	86,002
Unique reflections	17,605
Whole range	
Complete (%)	92.1
R_{merge}	4.4
$I/\sigma(I)$	16.86
Last shell	
Resolution range (Å)	1.6-1.7
Completeness (%)	76.9
R_{merge}	17.8
$I/\sigma(I)$	5.45

The native and derivative datasets were collected at the BW6 beamline in DESY, Hamburg. The structure was refined by the Refmac5 program (CCP4, 1994). Final electron density maps were of high quality; there were no interpretable densities for side chains of residues Glu 11, Arg16,

Leu42, Glu66 and Glu81 of NPB-4 and Lys27, Arg37, Arg50 of IGF-I. These side chains were removed from the model. The final R crystallographic factor was 0.186 and R_{free} 0.2582.

4.18.2 14-3-3σ protein

A 2.8 Å dataset was collected on the MPG/GBF beamline BW6 at DESY, Hamburg, Germany. Diffr -action data for the structure refinement was collected at 90K. Diffraction images were acquired with MARCCD detectors. The summaries of the data collection and refinement statistics are presented in the results and discussion part of the thesis. The collected data were integrated, scaled and merged by XDS and XSCALE programs (Kabsch, 1993). The structure was determined by molecular replacement using the Molrep program from the CCP4 suite. The structure of the 14-3-3σ isoform taken from the PDB entry 1QJB (Rittinger et al., 1999) was used as a probe structure after removing the phosphopeptide part. The initial R-factor of the model was 0.46. The model was then refined by Refmac5 and rebuilt by XtalViev/Xfit (McRee, 1999). Water was added by Arp/warp (Lamzin et al., 1993). The final R crystallographic factor was 0.22 and R_{free} 0.31. Most of the model had clear interpretable electron density, however, the loop regions of Glu71A-Lys77A, Ser210A-Asp212A and Glu72B-Gly73B had no interpretable density as well as certain solvent exposed side-chains, and those parts were omitted in the model.

4.19 NMR–experimental procedure

^{15}N uniformly labeled or ^{15}N specifically labeled Lysine samples were recorded at 300 K on a Bruker DRX 900 and 600 MHz spectrometer equipped with a cryoprobe. The NMR samples contained 0.3 mM of protein in 140 mM NaCl, 10 mM Na_2HPO_4, 2.7 mM KCl, 5 mM DTT, pH 7.5. For the spectras, a total of 1024 complex points in t_2 and 128 t_1 increments were acquired. Water suppression was carried out using the WATERGATE sequence. NMR datas were processed using the Bruker program Xwin-NMR version 3.5.

4.20 Isothermal titration calorimetry

All experiments were carried out according to the references provided by the manufacturer. Proteins (IGFBPs their separate domains and IGF-I) were used at 0.25-0.4 mM in PBS (140 mM NaCl, 2.7

mM KCl 10 mM Na_2HPO_4, 1.8 mM KH_2PO_4, 0.05 NaN_3, pH 7.3) and titrated from a 300 µl syringe into a sample chamber holding 1.43 measurements. Heat generated by protein dilution was determined in separate experiments by injecting protein solution into PBS filled sample chamber. All data were corrected for the heat of protein dilution. All data were corrected for the heat of protein dilution. Data were fitted using χ^2 minimization on a model assuming a single set of sites to calculate the binding affinity K_D except for tirations involving the NBP-4-IGF binary complex with CBP-4, where only a 2 binding site model could be applied. All steps of the data analysis were performed using ORIGIN (V 5.0) software provided by the manufacturer. The details of the experimental and injection parameters are described below.

Table 2. Parameters of the experiments

Total number of injections:	58
Volume of single injection [µl]:	05
Duration of an injection [sec]:	10
Intervals between injections [sec]:	400
Filter period [sec]:	02
Equilibrium cell temperature [°C]:	20
Initial delay [sec]:	60
Reference power [µCal/sec]:	15
Stirring speed [RPM]:	270

4.21 CD spectroscopy

All experiments were carried out in the JASCO J-175 CD spectrometer according to the references provided by the manufacturer. Proteins CDK2 and p27 were used at 5.8 mM concentration in PBS buffer containing 140 mM NaCl, 2.7 mM KCl, 10 mM Na_2HPO_4, 1.8 mM KH_2PO_4, pH 7.5.

Table 3. Parameters of the experiments

Band width	1.0 nm
Response	1 sec
Sensitivity	standard
Measurement range	260-195 nm
Data pitch	0.1 nm
Scanning speed	50 nm/min
Accumulation	4
Cell length	0.1cm
Temperature	21.92 ºC
Concentration of protein	0.2 mg/ml

5. Results and Discussion

A starting point in the design of a purification workflow is learning about properties of a protein of interest, such as its theoretical isoelectric point (pI), molecular mass (MW) and from the extinction coefficient at 280. This information can be deduced solely on the basis of the amino acid composition with the aid of an Internet engine, ProtParam on www.expasy.ch, for instance. Examination of already existing methods of purification of similar or homologous proteins can yield important information. Closer examination of the proteins' amino acid sequence may reveal potential cleavage/degradation sites.

With the knowledge of pI value a proper buffer and ion-exchanger (cation or anion exchanger) media combination can be chosen. It is common that a protein of an acidic pI would bind to a cation-exchanger resin at pH > pI. This can be observed for CDK2, which can bind Mono S medium in a buffer of pH 7.5. Masses of all proteins discussed in this work fall between fractionation ranges of the Superdex 75 resin, i.e. 3000-75000 Da. A known extinction coefficient of a protein enables quick estimation of the yield on the basis of the elution profile (height and area of the peak) monitored at a given wavelength.

Presence of the 6-His-tag in some of the expressed proteins enabled us to use the nickel affinity chromatography under reducing conditions. The pH of a supernatant prepared was adjusted to 7.0-7.5 with 1 M NaOH. Ni-NTA slurry was added and binding was performed for 1-2 h with agitation. The ratio of the Ni-NTA matrix used to the amount of the His-tagged protein is crucial for purity of the protein. It is more reasonable to use less resin and perform a stepwise elution to obtain a pure, concentrated protein in a much shorter time.

A high-resolution chromatographic medium, Mono S, was used at a second purification step in case of some proteins. Monodispersive, 5 μM beads support a large protein binding capacity, ranging up to 20 mg/ml, assured excellent resolution of absorbed proteins. Bound proteins were fractionated with a linear NaCl gradient.

This final step of purification is the gel filtration which, enabled separation of the proteins from digested tag peptides and the restriction protease used for tag cleavage. Complete exchange of the buffer was also possible, removing any low molecular weight substances, which could interfere with NMR measurements (such as Tris, EDTA, protease inhibitors, glycerol etc.) The 320-ml

Superdex 75 prep grade column is characterized by good resolution in the range 3-70 kDa. To make the best of its capability, low flow rates (0.75-1.25 ml/min) were used and samples not larger than 6 ml were loaded on the column.

To qualitatively assess binding activity of the purified proteins, an analytical-scale gel filtration-binding assay was carried out. The proteins were mixed in approximately equimolar ratios and separated on an analytical 23 ml Superdex 75 column. Different combinations of the proteins were examined to cover all possible interactions. To observe the formation of a stable protein complex in a gel filtration experiment, binding must occur with at least medium-low micromolar affinity. Higher K_D values cause the complex to dissociate on the column. Possible weak interactions between domains of proteins could not be therefore ruled out on the basis of this experiment. NMR spectroscopy was therefore used to address this problem, as NMR can detect even very weak interactions (i.e. in the millimolar range).

5.1 Experiments with CDK6
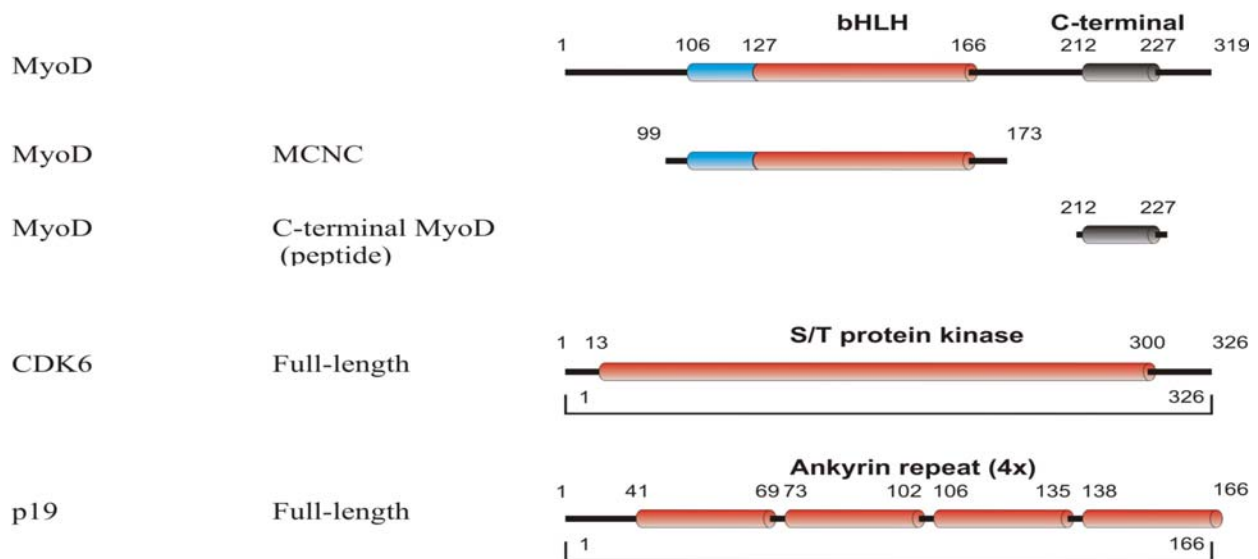
MyoD peptide sequence (human):   212-YSGPPSGARRRNCYEG-227

MyoD peptide sequence (chicken):   189-YSGPPCSSRRRNSYDS-204

Fig. 1. Schematic diagram of the constructs used in the experiments.

The full-length CDK6 was expressed in baculovirus and p19 was expressed in *E. coli*. The proteins CDK6 and p19 gave typical NMR intensity patterns of folded proteins Fig. 1. CDK6 forms a complex with p19 as shown by gel filtration chromatography and SDS-PAGE (Fig. 2A and 2B). The CDK6 protein was stable for weeks in 4 ºC.

Crystallization trials were performed to crystallize CDK6 alone in different buffer conditions. But no X-ray quality crystals of the protein were obtained. We concluded that the flexible loops cause hindrances in crystallization and this might be the reason why all the crystal structures of CDK6 were solved with its binding partners. The binding partners help in stabilizing the loops.
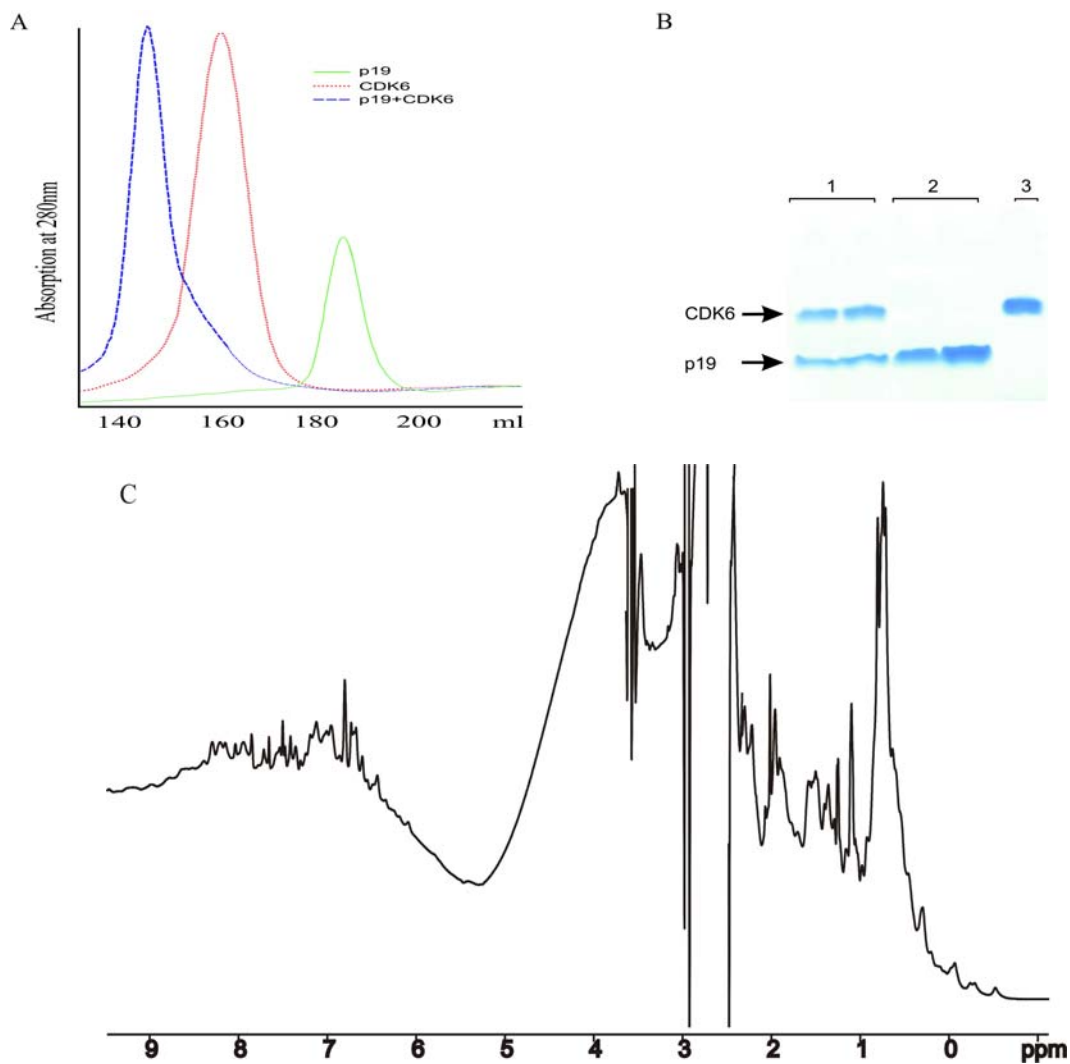
Fig. 2. A. The monitoring of formation of protein-protein complexes by gel filtration chromatography, CDK6-p19 complex (dash line), CDK6 alone (dotted line) and p19 alone (straight line). *B.* Shows the SDS-PAGE analysis of chromatography fractions. The lane marked 1 shows CDK6-p19 complex, lane marked 2 show p19, and lane marked 3 shows only CDK6. *C.* 1D proton spectrum of CDK6.

Mouse CDK4 and CDK6 were reported to interact with the C-terminal part of chicken MyoD (Zhang et al., 1999). We therefore tested the binding of the human and chicken MyoD, C-terminal 15-amino-acid peptides with CDK6 by the affinity chromatography pull-down assays, NMR spectroscopy, and gel filtration chromatography, followed by mass spectrometry.

In our affinity chromatography pull-down assays, GST-CDK6 served as the bait and the MyoD-C peptides as the prey. MyoD-C did not elute together with GST-CDK6. This indicated no binding between these two components. Both human and chicken MyoD-C peptides were titrated with CDK6 and no changes in peak positions were observed in the 1D proton NMR spectra, indicating that there is no interaction between the C-terminal part of MyoD and CDK6 (Fig. 3A and 3B).
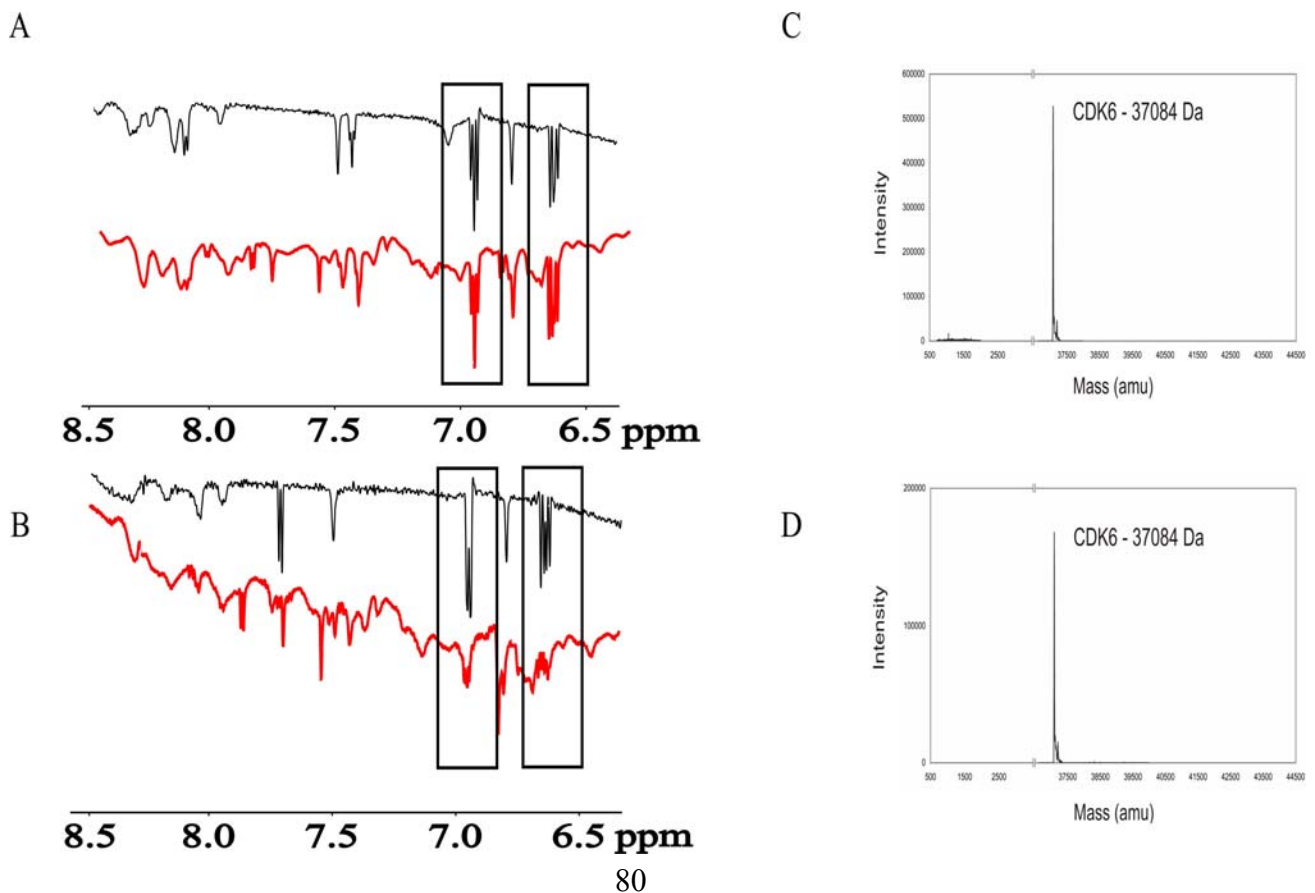
Fig. 3A & 3B. 1H proton NMR spectra of the human *(A)* and the chicken *(B)* C-terminal MyoD peptide, alone (black) and mixed with CDK6 (gray). Peptides were resuspended in modified PBS and pH was adjusted to 8.0. They were mixed with CDK6 in molar ratios of 1:1 *(A)* and 1:4 *(B)* (peptide:CDK6). Both MyoD peptides had two Tyr residues in position 1 from the N-terminal and position 3 from the C-terminal (sequences of peptides). The resonances of the aromatic protons of Tyr are highlighted by boxes. No changes in relative peak positions and intensities were observed, which means that the environments of these residues were unchanged. There was no interaction between the C-terminal MyoD peptides and CDK6. *3C & 3D.* Mass spectroscopy results: *C.* the gel filtration chromatography purified sample of mixture of 1:1 CDK6 with the C-terminal MyoD peptide and *D.* the detectable protein corresponds to CDK6 only.

After gel filtration chromatography of an equimolar mixture of human CDK6 and human or chicken MyoD-C peptides, the fraction corresponding to the CDK6 peak was examined by mass spectrometry for the presence of the MyoD-C peptide. Mass spectrometry showed the presence of only CDK6 (Fig. 3C & 3D). We concluded that there is no direct interaction between the C-terminal 15-amino-acid peptide of human (212-227) or chicken MyoD (189-204) and human CDK6 in vitro. Using the same biophysical methods, we were able to show the interaction between human p19 and human CDK6. Such cross-species interactions have high degree of uncertainty and do not necessarily represent physiological processes. The amino acid sequence of chicken MyoD that has been mapped for binding to mouse CDK4/6 differs substantially from that of human (Zhang et al., 1999). For example, cysteine residues that could be crucial for the interaction are situated at residues 6 and 13 in the human and chicken MyoDs, respectively. The closest homologs for the chicken and human MyoDs are *Xenopus borealis* and *Sus scrofa domestica* MyoDs, respectively. Human CDK4 and CDK6 are highly homologous proteins with a sequence homology of 71.1% (Kopp et al., 2004). CDK4 and 6 have compensating functions in the cell cycle (Helin et al., 1992) but there are also reports suggesting different functions of these two kinases (Hu et al., 1990). MyoD is proven to enhance the expression of the CDK inhibitor p21, which is shown to target and inhibit CDK6–cyclin D complexes in growth-arrested cells (Morgan et al., 1997).

In summary, our results show that the C-terminal part of human and chicken MyoDs does not interact with human CDK6 in vitro. Indirect interactions, through additional binding partners in multiprotein complexes or modulation of gene expression levels of these proteins, are therefore their probable modes of action. Protein–protein interactions can also be influenced to certain extent by post-translational modifications. It is also possible that other regions of these proteins may be required to maintain an interaction with those additional binding partners.

5.2 Experiments with 14-3-3 sigma protein

For crystallization the human 14-3-3σ protein was expressed in *E. coli*. The protein eluted as a dimer on the Superdex 75 gel chromatography column (Fig. 4A) and the purity of the protein was examined by SDS-PAGE (Fig. 4B). Folding pattern of the purified protein was analysed by NMR spectroscopy. (Fig. 5). In order to further confirm the functional integrity of the recombinant 14-3-3σ protein, the direct binding of recombinant 14-3-3σ to BAD, a previously characterized interaction (Subramanian et al., 2001), was tested in an overlay assay (Fig. 4C). Recombinant 14-3-3σ was found to interact with BAD and with 14-3-3σ expressed in HEK293T cells, indicating that the recombinant 14-3-3σ protein employed here adopts a functional conformation which allows interaction with known interacting proteins.
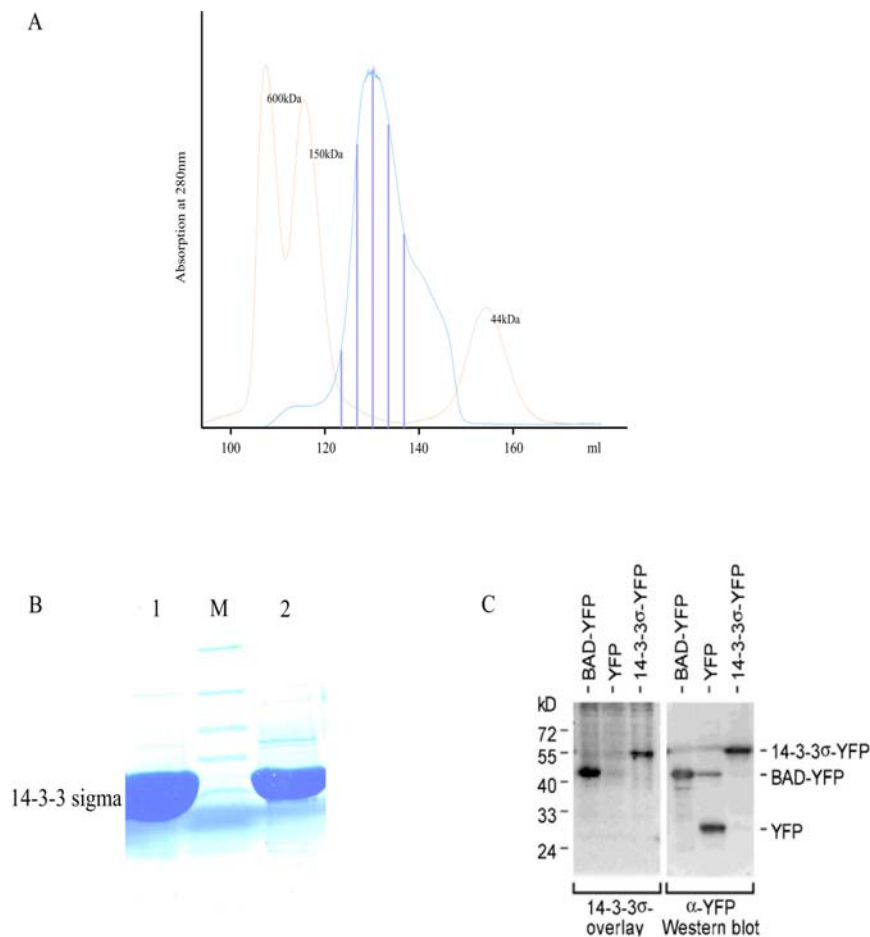
Fig. 4. A. Chromatogram showing the elution profile of the 14-3-3σ in the Superdex 75 gel chromatography column. *B.* The blue-striped portion of the eluted fractions were analysed with SDS-PAGE to check the purity of the protein. *C.* Binding of a bacterially produced 14-3-3σ to cellular BAD protein. HEK293T cells were transiently transfected with vectors encoding for YFP-tagged BAD (BAD-YFP) or 14-3-3σ (14-3-3σ-YFP) or a control vector (YFP) and harvested 24 h after transfection. 50 μg of total lysates were separated by SDS-PAGE, transferred to nitrocellulose membranes and incubated with DIG-labeled 14-3-3σ or anti-GFP antibodies.
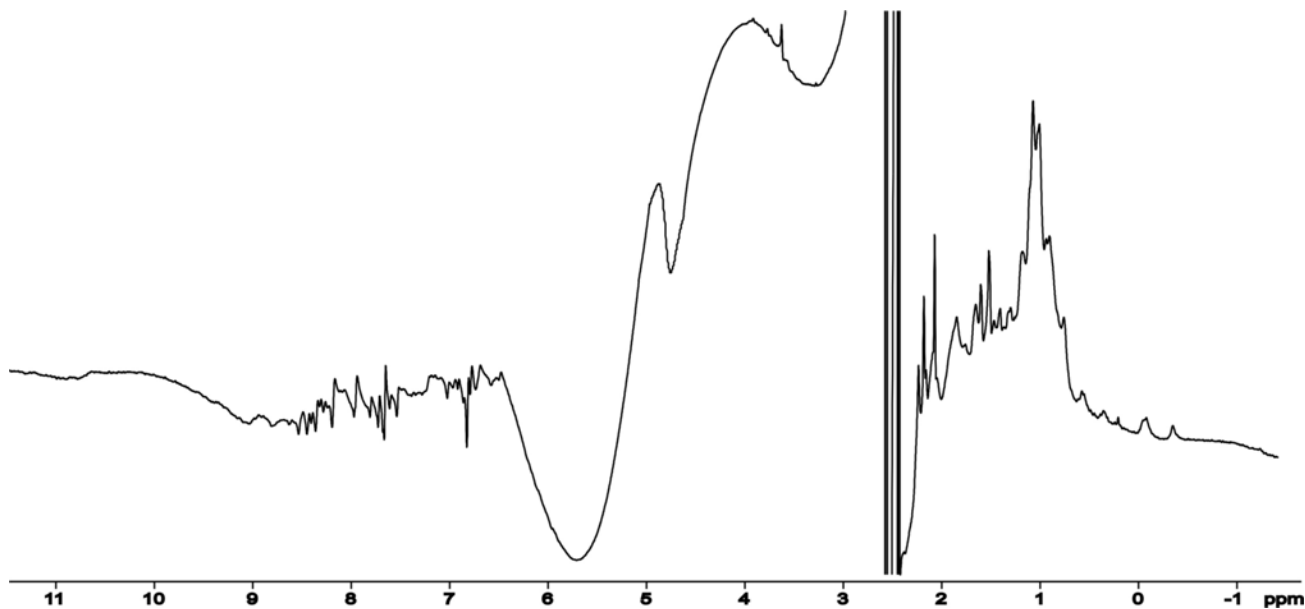
Fig. 5. 1D proton spectrum of the human 14-3-3σ protein showing the folded nature of the protein.

5.2.1 Crystal structure of the 14-3-3σ dimer

The structure of the 14-3-3σ dimer was solved by molecular replacement at a resolution of 2.8 Å. A ribbon plot of the 14-3-3σ structure is shown in Fig. 8 and details of data collection and refinement statistics are presented in Table 1. 14-3-3σ crystallized as a homodimer. Each monomer consists of nine anti-parallel helices forming an elongated bundle. The first four helices participate in the formation of the homodimer. The remaining five helices form a deep groove providing the phosphopeptide-binding site The overall root-mean-square-deviation (RMSD) between monomers calculated for the backbone atom is small (1.07 Å), but a clear difference is observed in the position of the ninth helix. This helix is shifted about 1.7 Å towards the ligand binding cleft in one monomer (chain A) compared to the second (chain B). As crystal packing probably causes this shift, it may indicate flexibility and adaptability of this region to structural changes that accompany ligand binding.
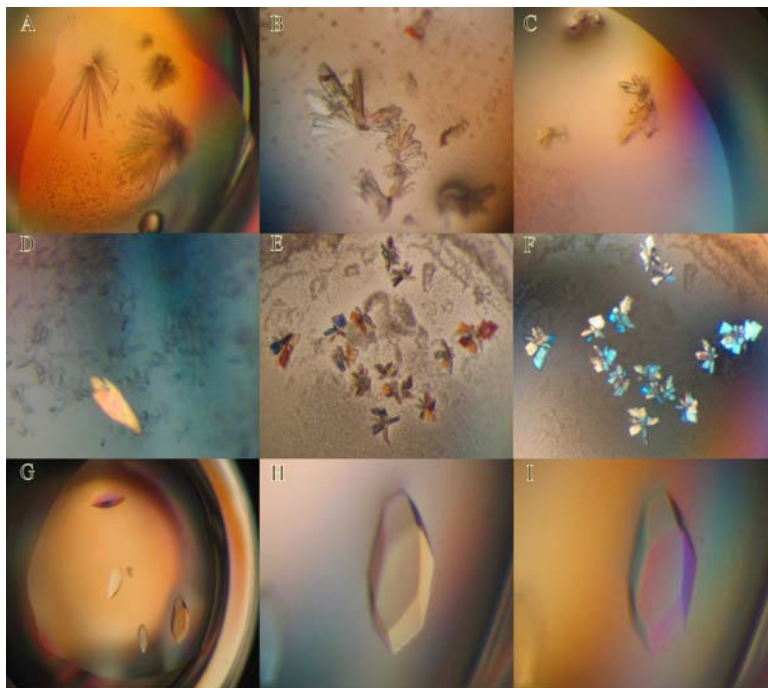
Fig. 6. Examples of the crystallization experiments. The protein crystallized under many different conditions, however it was difficult to obtain well-diffracting crystals. The best crystals were obtained from 40 % PEG 4000, 0.6 M ammonium sulfate and 0.1 M Tris pH 9.0. They appeared after several weeks and grew to a final size of ca. 0.3 × 0.2 × 0.1 mm. Crystals were flash frozen after soaking for ca. 30 sec in a drop of a reservoir solution containing 30% (v/v) glycerol as a cryoprotectant. The crystals belong to the space group P212121 with unit cell dimensions a =71.65 Å, b = 80.85 Å, c = 99.13 Å and contained one dimer molecule per an asymmetric unit.
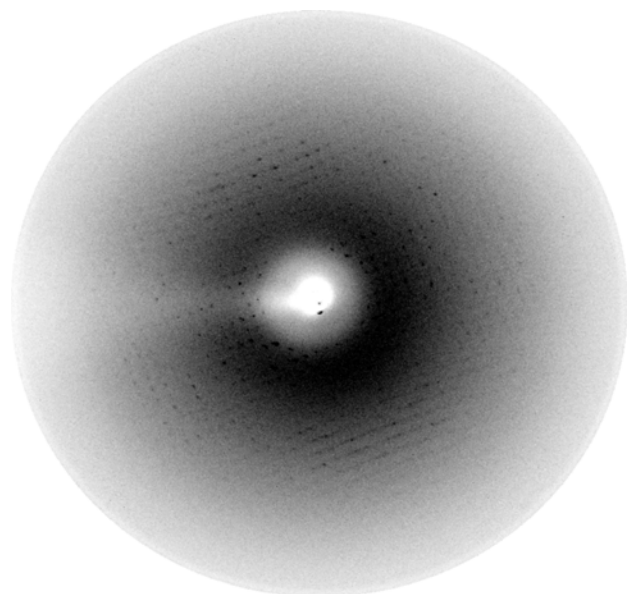
Space group	$P2_12_12_1$
Cell constants (Å)	a = 71.650
	b = 80.850
	c = 99.130
Resolution range (Å)	30-2.8
Wavelength (Å)	1.05
Observed reflections	124574
Unique reflections	19297
Completeness (%)	99.4
R_{merge}	4.5
I / σ(I)	11.8
Last resolution shell:	
Resolution range (Å)	2.85-2.8
Completeness (%)	95.9%
R_{merge}	27.4
I / σ(I)	4.9

Fig. 7. Diffraction pattern of crystals of the 14-3-3σ frame from the MAR CCD165 (BW6, DESY, Hamburg) and the table represents the data collection and refinement statistics.
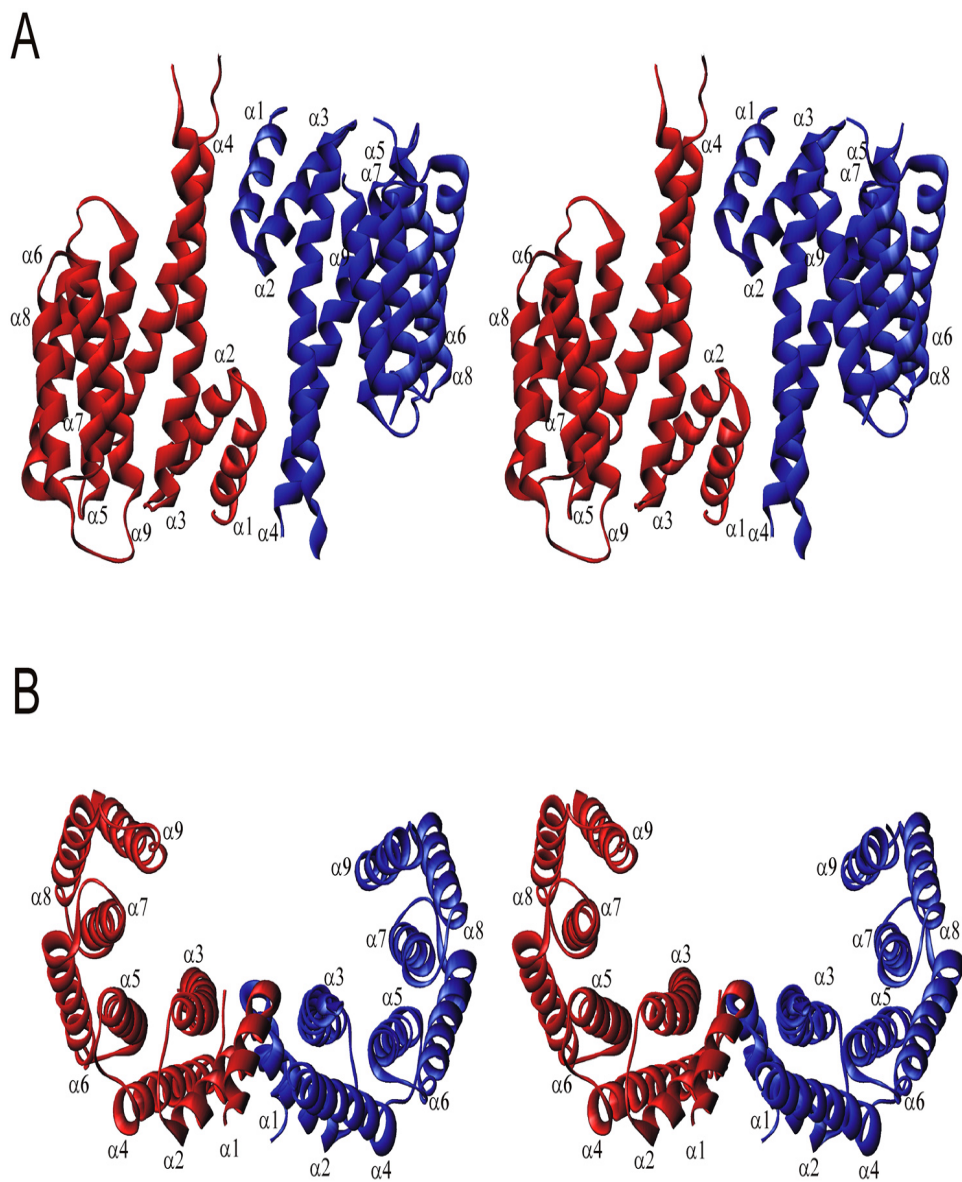
Fig. 8. An overall ribbon plot of the 14-3-3sigma homodimer. Each monomer consists of nine antiparallel helices and the protein dimerizes in a perfect 2-fold symmetry. The dimer forms a large cup-shaped space between monomers with two phosphopeptide binding sites at its sides. The C-terminal helix of the monomer A (blue) is significantly shifted toward the binding site; chain B is shown in dark-red. *A.* A view perpendicular to the helices axis is presented. *B.* A view parallel to this axis.

5.2.2. Structural comparison of 14-3-3σ, τ, and ζ

We compared our structure of 14-3-3σ to the previously published structures of 14-3-3ζ and 14-3-3τ (Yaffe et al., 1997; Liu et al., 1995; Obsil et al., 2001, Xiao et al., 1995). Only the structure of 14-3-

3ζ solved by Liu *et al* was determined in an unliganded form, i.e. in the same state as 14-3-3σ determined here. The two additional structures of 14-3-3ζ and 14-3-3τ were determined bound to a phosphopeptide or a sulfate group, respectively. In addition, the structure of 14-3-3ζ has the same overall fold compared to the published structures of the ζ and τ isoforms (Obsil et al., 2001). The structure of 14-3-3σ has the same overall fold as the known fold of the ζ and τ isoforms (Fig. 9).
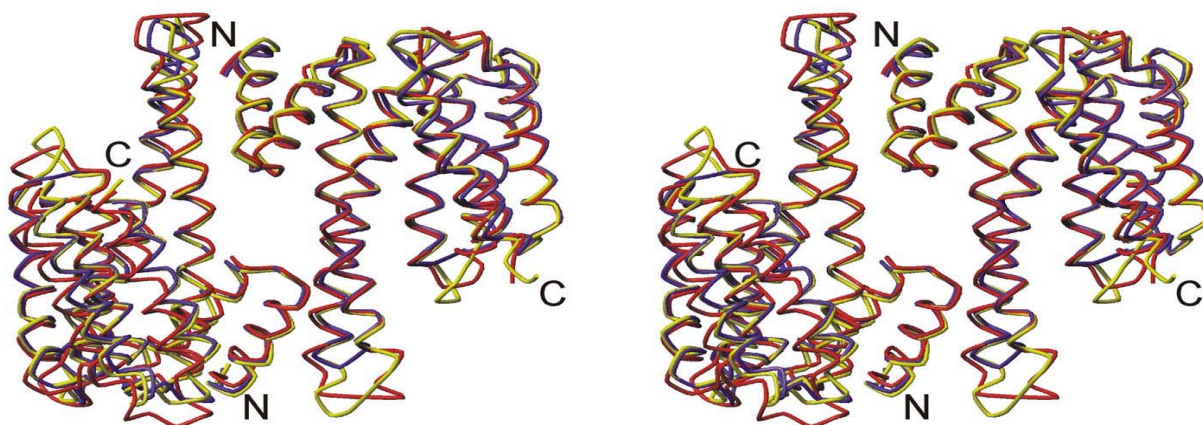
Fig. 9. Comparative superposition of 14-3-3σ, ζ and τ. This main chain trace representation shows 14-3-3σ in red, 14-3-3ζ in blue and 14-3-3τ in yellow. RMSD between 14-3-3σ and 14-3-3ζ for backbone atoms are 1.15 Å, between 14-3-3σ and 14-3-3τ 1.18 Å and between 14-3-3ζ and 14-3-3τ 0.71 Å.

The interface mechanism responsible for dimerization is identical for the three 14-3-3 isoforms. Most residues not conserved between isoforms are localized on the outer surface of the molecule, while the phosphopeptide-binding cleft is highly conserved (Fig. 10). The dimerization surfaces of the 14-3-3σ, ζ, and τ isoforms display several differences, which may alter the binding constant of different isoform combinations and result in limited heterodimerization among the isoforms (Fig. 11 and: residues in red): the most significant changes between the σ isoform and the two other isoforms are Ser5(σ)-Glu5(ζ, τ), Glu20(σ)-Asp20 (ζ, τ), Phe25(σ)-Cys25(ζ, τ), Gln55(σ)-Arg55(ζ, τ) and Gln80(σ)-Met78(ζ)-Leu(τ). In the 14-3-3τ isoform the loop Glu131-Thr141 has adopted a different main chain conformation than in 14-3-3σ and ζ, however, these loop residues have the same character and it is unlikely that they affect 14-3-3 dimerization.

The most significant difference between the structures of 14-3-3 isoforms solved so far and our structure of 14-3-3σ is seen in the configuration of the loop located between Ala203 and Asp215

(Fig. 11). This component of the structures is in "an open conformation" relative to the ligand binding site in 14-3-3σ and has a different position when compared to the peptide/small molecule bound 14-3-3ζ and τ isoforms and also a different fold in the 14-3-3ζ serotonin N-acetyltransferase complex. The movement of this fragment is large between the 14-3-3σ and the peptide bound 14-3-3ζ structures (about 4.2 Å between Cα of Ser207ζ and Ser209σ).
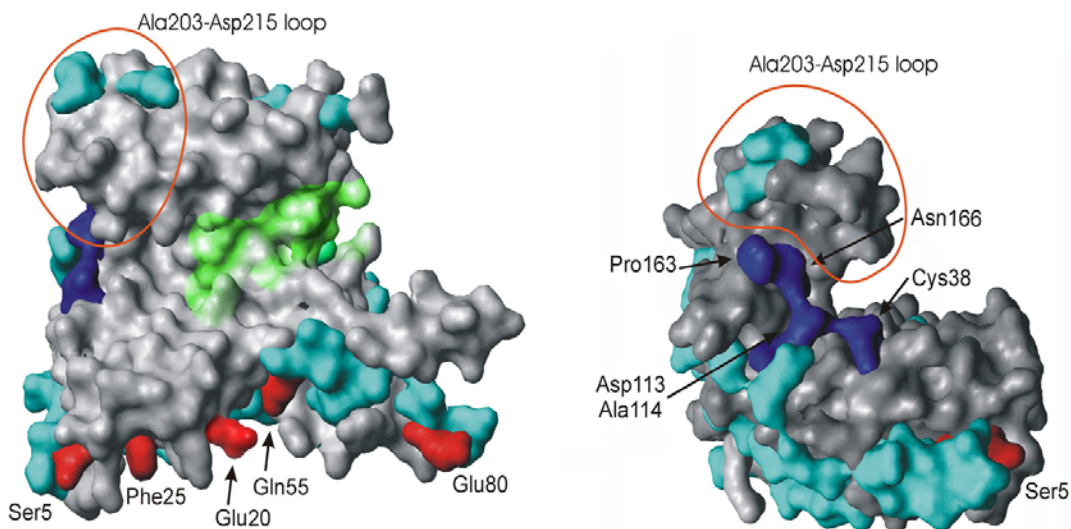

Fig. 10. Comparative, structural analysis of phosphopeptide binding and dimerization interfaces in 14-3-3 proteins. Surface plot of the 14-3-3σ monomer. Residues belonging to the dimerization surface that differ significantly from other isoforms are shown in red. Residues forming the edge of the peptide binding site which differ from the 14-3-3τ and ζ isoforms are shown in dark blue. Other non-conserved residues are shown in green whereas conserved parts are in gray. The Ala203-Asp215 loop has been marked by a circle (in red line). The phosphopeptide binding region is highlighted in light green.

In the structures of the 14-3-3ζ and τ isoforms this loop partly folds upon itself producing "a closed conformation". In the structure of 14-3-3ζ bound to serotonin N-acetyltransferase, the C-terminal portion of the loop is pushed away from the (Obsil et al., 2001) phosphopeptide binding cleft by the intruding serotonin N-acetyltransferase molecule PDB 1IB1). The long axis of the loop, which runs from Ala203 to Asp215, is rotated 90° relative to the position of this axis in 14-3-3σ. Taken together, the leading difference among the 14-3-3 isoforms is seen in the position of loop 203-215 relative to the phosphopeptide binding site in 14-3-3 structures. These differences suggest that this area is the major ligand-specificity region. In the 14-3-3σ structure this loop is well determined in one monomer (chain B), and partially defined in the other (chain A, no electron

density was seen for tip residues Glu210-Ser212). However, in the parts of the chain A loop with interpretable electron densities the fold of the loop is identical in both monomers, indicating that this difference is not caused by crystal packing as each monomer is in a different environment. In the only other structure of a completely free 14-3-3, the ζ isoform presented by Liu *et al*, this segment of the structure is missing. Our data and the structure determined by Liu *et al* indicate that this loop might be flexible. This feature however would not interfere with its proposed function of a major ligand-specificity region, which utilizes both sequential and structural diversities of this region to select for isoform-specific binding partners.
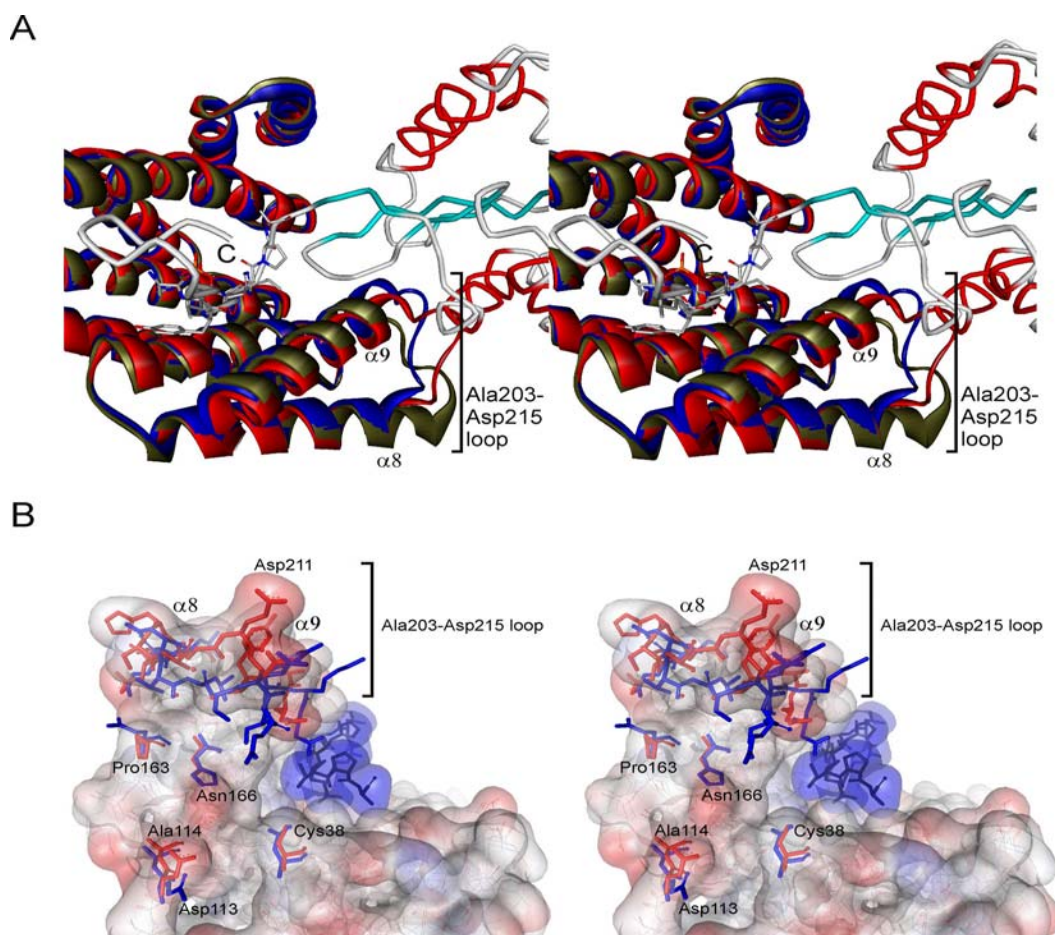
Fig. 11. Ligand recognition by 14-3-3 proteins. *A*. Unbound σ (red) and ζ (blue) are superimposed with the structure of the zeta isoform (green) bound to serotonin N-acetyltransferase (Cα trace) to indicate the structural diversity of the Ala203 and Asp215 loop area. *B*. Structures of ζ (blue) and σ (red) are overlaid. The molecular surface of the sigma isoform is shown half-transparent. The structure and surface of the phosphopeptide from the 1QJA model is shown in light blue. Non-conserved residues in this area are labeled for the sigma isoform. Significant difference in the Ala203 and Asp215 loop are evident.

The most significant divergence in amino acid types towards other 14-3-3 isoforms is seen in the same area: at the edge of the phosphopeptide-binding groove at the 14-3-3-residues marked in blue in Fig. 12. This part has a strictly preserved backbone structure among the 14-3-3 proteins and is in a significant distance (ca. 20 Å) from the primary phosphoserine binding site. Since structural properties of the binding site are analogous for the isoforms for which structures have been determined, the specific amino acids in this part are also prime candidates for determining the isoform-specificity towards ligands. The most important changes in amino acid character in this region are: Asn166(σ)-His164(ζ, τ), Pro163(σ)- Gln161(ζ, τ), Cys38(σ)-Asn38(ζ, τ), Asp209/211 (σ, τ)-Glu209 (ζ) and Asp113(σ)-Asn111(τ)-Gln111(ζ). In conclusion, the periphery of the phosphopeptide-binding cleft accumulates significant differences both in the fold (residues 203-215 in σ) and residue properties (the σ residues 38, 113, 163, 166, 209). Based on comparison of all mentioned structures, we propose that the Ala203 and Asp215 loop and its neighbourhood represent the major ligand specificity region (Figs. 11 and 12). On the primary sequence level this loop is highly conserved between the seven isoforms, but contains 3 unique amino acids (Met202, Asp204, His206) in 14-3-3σ, which are not found in any other 14-3-3 isoforms (see Fig. 14) (Yaffe et al., 2002).
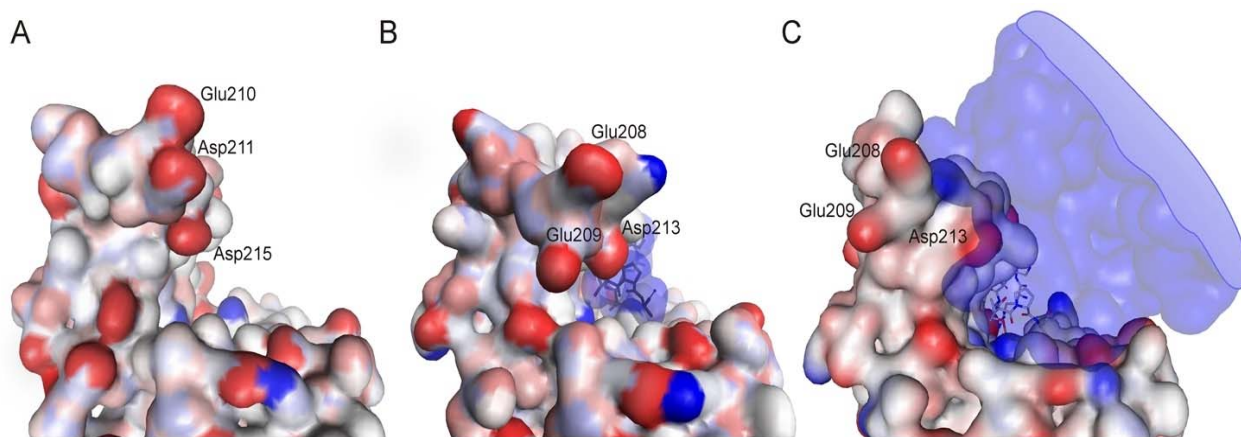
Fig. 12. Proposed major ligand specificity region of 14-3-3σ. The figure shows the edge of the phosphopeptide binding groove, from the C-terminal side of a phosphopeptide. *A.* the molecular surface of the 14-3-3σ isoform colored by atom charge. The structure presents an "open" conformation of the cleft edge. *B.* The same area of the 14-3-3ζ isoform has a "closed" conformation. *C.* Serotonin N-acetyltransferase in complex with 14-3-3ζ shown as a semi-transparent surface plot; the phosphoserine region is shown as a stick model. Except for the phosphopeptide cleft, the only possible contact area is localized at the edge of the 14-3-3ζ molecule, thus indicating that this part may be responsible for selective ligand binding.

The structure of the phosphopeptide binding site of the 14-3-3σ molecule is identical to the ζ and τ isoforms with bound ligands (structures 1QJA and 1QJB) (Fig. 13A, but not to the ζ isoform in its free form (1A4O). This difference is especially pronounced in the conformations of Trp230 and Tyr181, which form an aromatic environment at the N-terminus of a potential 14-3-3-binding peptide. As shown in Fig. 13B the aromatic rings of Trp230 and Tyr181 in 14-3-3σ are oriented in the same plane as in the ζ isoform with a bound phosphopeptide, while in the free form of the ζ isoform they adopt a different orientation.
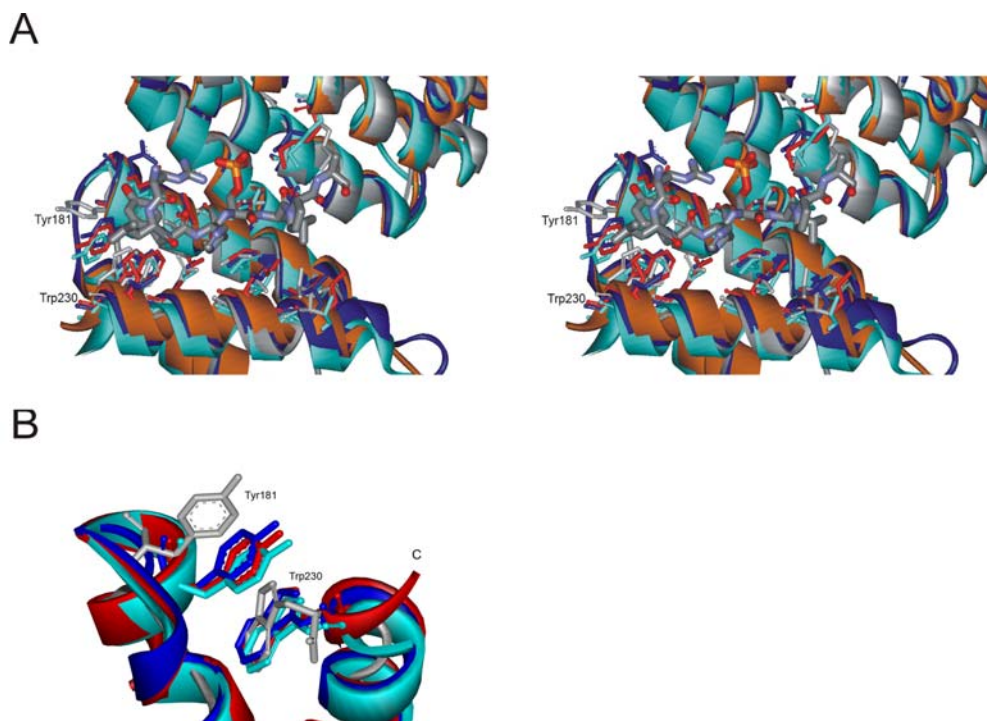
Fig. 13. Details of phosphopeptide binding pockets in the 14-3-3 ζand σ isoforms. *A.* Comparison of the spatial organization of phosphopeptide binding sites in different 14-3-3 structures. ζ isoforms 1QJA (dark blue; bound to a peptide) and 1A4O (gray; without a bound peptide) were superimposed onto the solved 14-3-3σ monomers (chains A and B presented in brown and green, respectively). The phosphopeptide from the 1QJA structure is shown as a bold stick model with the phosphogroup in orange. *B.* The two aromatic residues that complete the binding site are shown. ζ isoforms 1QJA (dark blue) and 1A4O (gray) are compared to the σ chains A and B presented in red and green, respectively. Positions of side chains in the free σ isoform resemble those of bound ζ isoforms. The free ζ form 1A4O differs significantly from the two other models.

The conformation of additional side chains of the phosphopeptide binding site in 14-3-3σ also resembles the ζ isoform complexed, with a peptide more than the uncomplexed 14-3-3ζ. This conformation of 4-3-3σ could therefore result in an increased stability of 14-3-3σ-ligand interactions

when compared to 14-3-3ζ interactions. As expression of 14-3-3σ is rapidly induced after DNA-damage, a displacement of other 14-3-3 isoforms or preferential binding to ligands by 14-3-3σ may therefore be possible. As discussed above, multiple examples of selective ligand binding by different 14-3-3 isoforms exist. We recently used a targeted proteomics approach to identify 14-3-3σ-associated proteins *in vivo* (Benzinger et al., 2005). Interestingly, we found that in colorectal cancer cells 14-3-3σ was only present as a homo-dimer or as a hetero-dimer with 14-3-3γ indicating selective dimerization, which may be due to the putative dimerization determinants identified here (Benzinger et al., 2005). The data presented here provides a basis for the experimental validation of determinants of ligand and dimerization specificity by mutational analysis.
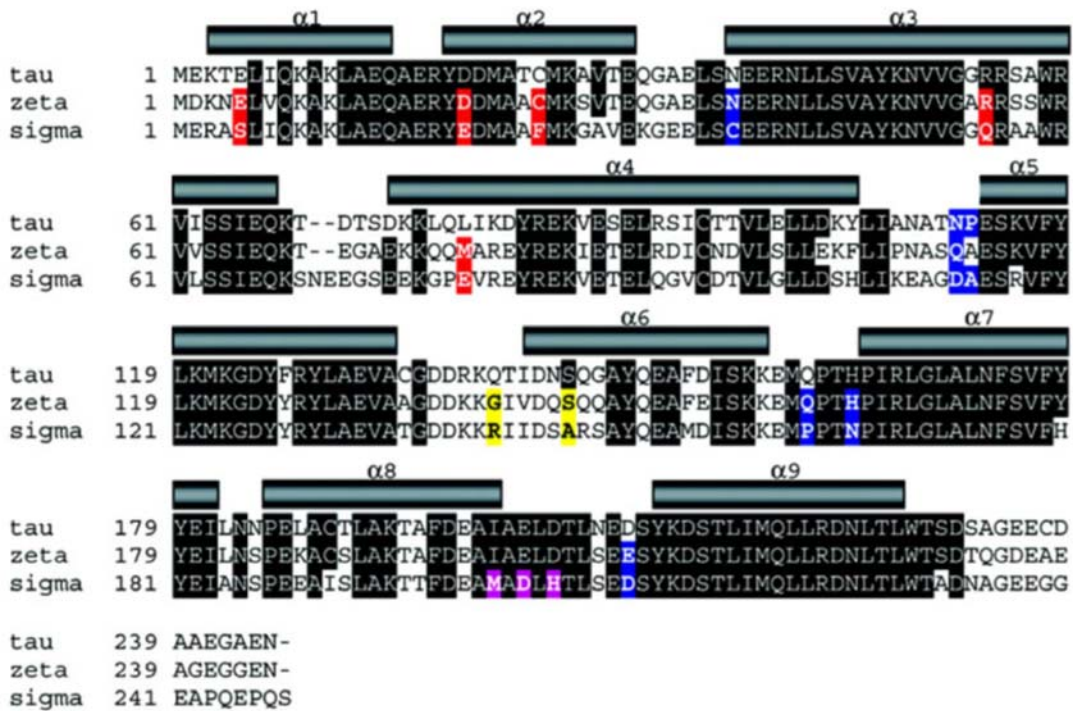
Fig. 14. Alignments of primary sequences of 14-3-3σ, ζ and τ. Differences in the structures identified here are highlighted in colors. Amino acid residues shown with a black background are conserved in at least 6 of the 7 human 14-3-3 isoforms according to reference 14. The positions of α helices (α1 to α9) are indicated by rods above the alignment. Residues in red presumably determine 14-3-3 dimerization specificity. For 14-3-3σ and 14-3-3ζ these residues are Ser5-Glu5, Glu20-Asp20, Phe25-Cys25, Gln55-Arg55 and Glu80-Met78, respectively. Residues constituting the ligand-specificity region proposed here are shown in blue for 14-3-3σ and ζ, respectively: Cys38-Asn38, Asp113-Gln111, Pro163-Gln161, Asn166-His164 and Asp211-Glu209. For comparison between 14-3-3σ and τ Asp113-Asn111 and Ala114-Pro112 are marked in blue. The yellow residues (Arg142-Gly140, Ala147-Ser145) may be of minor importance for ligand-specificity of 14-3-3σ and ζ. Three 14-3-3σ-specific residues present in the potential ligand-specificity region Ala203-Asp215 are shown in magenta (Met202, Asp204, His206).

5.3 Experiments with cyclin A2

The full-length protein with a GST-tag was cloned into the pGEX-4T-2 vector and expressed in *E. coli* in BL 21 cells. The yield was low, the protein was impure and susceptible to degradation (Fig. 15)
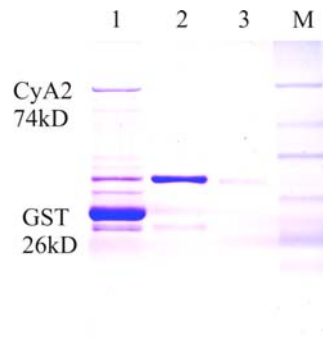

Fig. 15. The SDS-PAGE analysis of gel chromatography fractions of cyclin A2. The lane marked 1 shows cyclin A2 tagged with GST and GST alone, lanes 2 and 3 contain bacterial proteins and lane M is the marker.

Fig. 16. Schematic diagram of the constructs of human cyclin A2 used in the study. Residues 47-57 represent the destruction box. Ser154 is the phosphorylation site and the cyclin box (with the two cyclin box folds) is shown. Numbers represent the amino acid positions.

Cyclin A2 has a nine amino acid destruction box situated at the N-terminus and is required for ubiquitin-mediated degradation. The protein was re-cloned in pET28 vector with a 30 amino acid long histidine tag and the degradation box from the sequence was deleted. The construct contained the region from residues 173 to 432 (Fig. 16). This construct retains a CDK2 binding activity and is constitutively active (Brown et al., 1995). The expression of the protein increased drastically and the protein eluted as a monomer in gel filtration (Fig. 17A). The fractions were analysed with SDS-

PAGE (Fig. 17B). Later, to shorten the tag it was again cloned in pET46 Ek/LIC vector with a 15 amino acid histidine tag. The expression was similar to that of the earlier prep. The protein was checked by NMR and mass spectroscopy for its folding pattern and purity. The protein was stable for a week at 4 ˚C. The presence of $MgCl_2$ was very important to keep the protein in a monomeric form. The purified protein was used for binding studies. It was mixed in an equimolar ratio with CDK2 to make binary complexes that were required for binding with p53, pRb, and p27.
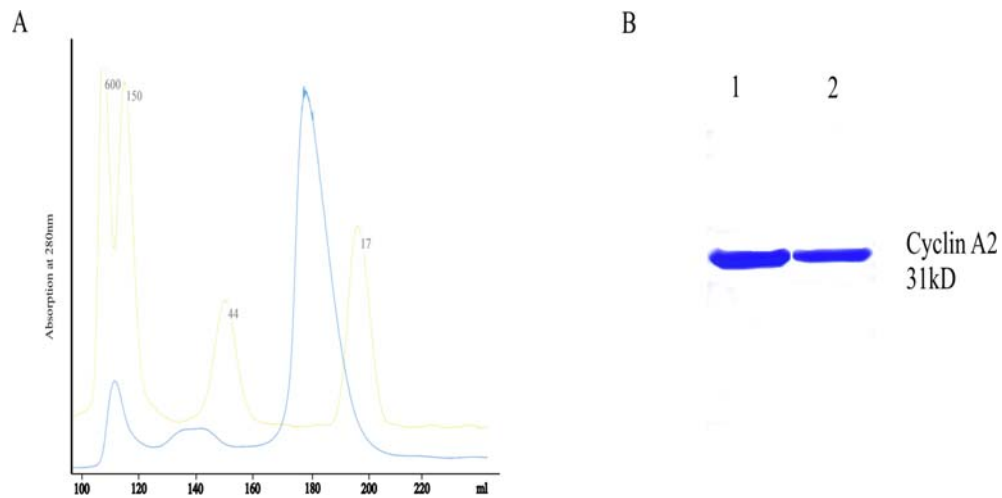
Fig. 17. A. Elution of the cyclin A2 in the Superdex 75 gel chromatography. *B.* Fractions were analysed with SDS-PAGE to check the purity of the eluted protein.

5.4 Experiments with CDK2

The full length human CDK2 was first cloned into the pET28 vector and then recloned to pET46 Ek/LIC to shorten the histidine tag. An unphosphorylated CDK2 was expressed in BL 21 (DE3) cells in *E. coli*. After the N-NTA elution (Fig. 18A), the protein was subjected to cation exchange chromatography (Fig. 18B). The fractions in the blue striped region of the chromatogram in Fig. 18B were collected, concentrated and loaded on the Superdex 75 gel filtration column. The protein eluted as a monmer (Fig. 18C). The Western blot analysis, SDS–PAGE and mass spectrometry confirmed the presence of CDK2. The protein was 99% pure as visualized in SDS-PAGE (Fig. 19A). In one of the construct thrombin site was introduced to cleave the histidine tag. Due to

internal unspecific cleavage by thrombin it was not possible to cleave the tag (Fig. 19B). For confirmation, Western blot was carried out with CDK2 antibody. Fig. 19C shows the Western blot before cleavage and Fig. 19D shows the western blot after cleavage. The positive signal in the two lanes of Fig. 19D confirms the internal unspecific cleavage. We decided therefore to continue our experiments with the His-tagged protein.
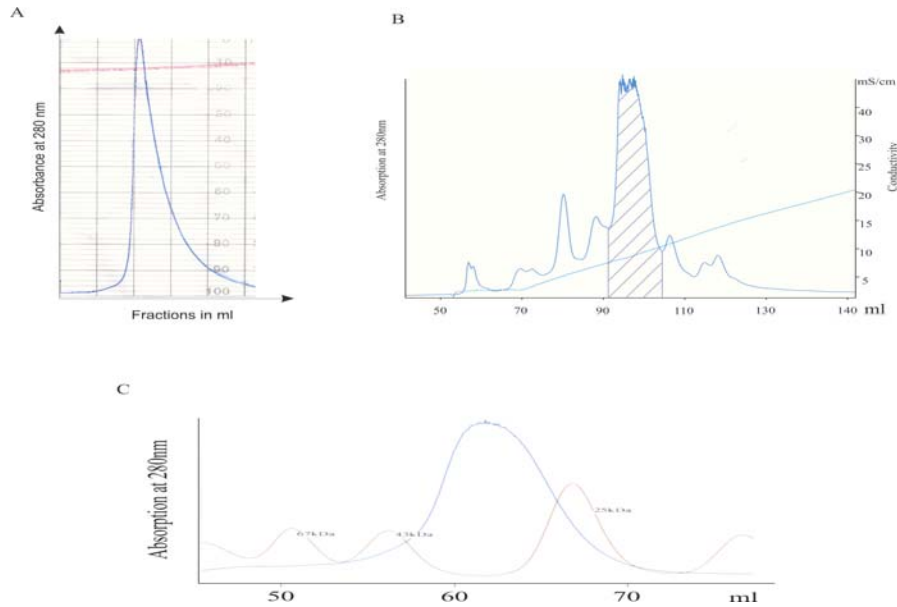

Fig. 18. A. The elution profile of CDK2 in the Ni-NTA column. *B.* Shows the separation of CDK2 in a 8 ml cation exchange column. *C.* Chromatogram showing the elution profile of the CDK2 in the Superdex 75 gel chromatography.
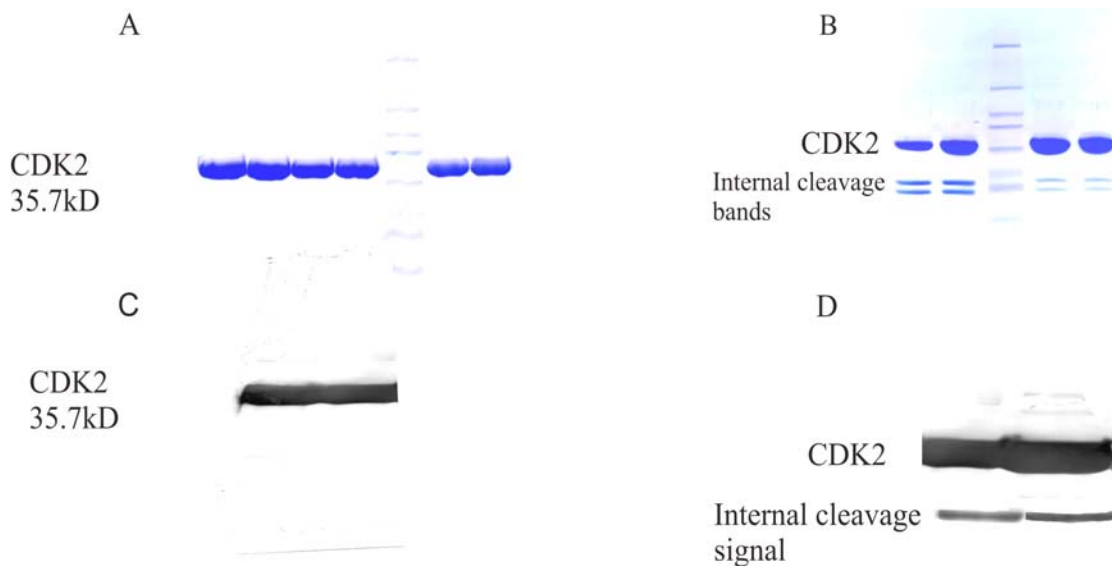
Fig. 19. A. SDS-PAGE of the CDK2 samples after gel filtration chromatography. *B*. SDS-PAGE showing CDK2 after cleavage. *C*. Western blot of CDK2. *D*. Western blot of CDK2 after thrombin cleavage.

The 1D NMR proton spectrum showed well dispersed signals between 8 to 11 ppm region and 0 to -1 ppm, characteristic of a folded protein (Rehm et al., 2002). A CD spectrum was recorded for the protein, which showed the protein to be a mixture of α- helixes and β- sheets (Fig. 21).
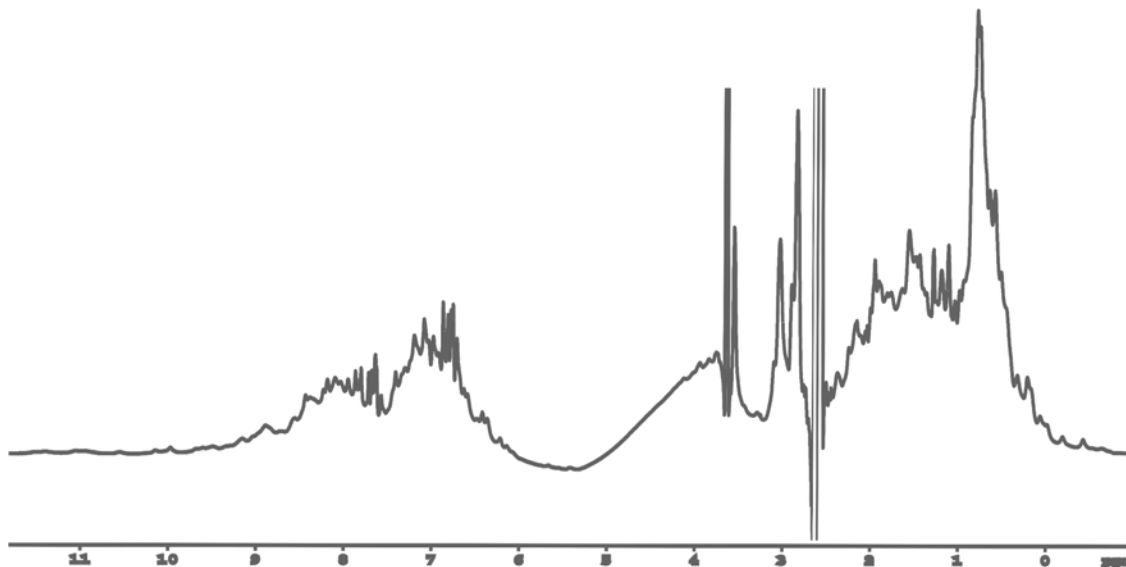

Fig. 20. 1D proton spectrum of human CDK2 showing the folded nature of the protein.

CDK2 with His-tag
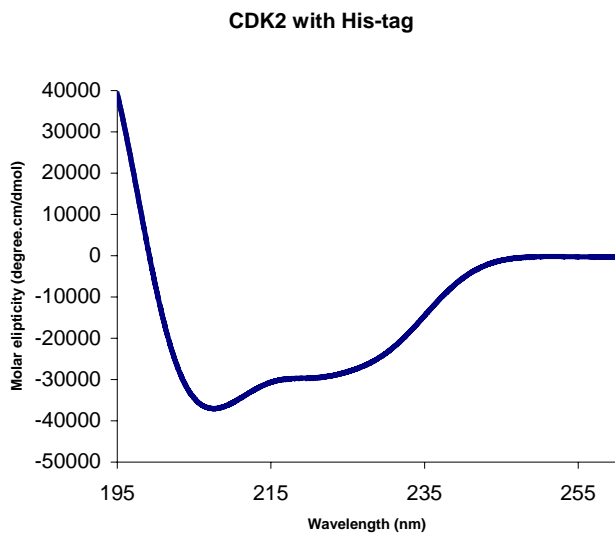
Fig. 21. CD spectrum of the CDK2, showing the absorption at 205 for βsheet and 220 for α helix.

The protein was mixed with cyclin A2 and was loaded onto the Superdex 75 column to form an equimolar, pure complex. Fig. 22A. To check its purity the sample was analyzed with SDS-PAGE, which is shown in Fig. 22B. The complex was almost 95% pure. The binary complex eluted as a monomer in gel filtration but the elution was later comparative to its mass because of its proper fold and globular tertiary structure. To check the proper folding of the complex, 1D proton spectra was recorded which is shown in the Fig. 23.
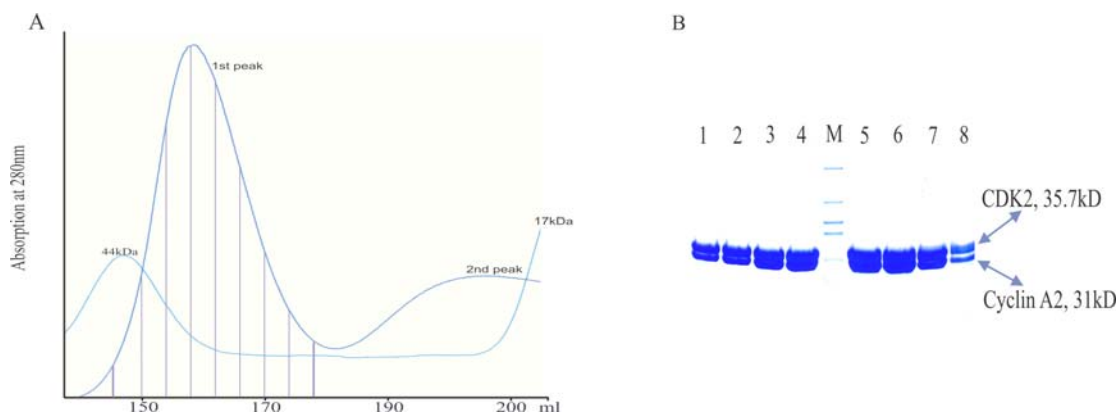
Fig. 22. A. Chromatogram showing the elution of the CDK2-cyclin A2 in the Superdex 75 gel chromatography. The first peak corresponds to the complex and the second peak corresponds to the excess of CDK2 in the protein mix. *B.* SDS-PAGE of the CDK2-cyclin A2 complex after gel filtration chromatography. M-represents the marker.
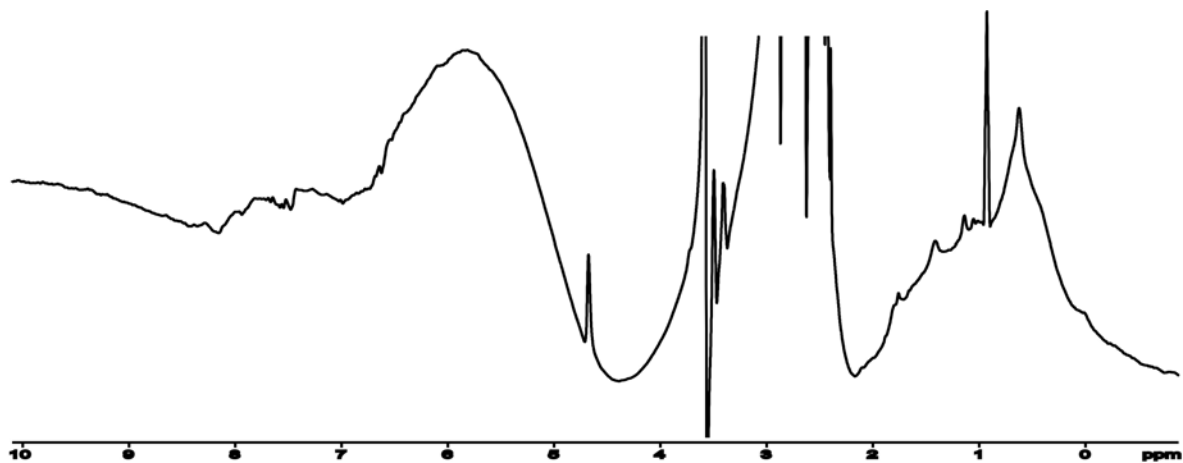

Fig. 23. 1D proton spectrum of the complex of cyclin A2-CDK2 showing the folded nature of the complex.

As the protein size was larger (around 65 kDa), so it was difficult to predict in detail the folded nature of the protein through NMR. The line widths were broad due to the size of the protein

complex. But there were characteristic signals in the region of 0 to –1 and around 8 to 10 ppm region, which suggested that the protein complex as folded. This complex was used for binding and crystallization studies with the pRb C-terminal domain, p53 C-terminal domain, p27 N-terminal domain and INCA1.

5.5 Experiments with p27

The recombinant p27 (residues 1-96) was over-expressed at 37 °C in BL 21 (DE3) in *E. coli* using a pET28 vector. The protein was purified under native condition using Ni-NTA Agarose (Qiagen).
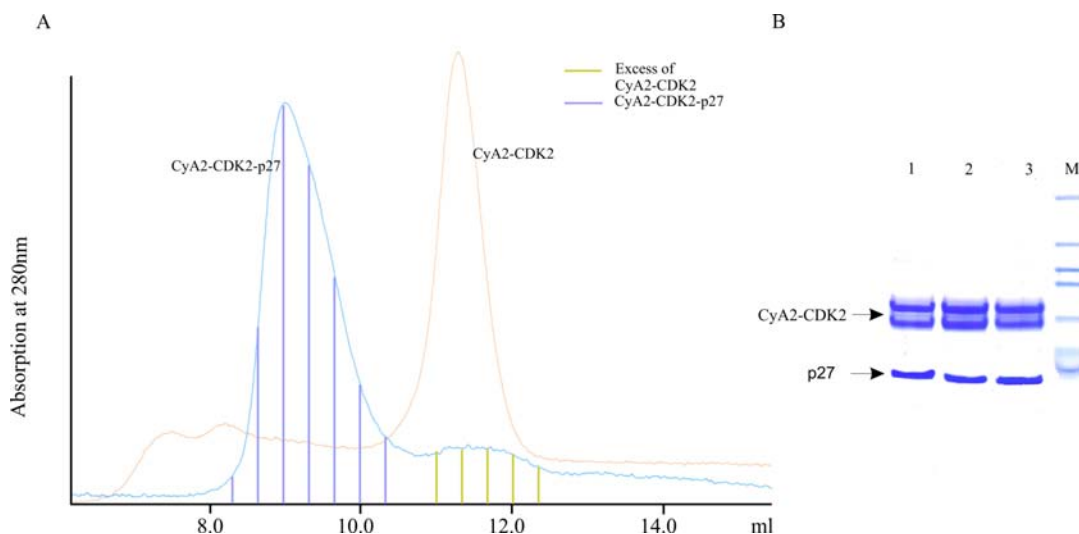
Fig. 24. A. Chromatogram showing the elution profile of the ternary complex p27-cyclinA2-CDK2 (the Superdex 75 analytical column). Green striped portion represent the excess of cyclin A2-CDK2. *B.* SDS-PAGE analysis of different fractions after gel filtration. M represents the marker.

Binding studies of p27 were performed with cyclin A2-CDK2. The p27 (residues 1-96) was mixed with the cyclin A2-CDK2 complex and loaded onto the Superdex 75 analytical gel filtration column to observe the binding. Fig. 24A shows two chromatograms overlaid over each other. The blue striped portion represents the ternary complex of cyclin A2-CDK2-p27, whereas the green striped portion shows the excess of the binary complex of cyclin A2-CDK2. The fractions were analysed with SDS-PAGE (Fig. 24B), which showed the presence of p27 N-terminal protein with the fractions of cyclin A2-CDK2.
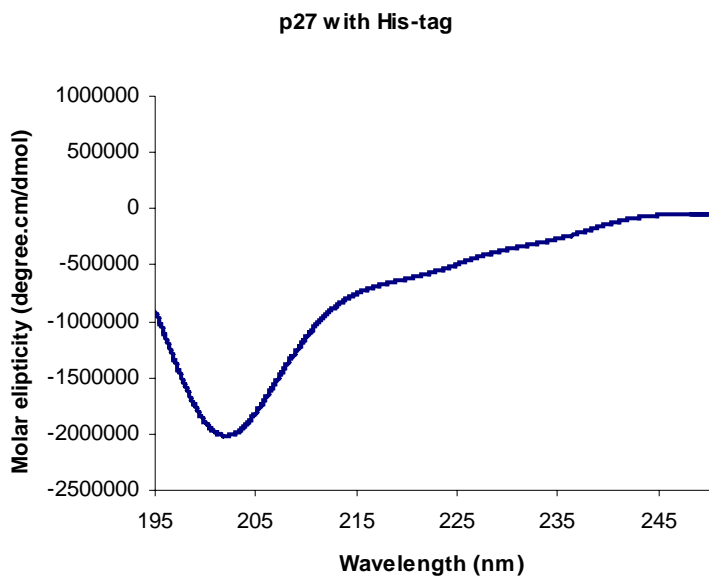
p27 with His-tag

Fig. 25. CD spectrum of the p27 protein, which shows the protein as unstructured.

The 1D proton spectrum and the CD spectrum of the p27 showed that the protein had unfolded region (Fig. 25 and 26). Further studies were conducted with a uniformly ^{15}N labeled p27. In ^{1}H-^{15}N HSQC spectra of p27 (Fig. 27A) the peaks at 8.3 ppm showed little signal dispersion, which characterised the protein to be mostly unstructured.
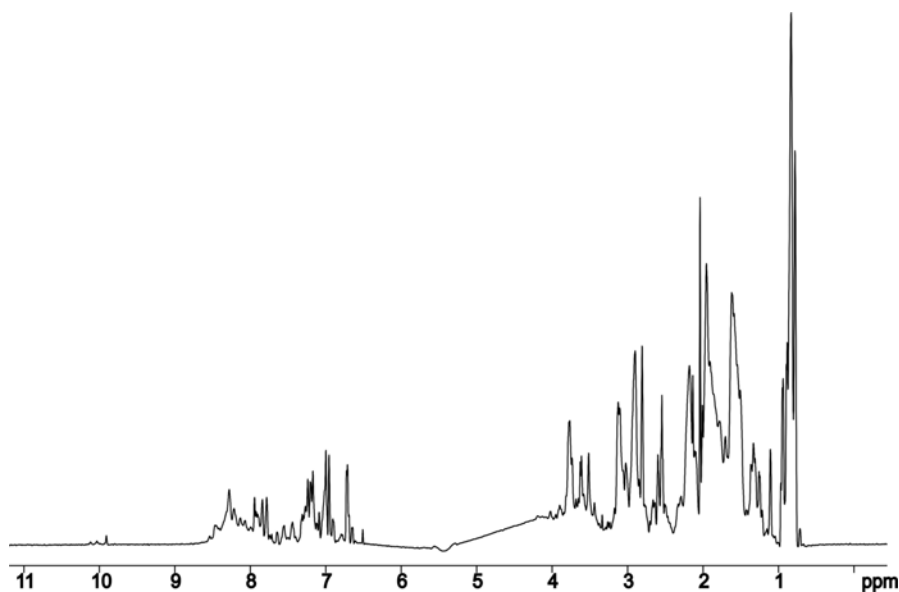

Fig. 26. 1D proton spectrum of the p27 construct. Details' regarding the folding is described in the text.

The two-dimensional experiments, are frequently used for screening and binding studies. The simplest and most powerful among them is the heteronuclear single-quantum coherence (HSQC) experiment. ^{15}N-HSQC is the first step in any structure elucidation, as it maps the backbone amide groups of a protein according to their proton and nitrogen frequencies. For this kind of spectrum, ^{15}N-labeled protein samples are required.
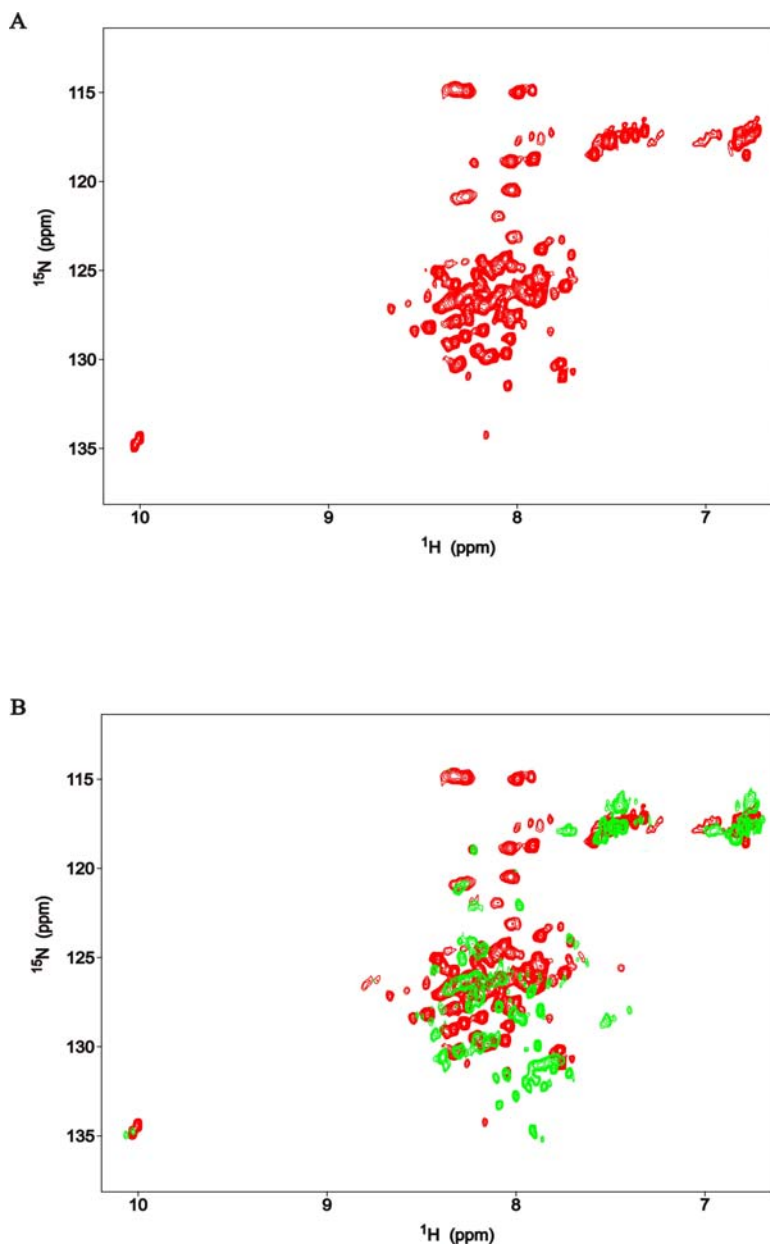

Fig. 27. A. ^{1}H-^{15}N HSQC spectrum of the ^{15}N uniformly labeled p27. *B.* ^{1}H-^{15}N HSQC spectrum of the ^{15}N uniformly labeled p27 titrated with cyclin A2-CDK2. Reference in red and the last step of titration is in green. For details consult the text.

The HSQC shows one peak for every proton bound directly to a nitrogen atom and, thus, exactly one signal per residue in the protein (apart from proline, which is devoid of proton-bound nitrogen, and some additional side chain signals, which can easily be identified, appear). The positions of the peaks are indicative of structured or disordered proteins in the same way as described for the one-dimensional spectrum. When the uniformly ^{15}N labeled sample was titrated with cyclin A2-CDK2 there was clear disappearance of ca. 50% of the peaks and the peaks at around 8.3 ppm showed signal dispersion. The ternary complex that was formed was around 80 kDa. The disappearance of the peaks was due to broadening of their line widths because of the formation of the ternary complex.

Fig. 27B shows the changes observed after titration with cyclin A2-CDK2. The experiments proved that the cyclin A2-CDK2 complex introduced structured parts in p27, which was in accordance with the previous studies conducted with the ternary complex.

5.6 Experiments with the p53 C-terminal domain

Four different constructs of the C-terminal domain of p53 were cloned in pET46 Ek/LIC vector. Fig. 28 shows different constructs that were made for the study with cyclin A2 and CDK2. All these constructs were expressed in *E. coli* in BL 21 (DE3) cells. The protein sequences of the constructs are given in Fig. 29.
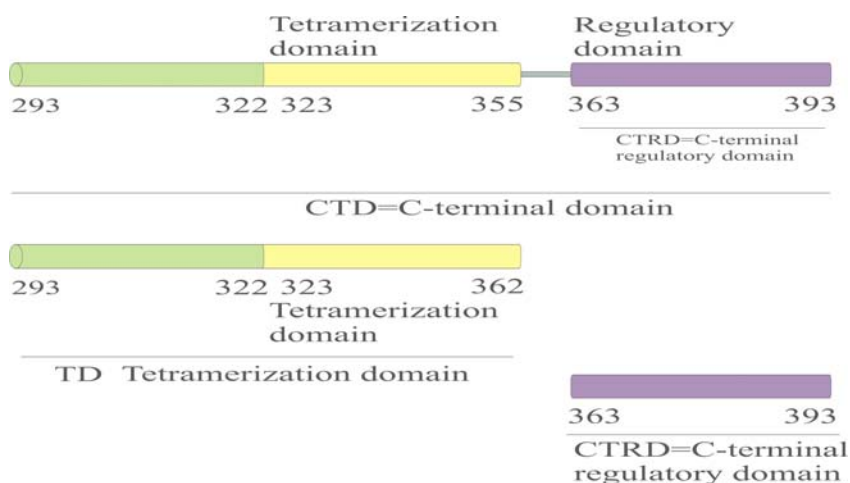

Fig. 28. Schematic representation of the constructs of the C-terminal domain of p53 used in the study.

p53 CTD 293-393

*MAHHHHHHHVDDDDK*KKGEPHHELPPGSTKRALPNNTSSSPQPKK*KPL*DGEYFTLQIRGRER
FEMFRELNE ALELKDAQAG KEPGGSRAHS SHLKSKKGQS TSRH*KKL*MFK TEGPDSD

p53 TD 293-356
*MAHHHHHHHVDDDDK*KKGEPHHELPPGSTKRALPNNTSSSPQPKK*KPL*DGEYFTLQIRGRER
FEMFRELNE ALELKDAQAG

p53 CTRD 363-393
*MAHHHHHHHVD DDDK*RAHS SHLKSKKGQS TSRH*KKL*MFK TEGPDSD

p53CTRD (Trp mutant) 362-393
*MAHHHHHHHVD DDDK*WRAHSS HLKSKKGQST SRH*KKL*MFKT EGPDSD

Fig. 29. Protein sequences of all the constructs made. The highlighted regions in teal colour represent the histidine tag from the vector and the blue represents the probable binding regions to cyclin A2.

The elution profiles of all the constructs are shown in Fig. 30. The expression and purity of the constructs varied. The expression of CTD and TD domains were high (with impurities) whereas the expression of CTRD was comparatively low. CTD and TD constructs eluted as tetramers in gel filtration whereas the CTRD eluted as a monomer. In the CTRD construct a tryptophan was added for detection in the gel filtration. The elution of the proteins were analysed through SDS-PAGE (Fig. 31). The protein p53-CTD was 80% pure compared to the others. Purest of them was the p53-CTRD.
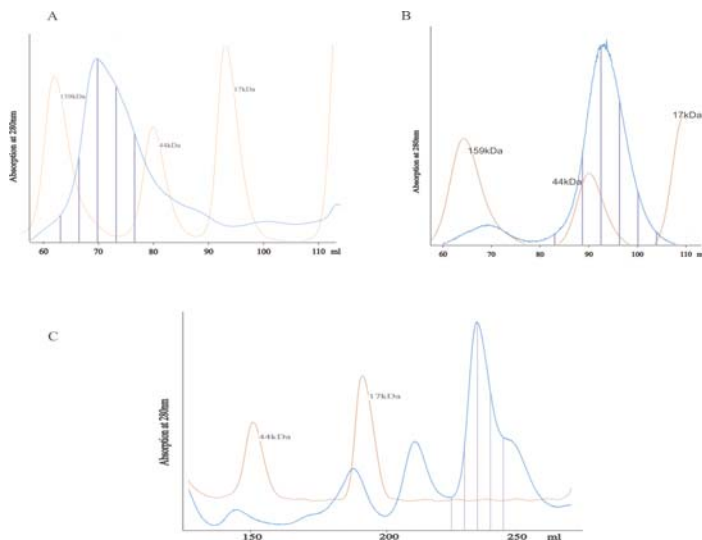

Fig. 30. Chromatograms showing the elution profile of different p53 constructs. *A.* Elution of p53-CTD in the Superdex 200 gel filtration. *B.* Elution of p53-TD in the Superdex 200 gel filtration. *C.* Elution of p53-CTRD in the Superdex 75 chromatography.

101

The folding pattern was analysed with the help of the NMR. The 1D proton spectra were recorded for the different p53 constructs. Figs. 32A, B and C show three spectra of the three different p53 constructs.
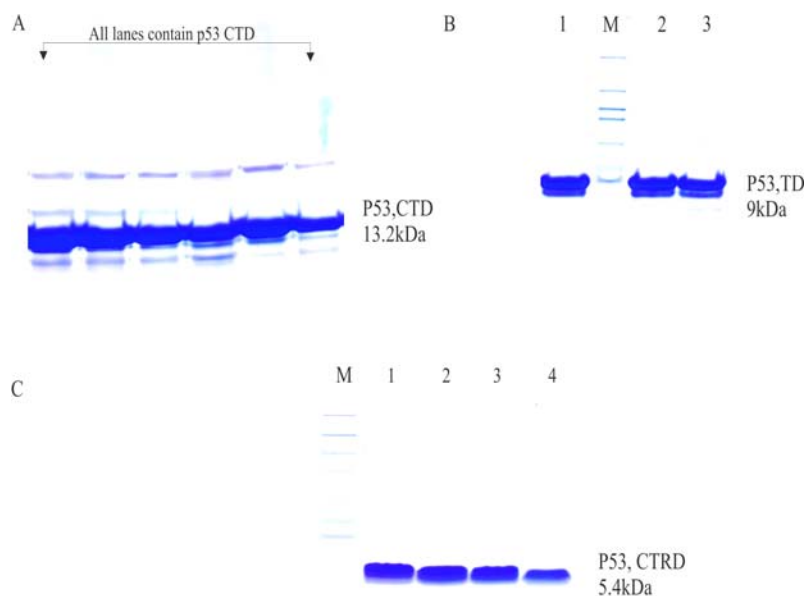

Fig. 31. SDS-PAGE analysis of the different constructs. *A*. p53-CTD. *B*. p53-TD. *C*. p53-CTRD.

In the upper spectrum, a mixture of approximately 50% folded and 50% unfolded protein can be identified by observing the signal dispersion and the prominent peak at 8.3 ppm compared to the spectrum of Fig. 32C. While the signal dispersion of the resonances is generally connected to folding, aggregation can be detected by observing the line width of the signals. Because of faster relaxation mechanisms, the NMR signal from larger molecules will decay much faster than that from smaller ones. This, in turn, will produce broader lines for the resonances of larger molecules. Thus, the line widths of the signals in any NMR spectrum are correlated to the size of the molecule. Both these aspects may be appreciated in the Figs. 32A and 32B.

The appearance of intensities at chemical shifts near ~8.3 ppm in Fig. 32C, is an excellent indicator for a disordered protein. Strong signals appear around this region characteristic for amide groups in random-coil conformation. No signal dispersion is visible below approximately 8.5 ppm.

Also, to the right of the strong methyl peak at 0.8 ppm, no further signals show up. In conclusion the domains of p53-CTD and -TD was 50% structured and the domain CTRD was completely unstructured.
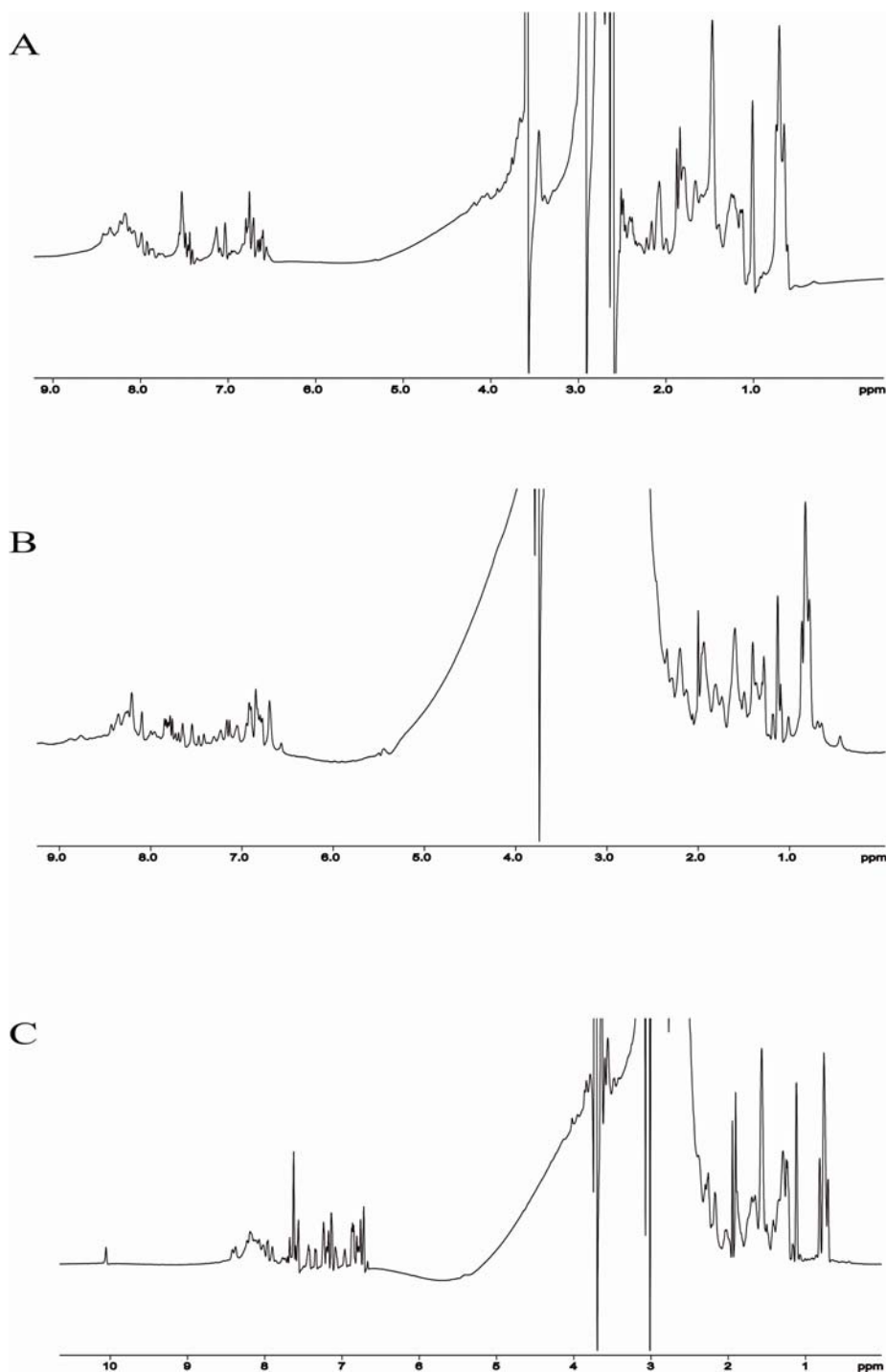

Fig. 32. 1D proton spectra of the different p53 constructs. *A.* p53-CTD. *B.* p53-TD. *C.* p53-CTRD (Trp mutant). Details regarding the folding are described in the text.

We continued our binding studies with the proteins and cyclin A2-CDK2. The proteins were mixed and loaded onto the gel filtration column. In the elution profile in Fig. 33A, the blue lines indicate the ternary complex whereas the green lines represent the excess of the p53-CTD protein. The SDS-PAGE analysis of fractions confirmed the results.
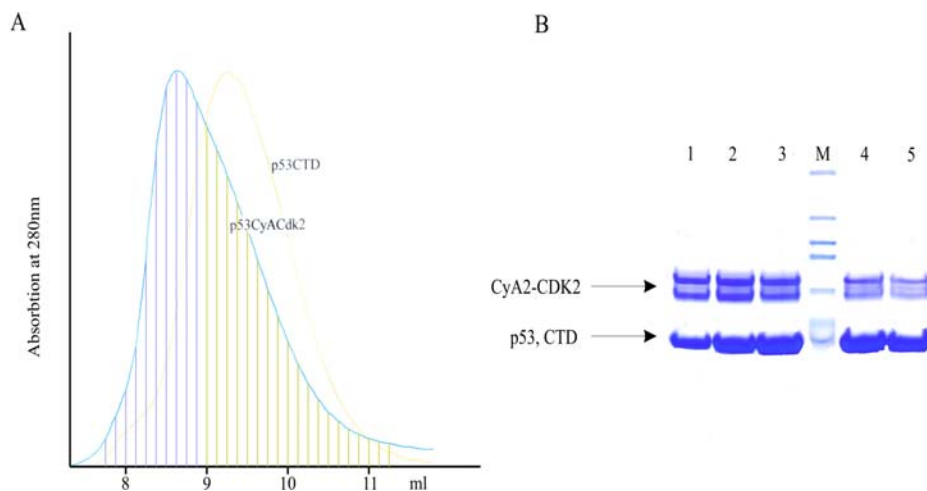

Fig. 33. A. Chromatogram showing the elution profile of the ternary complex (p53-CTD-cyclin A2-CDK2) in the Superdex 75 analytical column. *B*. SDS-PAGE analysis of the different fractions after gel filtration. M represents the marker.

We have clearly seen that the intensity of the bands of the complex cyclin A2–CDK2 decreased in lanes 4 and 5 but the intensity of the p53-CTD remained almost the same throughout the lanes. In conclusion the 'earlier' lanes made the ternary complex in equimolar ratio and in the later fractions the excess of p53-CTD was visible. So the fractions of lanes 1 and 2 were concentrated and given for NMR spectroscopy. Fig. 34 shows that the formation of complex did not change the unfolded region of the p53-CTD. It was a mixture of folded and unfolded proteins.

The next construct of p53, CTRD, was used for our further studies. The protein was mixed with cyclin A2-CDK2 and loaded onto the gel filtration column. The chromatogram in Fig. 35A represents the elution profile. The fractions were analysed in a SDS-PAGE for a 1:1 complex. The blue stripes represent the complex in equimolar ratio, which was confirmed by the SDS-PAGE analysis in Fig. 35B.
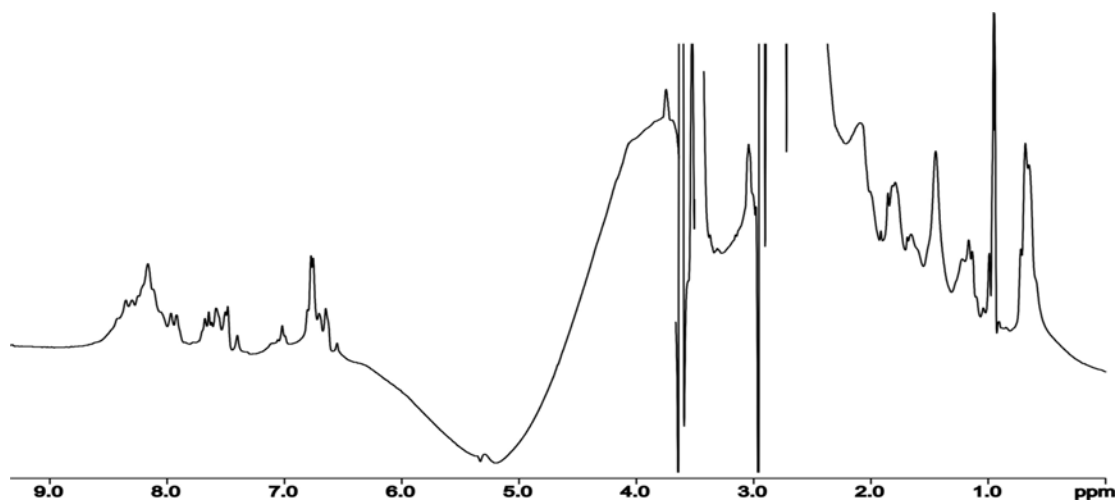
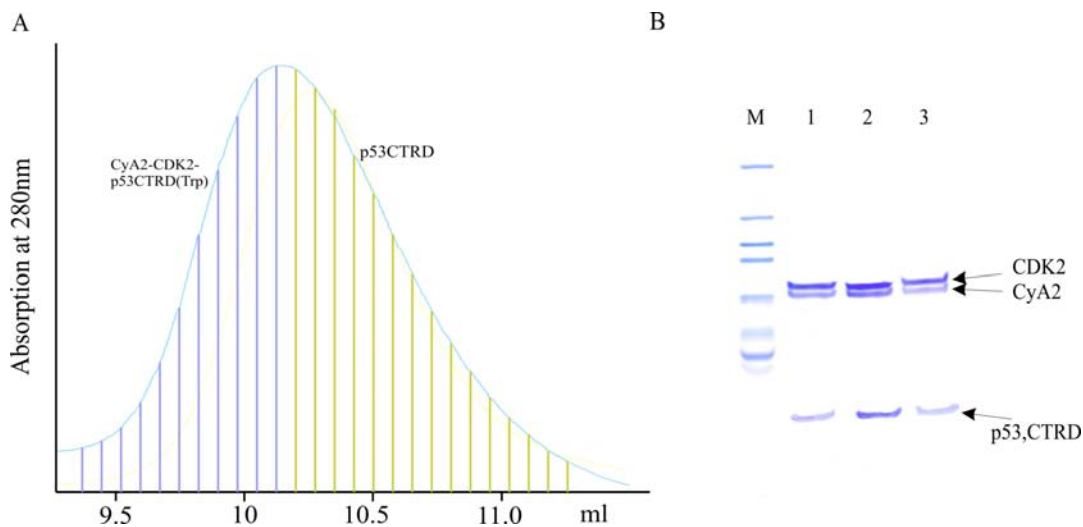*Fig. 34.* 1D proton spectrum of the ternary complex of p53-CTD-cyclinA2-CDK2.

Fig. 35. A. Chromatogram showing the elution profile of the ternary complex (p53-CTRD-cyclin A2-CDK2) in the Superdex 75 analytical column. *B.* SDS-PAGE analysis of the different fractions after gel filtration. M represents the marker.

In the ^{1}H-^{15}N HSQC spectrum of the ^{15}N uniformly labeled of p53-CTRD (Fig. 36A), almost all the signals clustered in a characteristic "blob" around a ^{1}H frequency of 8.3 ppm, with little signal dispersion in both dimensions, which is a characteristic of an unfolded protein. In the ^{1}H-^{15}N HSQC spectrum of the ^{15}N uniformly labeled sample of p53 CTRD titrated with cyclin A2-CDK2, there were no signal dispersion (Fig. 36B) and the changes observed were more in the unfolded

region of the protein. However it was not possible to identify the exact regions involved in binding to the binary complex of cyclin A2-CDK2.
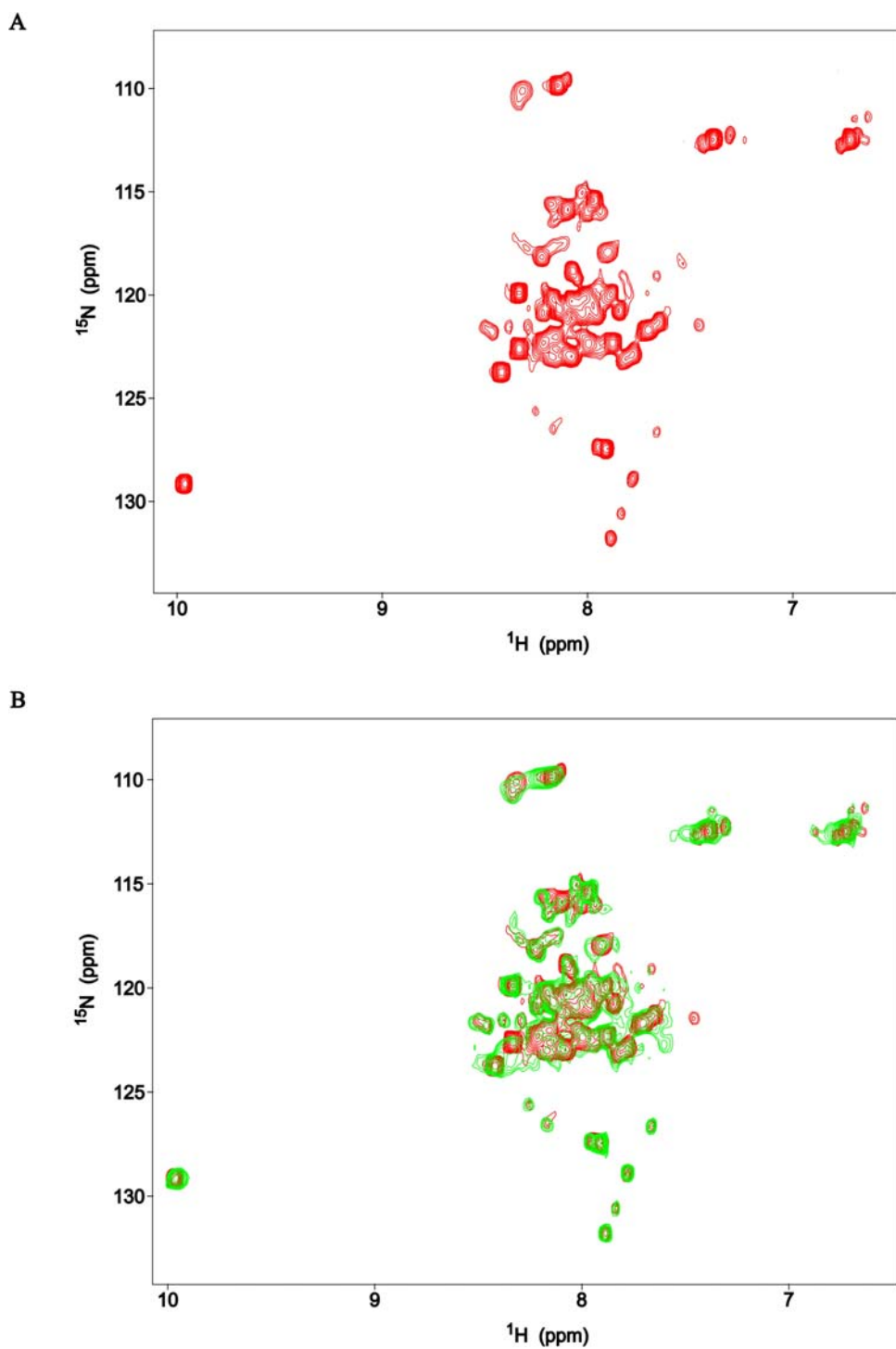
A

B

Fig. 36. A. ^{1}H-^{15}N HSQC spectra of the ^{15}N uniformly labeled p53-CTRD. *B.* ^{1}H-^{15}N HSQC spectrum of the ^{15}N uniformly labeled sample of p53-CTRD titrated with cyclin A2-CDK2. Reference in red and the last step of titration is in green. For details consult the text.

5.7 Experiments with INCA1

The nuclear INCA1 protein is evolutionarily conserved and lacks homology to any known gene. This novel protein served as substrates for the cyclin A1-CDK2 kinase complex. Cyclin A1 and all its interaction partners were highly expressed in testis with varying degrees of tissue specificity. The highest expression levels were observed at different time points during testis maturation, whereas expression levels in germ cell cancers and infertile testes decreased.
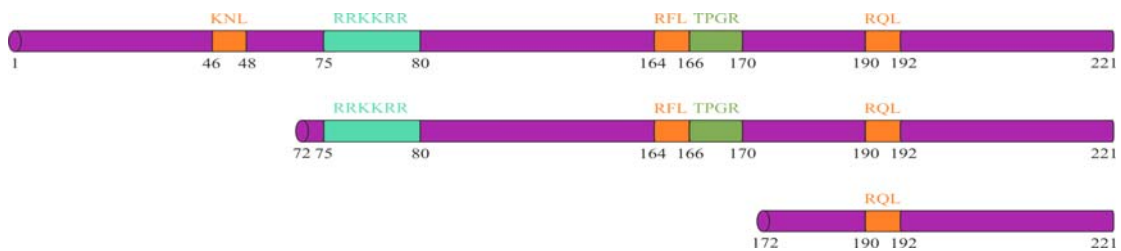

Fig. 37. Schematic diagram of the constructs used in the study. KNL, RFL and RQL show the probable binding regions for cyclin A2. RRKKRR represent the nuclear localization signal and TPGR is the recognition site for phosphorylation.
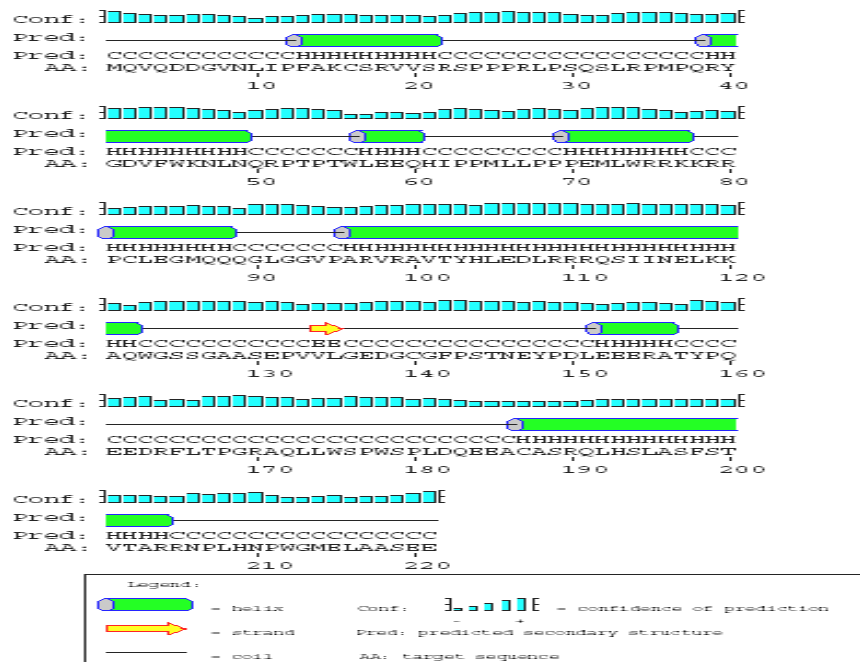

Fig. 38. A secondary structure prediction of the INCA1 determined the protein to be α-helical.

The above constructs (Fig. 37) were made for the expression and purification of the protein. They were cloned in pET46 EK/LIC and pET41 EK/LIC vectors. It was difficult to express the first two constructs because the proteins degraded rapidly. The last construct expressed with very low yield and was not pure. Fig. 39A shows the elution profile of the protein in the gel filtration. The protein eluted at a higher mass than expected. The fractions shown in blue stripes were analysed through SDS-PAGE (Fig. 39B). The protein was 80% pure.
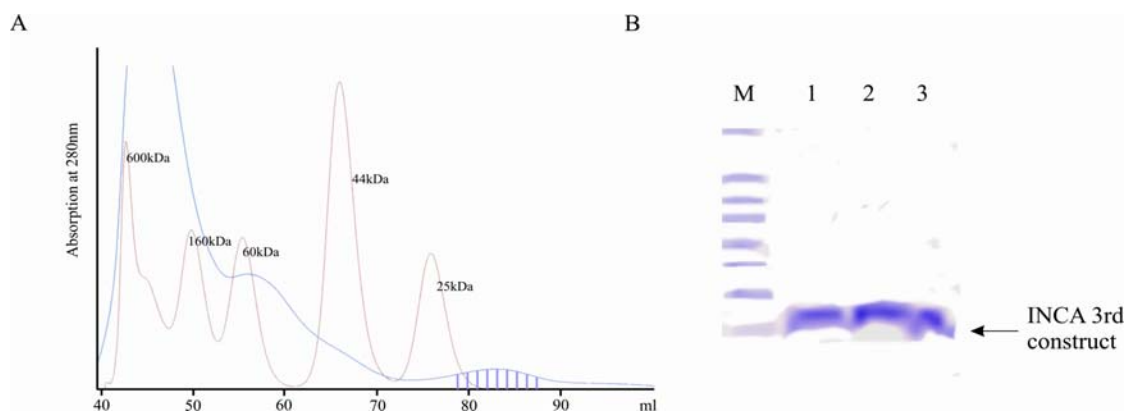
Fig. 39. A. Chromatogram showing the elution profile of the 3rd construct of INCA1 in Superdex 75 gel filtration column. Blue striped portion represent the protein. *B*. SDS-PAGE analysis of the different fractions after gel filtration. M-represent the marker.

The 1D proton spectra of the protein revealed the presence of flexible regions (Fig. 40). Further studies were not possible with these constructs and the protein because of high rate of degradation and the presence of unstructured parts.
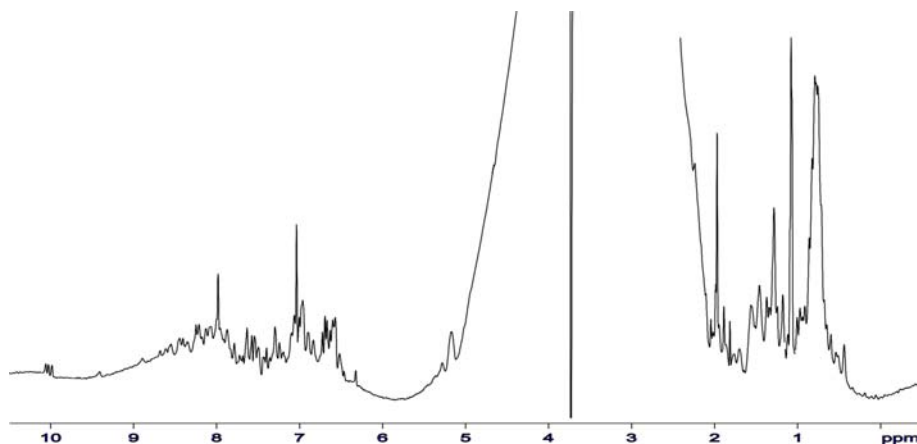
Fig. 40. 1D proton spectrum of the 3rd construct of INCA1 (residues 172-221).

5.8 Experiments with the C-terminal domain of pRb

The following pRb constructs were made and cloned in a pET46 Ek/LIC vector. They were expressed in BL21 (DE3) cells in *E. coli* at 20 ºC after induction at an OD_{600} of 0.7.
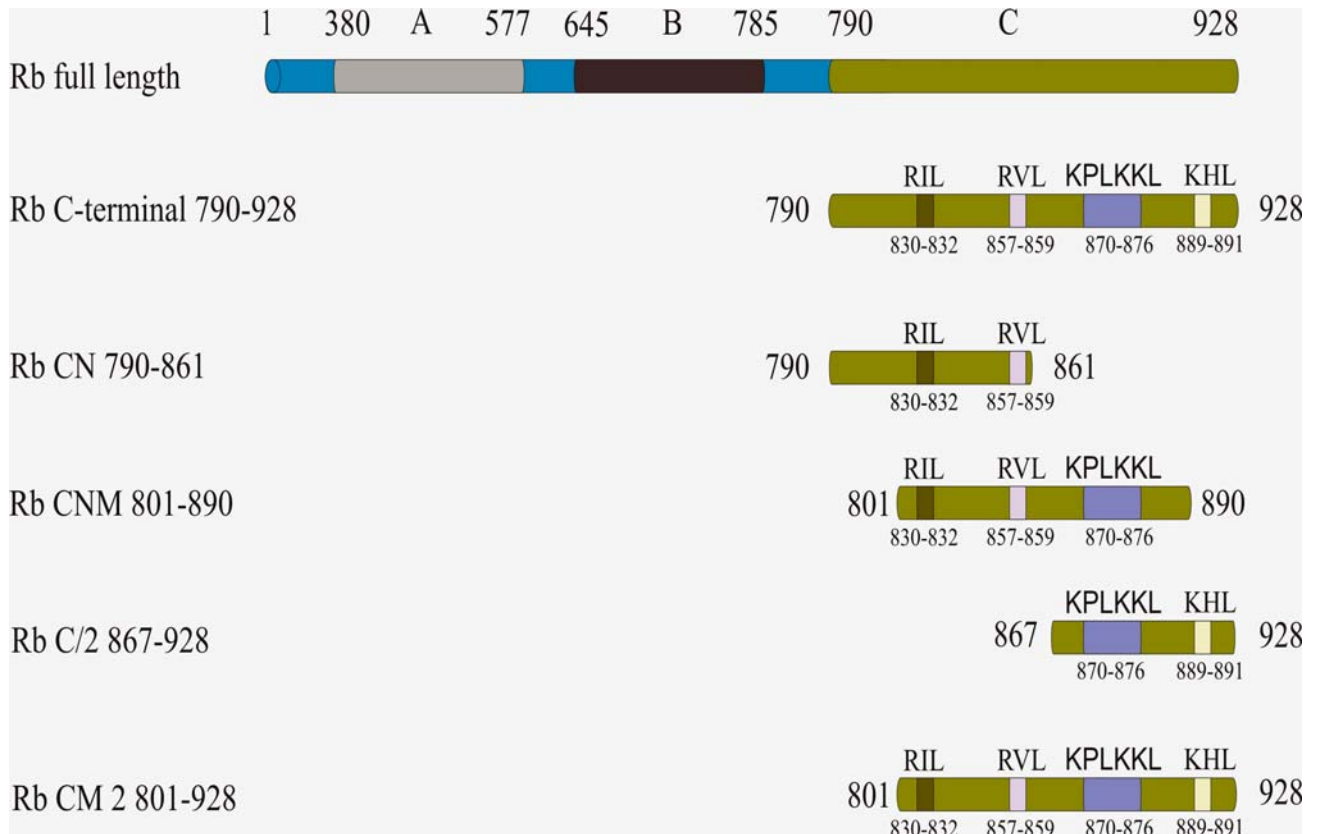
Fig. 41. Schematic diagram of the constructs used in the study. A and B represent the A and B pockets of pRB and C denotes the C-terminus. All *RXL* and *KXL* motifs are marked in the C-terminal domain.

The constructs were made according to the probable binding regions with cyclin A2. Fig. 41 shows all the *RXL* and the *KXL* motifs in the C-terminus part of pRb. Expressions of the proteins were high and all eluted as a monomer in the Superdex 75 gel filtration column. Binding studies were performed with cyclin A2-CDK2.

The C-terminus of pRb, residues 790-928 were mixed with the cyclin A2-CDK2 complex and loaded on the Superdex 75 gel filtration column to observe the binding. Fig. 42A shows two chromatograms overlaid on each other. The one in green represents the binary complex of cyclin

A2-CDK2 whereas the blue denotes the ternary complex (pRb C-terminus-cyclin A2-CDK2). The fractions were analysed in the SDS-PAGE (Fig. 42B), which showed the presence of pRb C-terminal domain in the fractions of cyclin A2-CDK2. A uniformly labeled sample was made of this pRb protein to check the purity by NMR spectroscopy. The sample degraded fast and it was not possible to record the proper titration spectrum.

Fig. 42. A. Chromatogram showing the elution profile of the ternary complex (pRb C-terminus-cyclin A2-CDK2) in the Superdex 75 analytical column. *2B.* SDS-PAGE analysis of different fractions after gel filtration. M-represents the marker.

The next construct that we used in our study was pRb-CNM (801-890). We deleted the last *RXL* motif from the C-terminus part. The binding study with the binary complex was performed with the Superdex gel filtration column and the fractions analysed by SDS-PAGE. The elution profile is shown in Fig. 43A. The two chromatograms were overlaid. The blue stripe portion represents the ternary complex, whereas the green one represents only CDK2-cyclin A2. In the

SDS-PAGE (Fig. 43B) analysis we could clearly visualise the band of the pRb corresponding to its mass. We uniformly labeled the protein and titrated it with cyclin A2-CDK2.
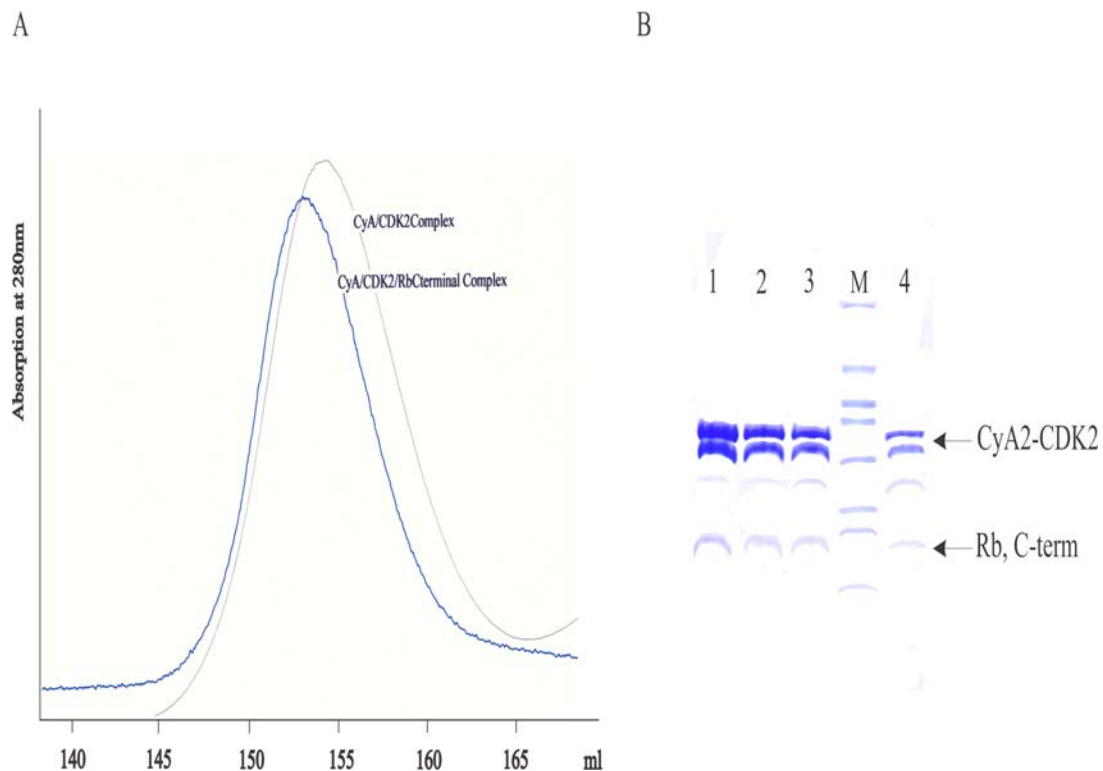

Fig. 43. A. Chromatogram showing the elution profile of the ternary complex pRb-CNM (801-890)-cyclin A2-CDK2) in the Superdex 75 analytical column. The blue striped portions represent the ternary complex whereas the green-stripped portions represent the presence of cyclin A2-CDK2 *B*. SDS-PAGE analysis of the different fractions after gel filtration. M-represent the marker.

Fig. 44A shows a uniformly labeled pRb-CNM (801-890). As the protein was unfolded so the dispersion of the peaks at around 8.3 ppm was low. In the Fig. 44B the two spectra are overlaid to distinguish the probable changes. The spectrum in green represents the last step of titration and the spectrum in red was the reference. 5 peaks disappeared and 9 peaks showed perturbation in NMR chemical shifts.

The other constructs that we studied were pRb-CN (residues 790-861), pRb-C/2 (residues 867-928) and pRb-CM2 (residues 825-928). The binding studies were performed by gel filtration with cyclin A2-CDK2 and a uniformly labeled sample of pRb construct was made for the positive result obtained for binding. The construct CN did not bind to the binary complex of cyclin A2-CDK2 and the pRb-CM2 eluted in the same column volume as cyclin A2-CDK2 in the Superdex analytical column (Fig. 45). It was therefore difficult to predict the binding.

111

The construct pRb-C/2 (residues 867-928) showed positive interaction in gel filtration and a uniformly labeled sample of the protein pRB-C/2 was titrated with the complex of cyclin A2-CDK2. Few changes were observed in the spectrum.

A

B
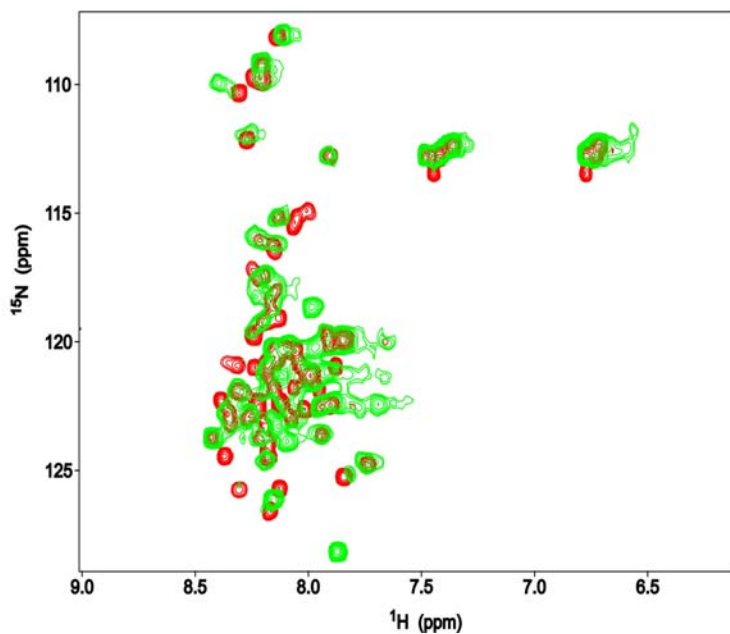
Fig. 44. A. ^{1}H-^{15}N HSQC spectrum of the ^{15}N uniformly labeled sample of pRb-CNM (801-890). *4B*. ^{1}H-^{15}N HSQC spectrum of the ^{15}N uniformly labeled sample of pRb titrated with cyclin A2-CDK2. Reference in red and the last step of titration is in green. For details consult the text.
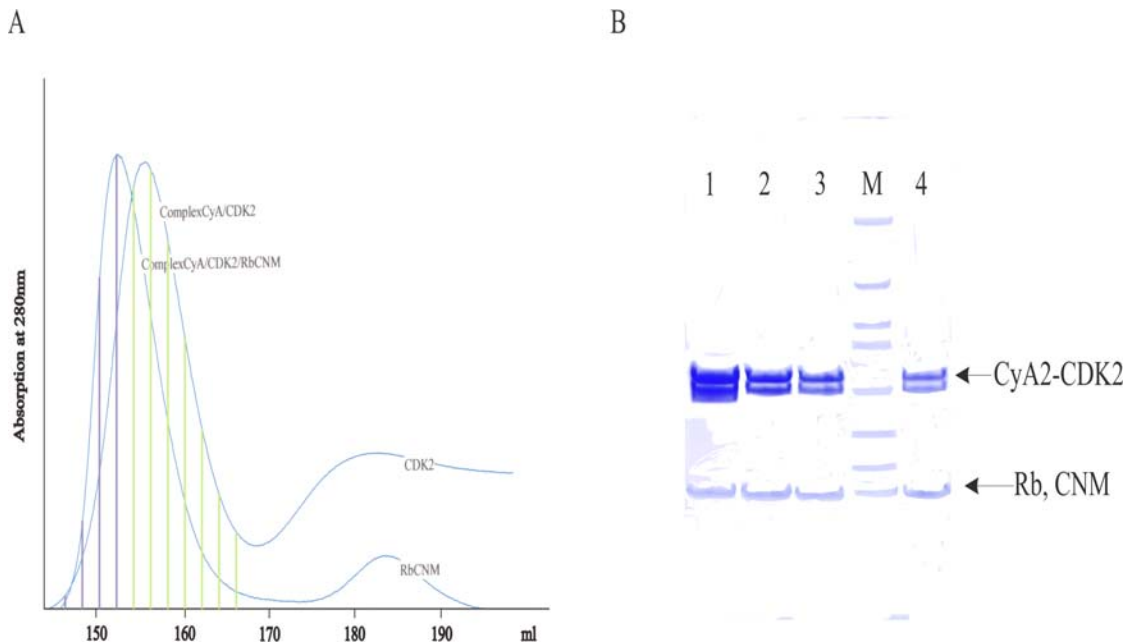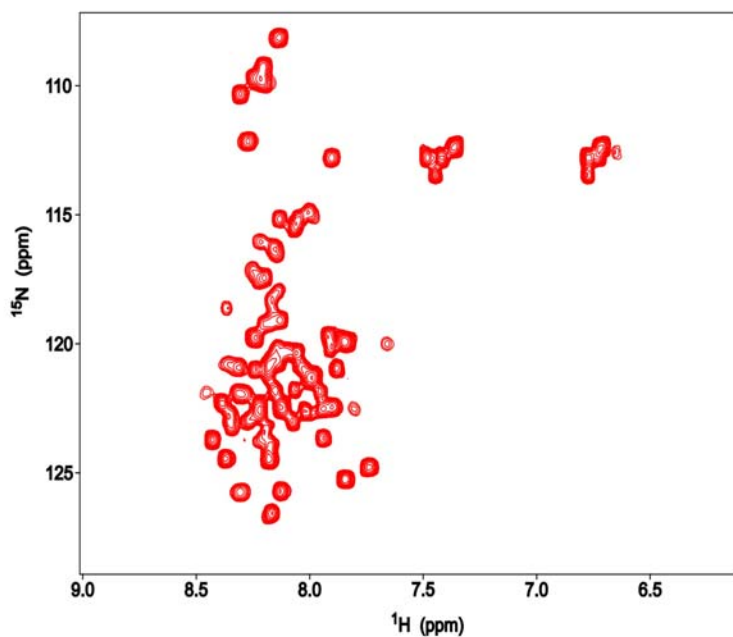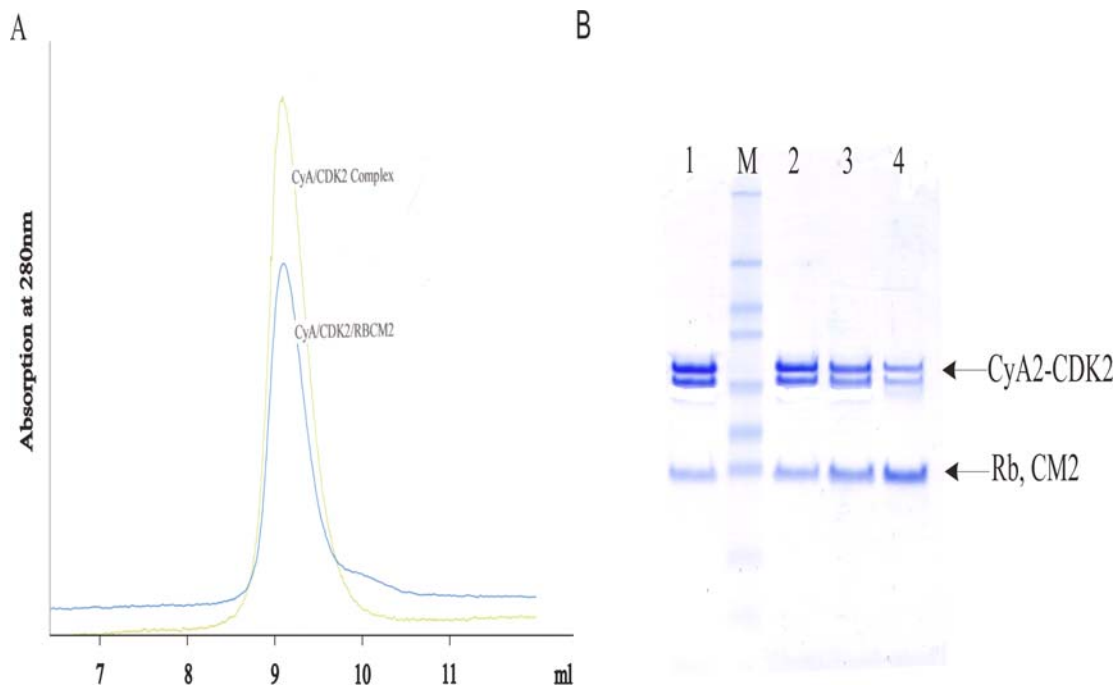
Fig. 45. A. Chromatogram showing the elution profile of the ternary complex (pRb-CM2 (825-928)-cyclin A2-CDK2) in the Superdex 75 analytical column. *B.* SDS-PAGE analysis of different fractions after gel filtration. M-represents the marker.

Fig. 46A shows the reference spectra of the protein pRb-C/2 and Fig. 46B shows the overlaid spectra of the reference and the last step of the titration with cyclin A2-CDK2. In the second Figure we can clearly see that two peaks disappeared and seven peaks showed induced changes in chemical shifts.

The Fig. 47 shows overlaid spectra of the reference of pRb-CN (790-861) and the last step of titration with cyclin A2-CDK2. There were no significant chemical changes observed between the spectra. This shows that the residues 790-861 (pRb-CN) were not required for binding.

In conclusion significant changes in NMR chemical shifts were observed for the construct pRb-CNM (residues 801-890) and no changes were visible with the construct pRb-CN (residues 790-861). This demonstrates that the two *RXL* motifs present in this last construct were not involved in binding. It also proved that the two *RXL* motifs present in the CNM construct (870-876) were responsible for the binding. We tried to crystallize the ternary complex (pRb-CNM-cyclin A2-CDK2) as well as the pRb-CNM alone. Until now we did not get any crystals of either the protein or the ternary complex.
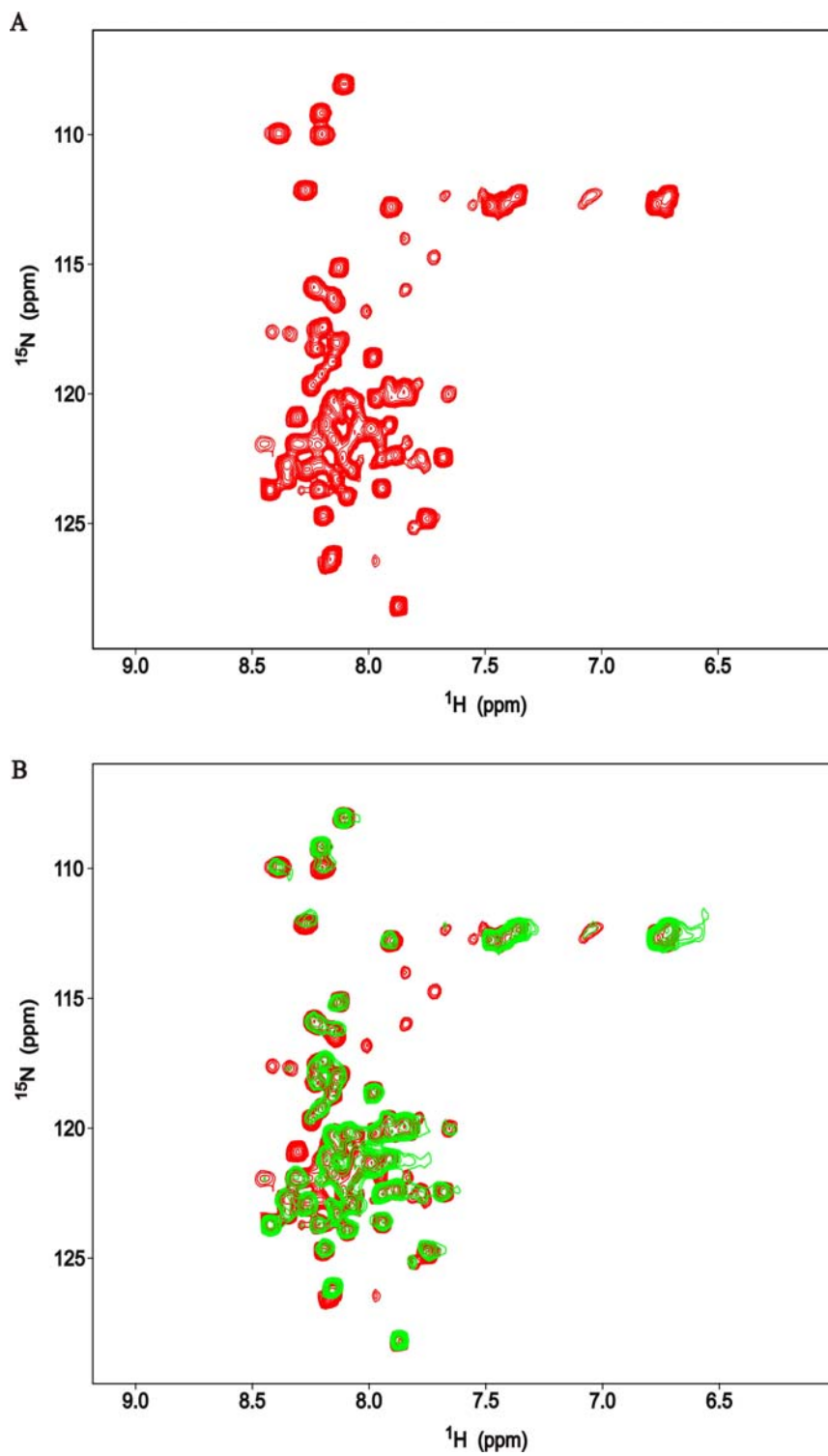
Fig. 46. ^{1}H-^{15}N HSQC spectrum of the ^{15}N uniformly labeled sample of pRb-C/2 (867-928). *B.* ^{1}H-^{15}N HSQC spectrum of the ^{15}N uniformly labeled sample of pRb titrated with cyclin A2-CDK2. Reference in red and the last step of titration is in green. For details consult the text.
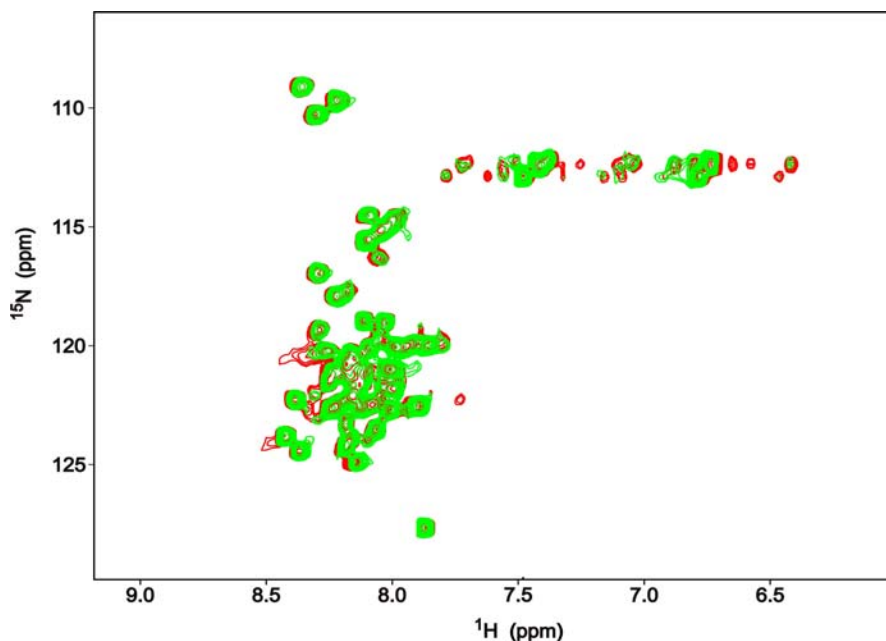
Fig. 47. ^{1}H-^{15}N HSQC spectrum of the ^{15}N uniformly labeled sample of pRb-CN (790-861) overlaid on ^{1}H-^{15}N HSQC spectrum of the ^{15}N uniformly labeled sample of pRb titrated with cyclin A2-CDK2. Reference in red and the last step of titration is in green. For details consult the text.

5.9 Interaction studies of CDK2 with chalcones

Chalcones are derivatives of flavonoids and isoflavonoids, and are abundant in some edible plants or plant extracts and have been used over decades as remedies against various chronic diseases. Chemically they consist of open chain flavonoids in which the two aromatic rings are joined by a three-carbon α, β-unsaturated carbonyl system. Chalcones can be synthesized using Claisen-Schimdt aldol condensation. (Stoll et al., 2001). They are a class of anticancer agents that have shown promising thearuptic efficacy for the management of human cancers. Some of them include inhibition of angiogenesis, interfering with p53-MDM2 interaction, induction of mitochondrial uncoupling and membrane collapse, and disruption of the cell cycle (Nguyen-Hai et al., 2003; Stoll et al. 2001; Kumar et al., 2003; Won et al., 2005; Ducki et al., 1998; Lawrence et al., 2003). The methoxylated chalcone is probably the most potent inhibitor of microtubule assembly in human leukemia cells (Lawrence et al., 2003). Butein (3,4,2',4'-tetrahydroxychalcone) a plant phenol, is one of the major biologically active components of the bark and stems of *Rhus verniciflua*. Butein

was first used as an inhibitor of cAMP-dependent phosphodiesterase (Yu et al., 1995). The compound was isolated from the plant *Dalbergia odorifera T Chen*. Later studies revealed that it specifically inhibited the tyrosine kinase specific activities of the EGF receptors. In the recent studies with the piepridinyl chalcones it has been proved that the levels of pRb, CDK4 and E2F go down in the cells treated with these compounds (Go et al., 2005). These broad antitumor properties of chalcones prompted us to study the effect of some of these compounds on CDK2. We studied by NMR the evidence for binding of these compounds in the ATP binding cleft of the human CDK2.
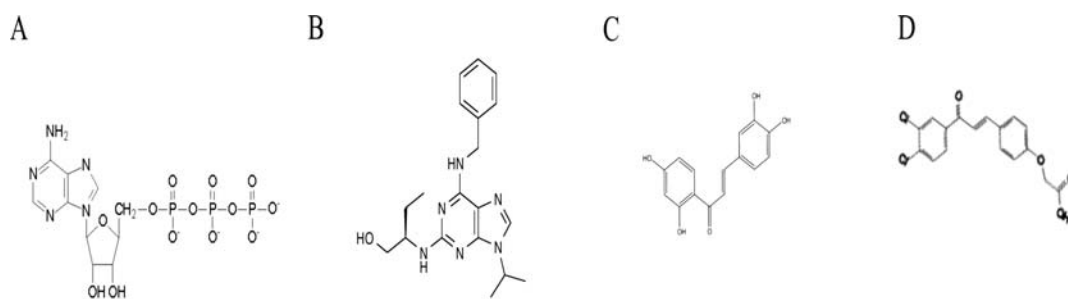
Fig. 48. Chemical structures of the compounds studied in the experiments. *A.* ATP *B.* Roscovitine *C.* Butein *D.* Dichloro-chalcone.

The chalcones that we studied in our experiments are dicholoro chalcone (Fig. 48D) and butein (Fig. 48C). We used ATP and roscovitine (purine derivative) as positive controls for the experiment. NMR spectroscopy was used to determine the binding and the K_D values of the compounds. The compounds were soluble in DMSO and lowering the concentration of DMSO to 5%, precipitated the compound; so it was not possible to carry out the titration by ITC (Isothermal Titration Calorimetry).

Determination of binding sites of chalcone compounds was carried out with a series of HSQC spectra, using uniformly labeled ^{15}N and for selectively labeled ^{15}N lysine of human CDK2. The NMR chemical shift perturbation methods have been successfully used for mapping binding interfaces in proteins and for screening small molecule lead compound in ligand–protein interactions (Stoll et al., 2001; D'Silva et al., 2005). The HSQC shows one peak for every proton bound directly to a nitrogen atom and, thus, exactly one signal per residue in the protein (apart from proline, which is devoid of proton-bound nitrogen), and some additional side chain signals, which can easily be

identified, appeared in the spectrum. A general requisite for mapping interactions of the protein complexes is that the assignment of the NMR spectrum of the protein is known. The assignment is not necessary if it is just to find the interaction at a specific place because the positive compound serves as the reference for the study.

A

B

Fig. 49. ^{1}H-^{15}N HSQC spectra. *A.* ^{1}H-^{15}N HSQC spectrum of the ^{15}N uniformly labeled CDK2. *B.* ^{1}H-^{15}N HSQC spectrum of the ^{15}N selectively labeled lysine sample of CDK2.
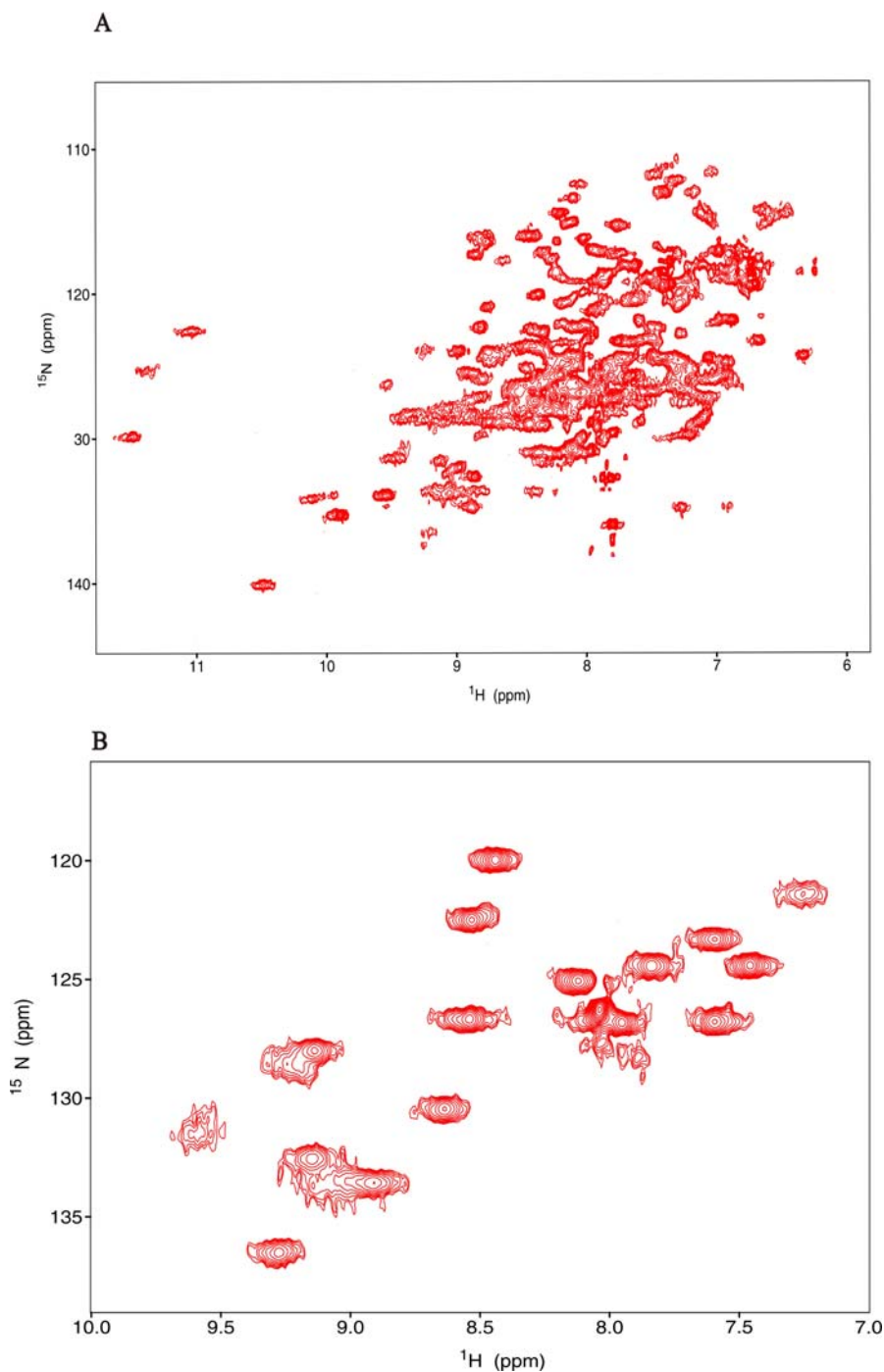
We first tried to test the inhibitors with the ^{15}N uniformly labeled sample of full-length CDK2. CDK2 is a 34 kDa protein and it has 7α- helices, 8β- sheets and 16 loops (Bondt et al., 1993). NMR signals from the α helices are not resolved well in the proton NMR frequency due to overlap of resonances, so it was difficult to determine the (specific) binding site on the protein on addition of the compounds. Selective ^{15}N amino acid labelling was employed in order to overcome the problem of overlap. By comparing the crystal structure of CDK2 bound to roscovitine, flavopiridol, and ATP, we found that the residues of CDK2, which are common to all these compounds, were Lys33, Iso10, Val18, Ala31, Leu134, Phe 80 and Phe 82.
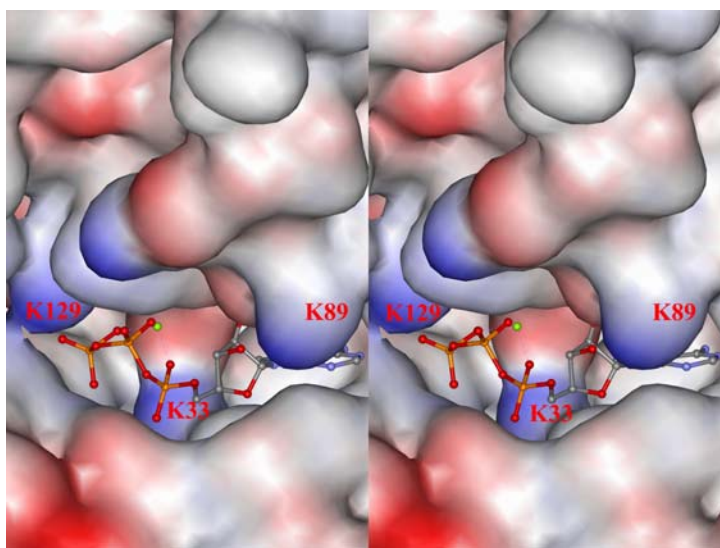
Fig. 50. Stereo view of the crystal structure of CDK2 bound to Mg-ATP (taken from PDB). The ATP region is shown in the structure and the lysines involved in the binding with ATP are numbered and shown in red. The ball and stick form represents the ATP molecule.

In the ATP region of CDK2 there are two lysine residues that take part in the binding, Lys33 and Lys89 (for the inhibitors) and Lys33 and Lys129 (for ATP) (Fig. 51). Lys33 and Lys89 are present in the β3 and α2 helix, respectively (Fig. 50). Lys33 is important for ATP binding because it forms salt bridges with γ-phosphate of ATP and Asp145 residue involved in ATP-Mg^{2+} binding. This behaviour of the Lys33 side chain could be important for drug design because it is possible that the cavity formed by (Val18, Ala31, Lys33, Val64, Phe80 and Asp145) can accommodate larger groups (Azevedo et al., 1996; Legraverend et al., 2000; Otyepka et al., 2002). We chose to

selectively label all the lysines present in the CDK2 (21 lysines) (Bondt et al., 1993). In this construct the histidine-tag bound to the CDK2 has one more lysine. Of the total 22 peaks, 20 are visible in the 2D HSQC spectrum (Fig. 49A). In the spectrum the signals cluster around a ^{1}H frequency of 8.3 ppm, with small as expected for lysines in α helical structures.

```
          histag                                         β₃ sheet
MAHHHHHHVD DDDKM MENFQ KVEKIGEGTY GVVYKARNKL TGEVVALKKI RLDTETEGV
         enterokinase site                                  33
                                              α₂ helix
PSTAIREISLL KELNHPNIVK LLDVIHTENK LYLVFEFLHQ DLKKFMDASA LTGIPLPLI
                                                89

KSYLFQLLQGL AFCHSHRVLH RDLKPQNLLI NTEGAIKLAD FGLARAFGVP VRTYTHEVV

TLWYRAPEILL GCKYYSTAVD IWSLGCIFAE MVTRRALFPG DSEIDQLFRI FRTLGTPDE

VVWPGVTSMPD YKPSFPKWAR QDFSKVVPPL DEDGRSLLSQ MLHYDPNKRI SAKAALAHP

FFQDVTKPVPH LRL
```

Fig. 51. CDK2 protein sequence, with the histidine-tag in italics and the lysines marked by blue letters. Lys33 and Lys89 are highlighted according to their presence in the structure.

We used ATP and roscovitine as positive control for our studies:

ATP: (Fig. 48A) In the crystal structure of CDK2/ATP, the interactions with ATP are characterized by predominantly hydrophobic and van der Waals interactions between the protein and the adenine base, ionic interactions, hydrogen bonds, and van der Waals interactions with the ribose and triphosphate of ATP. In total, there are 26, 15, and 38 contacts between CDK2 and the adenine base, ribose and phosphates, respectively. There are at least 17 hydrogen bonds between the protein and the ATP (Bondt et al., 1993). We titrated the ATP with the ^{15}N lysine selectively labeled CDK2. Addition of Mg-ATP caused 5 changes in the ^{1}H-^{15}N HSQC spectrum (Fig. 52A). Peaks numbered 1, 3, 4 and 5 showed shifts whereas the intensity of peaks numbered 2 and 6 weakened.

Roscovitine: (Fig. 48B) *R*oscovitine [2-(R)-(1ethyl-2-hydroxyethylamino)-6-benzylamino-9-isopropylpurine] has an IC^{50} value of 0.45 µM for CDK2 and the crystal structure with the kinase is known. The purine portion of the inhibitor binds to the adenine-binding pocket of CDK2. There is only one hydrogen bond formation with Leu83 while there are 12 van der Waals interactions (Legraverend et al., 2000). The position of the benzyl ring of the inhibitor enables the inhibitor to make contacts with the enzyme not observed in the ATP-complex structure. There are 20 van der

Waals interactions with the benzyl ring. The total contacts of CDK2 and roscovitine are 53 (De Azevedo et al., 1997). When the ^{15}N lysine sample of CDK2 was titrated with roscovitine there were clear shifts noticeable in the ^{1}H-^{15}N HSQC spectra. In Fig 52B, peaks 1, 3, 4, 5, and 7 shows distinct chemical shifts compared to the others. Whereas the intensity of peaks numbered 2 and 6 weakened. As roscovitine is a competitive analog of ATP, the binding of roscovitine with CDK2 is stronger than ATP and this is clearly seen in the HSQC spectrum.
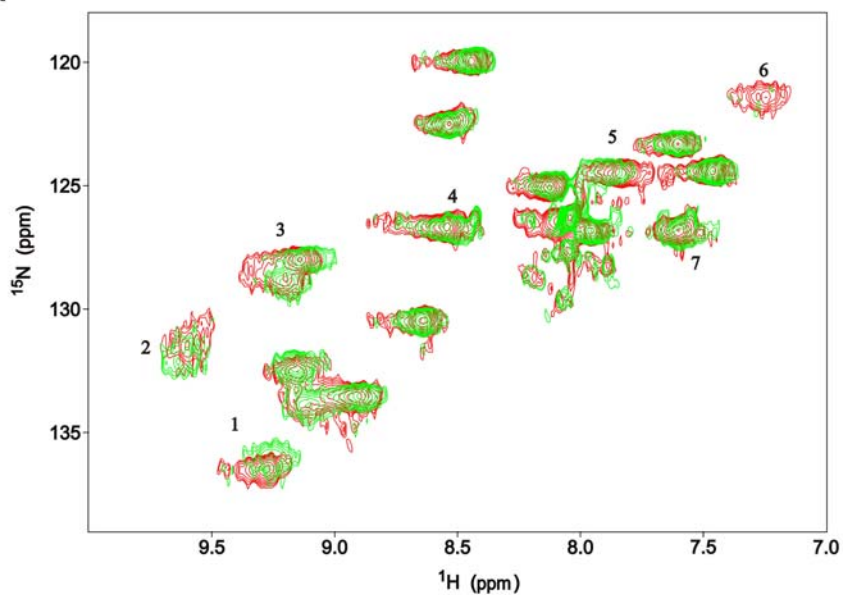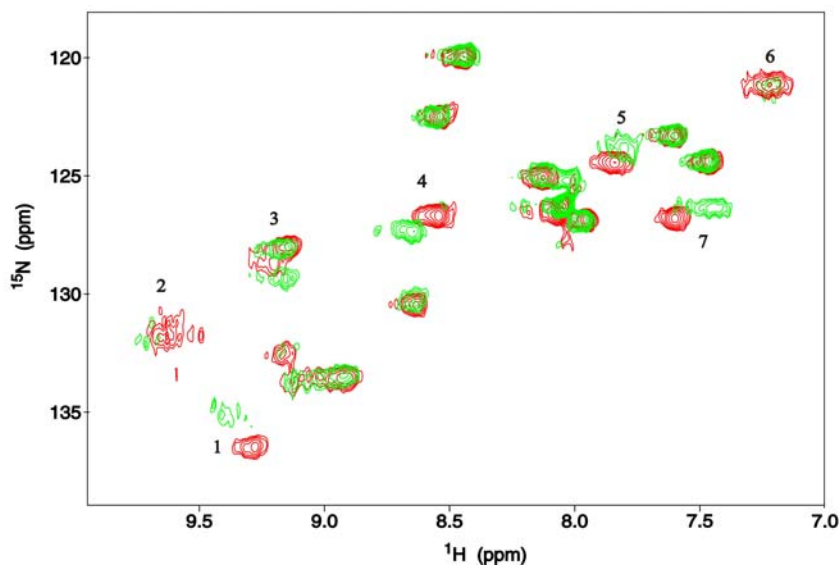
Fig. 52. ^{1}H-^{15}N HSQC spectra. *A.* ^{1}H-^{15}N HSQC spectrum of the ^{15}N selectively labeled lysine of CDK2 titrated with ATP. The reference is in red and the last step of the titration is in green. Both spectra are overlaid over each other to show the exact chemical shifts of the peak. For convenience the peaks, which show chemical shifts or disappear are numbered. *B.* ^{1}H-^{15}N HSQC spectrum of the ^{15}N selectively labeled lysine of CDK2 titrated with roscovitine. Reference in red and the last step of titration is in green. For details consult the text

Dichlorochalcone: (Fig. 48D) When ^{15}N lysine sample of specifically labeled CDK2 was titrated with this compound there were hardly any changes seen in the ^{1}H-^{15}NHSQC spectrum. The intensity of the peaks numbered 2 and 6 weakened whereas the peak numbered 1 shows a small insignificant chemical shift. This compound also precipitated the protein. The binding of this compound with CDK2 was weaker compared to the other inhibitors (Fig. 53A).

A

B
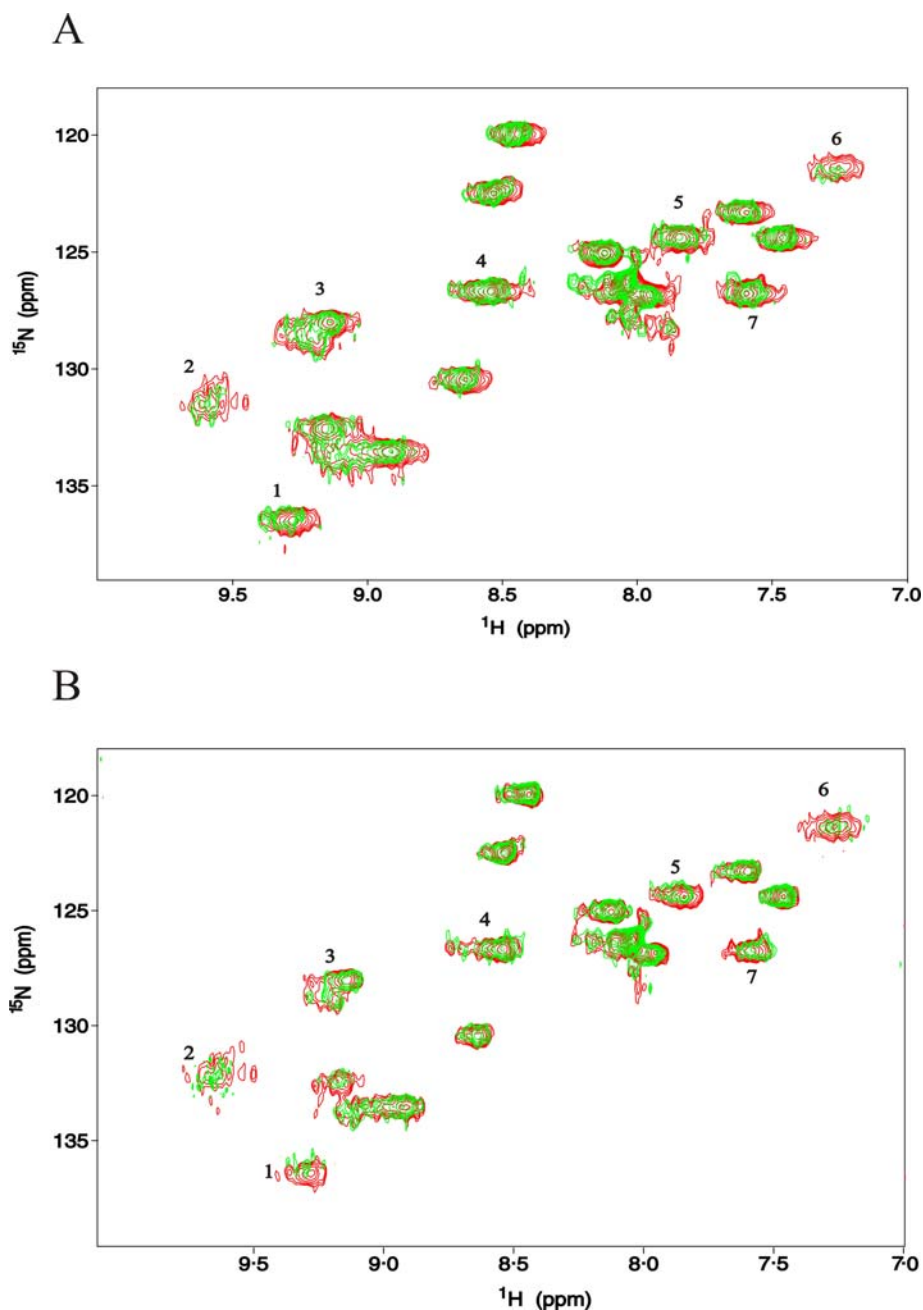
Fig. 53. ^{1}H-^{15}N HSQC spectrums. *4A..*^{1}H-^{15}N HSQC spectrum of the ^{15}N selectively labeled lysine sample of CDK2 titrated with dichloro-chalcone. Reference in red and the last step of titration is in green. For details consult the text. *4B.* ^{1}H-^{15}N HSQC spectrum of the ^{15}N selectively labeled lysine sample of CDK2 titrated with butein. Reference in red and the last step of titration is in green. For details consult the text.

Butein: (Fig. 48C) Butein also inhibited the PKC (protein kinase C), which is a serine–threonine kinase and protein kinase A (cAMP dependent). The inhibition was competitive to ATP and non-competitive to the phosphate acceptor for EGF receptor (Yang. et al., 1998). This made us to test the compound on the CDK2, which is also a serine threonine kinase. When the ^{15}N specifically labeled lysine of CDK2 was titrated with butein the peak numbers 1, 5 and 7 showed changes in chemical shift whereas the peaks 2 and 6 disappeared, confirming that the interaction was stronger compared to the other chalcones (Fig. 53B).
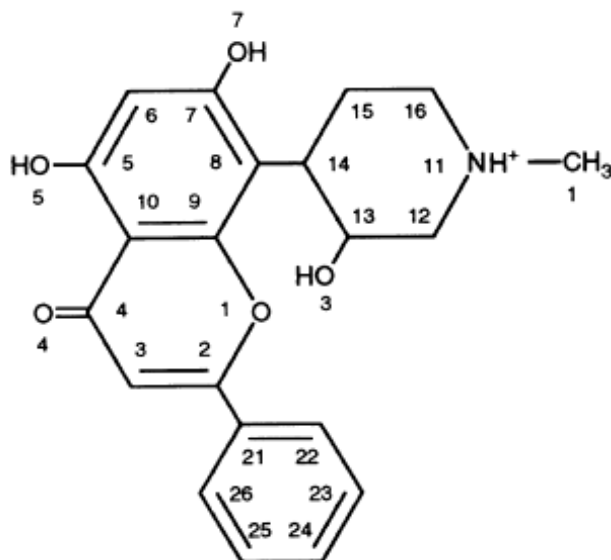
Fig. 54. Molecular structure of (-)-cis-5,7-dihydroxyphenyl-8-[4-(3-hydroxy-1-methyl)piperidinyl]-4H-1-benzopyran-4-one hydrochloride hemihydrate (L868276).

In these above experiments it was possible to detect the binding of chalcones to the ATP binding site of CDK2. Butein proved to be the stronger binding partner compared to the other chalcones. If we compare the chemical structure of flavopridol (Fig. 54) and Butein (Fig. 48C) we can clearly visualize that the presence of OH groups in position 7 and 5 which makes hydrogen bonds and van der Waals bond with the CDK2 in flavopiridol are also present in the compound (Butein). So we conclude that the presence of the OH groups in this region is important for binding to the ATP region of CDK2.

6. Experiments with IGFBP-4

The X-ray analysis was carried out for the binary (NBP-4(3-82)/IGF-I and NBP-4(1-92)/IGF-I) complexes. Purification of all IGFBPs constructs followed similar protocol, involving three different liquid chromatography steps: immobilized metal affinity chromatography on Ni-NTA, cation exchange, followed by gel filtration chromatography.

Cells were grown at 37 °C at an OD_{600}=0.8, induced with 1 mM IPTG and harvested after 3 h. Solubilization was achieved by the 12 h incubation in 6 M guanidinium hydrochloride, under strong reducing conditions (20 mM β-ME), accompanied by vigorous stirring of previously disrupted cells. Insolubilities were removed and samples were clarified by centrifugation.

Presence of the 6-His-tag in all the expressed proteins enabled the use of nickel affinity chromatography under reducing conditions. Ni-NTA slurry was added and binding was performed for 1 h with agitation. After an initial IMAC purification performed under denaturing conditions, the fractions containing target proteins were pooled, 10 mM of β-ME was added, and the pool was dialyzed against 6 M GuHCl at pH 3.0. Recreation of disulfide bridges cannot occur at low pH due to the SH protonation.
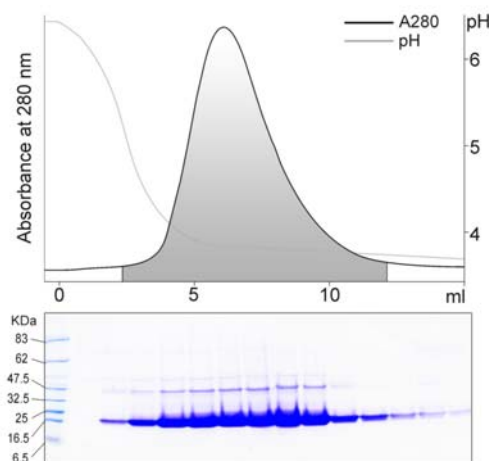
Fig. 55. His/T7-CBP-4 was eluted from 3 ml of the Ni-NTA matrix in a single step at 0.5 ml/min. Fractions of 1 ml were collected and analyzed by PAGE (lanes 2-14). Pools are indicated as gray areas.
Refolding is initiated by reducing the concentration of a denaturant.

For refolding of the IGFBP constructs, a rapid (pulse) dilution technique was applied. The volume of the refolding buffer was adjusted to the total amount of the protein to maintain its final concentration at a range of 0.1 − 0.2 mg/ml. The volume ratio of the denaturant containing

sample to the buffer was kept at 1:50, resulting in the final Gua-HCl concentration of less than 0.15 M. Dilution of the the protein containing solution was accomplished by injecting 100-200 μl aliquots into a refolding solvent, and refolding was allowed to occur for a period of 10-20 min before addition of the next aliquot. Arginine-HCl and glycerol were present as aggregation suppressors, and GSH-GSSG redox system was supplied to enable shuffling of the disulfide bridges. Glutathiones exert their function by cycles of covalent binding to the free thiol groups and their release with assistance of atmospheric oxygen, producing GSSG, H_2O and Cys-Cys bridges. This disulfide shuffling mimics the action of the disulfide isomerase enzyme *in vivo*, preventing the structure from being prematurely rigidified by forming disulfide linkages. Sufficient time is thus given for the protein to collapse into a global free energy minimum state. The refolding was conducted for 3 days with vigorous steering and free access of air. The recovery of the protein of interest varied between 70-95%. In general, the C-terminal constructs of IGFBPs were more susceptible to aggregation than N-terminal ones.
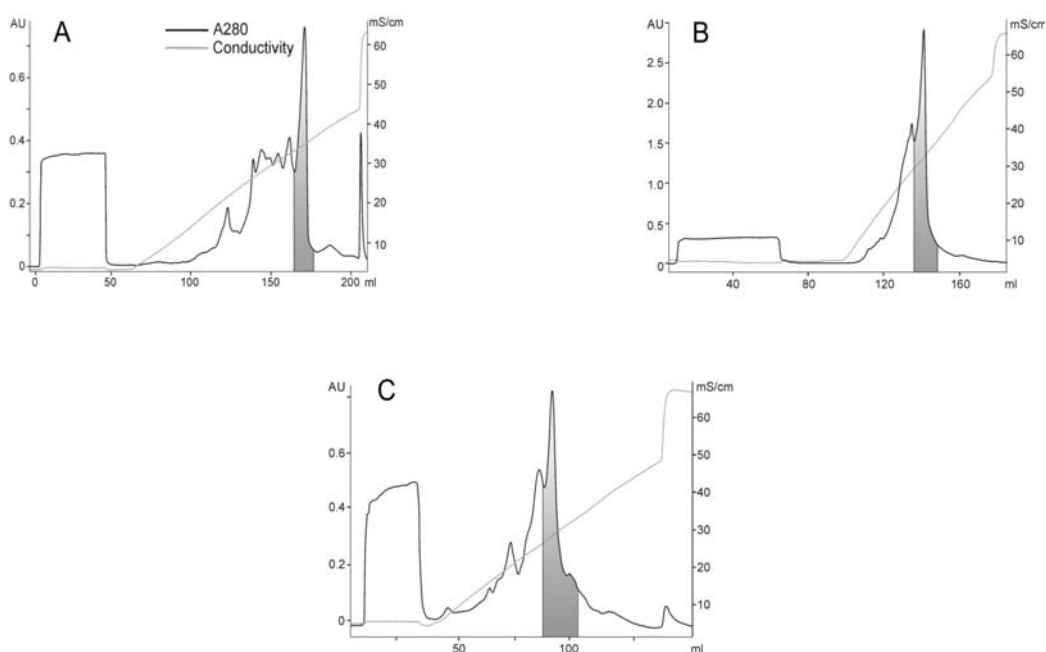
Fig. 56. Three examples of separations of various IGFBP constructs by chromatography on a 8-ml cation exchange column. *A*: purification of CBP-4; bound proteins were fractionated with a 10-700 mM NaCl gradient in 17.5 column volumes (CV); *B*. NBP-4(3-82) was eluted with a 20-800 mM NaCl gradient in 5 CV; *C*: NBP-4(1-92) was fractionated with a 15 CV, 10-700 mM NaCl gradient. Pooled fractions are indicated as gray areas.

A high-resolution chromatographic medium, Mono S, was used at a second purification step. Bound proteins were fractionated with a linear NaCl gradient, the length of which was

chosen individually for each construct on the basis of pilot experiments. The final step of purification, gel filtration enabled separation of the proteins from digested tag peptides, and the restriction protease used for tag cleavage.

6.1 Binding studies with IGF

To qualitatively assess IGF-I binding activity of the purified proteins, an analytical-scale gel filtration-binding assay was carried out. The proteins were mixed in approximately equimolar ratios and separated on an analytical 23 ml Superdex 75 column. Different combinations of the proteins were examined to cover all possible interactions. Fig. 57 summarizes the results of an assay performed for miniNBP-5, CBP-5, and IGF-I.
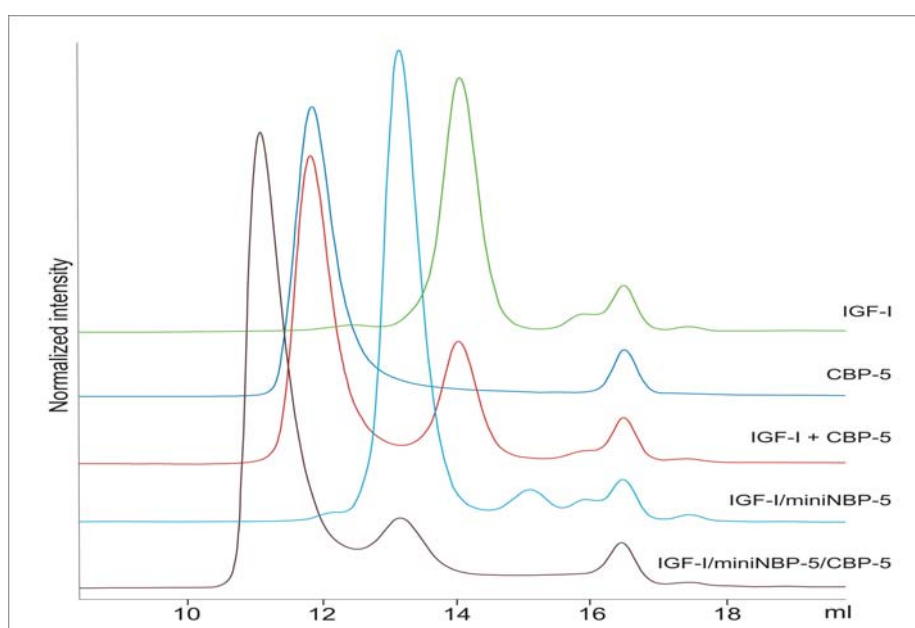
Fig. 57. The gel filtration binding assay for miniNBP-5, CBP-5, and IGF-I. The proteins were mixed in approximately equimolar ratios in the indicated combinations, and separated on the analytical Superdex 75 10/30 column. Elution profiles are superimposed to visualize peak shifts.

To observe the formation of a stable protein complex in a gel filtration experiment, binding must occur with at least medium-low micromolar affinity. Higher K_D values cause the complex to dissociate on the column. Possible weak interactions between the C-terminal domains and IGF-I or C-domains and N-terminal constructs could not be therefore ruled out on the basis of this experiment. NMR spectroscopy can detect even very weak interactions (i.e. in

the millimolar range), therefore it was used to address the problem of inter-domain and C-domain-IGF-I interaction.

6.2 NMR studies on the domain organization of IGFBPs

A typical intensity pattern of a folded protein can be observed in spectra of the N-terminal domain of IGFBP-4 (residues 1-92) and IGFBP-5 (residues 1-83). The spectra of the C-terminal fragments, CBP-4(151-232) and CBP-5(170-247) indicate that there are some unstructured regions located also in the C-terminal fragments (Fig. 58).
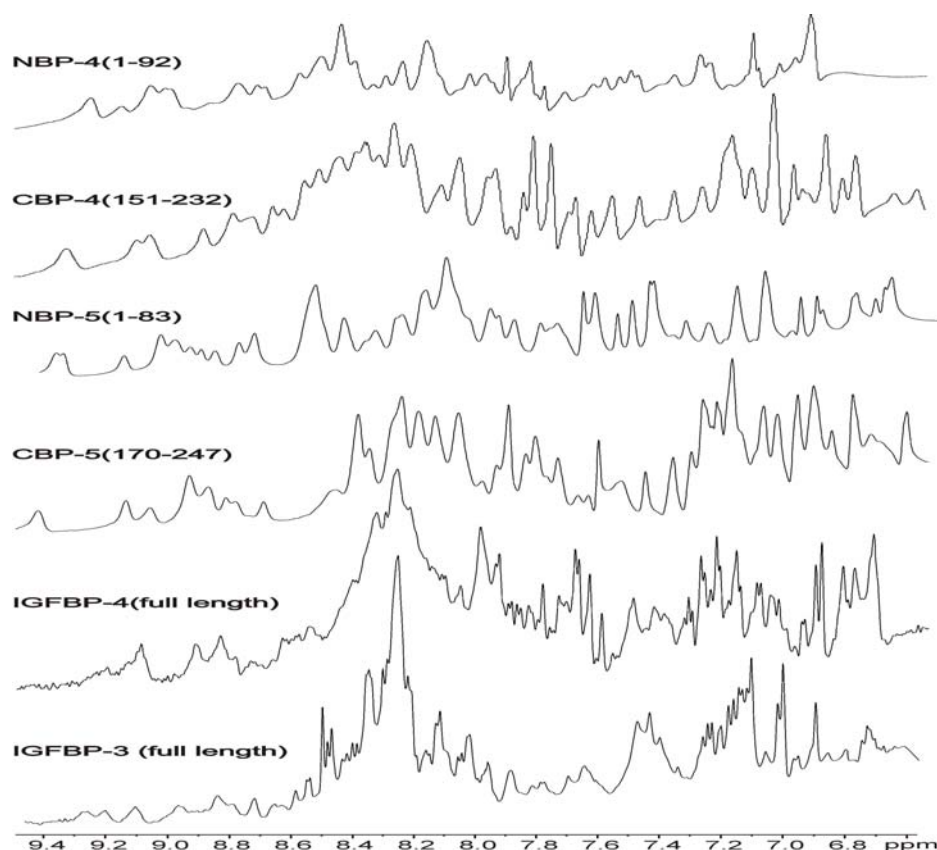
Fig. 58. Characterization of IGFBP structures by one-dimensional NMR spectroscopy. Amide regions of ^{1}H NMR spectra of the full length IGFBP-3, –4, and the isolated N- and C-domains of IGFBP-4 and –5.

Based on these spectra it can be concluded that the whole central variable domain of IGFBP-4 and -5 is in a random coil conformation. The amide region of a 1D spectrum of the full length IGFBP-3 obtained from human cell cultures is also shown to compare its extent of folding

to that of the artificially refolded proteins. Thus, structure-wise, the properties of IGFBPs are the same whether expressed in *E. coli* or in the mammalian expression system.

On the basis of 1D NMR spectra of the intact IGFBP-4 and −5 and their N- and C-domains we concluded that central variable domain is largely disordered, while the first ca. 90 amino acids from the N-terminus form a folded structure. The spectra of the C-terminal fragments indicate presence of disordered regions within the carboxyl-domains. Comparison of 1D NMR spectra of the *E. coli* expressed full-length recombinant IGFBPs with that of IGFBP-3 produced in mammalian cell cultures show no noticeable differences in the folding extent, indicating that the in vitro refolding recreates protein structures seen in the mammalian expression system.

6.3 Structure of IGFBP-4

6.3.1 Crystallization of the binary complexes

Purity, homogeneity, and folding of the proteins to be used in crystallization trials were evaluated using mass spectroscopy, amino-terminal sequencing, and NMR. Three protein complexes, NBP-4(3-82)/IGF-I, NBP-4(1-92)/IGF-I and NBP-4(3-82)/CBP-4/IGF-I, were prepared by mixing approximately equimolar amounts of respective components. The complexes were separated from any excess of either protein by gel filtration on the Superdex 75 prep grade 26/60 column (Fig. 59).
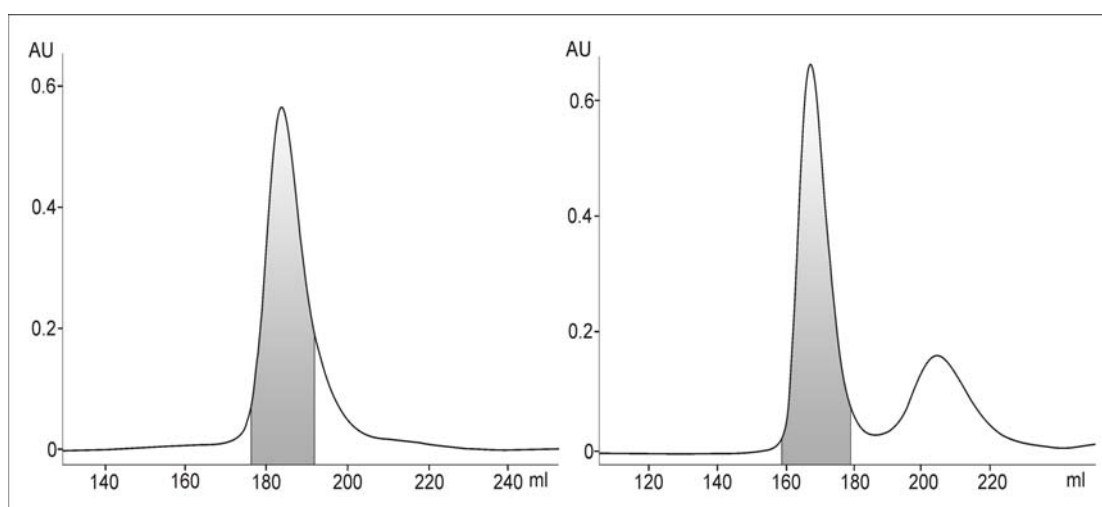
Fig. 59. Purification of the complexed proteins by gel filtration on the Superdex 75 column. Right panel: NBP-4(3-82)/IGF-I binary complex purification; left panel: CBP-4/ NBP-4(3-82)/IGF-I ternary complex purification. Buffer used in both chromatographic runs: 50 mM NaCl, 5 mM Tris, pH 8.0, 0.02% NaN$_3$; flow rate: 0.75 ml/min; pooled fractions are indicated

A precise estimation of the protein ratio in the mixture was more important for the binary than the ternary complexes preparation. In the former case, excess of either NBP-4 or IGF-I in the sample would not be entirely separated from the binary complex using gel filtration (the difference of masses of binary complex and each of its components being not sufficient). Any surplus proteins were thus easily separated from the ternary complex (Fig. 59, right panel). The solvent used contained low salt (50 mM NaCl) and buffering substance (5 mM Tris, pH 8.0) to minimize any possible interference with crystallization reagents. Fig. 60 shows photomicrographs of crystallization experiments described.
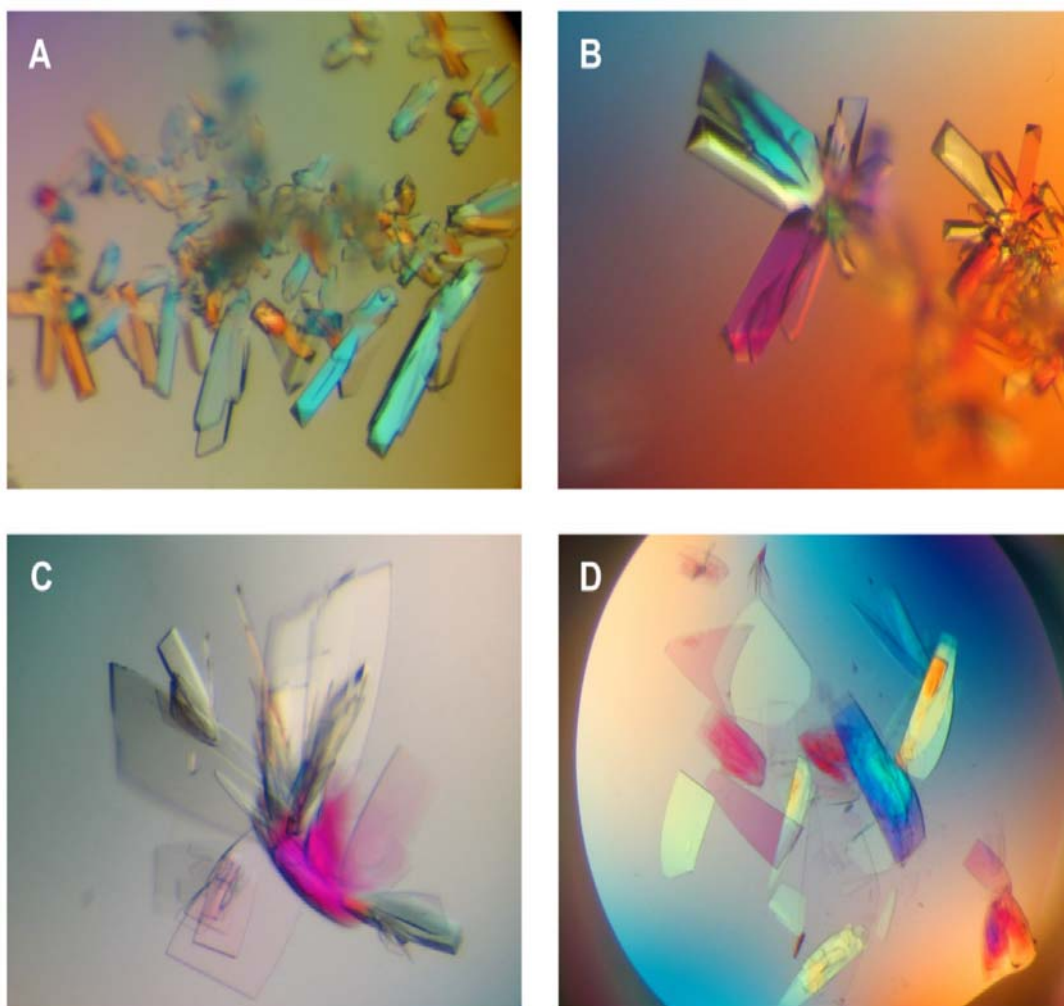
Fig. 60. Examples of the crystallization experiments. *A; B.* X-ray quality orthorhombic crystals of the NBP-4(3-82)/IGF-I binary complex belonging to the $P2_12_12_1$ space group, grown from 23% PEG 1500, 50 mM Tris pH 8.2. The noticeable growth along a streak line arises from the micro-seeding technique used. *C; D.* the monoclinic plate crystals of the NBP-4(1-92)/IGF-I binary complex, obtained from 0.2 M lithium sulfate, 0.1 M Bis-Tris pH 5.5 and 25% w/v PEG 3350. The crystals belong to the $P2_1$ space group.
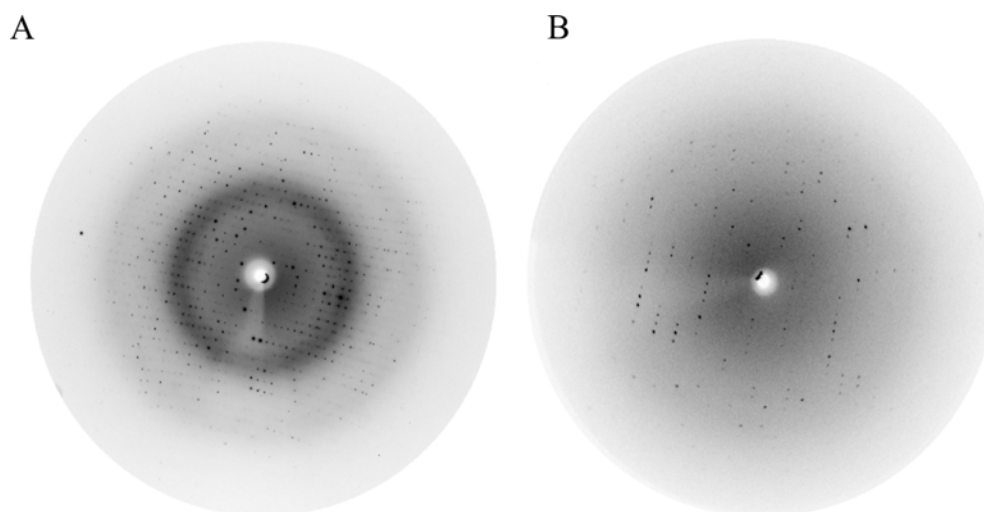
Fig. 61. Diffraction patterns of crystals of the binary complexes. *A*. A frame from the MAR CCD165 (BW6, DESY, Hamburg). The crystal of NBP-4(3-82)/IGF-I (space group $P2_12_12_1$) was rotated 2°. The edge of the image is about 1 Å. *B*. A frame from the MAR 345 image plate, in-house rotating copper anode X-ray source. The $P2_1$ crystal of NBP-4(1-92)/IGF was rotated 3°. Resolution at the edge of the detector is ca. 1.5 Å.

6.3.2 Overall structure of the NBP-4(3-82)/IGF-I binary complex

Fig. 62 shows the structure of the NBP-4 (3-82)/IGF-I complex. NBP-4 has an L-like shape and covers both the N- and C-terminal parts of IGF-I. Features of the NBP-4 structure itself will be discussed first; details of the IGF/BP-4 interactions are covered in a separate section below. The global folds of NBP-4 (residues Ala39-Leu82) and miniNBP-5 (residues Ala40-Glu83) are almost identical in both complex structures, with main chain RMSD of 0.77 Å; the RMSD IGF/minNBP-5 vs. IGF/minBP-4 is 0.50 Å (Fig. 61A).

The core of the NBP-4(3-38) subdomain presents a novel fold stabilized by a short two-stranded β-sheet and 4 disulfide bridges forming a disulphide bond ladder-like structure (Figs. 62 and 63B). This structure is connected to the miniNBP fragment only by a short stretch of amino acids, which include Ala39, Leu40 and possibly Gly41. The X-ray structure shows extensive interactions between NBP-4(3-38) and miniNBP-4 around this region. There are several hydrogen bonds between Arg50 and Ser53 of the NBP-4(3-38) subdomain and Glu23, Glu27, and Glu29 of the miniNBP-4 fragment. Additionally the linker residues make backbone hydrogen bonds to Cys77, Met42, Gly52 and Arg50 of NBP-4(3-38). This network of H-bonding assures high degree of rigidity. The two subdomains are perpendicular to each other, creating the

129

"L" shape for the whole N-domain. The miniNBP is globular, whereas in NBP-4(3-38) the β-sheet and disulfide bridges are all in one plane making the structure appear flat from one side.

Fig. 62. Structure of the NBP-4(3-82)/IGF-I complex. Heavy atom *(A)* and ribbon *(B)* plots of the binary complex. NBP-4 is shown in blue, IGF-I in green. Residues shown in violet constitute the binding site for interaction with NBP-4. Residues marked in red are determinants for binding to IGF-IR.
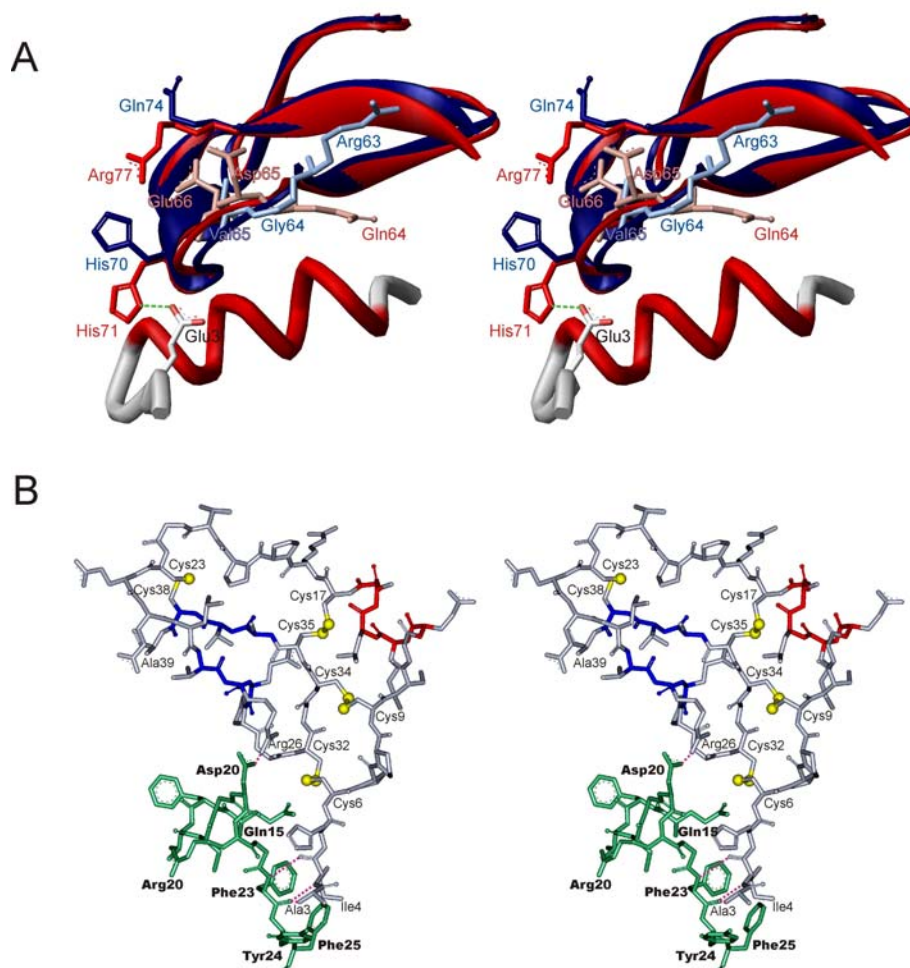
Fig. 63. Structures of the NBP-4(3-82)/IGF-I complex. *A*. Comparison of miniNBP-5 and miniNBP-4 interactions with IGF-I. MiniNBP-5 (red) and miniNBP-4 (blue) were fitted with Swiss-PdbViewer 3.7. *B*. The structure of the N-terminal subdomain of NBP-4 and its interaction with IGF-I. Residues Ala3-Ala39 of IGFBP-4 are colored in gray, with secondary structure elements in blue (for β-sheet) and red (for α-helix). The IGF-I fragment (Gln15-Phe25) is in green. The planar arrangement of disulphide bridges (yellow) is clearly seen.

The core of the NBP-4(3-38) subdomain can be therefore visualized as a "palm" of a hand. The palm is extended with a "thumb" segment of 4-12 residues in various IGFBPs. The thumb segment consists of the very N-terminal residues up to the equivalent of Cys6 in IGFBP-4 and contains a consensus XHHYC motif, where h is a hydrophobic amino acid and y is positively charged.

The structure of IGF-I shown here is of the highest resolution to date (1.6 Å). Only very recently have X-ray structures of IGFs been published, with resolutions ranging from 1.8-2.5 Å (Vajdos et al., 2001; Brzozowski et al., 2002). In our structure a fragment of IGF-I consisting of amino acids Gly32-Gly42 is clearly seen in the electron density map. This segment was not

previously defined but had apparently retained a natural flexibility in the crystal form in agreement with NMR data for free IGF-II (Torres et al., 1995). The fragment assumes a β-hairpin-like structure and appears to be stabilized by crystal packing, as several hydrogen bonds are present with neighboring NBP-4 molecules in the unit cell.

6.3.3 NBP4(3-82)/IGF-I vs. NBP4(1-92)/IGF-I

The first 92 residues of IGFBP-4 are 59% identical to the corresponding N-terminal residues of IGFBP-5, and the remaining residues are functionally conserved. For miniNBP-5 (residues 40-92), the last 9 amino acids showed no electron density in its IGF complex structure (Zeslawski et al., 2001) and were unstructured as determined by NMR (Kalus et al., 1998). Equivalent residues therefore were not expressed in the construct NBP-4(3-82) to aid crystallization of the complex. However, residues Glu90 and Ser91 of IGFBP-4 were reported to be significant for high affinity binding with IGFs (Qin et al, 1998), and therefore we decided to include these residues in our extended N-terminal construct. The two first N-terminal residues were also added because the IGFBP-4(3-82)/IGF-I structure revealed the importance of the two N-terminal hydrophobic residues conserved among IGFBPs. Possibility also existed that eliminating the two first negatively charged residues, Asp1 and Glu2, at the N-terminus in the IGFBP-4 could have changed the properties of this amino terminal part. These residues were therefore added to the refined N-terminal construct, generating NBP-4(1-92).
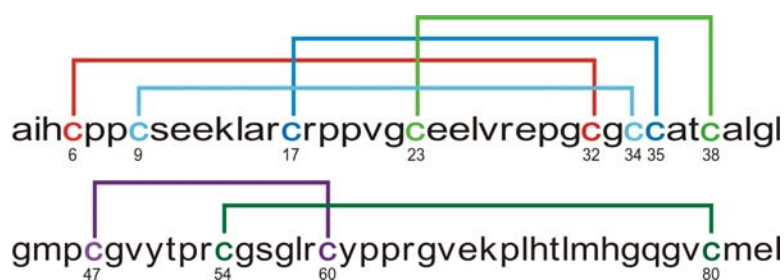
Fig. 64. Arrangement of the disulfide bridges of NBP-4.

       Examination of the structures of the two complexes reveals virtually no changes in positions of the backbone and most of the side chain atoms of both NBP-4 and IGF- heavy atoms RMSD of 0.75 Å. It can therefore be concluded that the presence of residues 1, 2 and 83-92 does not influence the fold of NBP-4 or IGF-I (Fig. 65C). Complexes of a longer and shorter NBP-4

with IGF-I crystallized in two different space groups; identity of the two structures therefore proves that crystal packing has no influence on their folds.
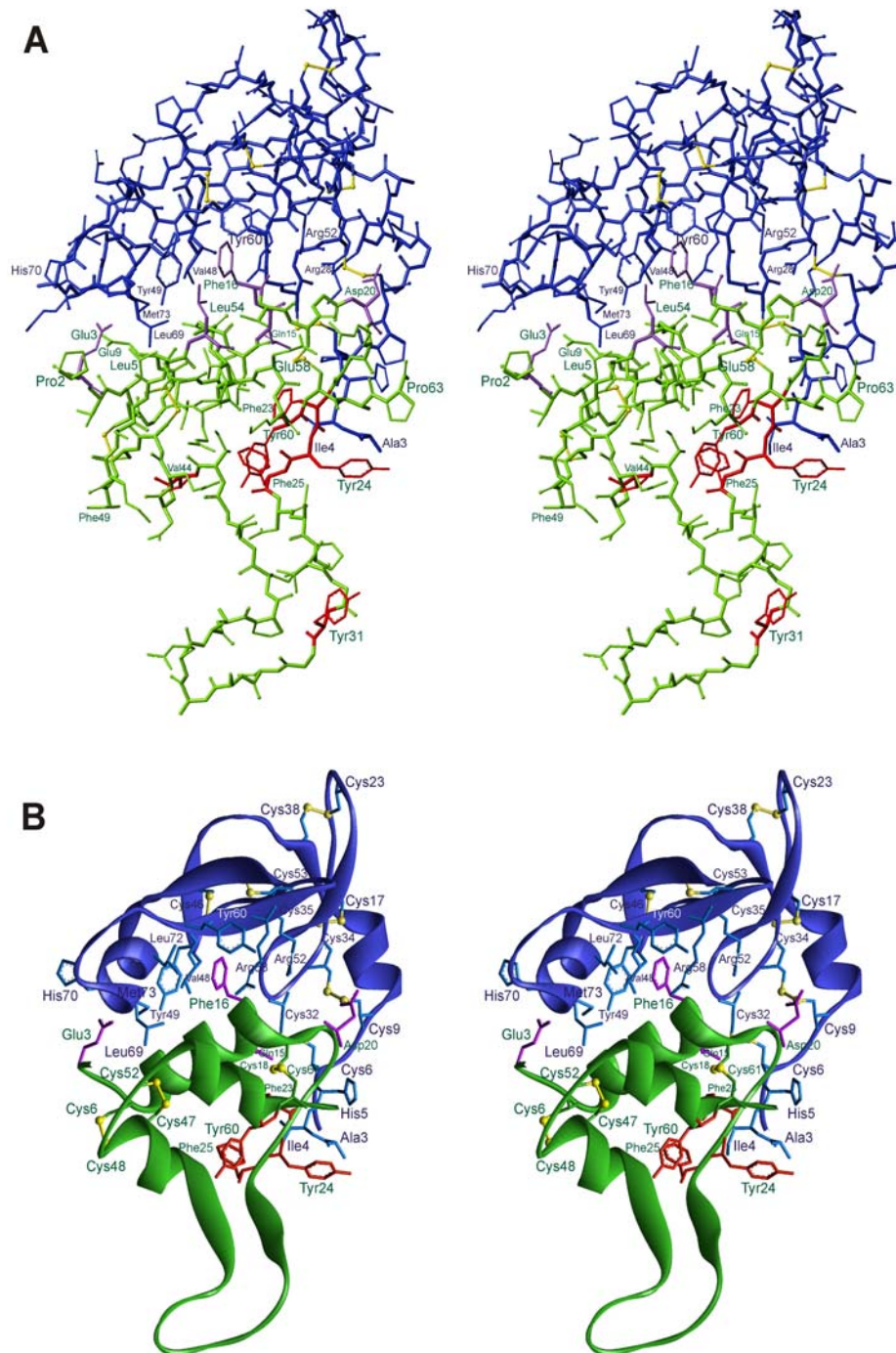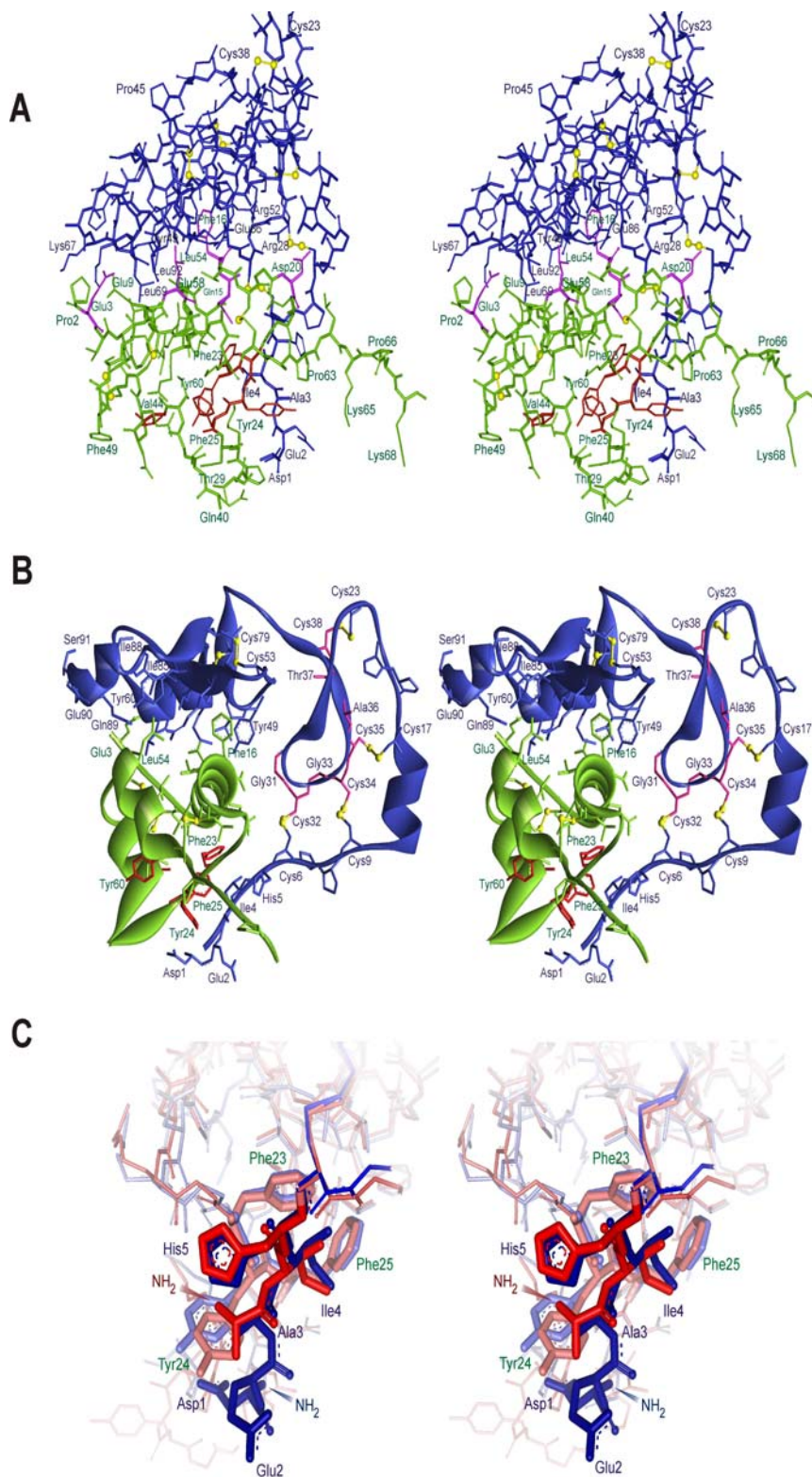

Fig. 65. Structure of the NBP-4(1-92)/IGF-I complex. Heavy atom *(A)* and ribbon *(B)* plots of the complex. NBP-4 is shown in blue, IGF-I in green. Residues shown in violet constitute the binding site for interaction with NBP-4. Residues marked in red are determinants for binding to IGF-IR. The GCGCCXXC consensus motif is shown in magenta *(B)*. Comparison of the IGF-I residues interacting with the "thumb" region in complex with NBP-4(3-82) (red) and NBP-4(1-92) (blue) *(C)*.

Crystal packing, however, had influence on the loose parts of the IGF-I molecule: the flexible loop spanning residues 30-40, clearly defined in the NBP-4(3-82)/IGF-I, showed no electron density in NBP-4(1-92)/IGF-I. The sequence Ala83-Leu92, of which the fragment Glu84-Glu90 forms a short helix, does not contact IGF directly. In the study of Qin et al. (1998), deletion of Glu90 and Ser91 led to the reduced IGF-I and –II binding activity, suggesting functional significance of these residues. Our crystallographic structure, however, shows no contribution of these two residues in formation of the IGF binding site. The presence of the 10-amino acid-long fragment may have, however, an indirect influence on IGF binding: side chains of Ile85, Ile88, and Gln89 shield Tyr60 side chain from the solvent and constrain its conformation of Tyr60 that otherwise would point away from the IGF surface, as can be seen in the NBP-4(3-82)/IGF-I complex structure. Tyr60 along with Pro61 form small hydrophobic cleft, in which Leu54 of IGF-I is inserted, thus extending the hydrophobic contact area of the two proteins.

The position of the His70 side chain in NBP-4(3-82) was rotated ca. 180° relative to the corresponding His71 of miniBP-5. In the structure of NBP-4(1-92), the imidazole ring of the histidine is however flipped back to the configuration observed in the miniNBP-5/IGF-I complex and forms a network of hydrogen bonds with side chains of Glu3 and Glu9 of IGF-I. Similarly, in the NBP-4(3-82)/IGF-I complex structure, IGFs' Phe16 was found rotated ca. 20° clockwise about the α-helix axis, when compared to its position in the miniBP-5/IGF-I complex. In the structure of IGF-I bound to NBP-4(1-92), Phe16 returns to the position found in the miniNBP-5/IGF-I.

6.3.4 The subdomain organization of NBP-4

The N-terminal domain, NBP-4, can be divided into two subdomains: the fragment from residues Asp1-Cys39 and the segment Met44-Glu90. The latter can exist autonomously and corresponds approximately to the mini-IGFBP-5 described by Kalus et al. (1998). The two subdomains are connected by a short stretch rich in Gly and Leu (i.e. Ala39, Leu40, Gly41, Leu42, and Gly43). In order to assess the flexibility of this short stretch, a selectively labelled ^{15}N-Gly and ^{15}N-Leu sample of NBP-4 has been prepared and then a ^{1}H-^{15}N het-NOE experiment was performed. The NOE values obtained for these residues are shown in the Fig. 66. It is seen from the Fig. 66 that only one peak is below the threshold level of the NOE intensity 0.5, indicating that the linker is

rigid. This one peak can be assigned with high probability to Gly56 present in the loop known to be flexible from mini-NBP-5 NMR studies.
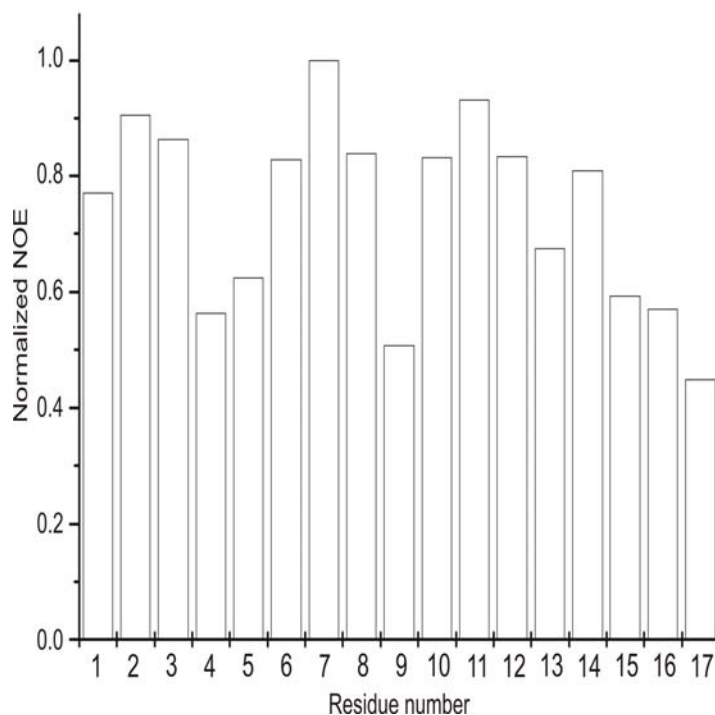
Fig. 66. NOE intensity values for all glycine and leucine residues of NBP-4(3-82). The numbers have been assigned randomly.

6.3.5 Ternary complex NBP-4(3-82)/IGF-I/CBP-4(151-232)

We have also obtained crystals of a ternary complex of NBP-4(3-82) and the C-terminal domain, CBP-4(151-232), with IGF-I. The structure of the binary segment NBP-4(3-82)/IGF-I in this complex could be readily solved by molecular replacement. Unfortunately, the C-domain produced electron densities in disconnected patches that could not be interpreted in detail. Only fragments of the domain in contact with or in proximity to NBP-4/IGF-I showed electron density sufficiently defined to allow incorporation of fragments of a polyalanine model. Identities of individual residues could not however be reliably established. The data allows identification of the C-domain interface surface of IGF-I and NBP-4 (Figs. 67, and 68). CBP-4 appears to exhibit a flat structure that has far-reaching interactions with the N terminal part of NBP-4 from Ala3 up to Tyr48 and also extensive contacts with IGF-I.
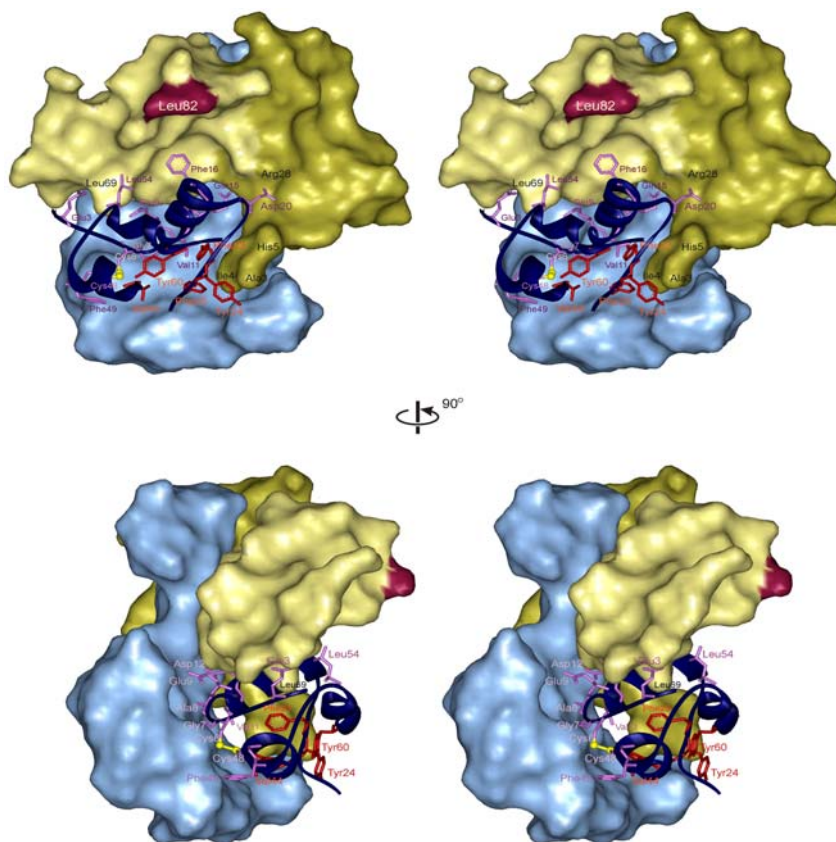
Fig. 67. Surface plot of the structure of the IGF-I/CBP-4/NBP-4 ternary complex. Side-chains of IGF residues important for IGF-IR binding are shown in red. Primary determinants of the IGF/IGFBP-4 interaction are shown in violet. The "base" region of NBP-4 is colored in lighter, "palm"-"thumb" in darker shades of yellow, IGF-I (dark blue ribbon); key IGF residues are numbered, IGF residues responsible for IGF-IR binding are shown in red; CBP-4 is presented as a light blue surface.
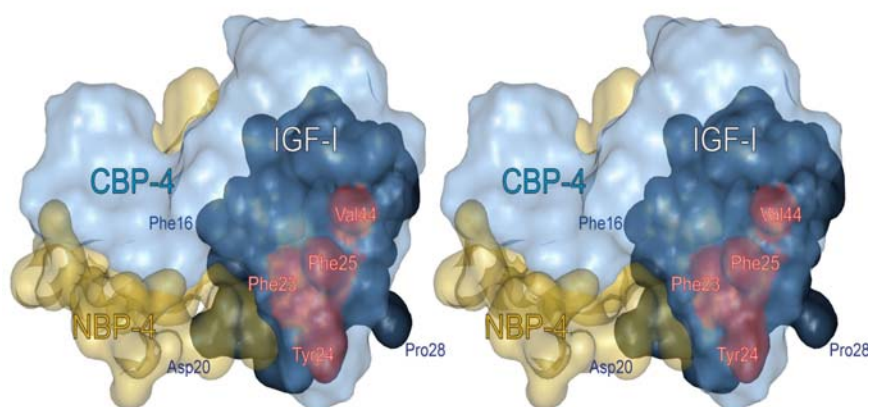
Fig. 68. A surface plot of the structure of the IGF-I/CBP-4/NBP-4 ternary complex. IGF-I(solid dark blue); key IGF residues are numbered, and IGF residues responsible for IGF-IR binding are shown in red. The NBP-4's transparent surface is shown in yellow. CBP-4 is presented as a transparent light blue surface.

6.3.6 The IGF-I/NBP-4 interaction for IGF-I binding to its receptor

The principal interface between IGF-I and NBP-4 is located in the miniNBP subdomain and comprises a hydrophobic sandwich that consists of interlaced protruding side chains of IGF-I and solvent-exposed hydrophobic side chains of the NBP-4. The side chains of IGF-I Phe16 and also Leu54 are inserted deep into a cleft present in NBP-4. This cleft is formed by side chains of Arg52 and Arg58 on one side of the molecule and by Val48, Leu69 and Leu72 on the opposite inner side, with a base formed by residues Gly47, Cys59 and Tyr60. Phe16 of IGF makes direct contacts with the backbone and side chain of Val48, and with Cys59 of NBP-4.

The IGF Phe16 NBP-4 interaction is closed on the solvent side by side chains of Glu3 and Glu9 of IGF-I, and by Tyr49, Thr50 and Pro30 of NBP-4.The N-terminal palm subdomain (between residues 6-38) and the thumb segment (residues 3-5) make several additional contacts to IGF-I. The "thumb" Ala3 and Ile4 of NBP-4 make major interactions by filling the hydrophobic patch created by IGF Phe23, Tyr24 and Phe25. The interaction is further strengthened by hydrogen bonding (Ile4 C=O to Phe23 NH, Ile4 NH to Phe23 C=O). The palm contacts IGF only from one edge mostly through BP-4 Arg28 (Arg28 NH1 to the IGF Asp 20 OD1). The C-domain appears to make extensive contacts to IGF. Contact residues on IGF are Cys6-Ala8, the sidechain of Glu9, Val11 and Asp12, Tyr24, Phe25, Asn26, Val44, Cys48 and Phe49 (Figs. 67 and 68).

6.4 Functional studies of IGFBP-4 – IGF interaction

In order to exclude any interaction that could be weak, these interactions have been tested by NMR using ^{15}N labeled CBP-4 or NBP-4. Addition of CBP-4 did not cause any changes in the ^{15}N–HSQC spectrum of ^{15}N labeled NBP-4, proving no interaction. In a similar manner, addition of IGF-I to ^{15}N-CBP-4 had no effect on the ^{15}N HSQC. In a positive control we were able to see clearly the interaction of NBP-4/IGF-I with ^{15}N-CBP-4 (Fig. 69).

Ligand binding–induced folding of partially unstructured proteins and peptides is an often-observed phenomenon (Weber et al., 2000). The experiments described above did not reveal such a behavior for CBP-4: no cross peaks emerged from the ^{1}H 8.3-ppm spectral region after addition of NBP-4/IGF-I (Fig. 69). Similarly, 1-D spectra of the full-length IGFBP-4/IGF-I complex do not show any improvement in terms of folding over free IGFBP-4. These experiments show that neither carboxyl-terminal unstructured regions nor the linker domain are

137

influenced by complex formation, and the overall folding pattern of IGFBP-4 is unaffected by IGF-I binding.
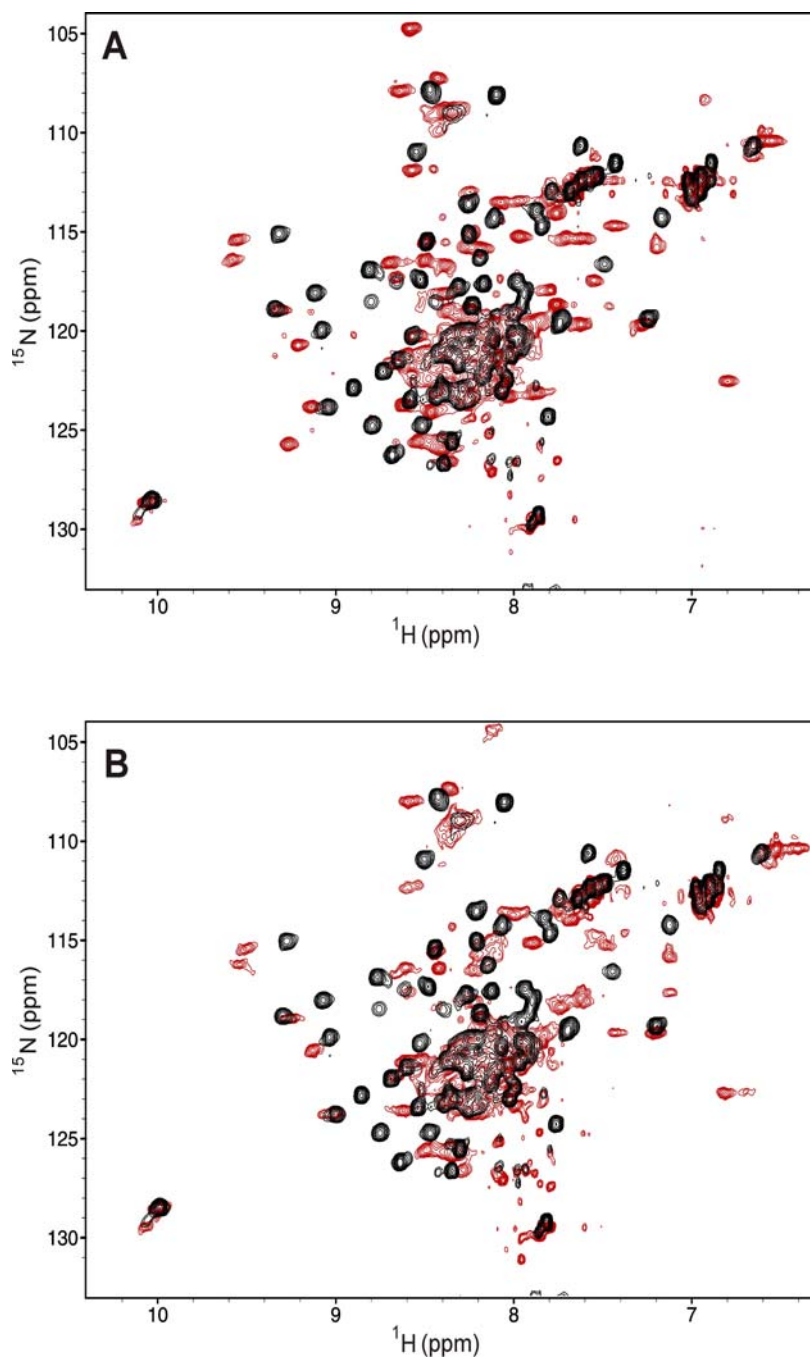
Fig. 69. Effect of the ternary complex formation on CBP-4 folding. Superimposed 2D-HSQC spectra of the ^{15}N-labeled CBP-4 in a free form (black) and bound to *(A)* the NBP-4(3-82)/IGF-I binary complex (red), and *(B)* the miniNBP-5/IGF-I binary complex.

138

6.4.1 Fine-tuning of the N-terminal "thumb" residues

The very first amino terminal residues of IGFBPs have been neglected to date in mutagenesis studies aiming at delineation of the proteins' structure/function relationships (reviewed in Clemmons, 2001).

To assess contribution of the "thumb" region of IGFBP to its IGF-I binding activity, a number of N-terminal mutants of NBP-4 was produced and their IGF-I binding activity was compared using isothermal titration calorimetry (Table 1). Differences in K_D values among the constructs, although not large, show that extra contacts made by the "thumb" residues present in our constructs do increase the strength of IGF-I bind.

Table 1. List of NBP-4 constructs

Construct	N-terminal sequence	K_D [nM]
NBP-4(1-82)	D E A I H C	317±19
NBP-4(3-82)	A I H C	865±78
NBP-4(6-82)	G C	3350±590
BP1-NBP4	A P W H C	544±45
BP3-NBP4	G A S S G G L G P V V H C	268±14
Cons BP3-NBP4	G A G A V G L G P V V R C	316±27
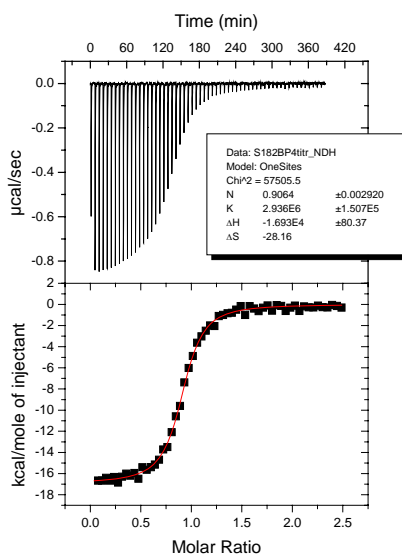
NBP-4(1-82) titrated with IGF   NBP-4(3-82) titrated with IGF
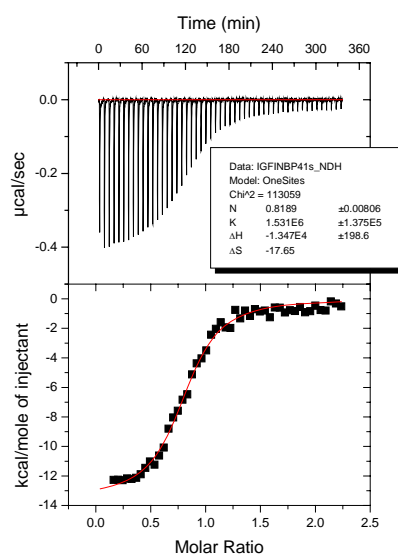
Data on structural determinants of IGFBP/IGF binding can be used for design of targets, which could regulate the actions of IGFs. This can be carried out either by site-directed mutagenesis of IGFBPs and thus producing IGFBPs of modified binding affinity, or by design of novel, low molecular weight ligands. Targeted release of IGF from their binding proteins might have therapeutic value for stroke and other IGF responsive diseases.

Inhibition of IGF-stimulated cancer cell growth via receptor intervention is a major strategy in anticancer drug discovery as shown by the efforts of pharmaceutical companies to develop both protein and small molecule antagonists toward the receptor (LeRoith and Helman, 2004; Ali et al., 2003; Mazerbourg et al., 2004; Firth and Baxter, 2002; Cohen et al., 2000; Khandwala et al., 2000; Bach, 1999). Mutagenesis of the thumb fragment to increase the IGF/BP fragments binding or to enhance their inhibition of IGF-IR action can therefore offer a therapeutic strategy against cancers that are the type I I-IGF receptor dependent.

7. Summary

The thesis carries information on the studies conducted by X ray crystallography and the nuclear magnetic resonance on the domain organization of different proteins and their structural necessities for binding to their respective partners.

14-3-3 proteins regulate many cellular processes that are important in cancer biology, such as apoptosis and cell-cycle checkpoints. There are seven human 14-3-3 genes and one of these, 14-3-3σ has been directly implicated in the aetiology of human cancer. Loss of 14-3-3σ expressions sensitizes cancer cells to conventional anticancer agents, so its inhibition could be exploited for therapeutic purposes. In order to identify structural differences between the 14-3-3 isoforms, the crystal structure of the human 14-3-3σ protein was solved at a resolution of 2.8 Å and compared it to the known structures of 14-3-3ζ and 14-3-3τ. The global architecture of the 14-3-3σ fold was similar to the previously determined structures of 14-3-3ζ and 14-3-3τ: two 14-3-3σ molecules form a cup-shaped dimer. Significant differences between these 14-3-3 isoforms were detected adjacent to the amphipathic groove, which mediates the binding to phosphorylated consensus motifs in 14-3-3 ligands. Another specificity determining region was localized between amino-acids 203 to 215. These differences presumably select for the interaction with specific ligands, which may explain the different biological functions of the respective 14-3-3 isoforms. Furthermore, the two 14-3-3σ molecules forming a dimer differ by the spatial position of the ninth helix, which was shifted to the inside of the ligand interaction surface, thus indicating adaptability of this part of the molecule. In addition, 5 non-conserved residues were located at the interface between two 14-3-3σ proteins forming a dimer and represented candidate determinants of homo- and hetero-dimerization specificity. The structural differences among the 14-3-3 isoforms described in the thesis presumably contributed to isoform-specific interactions and functions.

Cell proliferation requires precise coordination of cell cycle. This is achieved by direct interactions between proteins, indirect interaction in multiprotein complexes, and modulation of gene expression levels of partner proteins. The interactions of CDK6, p19, and MyoD peptides, CDK2-cyclin A2, and its binding partners: p53, pRb and p27 have been tested using *in vitro* biophysical and biochemical methods, which included mass spectrometry, nuclear magnetic resonance (NMR), the affinity chromatography pull-down assays, ITC and gel filtration chromatography. Using this multimethod approach, interactions between pRb, p27, and p53 with

CDK2-cyclin A2, CDK6 and p19 were documented. The techniques of nuclear magnetic resonance helped to gain a more detailed understanding of the domains of p53, pRb, p27, and their structural requirements for binding to CDK2-cyclin A2. Using the same methods, it was unambiguously shown that there was no direct protein–protein interaction in vitro between CDK6 and a 15-amino-acid peptide from the C-terminal domain of MyoD. Indirect interactions, through additional binding partners in multiprotein complexes or modulation of gene expression levels of these proteins, were therefore their probable mode of action. The flavonoid inhibitors of the ATP binding cleft of CDK2 were also studied through NMR spectroscopy, and butein (which is a flavonoid derivative) was found to be a competitive inhibitor of ATP. New insights were gained from these experiments into the involvement of CDKs and their cellular partners in controlling the cell cycle.

Insulin-like growth factor binding proteins (IGFBPs) control bioavailability, activity and distribution of IGF-I and –II in the serum. While IGFBPs also have IGF-independent actions, all IGF-dependent actions, positive or negative, i.e. potentiation or inhibition of its mitogenic and metabolic effects, depend on the formation of high-affinity complexes with IGFs. Amino- and carboxyl-terminal fragments of IGFBPs, form together a high-affinity IGF binding site, but their relative contribution to the binding affinity varies among IGFBPs. Structural studies conducted on different constructs of IGFBPs helped to determine the binding regions to IGFs. The structure of the complex of the N-terminal domain of IGFBP-4 (NBP-4, residues, 1-92) and IGF-I emphasizes a critical role of the first amino-terminal residues of IGFBPs for IGF signaling. A model of the ternary complex of IGF-I, NBP-4, and the C-terminal domain (CBP-4, residues 151-232) derived from diffraction data shows that CBP-4 contacts both (NBP-4 and IGFI) and also blocks the IGF-IR binding region of IGF-I.

8. Zusammenfassung

Die Doktorarbeit gibt neue Informationen zu Studien der Domänen-Organisation verschiedener Proteine und ihre strukturellen Voraussetzungen zur Bindung ihrer zugehörigen Partner mittels Röntgenkristalographie und Kern Spin Resonanz.

14-3-3 Proteine regulieren eine Vielzahl von zellulären Prozessen welche bedeutsam in der Krebsbiologie sind, wie z.B. Apoptose oder Check-point Kontrolle. Im menschlichen Genom gibt es insgesamt sieben 14-3-3 Gene und eines daraus, nämlich 14-3-3σ, stellt einen direkte Verbindung mit der Ätiologie von Krebs her. Der Verlust der 14-3-3σ Expression macht Krebszellen anfällig für konventionelle anticancer Wirkstoffe, d.h. die Inhibition von 14-3-3σ stellt ein mögliches neues Ziel für die Krebstherapie da. Um strukturelle Unterschiede zwischen den 14-3-3 Isoformen herauszufinden wurde die Kristallstruktur von 14-3-3σ bei einer Auflösung von 2.8 Å gelöst und mit den bekannten Strukturen von 14-3-3ζ und 14-3-3τ verglichen. Die globale Architektur von 14-3-3σ ist identisch zu denen der zuvor beschriebenen Isoformen 14-3-3ζ und 14-3-3τ. Zwei 14-3-3σ Moleküle bilden ein tassenförmiges Dimer. Signifikante Unterschiede zwischen den 14-3-3 Isoformen wurden entlang einer amphipathischen Furche gefunden, die die Bindung von phosphorylierten Konsensusmotifen in 14-3-3 Liganden steuert. Eine weitere spezifitätsbestimmende Region wurde zwischen der AS 203 und der AS 215 gefunden. Diese Unterschiede sind wahrscheinlich für die Selektion der spezifischen Liganden verantwortlich und sind die Grund für die unterschiedliche biologische Funktion der 14-3-3 Isoformen. Desweiteren unterscheidet sich das 14-3-3σ Dimer in der räumlichen Anordnung der neunten Helix von den anderen 14-3-3 Isoformen. Die Helix ist nach innen, in Richtung der Liganden Bindungsstelle, verschoben, was die Anpassungsfähigkeit dieses Bereichs des Moleküls zeigt. Zusätzlich wurde an der Kontakfläche zwischen den beiden 14-3-3σ Einheiten fünf nicht konservierte Reste entdeckt, die für die Homo- und Heterodimer Bildung wichtig sein könnten. Die strukturellen Unterschiede zwischen den 14-3-3 Isoformen, die in der Doktorarbeit vorgestellt werden, tragen zu den spezifischen Interaktionen und Funktionen der jeweiligen Isoform bei.

Zellproliferation benötigt eine präzise Kontrolle des Zellzyklus. Das wird durch direkte Protein-Protein Wechselwirkung, durch indirekte Wechselwirkung in Proteinkomplexen und durch Modulation der Genexpression von Partnerproteinen erreicht. Die Interaktion zwischen CDK6 und MyoD Peptiden bzw. p19, sowie zwischen CDK2/Cyclin A2 und dessen

Bindungspartnern: p27, p53 und pRB wurden *in vitro* mit biophysikalischen und biochemischen Methoden, wie Massenspektrometrie, Kern Spin Resonanz Spektroskopie (NMR), Affinitäts-chromatographie pull-down Experimenten, ITC und Gelfiltrationschromatographie, untersucht. Durch diesen Multimethoden Ansatz wurden die Wechselwirkungen zwischen p27, p53 und pRB einerseitz und CDK2/Cyclin A2 andererseits, sowie die Wechselwirkung zwischen CDK6 und p19 dokumentiert. Mit Hilfe der NMR Spektroskopie konnte ein genaueres Bild der Domänen von p27, p53 und pRB und deren strukturelle Voraussetzung für die Bindung an CDK2/Cyclin A2 gewonnen werden. Mit den gleichen Methoden konnte gezeigt werden, dass es keine direkte Protein-Protein Wechselwirkung zwischen CDK6 und einen 15 Aminosäure langen Peptid der C-terminalen Domäne von MyoD gibt. Indirekte Wechselwirkung über weitere Bindungspartner in Multiproteinkomplexen oder die Modulation der Genexpression sind daher die wahrscheinlicheren Aktionen. Die Flavonoid-Inhibitoren der ATP-Bindungstasche wurden ebenfalls mit NMR untersucht. Es konnte gezeigt werden, dass Butein (ein Flavonoid Derivat) ein kompetitiver Inhibitor für ATP in CDK2 ist. Es wurden durch diese Experimente neue Einblicke über die Aufgabe von CDK2 und dessen zellulären Partnern bei der Kontrolle des Zellzyklus gewonnen.

Insulin ähnliche Wachstumsfaktoren bindende Proteine (IGFBP) steuern die Bioverfügbarkeit, Aktivität und Verteilung von IGF-I und IGF-II im Serum. Während IGFBPs auch eine IGF unabhängige Funktion haben, ist die IGF abhängige Funktion, sei es positv oder negativ, z.B. Potenzierung oder Inhibition von mitogenen oder metabolischen Effekten, von der Bildung eines hochaffinen IGF/IGFBP Komplex abhängig. N- und C-terminale Fragmente von IGFBP bilden zusammen mit IGF eine hochaffine Bindung, die relative Verteilung der Bindungsaffinität variert aber unter den verschiedenen IGFBPs. Mit Hilfe von strukturellen Untersuchungen an verschidenen Konstrukten von IGFBP konnte die Bindungsstelle für IGF ermittelt werden. Die Struktur des Komplex mit der N-terminalen Domäne von IGFBP-4 (NBP-4, AS 1-92) und IGF-I zeigen eine kritische Aufgabe der ersten N-terminalen Reste von IGFBP-4, für den IGF Signalweg, auf. Ein Model eines tertiären Komplex mit IGF-I, NBP-4 und der C-terminalen Domäne (CBP-4, AS 151-232), das aus Diffraktionsdaten gewonnen wurde, zeigt dass CBP-4 Kontakte mit NBP-4 und IGF-I hat und dass es die IGF-IR Bindungsstelle auf IGF-I blockiert.

9. References

1.   Achenbach, T.V., Muller, R., and Slater, E.P. (2000) Bcl-2 independence of flavopiridol-induced apoptosis. *J. Biol. Chem.* **275***, 32089-32097.

2.   Adamczewski, J.P., Rossignol, M., Tassan, J.P., Nigg, E.A., Moncollin, V., and Egly, J.M. (1996) MAT1, CDK7 and cyclin H form a kinase complex which is UV light-sensitive upon association with TFIIH. *EMBO J.* **15**, 1877-1884.

3.   Adams, P.D., Li, X., Sellers, W.R., Baker, K.B., Leng, X., Harper, J.W., Taya Y., and Kaelin, W.G, Jr. (1999) Retinoblastoma protein contains a C-terminal motif that targets it for phosphorylation by cyclin-CDK complexes. *Mol. Cell Biol.* **19**, 1068-1080.

4.   Adams, P.D., Sellers, W.R., Sharma, S.K., Wu, A.D., Nalin, C.M., and Kaelin, W.G, Jr. (1996) Identification of a cyclin-CDK2 recognition motif present in substrates and p21-like cyclin-dependent kinase inhibitors. *Mol. Cell. Biol.* **16**, 6623-6633.

5.   Aitken, A., Collinge, D.B., van-Heusden, B.P, Isobe, T., Roseboom, P.H., Rosenfeld, G., and Soll, J. (1992) 14-3-3 proteins: a highly conserved, widespread family of eukaryotic proteins *Trends Biochem. Sci.* **17**, 498-501.

6.   Akiyama, T., Yoshida, T., Tsujita, T., Shimizu, M., Mizukami, T., Okabe, M., and Akinaga, S. (1997) G1 phase accumulation induced by UCN-01 is associated with dephosphorylation of Rb and CDK2 proteins as well as induction of CDK inhibitor p21/Cip1/WAF1/Sdi1 in p53-mutated human epidermoid carcinoma A431 cells. *Cancer Res.* **57**, 1495-1501.

7.   Ali, O., Cohen, P., and Lee, K.W. (2003) Epidemiology and biology of insulin-like growth factor binding protein-3 (IGFBP-3) as an anti-cancer molecule. *Hor. Met. Res.* **35**, 726-733.

8.   Andress, D.L. (1995) Heparin modulates the binding of insulin-like growth factor (IGF) binding protein-5 to a membrane protein in osteoblastic cells. *J. Biol. Chem.* **47**, 28289-28296.

9.   Andress, D.L., and Birnbaum, R.S. (1992) Human osteoblast-derived insulin-like growth factor (IGF) binding protein-5 stimulates osteoblast mitogenesis and potentiates IGF action. *J. Biol. Chem.* **267**, 22467-22472.

10.   Andress, D.L., Loop, S.M., Zapf, J., and Kiefer, M.C. (1993) Carboxy-truncated insulin-like growth factor binding protein-5 stimulates mitogenesis in osteoblast-like cells. *Biochem. Biophys. Res. Commun.* **195**, 25-30.

11.   Arata, Y., Fujita, M., Othani, K., Kijima, S., and Kato, J.Y. (2000) CDK2-dependent and-independent pathways in E2F -mediated S phase induction. *J. Biol. Chem.* **275**, 6337-6345.

12.   Arteaga, C.L, Kitten, L.J., Coronado, E.B., Jacobs, S., Kull Jr., F.C., and Osborne, K. (1989) Blockade of the type I somatomedin receptor inhibits growth of human breast cancer cells in athymic mice. *J. Clin. Invest.* **84**, 1418-1423.

13.   Aslanian, A., Iaquinta, P.J., Verona, R., and Lees, J.A. (2004) Repression of the Arf tumor suppressor by E2F3 is required for normal cell cycle kinetics. *Genes Dev.* **18**, 1413-1422.

14.   August, G.P., Nissley, S.P., Kasuga, M., Lee, L., Greenstein, L., and Rechler, M.M. (1983) Purification of an insulin-like growth factor II receptor from rat chondrosarcoma cells. *J. Biol. Chem.* **258**, 9033-9036.

15.   Avantaggiati, M.L., Ogryzko, V., Gardner, K., Giordano, A., Levine, A.S., and Kelly, K. (1997) Recruitment of p300/CBP in p53-dependent signal pathways. *Cell.* **89**,1175-1184.

16.   Babajko, S., and Binoux, M. (1996) Modulation by retinoic acid of insulin-like growth factor (IGF) and IGF binding protein expression in human SK-N-SH neuroblastoma cells. *E. J. Endocrinology*. **134**, 474-480.

17.   Bach, L.A., (1999) The insulin-like growth factor system: basic and clinical aspects. *Aust. N.Z. J. Med.* **29**, 355-361.

18.   Bagchi, S., Raychaudhuri, P., and Nevins, J.R. (1990) Adenovirus E1A proteins can dissociate heteromeric complexes involving the E2F transcription factor: a novel mechanism for E1A trans-activation. *Cell.* **62**, 659-669.

19.   Ballard, F.J., Wallace, J.C., Francis, G.L., Read, L.C., and Tomas, F.M. (1996) Des (1-3)-IGF-I: a truncated form of insulin-like growth factor-I. *Int. J. Biochem. Cell. Biol.* **28**, 1085-1087.

20.   Banin, S., Moyal, L., Shieh, S., Taya, Y., Anderson, C.W., Chessa, L., Smorodinsky N.I., Prives, C., Reiss, Y., Shiloh, Y., and Ziv, Y. (1998) Enhanced phosphorylation of p53 by ATM in response to DNA damage. *Science.* **281**, 1674-1677.

21.   Barak, Y., Juven, T., Haffner, R., and Oren, M. (1993) MDM2 expression is induced by wild type p53 activity. *EMBO J.* **12**, 461-468.

22.   Bartsch, O., Horstmann, S., Toprak, K., Klempnauer, K.H., and Ferrari, S. (1999) Identification of cyclin A/CDK2 phosphorylation sites in B-Myb. *Eur. J. Biochem*. **260**, 384-391.

23.   Bates, S., Phillips, A.C., Clarke, P., Stott, F., Peters, G., Ludwig, R.L., and Vousden, K.H. (1998) E2F-1 regulation of p14^{ARF} links pRB and p53. *Nature*. **395**, 124-125.

24.   Baxter, R.C. (1994) Insulin-like growth factor binding proteins in the human circulation: a review. *Horm. Res*. **42**, 140-144.

25.   Baxter, R.C., Bayne, M.L., and Cascieri, M.A. (1992) Structural determinants for binary and ternary complex formation between insulin-like growth factor-I (IGF-I) and IGF binding protein-3. *J. Biol. Chem*. **267**, 60-65.

26.   Beck, K.D., Knusel, B., and Hefti, F. (1993) The nature of the trophic action of brain- derived neurotrophic factor des(1-3)-insulin-like growth factor-1, and basic fibroblast growth factor on mesencephalic dopaminergic neurons developing in culture. *Neurosci*. **52**, 855-866.

27.   Benzinger, A., Muster, N., Koch, H.B., Yates JR 3rd, and Hermeking, H. (2005) Targeted proteomic analysis of 14-3-3σ, a p53 effector commonly silenced in cancer. *Mol. Cell Proteomics*. **6**, 785-795.

28.   Benzinger, A., Popowicz, G., Joy, J.K., Majumdar, S., Holak, T.A., and Hermeking, H. (2005) The crystal structure of the non-liganded 14-3-3sigma protein: insights into determinants of isoform specific ligand binding and dimerization. *Cell Res*. **15**, 219-227.

29.   Binoux, M., Lalou, C., and Mohseni-Zadeh, S. (1999) Biological actions of proteolytic fragments of the IGF binding proteins. In The IGF System: Molecular Biology, Physiology and Clinical Applications. M. Ron G. Rosenfeld, and J. Charles T. Roberts, Phd (eds.) Humana Press, Totowa, New Jersey. 281-313.

30.   Blain, S.W., Montalvo, E., and Massague, J. (1997) Differential interaction of the cyclin-dependent kinase (CDK) inhibitor p27Kip1 with cyclin A-Cdk2 and cyclin D2-CDK4. *J. Biol. Chem*. **272**, 25863-25872.

31.   Blaydes, J.P., and Hupp, T.R. (1998) DNA damage triggers DRB-resistant phosphorylation of human p53 at the CK2 site. *Oncogene*. **17**, 1045-1052.

32.   Bohannon, N.J., Corp, E.S., Wilcox, B.J., Figlewicz, D.P., Dorsa, D.M., and Baskin, D.G. (1988) Localisation of binding sites for insulin-like growth factor-I (IGF-I) in the rat brain by quantitative autoradiography. *Brain Res*. **444**, 205-213.

33.   Boisclair, Y.R., Rhoads, R.P., Ueki, I. Wang, J., and Ooi, G.T. (2001) Regulation of the acid-labile subunit of the 150-kDa IGF-binding protein complex and its role in the circulating IGF system. *J. Anim. Sci*. **79**, E41-E47.

34.   Booth, B.A., Boes, M., Andress, D.L., Dake, B.L., Kiefer, M.C., Maack, C., Linhardt, R.J., Bar, K., Caldwell, E.E., Weiler, J. et al. (1995) IGFBP-3 and IGFBP-5 association with endothelial cells: role of C-terminal heparin binding domain. *Growth Regulation*. **5**, 1-17.

35.   Bourne, Y., Watson, M.H., Hickey, M.J., Holmes, W., Rocque, W., Reed, S.I., and Tainer, J.A. (1996) Crystal structure and mutational analysis of the human CDK2 kinase complex with cell cycle-regulatory protein CksHs1. *Cell*. **84**, 863-874.

36.   Bresnahan, W.A., Thompson, E.A., and Albrecht, T. (1997) Human cytomegalovirus infection results in altered CDK2 subcellular localization. *J. Gen. Virol*. **78**, 1993-1997.

37.   Brotherton, D.H., Dhanaraj, V., Wick, S., Brizuela, L., Domaille, P.J., Volyanik, E., Xu, X., Parisini, E., Smith, B.O., Archer, S.J., Serrano, M., Brenner, S.L., Blundell, T.L., and Laue, E.D. (1998) Crystal structure of the complex of the cyclin D-dependent kinase CDK6 bound to the cell-cycle inhibitor p19^{INK4d}. *Nature*. **395**, 244-250.

38.   Brown, N.R., Noble, M.E.M., Endicot, J.A., and Johnson, L.N. (1999) The structural basis for specificity of substrate and recruitment peptides for cyclin-dependent kinases. *Nature Cell Biology*. **1**, 438 - 443.

39.   Brown, N.R., Noble, M.E.M., Endicott, J.A., Garman, E.F., Wakatsuki, S., Mitchell, E., Rasmussen, B., Hunt, T., and Johnson, L.N**.** (1995) The crystal structure of cyclin A. *Structure*. **15**, 1131-1134.

40.   Brzozowski, A.M., Dodson, E.J., Dodson, G.G., Murshudov, G.N., Verma, C., Turkenburg, J.P., de Bree, F.M., and Dauter, Z. (2002) Structural origins of the functional divergence of human insulin-like growth factor-I and insulin. *Biochemistry*. **41**, 9389-9399.

41.   Bunch, R.T., and Eastman, A. (1996) Enhancement of cisplatin-induced cytotoxicity by 7-hydroxystaurosporine (UCN-01), a new G2-checkpoint inhibitor. *Clin. Cancer Res*. **2**, 791-797.

42.   Cam, H., and Dynlacht, B.D. (2003) Emerging roles for E2F: beyond the G1/S transition and DNA replication. *Cancer Cell*. **3**, 311-316.

43.   Canman, C.E., Lim, D.S., Cimprich, K.A., Taya, Y., Tamai, K., Sakaguchi, K., Appella, E., Kastan, M.B., and Siliciano, J.D. (1998) Activation of the ATM kinase by ionizing radiation and phosphorylation of p53. *Science*. **281**, 1677-1679.

44.   Carrick, F.E., Wallace, J.C., and Forbes, B.E. (2002) The interaction of Insulin-like growth factors (IGFs) with Insulin-like growth factor binding proteins (IGFBPs): a review. *Lett. Pep. Sci*. **8**, 147-153.

45.   Casagrande, F., and Darbon, J.M. (2001) Effects of structurally related flavonoids on cell cycle progression of human melanoma cells: regulation of cyclin-dependent kinases CDK2 and CDK1. *Biochem. Pharmacol*. **61**, 1205-1215.

46.   CCP4, Collaborative Computational Project, Number 4. (1994) The CCP4 Suite: Programs for protein crystallography. *Acta Cryst*. **D50**, 760-763.

47.   Chan, F.K., Zhang, J., Cheng, L., Shapiro, D.N., and Winoto, A. (1995) Identification of human and mouse p19, a novel CDK4 and CDK6 inhibitor with homology to p16ink4. *Mol. Cell. Biol*. **15**, 2682-2688.

48.   Chan, J.M., Stampfer, M.J., Giovannucci, E., Gann, P.H., Ma, J., Wilkinson, P., Henneken, C.H., and Pollak, M. (1998) Plasma insulin-like growth factor-I and prostate cancer risk: A prospective study. *Science*. **279**, 563-566.

49.   Chelius, D., Baldwin, M.A., Lu, X., and Spencer, E.M. (2001) Expression, purification and characterization of the structure and disulfide linkages of insulin-like growth factor binding protein-4. *J. Endocrinol*. **168**, 283-296.

50.   Chen, J., Saha, P., Kornbluth, S., Dynlacht, B.D., and Dutta, A. (1996) Cyclin binding motifs are essential for the function of p21^{cip1}. *Mol. Cell Biol*. **16**, 4673-4682.

51.   Cheng, M., Olivier, P., Diehl, J.A., Fero, M., Roussel, M.F., Roberts, J.M., and Sherr, C.J. (1999) The p21^{Cip1} and p27^{Kip1} CDK "inhibitors" are essential activators of cyclin D-dependent kinases in murine fibroblasts. *EMBO J*. **18**,1571-1583.

52.   Cho, Y., Gorina, S., Jeffrey, P.D., and Pavletich, N.P. (1994) Crystal structure of a p53 tumor suppressor-DNA complex: understanding tumorigenic mutations. *Science*. **26**, 346-355.

53.   Clark, W., Black, E.J., MacLaren, A., Kruse, U., La-Thangue N, Vogt, P.K., and Gillespie, D.A. (2000) v-Jun overrides the mitogen dependence of S-phase entry by deregulating retinoblastoma protein phosphorylation and E2F-pocket protein interactions as a consequence of enhanced cyclin E-CDK2 catalytic activity. *Mol. Cell Biol*. **20**, 2529-2542.

54.   Classon, M., and Dyson, N. (2001) p107 and p130: versatile proteins with interesting pockets. *Exp. Cell Res*. **264**, 135-147.

55.   Clemmons, D.R. (2001) Use of mutagenesis to probe IGF-binding protein structure/function relationships. *Endocr. Rev*. **22**, 800-817.

56.   Clore, G.M., Ernst, J., Clubb, R., Omichinski, J.G., Kennedy, W.M., Sakaguchi, K., Appella, E., and Gronenborn, A.M. (1995) Refined solution structure of the oligomerization domain of the tumour suppressor p53. *Nature. Struct. Biol*. **2**, 321-333.

57.   Cohen, P. (2002) Protein kinases – the major drug targets of the twenty-first century. *Naure Review Drug Discovery*. **1**, 309-315.

58.   Cohen, P., Clemmons, D.R., and Rosenfeld, R.G. (2000) Does the GH-IGF axis play a role in cancer pathogenesis? Growth Hor. *IGF Res*. **10**, 297-305.

59.   Cohen, P., Lamson, G., Okajima, T., and Rosenfeld, R.G. (1993) Transfection of the human insulin-like growth factor binding protein-3 gene into Balb/c fibroblasts inhibits cellular growth. *Mol. Endocrinol*. **7**, 380-386.

60.   Cole, M.D. (1986) The myc oncogene: its role in transformation and differentiation. *Annu. Rev. Genet*. **20**, 361-384.

61.   Cooke, R.M., Harvey, T.S., and Campbell, I.D. (1991) Solution structure of human insulin-like growth factor 1: a nuclear magnetic resonance and restrained molecular dynamics study. *Biochemistry*. **30**, 5484-5491.

62.   Craig, A., Blaydes, J., Burch, L., Thompson, A., and Hupp, T. (1999) Dephosphorylation of human p53 at Ser20 in response to low doses of non-ionizing radiation. *Oncogene*. **18**, 6305-6312.

63.   Craig, A.L., Burch, L., Vojtesek, B., Mikutowska, J., Thompson, A., and Hupp, T.R. (1999) Novel phosphorylation sites of human tumour suppressor protein p53 at Ser20 and Thr18 that disrupt the binding of mdm2 (mouse double minute 2) protein are modified in human cancers. *Biochem. J*. **342**, 133-141.

64.   Crescenzi, M., Fleming, T.P., Lassar, A.B., Weintraub, H. and Aaronson, S.A. (1990) MyoD induces growth arrest independent of differentiation in normal and transformed cells, *Proc. Natl. Acad. Sci. U. S. A*. **87**, 8442-8446.

65.   Datta, S.R., Dudeck, H., Tao, X., Masters, S., Fu, H., Gotoh, Y., and Greenberg, M.E. (1997) Akt phosphorylation of BAD couples' survival signals to intrinsic machinery. *Cell*. **91**, 231-241.

66.   Davies, T.G., Pratt, D.J., Endicott, J.A., Johnson, L.N., and Noble, M.E.M. (2002) Structure-based design of cyclin-dependent kinase inhibitors. *Pharmacology and Therapeutics*. **93**, 125-133.

67. Davis, S.T., Benson, B.G., and Bramson, H.N. (2001) Prevention of chemotherapy-induced alopecia in rats by CDK inhibitors. *Science*. **291**,134-137.

68. De Azevedo W.F., Leclerc, S., Meijer, L., Havlicek, L., Strnad, M., and Kim, S.H. (1997) Inhibition of cyclin-dependent kinases by purine analogues: crystal structure of human CDK2 complexed with roscovitine. *Eur. J. Biochem*. **243**, 518-526.

69. De Meyts, P., Wallach, B., Christoffersen, C.T., Urso, B., Gronskov, K., Latus, L.J., Yakushiji, F., Ilondo, M.M., and Shymko, R.M. (1994) The insulin-like growth factor-I receptor: Structure, ligand-binding mechanism and signal transduction. *Horm. Res*. **42**, 152-169.

70. De-Bondt, H.L., Rosenblatt, J., Jancarik, J., Jones, H.D., Morgan, D.O., and Kim, S.H. (1993) Crystal structure of cyclin-dependent kinase 2. *Nature*. **363**, 595-602.

71. DeGregori, J., Leone, G., Ohtani, K., Miron, A., and Nevins, J.R. (1995) E2F -1 accumulation bypasses a G1 arrest resulting from the inhibition of G1 cyclin- dependent kinase activity. *Genes Dev*. **9**, 2873-2887.

72. Delbe, J., Blat, C., Desauty, G., and Harel, L. (1991) Presence of IDF45 (mIGFBP-3) binding sites on chick emryo fibroblasts. *Biochem. Biophys. Res. Commun*. **179**, 495-501.

73. Demetrick, D.J., Zhang, H., and Beach, D.H. (1994) Chromosomal mapping of human CDK2, CDK4, and CDK5 cell cycle kinase genes. *Cytogenet Cell Genet*. **66**, 72-74.

74. De-Stanchina E., McCurrach M.E., Zindy, F., Shieh, S.Y., Ferbeyre, G., Samuelson, A.V., Prives, C., Roussel, M.F., Sherr, C.J., and Lowe, S.W. (1998) E1A signaling to p53 involves the p19[ARF] tumor suppressor. *Genes Dev*. **12**, 2434-2442.

75. Diederichs, S., Bäumer, N., Ji, P., Metzelder, S.K., Idos, G.E., Cauvet, T., Wang, W., Möller, M., Pierschalski, S., Gromoll, J., Schrader, M.G., Koeffler, H.P., Berdel, W.E., Serve, H., and Müller-Tidow, C. (2004) Identification of interaction partners and substrates of the cyclin A1-CDK2 complex. *J. Biol. Chem*. **279**, 33727-33741.

76. Dowdy, S.F., Hinds, P.W., Louie, K., Reed, S.I., Arnold, A., and Weinberg, R.A., (1993) Physical interaction of the retinoblastoma protein with human D cyclins. *Cell*. **73**, 499-511.

77. Du, K., and Montminy, M. (1998) CREB is a regulatory target for the protein kinase Akt/PKB. *J. Biol. Chem*. **273**, 32377-32379.

78. Dunaief, J.L., Strober, B.E., Guha, S., Khavari, P.A., Alin, K., Luban, J., Begemann M., Crabtree, G.R., and Goff, S.P. (1994) The retinoblastoma protein and BRG1 form a complex and cooperate to induce cell cycle arrest. *Cell*. **79**, 119-130.

79. Duro, D., Bernard, O., Valle, V.D., Berger, R., and Larsen, C.J. (1995) A new type of p16[INK4/MTS1] gene transcript expressed in B-cell malignancies. *Oncogene*. **11**, 21-29.

80. Dynlacht, B.D., Moberg, K., Lees, J.A., Harlow, E., and Zhu, L. (1997) Specific regulation of E2F family members by cyclin-dependent kinases. *Mol. Cell Biol*. **17**, 3867-3875.

81. El-Deiry W.S, Tokino, T., Velculescu, V.E., Levy, D.B., Parsons, R., Trent, J.M., Lin, D., Mercer, E., Kinzler, K.W., and Vogelstein, B. (1993) WAF1, a potential mediator of p53 tumor suppression. *Cell*. **75**, 817-825,

82. El-Deiry, W.S., Kern, S.E., Pietenpol, J.A., Kinzler, K.W., and Vogelstein, B. (1992) Definition of a consensus binding site for p53. *Nature Genet*. **1**, 45-49.

83. Ewen, M.E., (1994) The cell cycle and the retinoblastoma protein family. *Cancer Metastasis Rev*. **13**, 45–66.

84. Fantl, W.J., Muslin, A.J., Kikuchi, A., Martin, J.A., MacNicol, A.M., Grosst R.W., and Williams., L.T. (2002) Activation of Raf-1 by 14-3-3 proteins. *Nature*. **371**, 612-614.

85. Feaver, W.J., Jesper, Q., Svejstru., N., Henry, L., and Kornberg, R.D. (1994) Relationship of CDK-activating kinase and RNA polymerase II CTD kinase TFIIH/TFIIK *Cell*. **79**, 1103-1109.

86. Fesquet, D., Labbe, J.C., Derancourt, J., Capony, J.P., Galas, S., Girard, F., Lorca, T., Shuttleworth, J., Doree, M., and Cavadore, J.C. (1993) The MO15 gene encodes the catalytic subunit of a protein kinase that activates cdc2 and other cyclin-dependent kinases (CDKs) through phosphorylation of Thr161 and its homologues *EMBO J*. **12**, 3111-3121.

87. Firth, S.M., and Baxter, R.C. (2002) Cellular actions of the insulin-like growth factor binding proteins. *Endocr. Rev*. **23**, 824-854.

88. Fisher, R.P., and Morgan, D.O. (1994) A novel cyclin associates with M015/CDK7 to form the CDK-activating kinase. **78**, 713-724.

89. Forbes, B., Szabo, L., Baxter, R.C., Ballard, F.J., and Wallace, J.C. (1988) Classification of the insulin-like growth factor binding proteins into three distinct categories according to their binding specificities. *Biochem. Biophys. Res. Commun*. **157**, 196-202.

90.   Forbes, B.E., Turner, D., Hodge, S.J., McNeil, K.A., Forsberg, G., and Wallace, J.C. (1998) Localization of an insulin-like growth factor (IGF) binding site of bovine IGF binding protein-2 using disulfide mapping and deletion mutation analysis of the C-terminal domain. *J. Biol. Chem*. **273**, 4647-4652.

91.   Ford, J.C., Al-Khodairy, F., Fotou, E., Sheldrick, K.S., Griffiths, D.J., and Carr, A.M. (1994) 14-3-3 protein homologs required for the DNA damage checkpoint in fission yeast. *Science*. **265**, 533-535.

92.   Francis, G.L., Upton, F.M., Ballard, F.J., McNeil, K.A., and Wallace, J.C. (1988) Insulin-like growth factors 1 and 2 in bovine colostrum. Sequences and biological activities compared with those of a potent truncated form. *Biochemical J*. **251**, 95-103.

93.   Frederic, B., Ahcene, B., Anne-Marie, M., Gwenaelle, C., and Attilio, D.P. (1999) Synthesis and biological activity of 4-alkoxychalcones: potential hydrophobic modulators of P-glycoprotein-mediated multidrug resistance. *Bioorg. Med. Chem*. **7**, 2691-2695.

94.   Fuchs, B., Hecker, D., and Scheidtmann, K.H. (1995) Phosphorylation studies on rat p53 using the baculovirus expression system. Manipulation of the phosphorylation state with okadaic acid and influence on DNA binding. *Eur. J. Biochem*. **228**, 625-639.

95.   Furnari, B., Rhind, N., and Russell, P. (1997) Cdc25 mitotic inducer targeted by chk1 DNA damage checkpoint kinase. *Science*. **277**, 1495–1497.

96.   Garrett, T.P., McKern, N.M., Lou, M., Frenkel, M.J., Bentley, J.D., Lovrecz, G.O., Elleman, T.C., Cosgrove, L.J., and Ward, C.W. (1998) Crystal structure of the first three domains of the type-1 insulin-like growth factor receptor. *Nature*. **394**, 395-399.

97.   Garriga J., Bhattacharya, S., Calbo, J., Marshall, R.M., Truongcao. M., Haines, D.S., and Grana, X. (2003) CDK9 is constitutively expressed throughout the cell cycle, and its steady-state expression is independent of SKP2. *Mol. Cell Biol*. **23**, 5165-5173.

98.   Ginsberg, D. (2004) E2F3-a novel repressor of the ARF/p53 pathway. *Dev. Cell* **6**, 742-743.

99.   Girnita, A., Girnita, L., del Prete, F., Bartolazzi, A., Larsson, O., and Axelson, M. (2004) Cyclolignans as inhibitors of the insulin-like growth factor-1 receptor and malignant cell growth. *Cancer Res*. **64**, 236-42.

100.   Glotzer, M., Murray, A.W., and Kirschner, M.W. (1991) Cyclin is degraded by the ubiquitin pathway. *Nature*. **349**,132-138.

101.   Grana, X., Luca, A.D., Sang, N., Fu, Y., Claudio, P.P., Rosenblatt, J., Morgan, D.O., and Giordano, A. (1994) *PITALRE* a nuclear CDC2-related protein kinase that phosphorylates the retinoblastoma protein in vitro. *Proc. Natl. Acad. Sci. USA*. **91**, 3834-3838.

102.   Grzmil, M., Hemmerlein, B., Thelen, P., Schweyer, S., and Burfeind, P. (2004) Blockade of the type I IGF receptor expression in human prostate cancer cells inhibits proliferation and invasion, up-regulates IGF binding protein-3, and suppresses MMP-2 expression. *J. Pathol*. **202**, 50-59.

103.   Gu, Y., Rosenblatt, J., and Morgan, D.O. (1992) Cell cycle regulation of CDK2 activity by phosphorylation of Thr160 and Tyr15. *EMBO J*. **11**, 3995-4005.

104.   Guan, K.L., Jenkins, C.W., Li, Y., Nichols, M.A., Wu, X., O,'Keefe C.L., Matera, A.G., and Xiong, Y. (1994) Growth suppression by p18, a p16$^{INK4/MTS1}$- and p15$^{INK4B/MTS2}$-related CDK6 inhibitor, correlates with wild-type pRb function. *Genes Dev*. **8**, 2939-2952.

105.   Gyuris, J., Golemis, E., Chertkov, H., and Brent, R. (1993) Cdi1, a human G1 and S phase protein phosphatase that associates with CDK2. *Cell*. **75**, 791–803.

106.   Hannon, G. J., and Beach, D. (1994) p15^{INK4B} is a potential effector of TGFβ-induced cell cycle arrest. *Nature*. **371**, 257-261.

107.   Hanon, G., Casso, D., and Beach, D. (1994) Kap: a Dsp that interacts with cyclin-dependent kinases. *Proc. Natl. Acad. Sci. USA*. **91**, 1731–1735.

108.   Hansen, S., Midgley, C.A., Lane, D.P., Freeman, B.C., Morimoto, R.I., and Hupp, T.R. (1996) Modification of two distinct COOH-terminal domains is required for murine p53 activation by bacterial Hsp70. *J. Biol. Chem*. **271**, 30922-30928.

109.   Harbour, J.W., Robin, X., Santi, L.A.D., Postigo, A.A., and Dean, D.C. (1999) CDK phosphorylation triggers sequential intramolecular interactions that progressively block Rb functions as cells move through G1. *Cell*. **98**, 859-869.

110.   Harding B.T., Binne, U.K., Korenjak, M., Brehm, A and Dyson, N.J. (2004) p55, the *Drosophila* ortholog of RbAp46/RbAp48, is required for the repression of dE2F2/RBF-regulated genes. *Mol. Cell. Biol*. **24**, 9124-9136.

111.   Harper, J.W., Adami, G.R., Wei, N., Keyomarsi, K., and Elledge, S.J. (1993) The p21 CDK-interacting protein Cip1 is a potent inhibitor of G1 cyclin-dependent kinases. *Cell*. **75**, 805-816.

112.   Hashimoto, R., Ono, M., Fujiwara, H., Higashihashi, N., Yoshida, M., Enjohkimura, T., and Sakano, K. (1997) Binding sites and binding properties of binary and ternary complexes of insulin-like growth factor-II (IGF-II), IGF-binding protein-3, and acid-labile subunit. *J. Biol. Chem*. **272**, 27936-27942.

113.   Hatakeyama, M., Brill, J.A., Fink, G.R., and Weinberg, R.A. (1994) Collaboration of G1 cyclins in the functional inactivation of the retinoblastoma protein. *Genes Dev*. **8**, 1759-1771.

114.   Haupt, Y., Maya, R., Kazaz, A., and Oren, M. (1997) MDM2 promotes the rapid degradation of p53. *Nature*. **387**, 296-299.

115.   Headey, S.J., Keizer, D.W., Yao, S., Wallace, J.C., Bach, L.A., and Norton, R.S. (2004) Binding site for the C-domain of insulin-like growth factor (IGF) binding protein-6 on IGF-II; implications for inhibition of IGF actions. *FEBS Lett*. **568**, 19-22.

116.   Helin, K., Lees, J.A., Vidal, M., Dyson, N., Harlow, E., and Fattaey, A. (1992) A cDNA encoding a pRB-binding protein with properties of the transcription factor E2F. *Cell*. **70**, 337-350.

117.   Hernandez-Sanchez, C., Blakesley, V., Kalebic, T., Helman, L., and LeRoith, D. (1995) The role of the tyrosine kinase domain of the insulin-like growth factor-I receptor in intracellular signalling, cellular proliferation and tumorgenesis. *J. Biol. Chem*. **270**, 29176-29181.

118.   Higashi, H., Suzukitakahashi, I., Taya, Y., Segawa, K., Nishimura, S., and Kitagawa, M. (1995) Differences in substrate specificity between CDK2-cyclin A and CDK2-cyclin E in vitro. *Biochem. Biophys. Res. Commun*. **216**, 520-525.

119.   Hinds, P.W., Mittnacht, S., Dulic, V., Arnold, A., Reed, S.I., and Weinberg, R.A. (1992) Regulation of retinoblastoma protein functions by ectopic expression of human cyclins. *Cell*. **70**, 993-1006.

120.   Hirai, H., Roussel, M.F., Kato, J., Ashmun, R.A., and Sherr, C.J. (1995) Novel INK4 proteins, p19 and p18, are specific inhibitors of the cyclin D-dependent kinases CDK4 and CDK6. *Mol. Cell. Biol*. **15**, 2672-2681.

121.   Hoeck, W.G., and Mukku, V.R. (1994) Identification of the major sites of phosphorylation in IGF binding protein-3. *J. Cell. Biochem*. **56***,* 262-273.

122.   Holmes, J.K., and Solomon, M.J. (1996) A predictive scale for evaluating cyclin dependent kinase substrates. *J. Biol. Chem*. **271**, 25240-25246.

123.   Honda, R., Tanaka, H., and Yasuda, H. (1997) Oncoprotein MDM2 is a ubiquitin ligase E3 for tumor suppressor p53. *FEBS Lett*. **420***,* 25-27.

124.   Hu, Q.J., Dyson, N., and Harlow, E. (1990) The regions of the retinoblastoma protein needed for binding to adenovirus E1A or SV40 large T antigen are common sites for mutations. *EMBO J*. **9**, 1147-1155.

125.   Huang, S.S., Leal, S.M., Chen, C-L., Liu, I-H., and Huang, J.S. (2004) Identification of insulin receptor substrate proteins as key molecules for the TβR-V/LRP-1-mediated growth inhibitory signaling cascade in epithelial and myeloid cells. *FASEB*. **18**, 1230-1254.

126.   Humbel, R.E. (1990) Insulin-like growth factor-I, and II. *Eur. J. Biochem*. **190**, 445-462.

127.   Hunter, T., and Pines, J. (1994) Cyclins and cancer. cyclin D and CDK inhibitors come of age. *Cell.* **79**, 573-582.

128.   Hupp, T.R., and Lane, D.P. (1995) Two distinct signaling pathways activate the latent DNA binding function of p53 in a casein kinase II-independent manner. *J. Biol. Chem*. **270**, 18165-18174.

129.   Hwa, V., Oh, Y., Burren, C.P., Choi, W.K., Graham, D.L., Ingermann, A., Kim, H.S., Lopez-Bermejo, A., Minniti, G., Nagalla, S.R., Pai, K., Spagnoli, A., Vorwerk, P., Wanek, D.L.V., Wilson, E.M., Yamanaka, Y., Yang, D.H., and Rosenfeld, R.G. (1999) The IGF binding protein superfamily. In Rosenfeld, R.G., and Roberts, C.T. (eds), The IGF system. Molecular biology, physiology, and clinical applications. Humana Press, Totowa, pp. 315-327.

130.   Jayaraman, L., and Prives, C. (1999) Covalent and noncovalent modifiers of the p53 protein. *Cell Mol. Life Sci*. **55**, 76-87.

131.   Jeffrey, P.D., Russo, Polyak, A.A., Gibbs, K., Hurwitz, E.J., Massague, J., and Pavletich, N.P. (1995) Mechanism of CDK activation revealed by the structure of a cyclin A-CDK2 complex. *Nature*. **376**, 313-320.

132.   Jones, J.L., Gockerman, A., Busby, W.H., Wrigh, G., and Clemmons, D.R. (1993) Insulin-like growth factor binding protein 1 stimulates cell migration and binds to the a5b integrin receptor by means of its Arg-Gly-Asp sequence. *Proc. Natl. Acad. Sci. USA*, **90**, 10553-10557.

133.   Kabsch, W. (1993) Automatic processing of rotation diffraction data from crystals of initially unknown symmetry and cell constants. *J. Appl. Cryst*. **26**, 795-800.

134.   Kalus, W., Zweckstetter, M., Renner, C., Sanchez, Y., Georgescu, J., Grol, M., Demuth, D., Schumacher, R., Dony, C., Lang, K., and Holak, T.A. (1998) Structure of the IGF binding domain of the insulin-like

growth factor-binding protein-5 (IGFBP-5): implications for IGF and IGF-I receptor interactions. *EMBO J.* **17**, 6558-6572.

135.   Kamb, A., Gruis, N.A., Weaver, F.J., Liu, Q., Harshman, K., Tavtigian, S.V., Stockert, E., Day, R.S., Johnson B.E, and Skolnick, M.H. (1994) A cell cycle regulator involved in genesis of many tumor types. *Science*. **264,** 436-440.

136.   Kamijo, T., Bodner, S., Kamp, E., Randle, D.H., and Sherr, C.J. (1999) Tumor spectrum in ARF-deficient mice. *Cancer Res*. **59**, 2217-2222.

137.   Kamijo, T., Weber, J.D., Zambetti, G., Zindy, F., Roussel, M.F., and Sherr, C.J. (1998) Functional and physical interactions of the ARF tumor suppressor with p53 and Mdm2. *Proc. Natl. Acad. Sci. USA*. **95**, 8292-8297.

138.   Kamijo, T., Zindy, F., Roussel, M.F., Quelle, D.E., Downing, J.R., Ashmun, R.A., Grosveld, G., and Sherr, C.J. (1997) Tumor suppression at the mouse *INK4a* locus mediated by the alternative reading frame product p19^{ARF}. *Cell*. **91***, 649-659.

139.   Kato, J., Matsushime, H., Hiebert, S.W., Ewen, M.E., and Sherr, C.J. (1993) Direct binding of cyclin D to the retinoblastoma gene product (pRb) and pRb phosphorylation by the cyclin D-dependent kinase CDK4. *Genes Dev*. **7**, 331-342.

140.   Khandwala, H.M., McCutcheon, I.E., Flyvbjerg, A., and Friend, K.E. (2000) The effects of insulin-like growth factors on tumorigenesis and neoplastic growth. *Endocr. Rev*. **21**, 215-244.

141.   Kim, J.H., Kang, M.J., Park, C.U., Kwak, H.J., Hwang, Y., and Koh, G.Y. (1999) Amplified CDK2 and cdc2 activities in primary colorectal carcinoma. *Cancer*. **85**, 546-553.

142.   Kim, S.G., Kim, S.N., Jong, H.S., Kim, N.K., Hong, S.H., Kim, S.J., and Bang, Y.J. (2001) Caspase-mediated CDK2 activation is a critical step to execute transforming growth factor-beta l-induced apoptosis in human gastric cancer cells. *Oncogene*. **20**, 1254-1265.

143.   Kitagawa, M., Higashi, H., Jung, H.K., Suzuki-Takahashi I, Ikeda, M., Tamai, K., Kato, J., Segawa, K., Yoshida, E., Nishimura, S., and Taya, Y. (1996) The consensus motif for phosphorylation by cyclin D1-CDK4 is different from that for phosphorylation by cyclin A/E-CDK2. *EMBO J*. **15**, 7060-7069.

144.   Knockaret, M., Greenard, P., and Meijer, L. (2002) Pharmacological inhibitors of cyclin-dependent kinases. *Trends in Pharmacological Sciences*. **23**, 9

145.   Knudsen, E.S., and Wang, J.Y. (1996) Differential regulation of retinoblastoma protein function by specific CDK phosphorylation sites. *J. Biol. Chem*. **271,** 8313-8320.

146.   Knudsen, E.S., and Wang, J.Y. (1997) Dual mechanisms for the inhibition of E2F binding to RB by cyclin-dependent kinase-mediated RB phosphorylation. *Mol. Cell. Biol*. **17**, 5771-5783.

147.   Ko, L.J., and Prives, C. (1996) p53: puzzle and paradigm. *Genes Dev*. **10**,1054-1072.

148.   Kobayashi, H., Stewart, E., Poon, R., Adamczewski, J.P., Gannon, J., and Hunt, T. (1992) Identification of the domains in cyclin A required for binding to, and activation of, p34cdc2 and p32cdk2 protein kinase subunits. *Mol. Biol. Cell*. **3**, 1279-1294.

149.   Kopp, J., and Schwede, T. (2004) The SWISS-MODEL repository of annotated three-dimensional protein structure homology models, *Nucleic Acids Res*. **32**, D230–D234, (database issue).

150.   Kornfeld, S. (1992) Structure and function of the mannose-6-phosphate/Insulin-like growth factor II receptors. *Annu. Rev. Biochem*. **61**, 307-330.

151.   Koundrioukoff, S., Jonsson, Z.O., Hasan, S., de Jong, R.N., van der Vliet, P.C., Hottiger, M.O., and Hübscer, U. (2000) A direct interaction between proliferating cell nuclear antigen (PCNA) and CDK2 targets PCNA-interacting proteins for phosphorylation. *J. Biol. Chem*. **275**, 30, 22882-22887.

152.   Krek, W and Nigg, E.A. (1991) Differential phosphorylation of vertebrate p34cdc2 kinase at the G1/S and G2/M transitions of the cell cycle: identification of major phosphorylation sites. *EMBO J*. **10**, 305-316.

153.   Kubbutat, M.H.G., Jones, S.N., and Vousden, K.H. (1997) Regulation of p53 stability by MDM2. *Nature*. **387**, 299-303.

154.   Kumar, S.K., Hager, E., Pettit, C., Gurulingappa, H., Davidson, N.E., and Khan, S.R. (2003). Design, synthesis, and evaluation of novel Boronic-chalcone derivatives as antitumor agents. *J. Med. Chem*. **46**, 2813-2815.

155.   LaBaer, J., Garrett, M.D., Stevenson, L.F., Slingerland, J.M., Sandhu, C., Chou, H.S., Fattaey, A., and Harlow, E. (1997) New functional activities for the p21 family of CDK inhibitors. *Genes Dev*. **11**, 847-862.

156.   Lai, A., Sarcevic, B., Prall, O.W.J., and Sutherland, R.L. (2001) Insulin/insulin-like growth factor-I and estrogen cooperate to stimulate cyclin E-CDK2 activation and cell cycle progression in MCF-7 breast cancer cells through differential regulation of cyclin E and p21$^{WAF1/CIP1}$. *J. Biol. Chem*. **276**, 25823-25833.

157.   Lamzin, V.S., and Wilson, K.S. (1993) Automated refinement of protein models. *Acta Cryst*. **D49**, 129-147.

158.   Landale, E.C., Strong, D.D., Mohan, S., and Baylink, D.J. (1995) Sequence comparison and predicted structure for the four exon-encoded regions of human insulin-like growth factor binding protein 4. *Growth Factors*. **12**, 245-250.

159.   Lane, D.P., and Crawford, L.V. (1979) T antigen is bound to a host protein in SV40-transformed cells. *Nature*. **278**, 261-263.

160.   Lane, M.E., Yu, B., Rice, A., Lipson, K.E., Liang, C., Sun, L., Tang, C., McMahon, G., Pestell, R.G., and Wadler, S. (2001) A novel CDK2-selective inhibitor, SU9516, induces apoptosis in colon carcinoma cells. *Cancer Res*. **61**, 6170-6177.

161.   Laronga, C., Yang, H.Y, Neal, C., and Lee, M.N. (2000) Association of the Cyclin-dependent Kinases and 14-3-3 Sigma Negatively Regulates Cell Cycle Progression. *J. Biol. Chem*. **275**, 30, 23106-23112.

162.   Lassar, A.B., Davis, R.L., Wright, W.E., Kadesch, T., Murre, C., Voronova, A., Baltimore, D., and Weintraub, H. (1991) Functional activity of myogenic HLH proteins requires hetero-oligomerization with E12/E47-like proteins in vivo. *Cell*. **66**, 305–315.

163.   Lawrence, N.J., Rennison, D., McGown, A.T., and Hadfield, J.A. (2003) The total synthesis of an aurone isolated from *Uvaria hamiltonii*: aurones and flavones as anticancer agents. *Bioorg. Med. Chem. Lett*. **13**, 3759-3763.

164.   Leal, S.M., Huang, S.S., and Huang, J.S. (1999) Interactions of high affinity insulin-like growth factor-binding proteins with the type V transforming growth factor-β receptor in mink lung epithelial cells. *J. Biol. Chem*. **274**, 6711-6717.

165.   Leal, S.M., Liu, Q., Huang, S.S., and Huang, J.S. (1997) The type V transforming growth factor β receptor is the putative insulin-like growth factor binding protein 3 receptor. *J. Biol. Chem*. **272**, 20572-20576.

166.   Lee, C.W., Sorensen, T.S., Shikama, N., and La-Thangue, N.B. (1998) Functional interplay between p53 and E2F through co-activator p300. *Oncogene*. **16**, 2695-2710.

167.   Lee, K-W., Liu, B., Ma, L., Li, H., Bang, P., Koeffler H.P., and Cohen, P. (2004) Cellular Internalization of insulin-like growth factor binding protein-3. *J. Biol. Chem*. **279**, 469-476.

168.   Lee, M.G., and Nurse, P. (1987) Complementation used to clone a human homologue of the fission yeast cell cycle control gene cdc2. *Nature*. **327**, 31-35.

169.   Lee, M.H., Reynisdottir, I., and Massague, J. (1995) Cloning of p57^{Kip2}, a cyclin-dependent kinase inhibitor with unique domain structure and tissue distribution. *Genes Dev*. **9**, 639-649.

170.   Lees, E.M and Harlow, E. (1993) Sequences within the conserved cyclin box of human cyclin A are sufficient for binding to and activation of cdc2 kinase. *Mol. Cell. Biol*. **13**, 1194-1201.

171.   Lees-Miller, S.P., Sakaguchi, K., Ullrich, S.J., Appella, E., and Anderson, C.W. (1992) Human DNA-activated protein kinase phosphorylates serines 15 and 37 in the amino-terminal transactivation domain of human p53. *Mol. Cell. Biol*. **12**, 5041-5049.

172.   Legraverend, M., Tunnah, P., and Noble, M. (2000) Cyclin-Dependent Kinase Inhibition by New C-2 Alkynylated Purine Derivatives and Moleculare Structure of a CDK2-Inhibitor Complex. *J. Med. Chem*. **43**, 1282-1292.

173.   LeRoith, D., and Helman, L. (2004) The new kid on the block(ade) of the IGF-1 receptor. *Cancer Cell*. **5**, 201-212.

174.   Lesniak, M.A., Hill, J.M., Kiess, W., Rojeski, M., Pert, C.B., and Roth, J. (1988) Receptors for insulin-like growth factors I and II: Autoradiographic localisation in rat brain and comparison to receptors for insulin. *Endocrinology*. **123**, 2089-2099.

175.   Levine, A.J. (1997) p53, the cellular gatekeeper for growth and division. *Cell*. **88**, 323-331.

176.   Levkau, B., Koyama, H., and Raines, E.W. (1998) Cleavage of p21 Cip1/Waf1 and p27Kip1 mediates apoptosis in endothelial cells through activation of CDK2: role of a caspase cascade. *Mol. Cell*. **1**, 553-563.

177.   Li, S., Janosch, P., Tanji, M., Rosenfeld, G.C., Waymire, J.C., Mischak, H., Kolch, W., and Sedivy, J.M. (1995) Regulation of Raf-1 kinase activity by the 14-3-3 family of proteins *EMBO J*. **14**, 685-696.

178.   Liu, D., Bienkowska, J., Petosa, C., Collier, R.J., Fu, H., and Liddington, R. (1995) Crystal structure of the ζ isoform of the 14-3-3 protein. *Nature*. **376**, 191-194.

179.   Lukas, J., Herzinger, T., Hansen, K., Moroni, M.C., Resnitzky, D., Helin, K., Reed, S.I., and Bartek, J. (1997) Cyclin E-induced S phase without activation of the pRb/E2F pathway. *Genes Dev*. **11**, 1479-1492.

180.   Lukas, J., Parry, D., Aagaard, L., Mann, D.J., Bartkova, J., Strauss, M., Peters, G., and Bartek, J. (1995) Retinoblastoma protein-dependent cell cycle inhibition by the tumor suppressor p16. *Nature*. **375**, 503-506.

181.   Lundberg, A.S., and Weinberg, R.A. (1998) Functional inactivation of the retinoblastoma protein requires sequential modification by at least two distinct cyclin CDK complexes. *Mol. Cell. Biol*. **18**, 753-761.

182.   Malumbres, M., and Barbacid, M. (2005) Mammalian cyclin-dependent kinases. *Trends in Biochemical Sciences*. **11**, 630-641.

183. Mannhardt, B., Weinzimer, S.A., Wagner, M., Fiedler, M., Cohen, P., Jansen-Durr, P., and Zwerschke, W. (2000) Human papillomavirus type 16 E7 oncoprotein binds and inactivates growth-inhibitory insulin-like growth factor binding protein 3. *J. Mol. Cell. Biol.* **20**, 6483-6495.

184. Mao, L., Merlo, A., Bedi, G., Shapiro, G.I., Edwards, C.D., Rollins, B.J., and Sidransky, D. (1995) A novel p16^{INK4a} transcript. *Cancer Res.* **55***, 2995-2997.

185. Martin, J.L., Ballesteros, M., and Baxter, R.C. (1992) Insulin-like growth factor-I (IGF-I) and transforming growth factor-beta 1 release IGF-binding protein-3 from human fibroblasts by different mechanisms. *Endocrinology.* **131**, 1703-1710.

186. Martin, J.L., Coverley, J.A., Pattison, S.T., and Baxter, R.C. (1995) IGFBP-3 and IGFBP-6 production by MCF-7 breast cancer cells: Stimulation by retinoic acid and cyclic AMP, and differential effects of estradiol. *Endocrinology.* **136**, 1219-1226.

187. Massari, M.E. and Murre, C. (2000) Helix–loop–helix proteins: regulators of transcription in eucaryotic organisms. *Mol. Cell. Biol.* **20**, 429-440.

188. Matsuoka, M., Kato, J.Y., Fisher, R.P., Morgan, D.O., and Sherr, C.J. (1994). Activation of cyclin-dependent kinase 4 (CDK4) by mouse MO15-associated kinase. *Mol. Cell. Biol.* **14**, 7265-7275.

189. Matsuoka, S., Edwards, M., Bai, C., Parker, S., Zhang, P., Baldini, A., Harper, J.W., and Elledge, S.J. (1995) p57^{KIP2}, a structurally distinct member of the p21^{CIP1} CDK inhibitor family, is a candidate tumor suppressor gene. *Genes Dev.* **9**, 650-662.

190. Matsushime, H., Ewen, M.E., Strom, D.K., Kato, J.Y., Hanks, S.K., Roussel, M.F., and Sherr, C.J. (1992) Identification and properties of an atypical catalytic subunit (p34PSKJ3/CDK4) for mammalian D-type G1 cyclins. *Cell.* **71**, 323-334.

191. Matsushime, H., Roussel, M.F., Ashmun, R.A., and Sherr, C.J. (1991) Colony-stimulating factor 1 regulates novel cyclins during the G1 phase of the cell cycle. *Cell.* **65**, 701–713.

192. Mazerbourg, S., Callebaut, I., Zapf, J., Mohan, S., Overgaard, M., and Monget, P. (2004) Update on IGFBP-4: regulation of IGFBP-4 levels and functions, in vitro and in vivo, *Growth Hormone & IGF Res.* **14**, 71-84.

193. McRee, D.E. (1999) XtalView/Xfit - A versatile program for manipulating atomic coordinates and electron density. *J. Struc. Biol.* **125**, 156-165.

194. Medema, R.H., Herrera, R.E., Lam, F., and Weinberg, R.A. (1995) Growth suppression by p16^{ink4} requires functional retinoblastoma protein. *Proc. Natl. Acad. Sci. USA.* **92**, 6289-6293.

195. Meijer, L., (2000) Cyclin-dependent kinases inhibitors as potential anticancer, antineurodegenerative, antiviral and antiparasitic agents. *Drug Resistance Updates.* **3**, 83-88.

196. Meijer, L., Jezequel, A., and Ducommun, B. (Eds) (2000) Progress in cell cycle research, vol. 4. Plenum Press, New York.

197. Meyerson, M., and Harlow, E. (1994) Identification of a G1 kinase activity for CDK6, a novel cyclin D partner. *Mol. Cell. Biol.* **14**, 2077-2086.

198. Meyerson, M., Enders, G.H., and Wu, C.L. (1992) A family of human cdc2-related protein kinases. *EMBO J.* **11**, 2909-2917.

199. Michels, A.A., Nguyen, V.T., Fraldi, A., Labas, V., Edwards, M., Bonnet, F., Lania, L., and Bensaude, O., (2003) MAQ1 and 7SK RNA interact with CDK9-cyclin T complexes in a transcription-dependent manner. *Mol. Cell. Biol.* **23**, 4859-4869.

200. Midgley, C.A., and Lane, D.P. (1997) p53 protein stability in tumour cells is not determined by mutation but is dependent on MDM2 binding. *Oncogene.* **15**, 1179-1189.

201. Mittnacht, S., Lees, J.A., Desai, D., Harlow, E., Morgan, D.O., and Weinberg, R.A. (1994) Distinct sub-populations of the retinoblastoma protein show a distinct pattern of phosphorylation. *EMBO J.* **13**, pp. 118-127.

202. Momand, J., Zambetti, G.P., Olson, D.C., George, D., and Levine, A.J. (1992) The mdm-2 oncogene product forms a complex with the p53 protein and inhibits p53-mediated transactivation. *Cell.* **69**, 1237-1245.

203. Mongay, L., Plaza, S., Vigorito, E., Serra-Pages, C., and Vives, J. (2001) Association of the cell cycle regulatory proteins p45(SKP2) and CksHs1. *J. Biol. Chem.* **276**, 25030-25036.

204. Morgan, D. (1997). Cyclin-dependent kinases engines, clocks, and microprocessors. *Annual Review Cell Developmental Biology.* **13**, 261-291.

205. Morgan, D.O., and De-Bondt, H.L. (1994) Protein kinase regulation: insights from crystal structure analysis. *Curr. Opin. Cell. Biol.* **6**, 239-246.

206. Motokura, T., Bloom, T., Kim, H.G., Juppner, H., Ruderman, J.V., Kronenberg, H.M., and Arnold, A. (1991) A novel cyclin encoded by a *bcl*1-linked candidate oncogene. *Nature.* **350**, 512-515.

207. Motwani, M., Li, X., and Schwartz, G.K. (2000) Flavopiridol, a cyclin-dependent kinase inhibitor, prevents spindle inhibitor-induced endoreduplication in human cancer cells. *Clin. Cancer Res*. **6**, 924-932.

208. Mukherjee, S., and Conrad, S.E. (2005) c-Myc suppresses p21[WAF1/CIP1] expression during estrogen signaling and antiestrogen resistance in human breast cancer cells. *J. Biol. Chem*. **280**, 17617-17625.

209. Müller, D., Bouchard, C., Rudolph, B., Steiner, P., Stuckmann, I., Saffrich, R., Ansorge, W., Huttner, W., and Eilers, M. (1997) CDK2-dependent phosphorylation of p27 facilitates its Myc-induced release from cyclin E/CDK2 complexes. *Oncogene*. **15**, 2561-2576.

210. Myers, M.G. Jr, and White, M.F. (1996) Insulin signal transduction and the IRS proteins. *Annu. Rev. Pharmacol. Toxicol*. **36**, 615-658.

211. Neuenschwander, S., Roberts Jr, C.T., and LeRoith, D. (1995) Growth inhibition of MCF-7 breast cancer cells by stable expression of an insulin-like growth factor I receptor antisense ribonucleic acid. *Endocrinology*. **136**, 4298-4303.

212. Neumann, G.M., and Bach, L.A. (1999) The N-terminal disulfide linkages of human insulin-like growth factor-binding protein-6 (hIGFBP-6) and hIGFBP-1 are different as determined by mass spectrometry. *J. Biol. Chem*. **274**, 14587-14594.

213. Nicolas, E., Roumillac, C., and Trouche, D. (2003) Balance between acetylation and methylation of histone H3 lysine 9 on the E2F-responsive dihydrofolate reductase promoter. *Mol. Cell. Biol*. **23**, 1614-1622.

214. Norton, J.D. (2000) ID helix–loop–helix proteins in cell growth, differentiation and tumorigenesis, *J. Cell Sci*. **113**, 3897-3905.

215. Obsil, T., Ghirlando, R., Klein, D.C., Ganguly, S., and Dyda, F. (2001) Crystal structure of the 14-3-3ζ :serotonin N-acetyltransferase complex: a role for scaffolding in enzyme regulation. *Cell*. **105**, 257-267.

216. Oh, Y., Müller, H.L., Lamson, G., and Rosenfeld, R. (1993) Insulin-like growth factor (IGF)-independent action of IGF-binding protein-3 in Hs578T human breast cancer cells. Cell surface binding and growth inhibition. *J. Biol. Chem*. **268**, 14964-14971.

217. Oliner, J.D., Pietenpol, J.A., Thiagalingam, S., Gyuris, J., Kinzler, K.W., and Vogelstein, B. (1993) Oncoprotein MDM2 conceals the activation domain of tumour suppressor p53. *Nature*. **362**, 857-860.

218. Otyepka, M., Kriz, Z., and Koca, J. (2002) Dynamics and binding modes of free cdk2 and its complexes with inhibitors studied by computer simulations. *J. Biol. Str. and Dynamics*. **20**, 141-154.

219. Peng, J., Marshall, N.F., and Price, D.H. (1998) Identification of a cyclin subunit required for the function of *Drosophila* P-TEFb. *J. Biol. Chem*. **273**, 13855-13860.

220. Peng, J., Zhu, Y., Milton, J.T. and Price, D.H. (1998) Identification of multiple cyclin subunits of human P-TEFb. *Genes Dev*. **12**, 755-762.

221. Pérez-Roger, I., Solomon, D.L.C., Sewing, A., and Land., H. (1997) Myc activation of cyclin E/CDK2 kinase involves induction of cyclin E gene transcription and inhibition of p27 (Kip1) binding to newly formed complexes. *Oncogene*. **14**, 2373-2381.

222. Perks, C.M., Newcomb, P.V., Norman, M.R., and Holly, J.M. (1999) Effect of insulin-like growth factor binding protein-1 on integrin signaling and the induction of apoptosis in human breast cancer cells. *J. Mol. Endocrinol*. **22**, 141–50.

223. Perrakis, A., Harkiolaki, M., Wilson, K.S., and Lamzin, V.S. (2001) ARP/wARP and molecular replacement. *Acta Cryst*. **D57**, 1445-1450.

224. Perrakis, A., Morris, R., and Lamzin, V.S. (1999) Automated protein model building combined with iterative structure refinement. *Nature Struct. Biol*. **6**, 458-463.

225. Pietenpol, J.A., Tokino, T., Thiagalingam, S., El-Deiry, W.S., Kinzler, K.W., and Vogelstein, B. (1994) Sequence-specific transcriptional activation is essential for growth suppression by p53. *Proc. Natl. Acad. Sci. USA*. **91**, 1998-2002.

226. Polyak, K., Kato, J.Y., Solomon, M.J., Sherr, C.J., Massague, J., Roberts, J.M., and Koff, A. (1994) p27[Kip1], a cyclin-CDK inhibitor, links transforming growth factor-ß and contact inhibition to cell cycle arrest. *Genes Dev*. **8**, 9-22.

227. Polyak, K., Lee, M.H., Erdjument-Bromage H., Koff, A., Roberts, J.M., Tempst, P., and Massague, J. (1994) Cloning of p27[Kip1], a cyclin-dependent kinase inhibitor and a potential mediator of extracellular antimitogenic signals. *Cell*. **78**, 59-66.

228. Pomerantz, J., Schreiber-Agus N., Liegeois, N.J., Silverman, A., Alland, L., Chin, L., Potes, J., Chen, K., Orlow, I., Lee, H.W., Cordon, C.C., and DePinho, R. (1998) The Ink4a tumor suppressor gene product, p19[ARF], interacts with MDM2 and neutralizes MDM2's inhibition of p53. *Cell*. **92**, 713-723.

229. Poon, R.Y., Yamashita, K., Howell, M., Ershler, M.A., Belyavsky, A., and Hunt, T. (1994) Cell cycle regulation of the p34cdc2/p33cdk2-activating kinase p40MO15. *J. Cell. Sci*. **107**, 2789-2799.

230.   Prall, OWJ., Carroll, J.S., and Sutherland, R.L. (2001) A low abundance pool of nascent p21WAF/CIP1 is targeted by estrogen to activate cyclin E-CDK2. *J. Biol. Chem.* **276**, 45433-45442.

231.   Qin, X.Z., Strong, D.D., Baylink, D.J., and Mohan, S. (1998) Structure-function analysis of the human insulin-like growth factor binding protein-4. *J. Biol. Chem.* **273**, 23509-23516.

232.   Quelle, D.E., Zindy, F., Ashmun, R.A., and Sherr, C.J. (1995) Alternative reading frames of the *INK4a* tumor suppressor gene encode two unrelated proteins capable of inducing cell cycle arrest. *Cell.* **83***, 993-1000.

233.   Radfar, A., Unnikrishnan, I., Lee, H.W., De-Pinho, R.A., and Rosenberg, N. (1998) p19^{ARF} induces p53-dependent apoptosis during Abelson virus-mediated pre-B cell transformation. *Proc. Natl. Acad. Sci. USA.* **95**,13194-13199.

234.   Rajah, R., Valentinis, B., and Cohen, P. (1997) Insulin-like growth factor (IGF)-binding protein-3 induces apoptosis and mediates the effects of transforming growth factor-b1 on programmed cell death through a p53- and IGF-independent mechanism. *J. Biol. Chem.* **272**, 12181-12188.

235.   Rayman, J.B., Takahashi, Y., Indjeian, V.B., Dannenberg, J.H., Catchpole, S., Watson, R.J., te Riele, H., and Dynlacht, B.D. (2002) E2F mediates cell cycle-dependent transcriptional repression in vivo by recruitment of an HDAC1/mSin3B corepressor complex. *Genes Dev.* **16**, 933-947.

236.   Rehm, T., Huber, R., and Holak, T.A. (2002) Application of NMR in structural proteomics: screening for proteins amenable to structural analysis. *Structure.* **10**, 1613-1618.

237.   Reynisdottir, I., and Massague, J. (1997) The subcellular locations of p15(Ink4b) and p27(Kip1) coordinate their inhibitory interactions with CDK4 and CDK2. *Genes Dev.* **11**, 492-503.

238.   Rittinger, K., Budman, J., Xu, J., Volinia, S., Cantley, L.C., Smerdon, S.J., Gamblin, S.J., and Yaffe, M.B. (1999) Structural analysis of 14-3-3 phosphopeptide complexes identifies a dual role for the nuclear export signal of 14-3-3 in ligand binding. *Mol. Cell.* **4**, 153-166.

239.   Roberts, J.M., Koff, A., Polyak, K., Firpo, E., Collins, S., Ohtsubo, M., and Massague, J. (1994) Cyclins, CDKs, and cyclin kinase inhibitors. *Cold Spring Harbor Symp. Quant. Biol.* **59**, 31-38.

240.   Robey, R.W., Medina-Perez W.Y., and Nishiyama, K. (2001) Overexpression of the ATP-binding cassette half-transporter, ABCG2 (MXR/BCRP/ABCP1), in flavopiridol-resistant human breast cancer cells. *Clin. Cancer Res.* **7**, 145-152.

241.   Rosenberg, A.H., Goldman, E., Dunn, J.J., Studier, F.W., and Zubay, G. (1993) Effects of consecutive AGG codons on translation in Escherichia coli, demonstrated with a versatile codon test system. *J. Bacteriol.* **175**, 716-722.

242.   Roy, R., Adamczewski, J.P., Seroz, T., Vermeulen, W., Tassan, J.P., Schaeffer, L., Nigg, E.A., Hoeijmakers, J.H.J., and Egly, J.M. (1994) The MO15 cell cycle kinase is associated with the TFIIH transcription-DNA repair factor. *Cell.* **79**, 1093-1101.

243.   Ruas, M., and Peters, G. (1998) The p16^{INK4a}/CDKN2A tumor suppressor and its relatives. *Biochim. Biophys. Acta Rev. Cancer.* **1378**, 115-177.

244.   Russo, A., Jeffrey, P.D., and Pavletich, N.P. (1996) Structural basis of cyclin dependent kinase activation by phosphorylation. *Nat. Struct. Biol.* **3**, 696-700.

245.   Russo, A.A., Jeffrey, P.D., Patten, A.K., Massague, J. and Pavletich, N.P. (1996) Crystal structure of the p27Kip1 cyclin-dependent-kinase inhibitor bound to the cyclin A-CDK2 complex. *Nature.* **382**, 325-331.

246.   Russo, A.A., Tong, L., Lee, J.O., Jeffrey, P.D., and Pavletich, N.P. (1998) Structural basis for inhibition of the cyclin-dependent kinase CDK6 by the tumor suppressor p16^{INK4a}. *Nature.* **395,** 237-243.

247.   Sausville, E.A., Arbuck, S.G., and Messmann, R. (2001) Phase I trial of 72-hour continuous infusion UCN-01 in patients with refractory neoplasms. *J. Clin. Oncol.* **19**, 2319-2333.

248.   Saville, M.K., and Watson, R.J. (1998) The cell-cycle regulated transcription factor B-Myb is phosphorylated by cyclin A/CDK2 at sites that enhance its transactivation properties. *Oncogene.* **17**, 2679-2689.

249.   Scharf, J.G., and Braulke, T. (2003) The role of the IGF axis in hepatocarcinogenesis. *Horm. Metab. Res.* **35**, 685-693.

250.   Schedlich, L.J., Young, T., Firth S., and Baxter, R. (1998) Insulin-like growth factor-binding protein (IGFBP9-3 and IGFBP-5 share a common nuclear trasport pathway in T47D human breast carcinoma cells. *J. Biol. Chem.* **273**, 18347-18352.

251.   Scheffner, M., Huibregtse, J.M., Vierstra, R.D., and Howley, P.M. (1993) The HPV-16 E6 and E6-AP complex functions as a ubiquitin-protein ligase in the ubiquitination of p53. *Cell.* **75**, 495-505.

252.   Schwartz, G.K., Ilson, D., and Saltz, L. (2001) Phase II study of the cyclin-dependent kinase inhibitor flavopiridol administered to patients with advanced gastric carcinoma. *J. Clin. Oncol.* **19**, 1985-1992.

253. Senderowicz, A.M. (1999) Flavopiridol: the first cyclin-dependent kinase inhibitor in human clinical trials. *Invest. New Drugs*. **17**, 313-320.

254. Senderowicz, A.M. (2003) Novel small molecule cyclin-dependent kinases modulators in human clinical trials. *Cancer Biology and Therapy*. **2**, Suppl.1, S84-S96.

255. Serizawa, H., Mäkelä, T.P., Conaway, J.W., Conaway, R.C., Weinberg, R.A., and Young, R.A. (1995) Association of CDK-activating kinase subunits with transcription factor TFIIH. *Nature*. **374**, 280-282.

256. Serrano, M., Hannon, G.J., and Beach, D. (1993) A new regulatory motif in cell cycle control causing specific inhibition of cyclin D/CDK4. *Nature*. **366**, 704-707.

257. Sherr, C.J. (1996) Cancer cell cycles. *Science*. **274**, 1672-1677.

258. Sherr, C.J., and Roberts, J.M. (1995) Inhibitors of mammalian G1 cyclin-dependent kinases. *Genes Dev.* **9**,1149-1163.

259. Shieh, S.Y., Ikeda, M., Taya, Y., and Prives, C. (1997) DNA damage-induced phosphorylation of p53 alleviates inhibition by MDM2. *Cell*. **91**, 325-334.

260. Shieh, S.Y., Taya, Y., and Prives, C. (1999) DNA damage-inducible phosphorylation of p53 at N-terminal sites including a novel site, Ser20, requires tetramerization. *EMBO J.* **18**, 1815-1823.

261. Shiffman, D., Brooks, E.E., Brooks, A.R., Chan, C.S., and Milner, P.G. (1996) Characterization of the human cyclin-dependent kinase 2 gene. *J. Biol. Chem*. **271**,12199-12204.

262. Shore, S.M., Byers, S.A., Maury, W., and Price, D.H. (2003) Identification of a novel isoform of CDK9. *Gen*. **307**, 175-182.

263. Singh, B., Charkowicz, D., and Mascarenhas, D. (2004) Insulin-like growth factor-independent effects mediated by a C-terminal metal-binding domain of Insulin-like growth factor binding protein-3. *J. Biol. Chem*. **279**, 477-487.

264. Siwanowicz, I., Popowicz, G.M., Wisniewska, M., Huber, R., Kuenkele, K.P., Lang, K.,Engh, R.A., and Holak, T.A. (2005) Structural basis for the regulation of Insulin-like growth factors by IGF binding proteins. *Structure*. **1**, 155-167.

265. Solomon, M.J., Harper, J.W., and Shuttleworth, J. (1993) CAK, the p34cdc2 activating kinase, contains a protein identical or closely related to p40MO15. *EMBO J*. **12**, 3133-3142.

266. Smialowski, P., Singh, M., Mikolajka, A., Majumdar, S., Joy, J.K., Nalabothula, N., Krajewski, M., Degenkolbe, R., Bernard H.U., and Holak, T.A. (2005) NMR and mass spectrometry studies of putative interactions of cell cycle proteins pRb and CDK6 with cell differentiation proteins MyoD and ID-2. *Biochem. Biophys. Acta Proteomics*. **1750**, 48-60.

267. Soos, T.J., Kiyokawa, H., Yan, J.S., Rubin, M.S., Giordano, A., De-Blasio, A., Bottega, S., Wong, B., Mendelsohn, J., and Koff, A. (1996) Formation of p27-CDK complexes during the human mitotic cell cycle. *Cell Growth Differ*. **7**, 135-146.

268. Spruck, C., Strohmaier, H., Watson, M., Smith, A.P., Ryan, A., Krek, T.W., and Reed, S.I. (2001) A CDK-independent function of mammalian Cks1: targeting of SCF(Skp2) to the CDK inhibitor p27Kipl. *Mol Cell*. **7**, 639-650.

269. Ständker, L., Braulke, T., Mark, S., Mostafavi, H., Meyer, M., Honing, S., Gimenez-Gallego, G., and Forssmann, W.G. (2000) Partial IGF affinity of circulating N- and C-terminal fragments of human insulin-like growth factor binding protein-4 (IGFBP-4) and the disulfide bonding pattern of the C-terminal IGFBP-4 domain. *Biochemistry*. **39**, 5082-5088.

270. Stevaux, O. and Dyson, N.J. (2002) A revised picture of the E2F transcriptional network and RB function. *Curr. Opin. Cell Biol*. **14**, 684-691.

271. Stoll, R., Renner, C., Hansen, S., Palme, S., Klein, C., Belling, A., Zeslawski, W., Kamionka, M., Rehm, T., Mühlhahn, P., Schumacher, R., Hesse, F., Kaluza, B., Voelter, W., Engh, R.A., and Holak, T.A. (2001) Chalcone derivatives antagonize interactions between the human oncoprotein MDM2 and p53. *Biochemistry*. **40**, 336-344.

272. Stone, S., Jiang, P., Dayananth, P., Tavtigian, S.V., Katcher, H., Parry, D., Peters, G., and Kamb, A. (1995) Complex structure and regulation of the p16(MTS1) locus. *Cancer Res*. **55**, 2988-2994.

273. Stott, F., Bates, S.A., James, M., McConnell, B.B., Starborg, M., Brookes, S., Palmero, I., Hara, E., Vousden K.H., and Peters, G. (1998) The alternative product from the human CDKN2A locus, p14[ARF], participates in a regulatory feedback loop with p53 and MDM2. *EMBO J*. **17**, 5001-5014.

274. Strausfeld, U., Labbe, J.C., Fesquet, D., Cavadore, J.C., Picard, A., Sadhu, K., Russell, P., and Doree, M., (1991) Dephosphorylation and activation of a p34cdc2/cyclin B complex in vitro by human CDC25 protein. *Nature*. **351**, 242–245.

275. Strober, B.E., Dunaief, J.L and Guha, G.SP. (1996) Analysis of promoter binding by the E2F and pRB families in vivo: distinct E2F proteins mediate activation and repression. *Mol. Cell. Biol*. **16**, 1576-1583.

276. Tao, W., and Levine, A.J. (1999) p19^ARF stabilizes p53 by blocking nucleo-cytoplasmic shuttling of MDM2. *Proc. Natl. Acad. Sci. USA*. **96**, 6937-6941.

277. Taylor, V.L., and Spencer, E.M. (2001) Characterisation of insulin-like growth factor-binding protein-3 binding to a novel receptor on human platelet membranes. *J. Endocrinol*. **168**, 307-315.

278. Tibbetts, R.S., Brumbaugh, K.M., Williams, J.M., Sarkaria, J.N., Cliby, W.A., Shieh, S.Y., Taya, Y., Prives, C., and Abraham, R.T. (1999) A role for ATR in the DNA damage-induced phosphorylation of p53. *Genes Dev*. **13**, 152-157.

279. Torres, A.M., Forbes, B.E., Aplin, S.E., Wallace, J.C., Francis, G.L., and Norton, R.S. (1995) Solution structure of human insulin-like growth factor II. Relationship to receptor and binding protein interactions. *J. Mol. Biol*. **248**, 385-401.

280. Toyoshima, H., and Hunter, T. (1994) p27, a novel inhibitor of G1 cyclin/CDK protein kinase activity, is related to p21. *Cell*. **78**, 67-74.

281. Tsuji, J.N., Nomoto, S., Yasuda, H., Reed, S.I., and Matsumoto, K. (1991) Cloning of a human cDNA encoding a CDC2-related kinase by complementation of a budding yeast cdc28 mutation. *Proc. Natl. Acad. Sci. USA*. **88**, 9006-9010.

282. Turner, R., and Tjian, R. (1989) Leucine repeats and an adjacent DNA binding domain mediate the formation of functional cFos-cJun heterodimers. *Science*. **243**, 1689-1694.

283. Twigg, S.M., Kiefer, M.C., Zapf, J., and Baxter, R.C. (2000) A central domain binding site in insulin-like growth factor binding protein-5 for the acid-labile subunit. *Endocrinology*. **141**, 454-457.

284. Vajdos, F.F., Ultsch, M., Schaffer, M.L., Deshayes, K.D., Liu, J., Skelton, N.J., and de-Vos, A.M. (2001) Crystal structure of human insulin-like growth factor-1: detergent binding inhibits binding protein interactions. *Biochemistry*. **40**, 11022-11029.

285. Valentinis, B., Bhala, A., DeAngelis, T., Baserga, R., and Cohen, P. (1995) The human insulin-like growth factor (IGF) binding protein-3 inhibits the growth of fibroblasts with a targeted disruption of the IGF-I receptor gene. *Mol. Endocrinol*. **9**, 361-367.

286. Wang, C., Fu, M., Mani, S., Wadler, S., Senderowicz, A.M., and Pestell, R.G. (2001) Histone acetylation and the cell-cycle in cancer. *Front. Biosci*. **6**, 610-629.

287. Wang, Y., and Prives, C. (1995) Increased and altered DNA binding of human p53 by S and G2/M but not G1 cyclin-dependent kinases. *Nature*. **376**, 88-91.

288. Weber, J.D., Taylor, L.J., Roussel, M.F., Sherr, C.J., and Bar-Sagi, D. (1999) Nucleolar Arf sequesters MDM2 and activates p53. *Nat. Cell Biol*. **1**, 20-26.

289. Weber, T., Baumgartner, R., Renner, C., Marahiel, M.A., and Holak, T.A. (2000) Solution structure of PCP, a prototype for the peptidyl carrier domains of modular peptide synthetases. *Struct. Fold. Des*. **8**, 407-418.

290. Webley, K., Bond, J.A., Jones, C.J., Blaydes, J.P., Craig, A., Hupp, T., and Wynford, T.D. (2000) Posttranslational modifications of p53 in replicative senescence overlapping but distinct from those induced by DNA damage. *Mol. Cell. Biol*. **20**, 2803-2808.

291. Weinberg, R.A. (1995) The retinoblastoma protein and cell cycle control. *Cell*. **81**, 323-330.

292. Weintraub, H., Davis, R., Tapscott, S., Thayer, M., Krause, M., Benezra, R., Blackwell, T.K., Turner, D., Rupp, R., Hollenberg, S., Zhuang, Y., and Lassar, A. (1991) The myoD gene family: nodal point during specification of the muscle cell lineage, *Science*. **251**, 761–766.

293. Wimmer, J., Fujinaga, K., Taube, R., Cujec, T.P., Zhu, Y., Peng, J., Price, D.H., and Peterlin, B.M. (1999) Interactions between Tat and TAR and Human Immunodeficiency Virus replication are facilitated by human cyclin T1 but not cyclins T2a or T2b. *Virology*. **255**, 182-189.

294. Won, S.J., Liu, C.T., Tsao, L.T., Weng, J.R., Ko, H.H., Wang, J.P., and Lin, C.N. (2005) Synthetic chalcones as potential anti-inflammatory and cancer chemopreventive agents. *Eur. J. Med. Chem*. **40**, 103-112.

295. Wu, H.B., Kumar, A., Tsai, W.C., Mascarenhas, D., Healey, J., and Rechler, M.M. (2000) Characterization of the inhibition of DNA synthesis in proliferating mink lung epithelial cells by insulin-like growth factor binding protein-3. *J. Cell. Biochem*. **77**, 288-297.

296. Wu, Y., Cui, K., Miyoshi, K., Hennighausen, L., Green, J.E., Setser, J., LeRoith, D., and Yakar, S. (2003) Reduced circulating insulin-like growth factor I levels delay the onset of chemically and genetically induced mammary tumors. *Cancer Res*. **63**, 4384-4388.

297. Wüthrich, K. (1986) NMR of Proteins and Nucleic Acids, Wiley-Interscience, New York.

298. Xiao, B., Smerdon S.J., Jones, D.H., Dodson, G.G., Soneji, Y., Aitken, A., and Gamblin, S.J. (1995) Structure of a 14-3-3 protein and implications for coordination of multiple signalling pathways. *Nature*. **376**, 188-191.

299.   Xiong, Y., Connolly, T., Futcher B., and Beach, D. (1991) Human D-type cyclin. *Cell*. **6**, 691-699.

300.   Yaffe, M.B. (2002) How do 14-3-3 proteins work?— Gatekeeper phosphorylation and the molecular anvil hypothesis. *FEBS Lett*. **513**, 53-57.

301.   Yaffe, M.B., Rittinger, K., Volinia, S., Caron, P.R., Aitken, A., Leffers, H., Gamblin, S.J., Smerdon, S.J., and Cantley, L.C., (1997) The structural basis for 14-3-3:phosphopeptide binding specificity. *Cell*. **91**, 961-971.

302.   Yam, C.H., Ng, R.W., Siu, W.Y., Lau, A.W., and Poon, R.Y. (1999) Regulation of cyclin A-CDK2 by SCF component Skp1 and F-box protein Skp2. *Mol. Cell. Biol*. **19**, 635-645.

303.   Yamasaki, H., Prager, D., and Melmed, S. (1993) Structure-function of the human insulin-like growth factor-I receptor: a discordance of somatotrophin internalisation and signalling. *Mol. Endocrinol*. **7**, 681-685.

304.   Yang, E.B., Zang, K., Cheng, L.Y., and Mack, P. (1998) Butein, a specific protein tyrosine kinase inhibitor. Biochemical and biophysical research communications. **245**, 435-438.

305.   Yu, S.M., Cheng, Z.J. and Kuo, S.C. (1995). Endotheliun-dependent relaxation of rat aorta by butein, a novel cyclic AMP-specific phosphodiesterase inhibitor. *E. J. Pharm*. **280**, 69-77.

306.   Zarkowski, T.U.S., Harlow, E., and Mittnacht, S. (1997) Monoclonal antibodies for underphosphorylated retinoblastoma protein identify a cell cycle regulated phosphorylation site targeted by CDKs. *Oncogene*. **14**, 249-254.

307.   Zeng, Y., Forbes, K.C., Wu, Z., Moreno, S., Piwnica-Worms, H. and Enoch, T., (1998) Replication checkpoint requires phosphorylation of the phosphatase Cdc25 by Cds1 or Chk1. *Nature*. **395**, 507–510.

308.   Zeslawski, W., Beisel, H.G., Kamionka, M., Kalus, W., Engh, R.A., Huber, R., Lang, K., and Holak T.A. (2001) The interaction of insulin-like growth factor-I with the N-terminal domain of IGFBP-5. *EMBO J*. **20**, 3638-3644.

309.   Zhang, H., Duan, H.O., Kirley, S.D., Zukerberg, L.R., and Wu, C.L. (2005) Aberrant Splicing of Cables Gene, A CDK Regulator, in Human Cancers. *Cancer Biol. Ther*. **8**, 4(11).

310.   Zhang, H.S., Gavin, M., Dahiya, A., Postigo, A.A., Ma, D., Luo, R.X., Harbour, J.W., and Dean, D.C. (2000) Exit from G1 and S phase of the cell cycle is regulated by repressor complexes containing HDAC-Rb-hSWI/SNF and Rb-hSWI/SNF. *Cell*. **101**, 79-89.

311.   Zhang, J.M., Wei, Q., Zhao, X., and Paterson, B.M. (1999) Coupling of the cell cycle and myogenesis through the cyclin D1-dependent interaction of MyoD with cdk4, *EMBO J*. **18**, 926–933.

312.   Zhang, J.M., Zhao, X., Wei, Q. and Paterson, B.M. (1999) Direct inhibition of G1 CDK kinase activity by MyoD promotes myoblast cell cycle withdrawal and terminal differentiation, *EMBO J*. **18**, 6983–6993.

313.   Zhang, Y., and Xiong, Y. (1999) Mutations in human ARF exon 2 disrupt its nucleolar localization and impair its ability to block nuclear export of MDM2 and p53. *Mol. Cell*. **3**, 579-591.

314.   Zhang, Y., Xiong, Y., and Yarbrough, W.G. (1998) ARF promotes MDM2 degradation and stabilizes p53: ARF-INK4a locus deletion impairs both the Rb and p53 tumor suppressor pathways. *Cell*. **92***,* 725-734.

315.   Zhu, L., Harlow, E., and Dynlacht, B.D. (1995) p107 uses a p21CIP1-related domain to bind cyclin/CDK2 and regulate interactions with E2F. *Genes Dev*. **9**, 1740-1752.

316.   Zhu, Y., Peery, T., Peng, J., Ramanathan, Y., Marshall, N., Marshall, T., Amendt, B., Mathews, M.B., and and David, H.P. (1997) Price transcription elongation factor P-TEFb is required for HIV-1 Tat transactivation in vitro. *Genes Dev*. **11**, 2622-2632.

317.   Ziebold, U., Bartsch, O., Marais, R., Ferrari, S., and Klempnauer, K.H. (1997) Phosphorylation and activation of B-Myb by cyclin A-CDK2. *Curr. Biol*. **7**, 253-260.

318.   Zindy, F., Eischen, C.M., Randle, D., Kamijo, T., Cleveland, J.L., Sherr, C.J., and Roussel, M.F. (1998) Myc signaling via the ARF tumor suppressor regulates p53-dependent apoptosis and immortalization. *Genes Dev*. **12***,* 2424-2433.

10. Appendix

Abbreviations and symbols

• 1D	one-dimensional	• 2D	two-dimensional
• Å	Ångstrom (10^{-10} m)	• aa	amino acid
• ALS	acid labile subunit	• APS	ammonium peroxodisulfate
• bHLH	basic helix loop helix	• bp	base pair
• BSA	bovine serum albumin	• cDNA	complementary DNA
• CDK2	cyclin dependent kinase 2	• CDK6	cyclin dependent kinase 6
• CTD	C-terminal domain	• CTRD	C-terminal regulatory domian
• CyA2	cyclin A2	• Da	Dalton (g mol-1)
• DMSO	dimethylsulfoxide	• DNA	deoxyribonucleic acid
• DnaseI	deoxyribonuclease I	• EDTA	ethylenediamine tetraacetic acid
• ELISA	enzyme-linked immunosorbant assay		
• g	gravity (9.81 m s^{-2})	• GH	growth hormone
• GSH	reduced glutathione	• GSSG	oxidized glutathione
• GST	glutathione S-transferase	• HSQC	heteronuclear single quantum coherence
• Hz	Hertz	• IGF	insulin-like growth factor
• IGFBP	IGF binding protein	• IGF-IR	IGF receptor type I
• IGF-IIR	IGF receptor type II		
• IMAC	immobilized metal affinity chromatography		
• INCA	inhibitor of CDK interacting with cyclin A2		
• IPTG	isopropyl-β-thiogalactopyranoside	• IR	insulin receptor
• ITC	isothermal titration calorimetry	• IRS	insulin receptor substrate(s)
• K_D	dissotation constant	• kDa	kilo dalton
• LB	Luria-Broth medium	• MAP	mitogen-activated protein kinase
• MM	minimal medium	• MW	molecular weight
• NiNTA	nickel-nitrilotriacetic acid	• NLS	nuclear localization signal
• NMR	nuclear magnetic resonance	• OD	optical density
• P3K	phosphatidylinositol 3-kinase	• PAGE	polyacrylamide gel electrophoresis
• ppm	parts per million	• pRb	retinoblastoma protein
• RMSD	root mean square deviation	• SDS	sodium dodecyl sulfate
• TB	terrific broth	• TD	tetramerization domain
• TEMED	N,N,N',N'-tetramethylethylendiamine		

Amino acids and nucleotides are abbreviated according to either one or three letter IUPAC code.
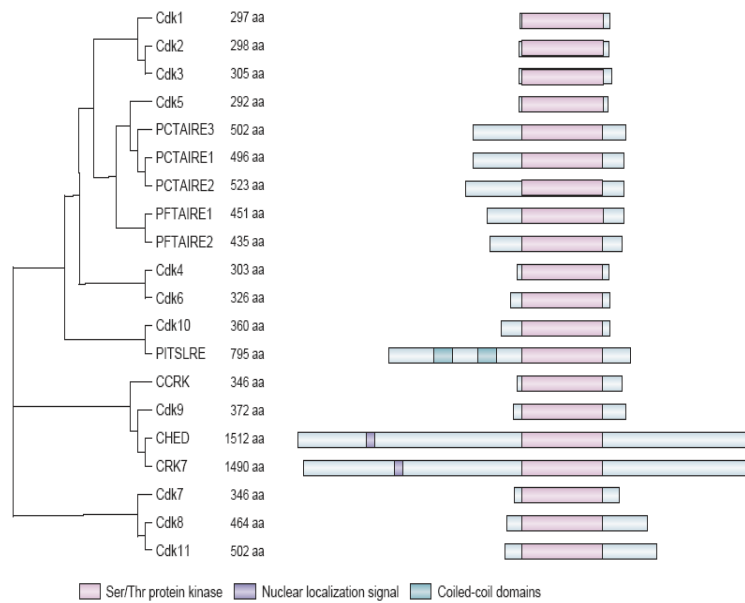
The mammalian CDK family. The number of amino acids (aa) deduced from the nucleotide sequence and the principal structural domains are indicated for each protein.
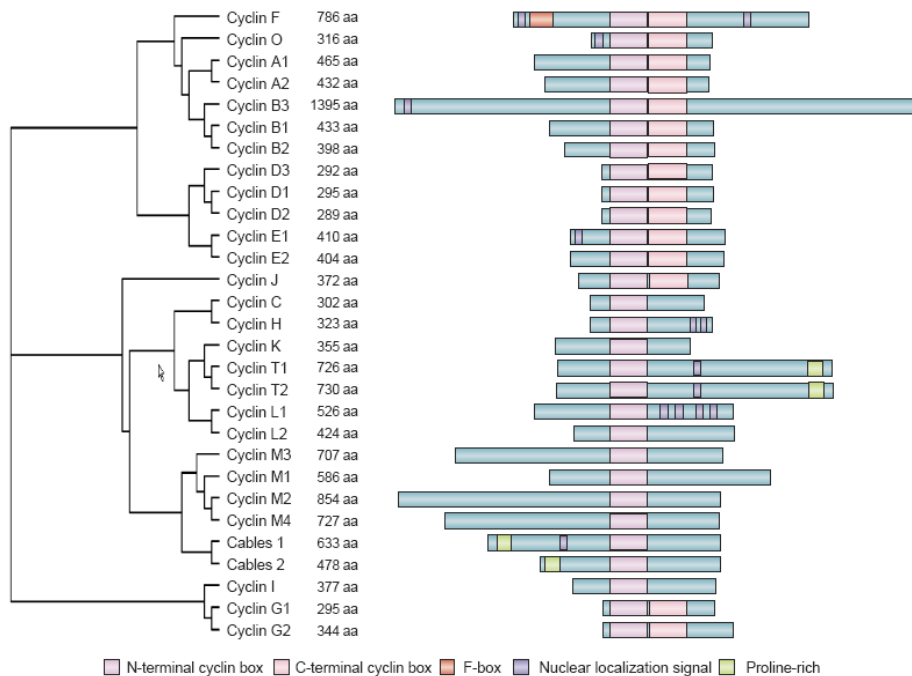
Mammalian protein with a cyclin domain. The number of amino acids (aa) deduced from the nucleotide sequence and the principal structural domains are indicated for each protein (Barbacid et al., 2005).
.